March 2018

DESIGN AND SYNTHESIS OF STIMULI-RESPONSIVE POLYMERIC NANOGELS TOWARDS THERAPEUTIC TRANSLATION

Mallory R. Gordon

DESIGN AND SYNTHESIS OF STIMULI-RESPONSIVE POLYMERIC NANOGELS TOWARDS THERAPEUTIC TRANSLATION

A Dissertation Presented

by

MALLORY R. GORDON

Submitted to the Graduate School of the
University of Massachusetts Amherst in partial fulfillment
of the requirements for the degree of

DOCTOR OF PHILOSOPHY

February 2018

Chemistry

DESIGN AND SYNTHESIS OF STIMULI-RESPONSIVE POLYMERIC NANOGELS TOWARDS THERAPEUTIC TRANSLATION

A Dissertation Presented

by

MALLORY R. GORDON

Approved as to style and content by:

_____
Sankaran Thayumanavan, Chair

_____
Richard W. Vachet, Member

_____
Min Chen, Member

_____
Gregory N. Tew, Member

_____
Richard W. Vachet, Department Head
Chemistry Department

DEDICATION

To my parents, who have unconditionally supported all life pursuits, academic or otherwise.

ACKNOWLEDGMENTS

Completion of this dissertation would not have been possible without the help and support of many individuals at the University of Massachusetts throughout my doctoral study. I would like to take this opportunity to say thank you and convey my sincere gratitude to many of these individuals.

First, I would like to thank my advisor Professor Sankaran Thayumanavan (Thai) for all his guidance, support, and understanding. Professor Thai has guided his group members in both scientific development and professional growth. I want to thank him for his creativity and passion for scientific research, and his resolution in pursing challenging problems. Throughout my time in his group, he has encouraged his students to collaborate, both academically and industrially, to apply for awards, certificate programs, and fellowships, and develop our scientific communication skills in presentations. We are fortunate to have his support in attending conferences, participate in grant proposal processes, and a degree of autonomy in project direction.

I would like to thank my committee members Professor Richard W. Vachet, Professor Min Chen, and Professor Gregory N. Tew for their in-depth engagement, productive criticism, and insightful suggestions during all candidacy presentations. All feedback has been immensely beneficial to my work, scientific development, and research communication.

I am very grateful to all the members of Thai Group, past and present. I would like to thank all my project collaborators in the Thai Lab throughout the years, which include Dr. Jiaming Zhuang, Dr. Judy Ventura, Dr. Longyu Li, Dr. Kishore Raghupathi, Bo Zhao, Francesca Anson, Ann Fernandez, Celia Homyak, Khushboo Singh, and Mine Canakci. I

am so appreciative of all the ideas, support, and expertise they have provided, as well as generosity with their time.

I would like to thank industrial collaborator Dr. Edward Lawson at Johnson & Johnson, for both the financial support for experimental pursuits and the astute direction. I wish to thank Tracey Woolliscroft, Christopher Bull, Deepa Balagurunathan, Lisa Repke, Patrick McConville, Erin Trachet, John L. Chunta, Deanne Lister, Scott Wise at Molecular Imaging Inc., for their involvement in animal biodistribution work. I also wish to thank Jianyun Deng, Jennifer Zhang, Debbie Snyder, Michelle Mack, Chelsea Bailey, at Crown Bioscience Inc., for their involvement in animal efficacy and safety work.

I would like to thank the Chemistry Biology Interface (CBI) for greatly improving my multidisciplinary scientific and personal development, and I am grateful to have received essential financial support for two years during my doctoral study as a Trainee. Specifically, I would like to thank Professor Lynmarie Thompson for her leadership in developing and maintaining CBI so that I, and many others, could benefit from such an excellent certificate program.

I would like to thank Karen Hakala for her practical assistance to everyone in the Thai lab. Her kindness and generosity are exemplary, and we are so appreciative for all her help. I would like to thank all my friends in Thayumanavan lab, at the University of Massachusetts, and the Amherst area. Their support and camaraderie have made these last six years enjoyable and inimitable, and I will cherish their relationships for years to come. To my family and my husband, who are always there, words cannot express my love and appreciation throughout this process.

ABSTRACT

DESIGN AND SYNTHESIS OF STIMULI-RESPONSIVE POLYMERIC NANOGELS TOWARDS THERAPEUTIC TRANSLATION

FEBRUARY 2018

MALLORY R. GORDON

B.A., FRANKLIN & MARSHALL COLLEGE

Ph.D., UNIVERSITY OF MASSACHUSETTS AMHERST

Directed by: Professor Sankaran Thayumanavan

In the application of delivery of therapeutics, nanostructures of various composition have been employed due to their capacity to act as a host for lipophilic payloads. Advances in the synthetic preparation, size, morphology, and chemical or physical characteristics of polymers have impacted their development and versatility. A detailed understanding of polymeric nanoparticle host-guest properties is crucial to their practical translation to specific delivery applications. Further, these features must be highly tailorable to overcome biological barriers, stably encapsulate their therapeutic contexts, and exhibit payload release selectively in the target environment. In this dissertation, we aim to rationally design polymeric nano-scale assemblies with well-defined compositions and unique stimuli-responsiveness to achieve desirable host properties and interfacial characteristics. While each chapter is specific in focus, we expect that the fundamental findings in this dissertation to broadly impact principles in drug delivery, including nanoparticle biodistribution (chapter 2), hydrophobic delivery (chapter 3), stimuli-responsive "smart" materials (chapter 4), and polymeric composition development (chapter 5).

TABLE OF CONTENTS

Page

LIST OF TABLES

Table Page

LIST OF FIGURES

Figure Page

CHAPTER 1

INTRODUCTION

The field of nanotechnology encompasses the development of materials in the range of 1 to 100 nanometers, and is of considerable interest towards various applications due to the morphological and chemical diversity, high surface to volume ratio, and capacity to either adsorb or encapsulate compounds at that scale.[1-4] The material's chemical composition, such as polymers, inorganic materials, metals and biologics,[5-11] as well as their morphology, such as spheres, disks, or cylinders,[12-16] are specific and adaptable to the purpose of interest. This rich diversity has implications in fundamental science and many fields including biotechnology, micro and photoelectronics, and optical materials.[17-21] In the application of delivery of therapeutics, nanostructures of various composition been employed including polymeric nanoparticles,[22-24] liposomes,[25-27] gold nanoparticles,[28, 29] carbon nanotubes,[30, 31] iron oxide nanoparticles,[32-34] and dendrimers[35, 36] Advances in the synthetic preparation, size and morphological control, and chemical or physical characteristics of polymers have aided in their development and practical application. Here will discuss polymeric nanoassemblies in the context of drug delivery of hydrophobic guests, with specific focus on the stimuli-responsivity of such materials and their material requirements for biological application in therapeutics.

1.1 Supramolecular Self-Assembly

Supramolecular materials of various structures, including micelles, vesicles, helices, and fibers, are formed through spontaneous non-covalent self-organization of amphiphiles that minimize its free energy to reach thermodynamic equilibrium in the system.[37-41] In aqueous media, this self-assembly is dictated by the differential interactions

of the amphiphile hydrophilic functionalities with the bulk solvent and hydrophobic functionalities among themselves. Those that display the capacity to encapsulate contents in their water-excluded interior such as drug molecules or reporters have vast implications in therapeutics and diagnostics.[42-45] The relative volume and position of hydrophobic and hydrophilic functional groups dictate the type of assembly that forms, and the concentration of amphiphile dictates the capability for assembly formation.[46-48] This critical aggregation concentration (CAC) are often large for small molecules amphiphiles such as detergents and have low mechanical stabilities. Macromolecules such as amphiphilic polymers, however, generally have assemblies with low CAC values and higher stability, yielding practical application in their use to retain guest molecules.[49-55]

1.2 Amphiphilic Random Copolymers

Advances in in controlled polymerization techniques, such as reversible addition–fragmentation chain transfer polymerization (RAFT), atom transfer radical polymerization (ATRP), ring-opening mediated radical polymerization (ROMP), and as nitroxide mediated radical polymerization (NMP), has led to significant progress in synthesis of diverse copolymers, both block and random.[56-61] Block copolymer are arranged where each block in the chain contains repetition of a particular monomer, while random copolymers have different monomer components indiscriminately arranged throughout the chain. Block copolymers' reproducible access to unique self-assembled morphologies has led to substantial focus towards understanding their supramolecular behaviors.[62-64] Synthesis, however, requires consecutive controlled polymerization reactions or post modifications through reactions such as substitutions, grafting, or assorted "click" chemistries.[65-67] Random copolymers, alternatively are more synthetically facile, and can be prepared with

different monomers copolymerized in one step. Investigation of nanomaterial capabilities using random copolymers can potentially expand their versatility towards various fields of study.

1.3 Nanoparticles for Drug Delivery and Passive Targeting

Many small molecule therapeutics, including chemotherapeutics, are lipophilic and suffer from poor aqueous solubility and are susceptible to decomposition through hydrolysis. This can require frequent administration to achieve therapeutic benefits due to short half-life, and low efficacy and tissue selectivity, and deleterious side effects.[68, 69] Nanoparticles can potentially improve the therapeutic profiles of such drugs through improved solubility and stability, and by minimizing toxicity from side effects. In the treatment of solid tumor-type cancers, nanoparticles have gained increased interest due to their observed increased tumor accumulation due to the enhanced permeation and retention (EPR) effect.[70, 71] This phenomena is a result of extravasation of nano-sized macromolecules through fenestrated blood vessels from rapid and irregular growth in angiogenesis, and poor lymphatic drainage of contents.[72] Biological physical barriers for particles include accumulation from the leaky endothelium of other organs such as the liver and spleen, and renal clearance through filtering of small particles (<10 nm) the kidneys.[73, 74] Also, nanoparticles face recognition and clearance through the reticuloendothelial system (RES), from immune cells in circulation, liver, lymph nodes and spleen.[75-77] This clearance is often occurs through the pathway of opsonization, which occurs when plasma proteins, or opsonins, are adsorbed onto the particle surface.[76] To achieve stealthy character and extended circulation half-lives for tumor accumulation through the EPR effect, a mechanism called “passive” targeting, nanocarriers are often coated with poly(ethylene

glycol) (PEG). PEG imparts a well hydrated corona to the surface of these nanoassemblies, generating steric stabilization and non-fouling characteristics to reduce non-specific interactions with proteins.[77-79] The grafting, conjugation, and adsorption of PEG to nanoparticle surfaces have been shown to decrease protein adsorption and improve residence times.[80-82] Even with PEG incorporation to the corona, several parameters including size, morphology, and chemical composition can influence non-specific interactions and impact biodistribution, leading to some contrasting trends depending on nanomaterial.

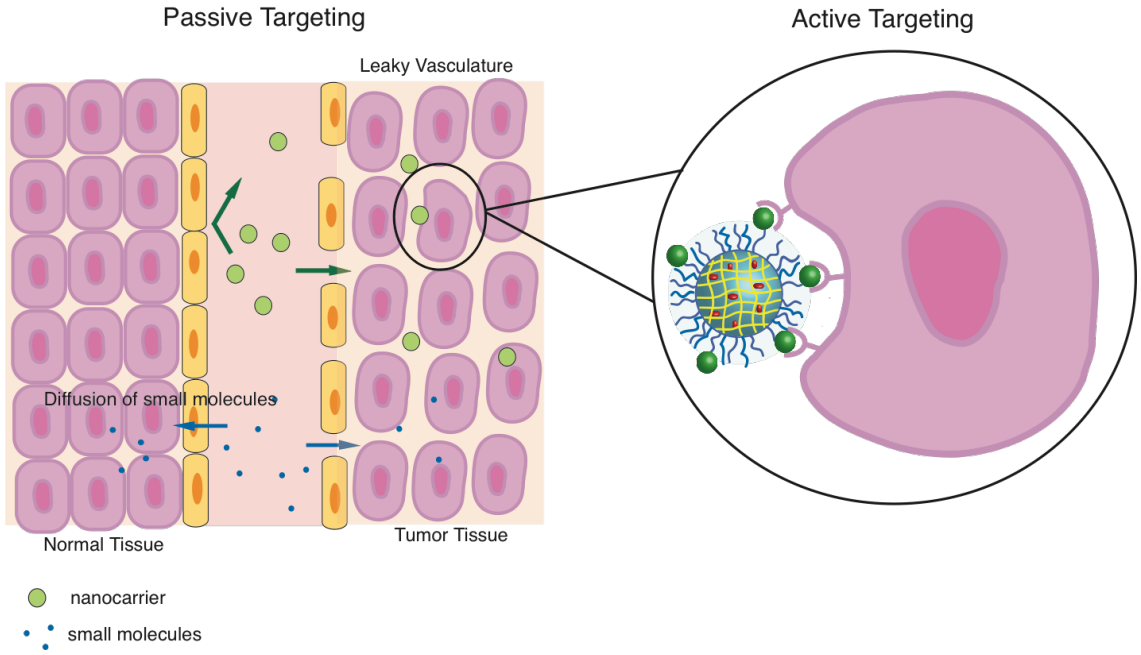

Figure 1. Schematic representation of passive targeting via the enhanced permeation and retention (EPR) effect and active targeting through ligands and cell surface receptors.

1.4 Active Targeting for Drug Delivery

Passive targeting have inherent limitations including inability distinguish disease tissue form healthy tissue, and reduced endosomolytic activity from inhibited cellular interactions.[83, 84] Active targeting aims to achieve cell-type selectivity though binding unique or over expressed surface receptors on cancer cells through receptor-mediated

endocytosis.[70, 85] Incorporation of ligands such as cell-penetrating peptides, targeting peptides, monoclonal antibodies, or small molecules can vastly improve the selective cellular internalization of nanoparticles.[86-89] This surface decoration, however, can increase the ability for RES recognition and in vivo clearance.[90] An approach to this concern is development of "smart" nanoparticles that can change their physical or chemical properties to expose targeting ligands or achieve "active" characteristics in response to stimuli.

1.5 Delivery Vehicle Requirements

Considering the afore mentioned biological considerations, the design and development of delivery vehicles must satisfy extensive criteria. Delivery vehicles should be able to *i)* stably encapsulate hydrophobic compounds such as drugs at their core without non-specific release *ii)* possess appropriate size and surface chemistry to achieve stealthy character to benefit from the EPR effect, *iii)* have the capability for surface modification for active targeting strategies through ligands or "smart" strategies, *iv)* release contents according to a specific stimulus in a desired location, and *v)* be biocompatible and exhibit low toxicity. Some current advances in the engineering of "intelligent" polymeric based nanomaterials in stimuli responsiveness, encapsulation stability, size control, and surface modification chemistries aim to fulfill these requirements.

1.6 Stimuli-Responsive Polymeric Nanomaterials

Stimuli responsive nanoparticles are materials that contain components that can respond to a stimulus in the local environment in a chemical or physical manor. The applications of such systems have implications in many fields including drug delivery, sensing, catalysis, surface coating, and tissue engineering.[91-97] Stimuli can be broadly categorized as chemical, physical, or biological.[98] Chemical stimuli can include pH, redox

potential, and ionic strength. Physical stimuli are those such as temperature, light, mechanical force, ultrasound, and electric or magnetic field. Biological stimuli can encompass proteins, enzymes, nucleic acids, among others. Our interests reside in polymeric nanoparticles that are responsive to inherent biological and chemical stimuli that provide tools in improving site-selectivity of therapeutic delivery. Here we will introduce the developments of polymeric nanogels with redox-sensitivity, followed by developments which expand upon the amphiphilic random copolymer nanogel platform.

1.6.1 Redox-Responsive Polymeric Nanogels

Redox responsive nanomaterials are attractive for biological purposes to the high intracellular concentration of reducing agents such as glutathione (GSH) and thioredoxin.[99-105] Serum and extracellular concentrations of GSH is low micromolar, while in cytosol concentrations are about 10 mM.[106] Further, the cytosolic GSH concentration in cancer cells are much higher than those in healthy normal cells. Therefore, nanoparticle systems that are responsive to reducing conditions have the capacity for selective intracellular release of encapsulated contents. The most heavily employed strategy for introducing GSH responsivity is the incorporation of disulfide functionality in the polymer. Disulfides can be synthetically installed in either the polymer backbone or side chains to achieve distinctive structural responsivity to reducing conditions. For example, one investigation achieved the cargo release of doxorubicin in the cytoplasm of cells through deshielding of poly(ethylamine) shells from disulfide incorporation in the polymer backbone of polymeric micelles.[107] Alternatively, GSH responsivity in the core or shell of aggregates is can be achieved by disulfide incorporation in polymer side chains. Our group has developed the GSH responsivity of amphiphilic random copolymers with hydrophilic

tri(ethylene glycol) moieties and hydrophobic alkyl moieties containing disulfide functionality prepared by free radical polymerization.[106] These polymers, capable of forming micelle-type assemblies and encapsulate lipophilic guests, displayed disassembly and release of guest in response to reducing agent. The disintegration is due to cleavage of alkyl disulfide and loss in assembly hydrophobicity.

These findings inspired introducing strategies to improve the aggregate stability. Upon dilution, these micelle-type copolymer aggregate were destabilized, leading to release. A strategy to introduce chemical crosslinking between and within chemical chains was developed to maintain their structural integrity and control their stimuli-specific guest release.[108, 109] The random copolymer prepared by RAFT polymerization in comprised of hydrophilic oligoethylene glycol (OEG) and hydrophobic pyridyldisulfide (PDS) moieties as side chain functionalities. The amphiphilic copolymer self-assembles in aqueous medium with the PDS units at the core. Addition of reducing agent dithiothreitol (DTT) results in a stoichiometric generation of free thiols from PDS units at the particle interior, which results in intra- and inter-polymer chain disulfide exchange reactions with adjacent PDS moieties, affording core crosslinked nanogels. These nanogels were capable of stably encapsulating hydrophobic guest molecules, and releasing them in response to reducing environment due to the disulfide core. Further, the polymer molecular weight and relative monomer composition were shown to tune the size of the aggregates.

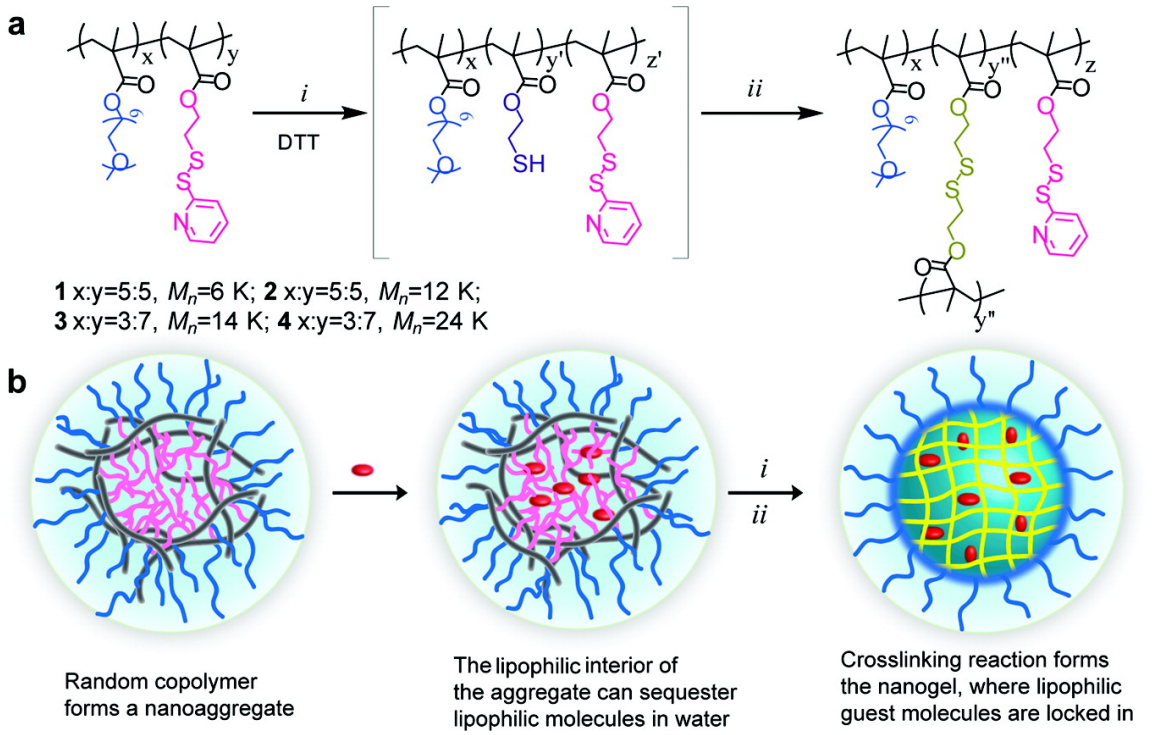

Figure 2. (a) Polymer structure of precursors and nanogels: (i) DTT cleavage of deficient amount of PDS functional groups, and (ii) inter and intra-chain crosslinking and nanogel formation. (b) Schematic representation of the preparation of the GSH-responsive nanogels (reprinted with permission from reference[108]. Copyright 2010 American Chemical Society).

The encapsulation stability of these nanogels were probed by guest exchange dynamics using a fluorescence resonance energy transfer (FRET) based method.[110] Fret donor and acceptor, 3,3′-dioctadecyloxacarbocyanine perchlorate (DiO) and 1,1′-dioctadecyl-3,3,3′,3′-tetramethylindocarbocyanine perchlorate (DiI), respectively, were separately encapsulated in nanogels. When the solutions of the two nanogels are mixed, no FRET observation indicates the distance between FRET pairs is longer than their Förster radius, signifying stable encapsulation in separate containers. However, unstable encapsulation is expected to allow guest exchange, resulting in an increased in observed FRET. The dynamics of exchange determined from FRET ratio over time demonstrated that the encapsulation stability is depended on the percentage of crosslinking.

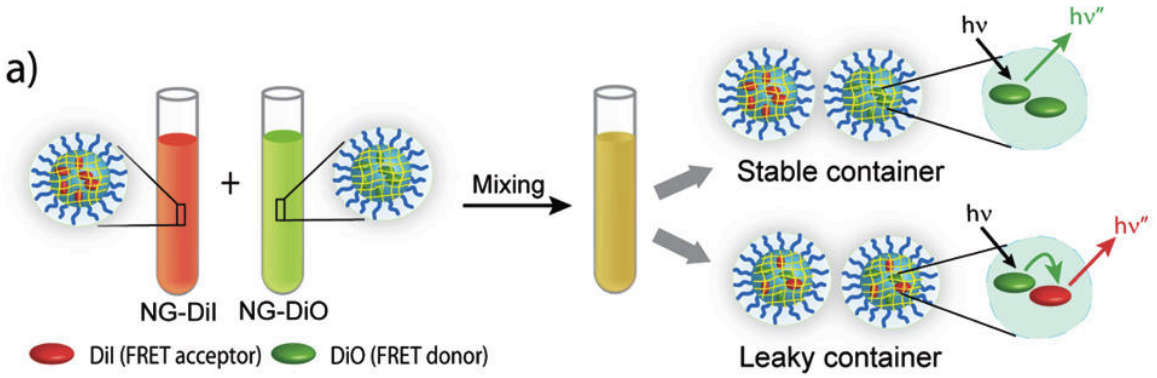

Figure 3. a) Nanogels encapsulated with DiI or DiO and FRET behavior of mixed solutions of stable containers and leaky containers (adapted with permission from reference[110]. Copyright 2010 American Chemical Society).

The dynamics were further probed to establish whether these guests are exchanging by collision-based collision-exchange-separation mechanism or diffusion-based exit-re-entry mechanism.[111] the former depends on the particle collision frequency, while the later depends on the ability of guest molecule to exit and re-enter the particle. The dynamics were investigated using the FRET method, and found that exchange in guest increased with particle concentration, supporting exchange occurs dominantly according to the collision-based mechanism. Investigation with pH sensitive host found that when the nanogel interior was hydrophobic, the collision-based mechanism, like non-pH sensitive control, was dominant. However, under pH conditions when the particle interior hydrophobicity was compromised, the dominant pathway observed to be the diffusion-based mechanism.

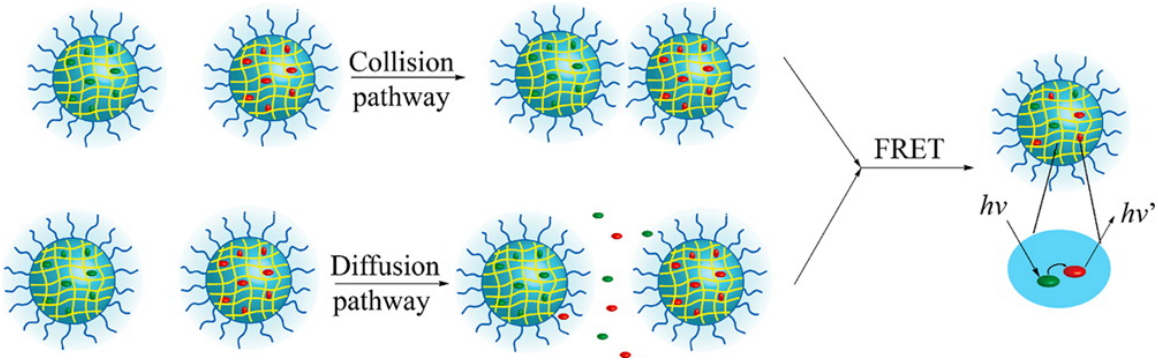

Figure 4. Schematic representation of (top) Collision-Exchange-Separation mechanism, and (bottom) Exit-Re-entry Mechanism for encapsulated guest exchange (reproduced with permission from reference[111]. Copyright 2014 American Chemical Society).

1.6.2 pH-Responsive Polymeric Nanoparticles

The varied environmental pH of different organs, extracellular tissues, and subcellular compartments is an attractive means to achieve unique nanoparticle responsiveness. Methods for oral delivery are often designed depending on the pH of intended locale in the gastrointestinal tract, for instance. A common technique to bypass digestion in the acidic stomach (pH 1-3) to achieve drug release in the upper tract of the intestines (pH 5-7.5) is the use of methacrylic acid copolymers as enteric coatings, such that they are collapsed as protonated carboxylic acid in low pH and swollen as deprotonated carboxylate at increased pH.[112-115]

In application of chemotherapeutic delivery, nanomaterials with pH sensitivity have been well explored because tumor anaerobic hypoxia results in lactate production a pH decrease (6.2-6.9) in the extracellular milieu compared to normal healthy tissue (7.2-7.4).[116] Thus, extensive work on nanoscopic systems that undergo chemical or physical changes at reduce pH has been explored to develop cationic character to induce local drug release or facilitate cellular internalization. [117-126] The former is a common strategy in developing systems with enhanced aqueous solubility at decreased pH, such that the hydrophobic-hydrophobic balance is disrupted resulting in content release. An example of this is the protonation of hydrophobic β-amino ester-containing polymers below pH 6.5, converting the polymer to hydrophilic.[117, 118] The latter is motivated by the affinity of cationic materials to the anionic phospholipid bilayer of cell membranes resulting in rapid internalization.[127, 128] Cationic polymers including polylysine, polyamidoamine, and polypropylene have been used towards this aim, particularly for layer-by-layer techniques for anion contents such as siRNA, mRNA, and DNA.[129] However, the indiscriminate cellular internalization and the adsorption of proteins on cationic nanomaterials limits their

practicality for *in vivo* translation.[130-132] Stimuli-specific charge development thus aims improve specificity and avoid the RES clearance of such materials.

Nanogels that are responsive to changes in have been developed within the group.[119, 120] One approach that was investigated involved using electrostatic complementarity to coat polycationic nanogels with a polyanionic nanogel.[119] The polycationic nanogel was achieved by incorporating quaternary ammonium and *N*-isopropyl moieties into the amphiphilic polymer. The coating polymer contained pH-sensitive and anionic tetrahydrophthalic acid units, such that when the pH is decreased the tetrahydrophthalic acid is cleaved, converting the coating to a polycationic material. The charge repulsion causes this coating to shed, and reveals the underlying cationic nanogel. This aim was pursued with interest that cationic materials internalize much more rapidly in cells, but have an inherent lack of specificity and are not applicable for direct use *in vivo*.

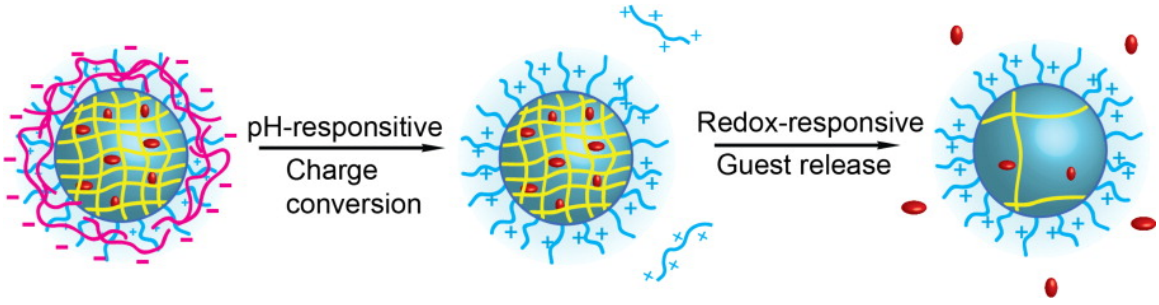

Figure 5. Schematic representation of the polymer nanogel coating with charge complementarity electrostatic assembly, followed by pH-induced charge conversion and redox-induced release processes (reproduced with permission from reference[119]. Copyright 2014 American Chemical Society).

Similarly, a pH-responsive nanogel system was developed in the group, which was achieved by incorporation of pH-sensitive 2-diisopropyl amine moieties into the amphiphilic polymer.[120] These groups are hydrophobic and buried under physiological pH (7.4), however become protonated at hydrophilic when the pH is decreased to 6.5,

representative of tumor extracellular milieu. This conversion was monitored by zeta potential change, and it was that the pH of charge conversion from negative to positive was dependent on the extent of 2-diisoproylamine groups present in the particle. Enhanced cellular uptake under mildly acidic conditions was demonstrated, supporting the potential of such systems to improve specificity and extent of delivery.

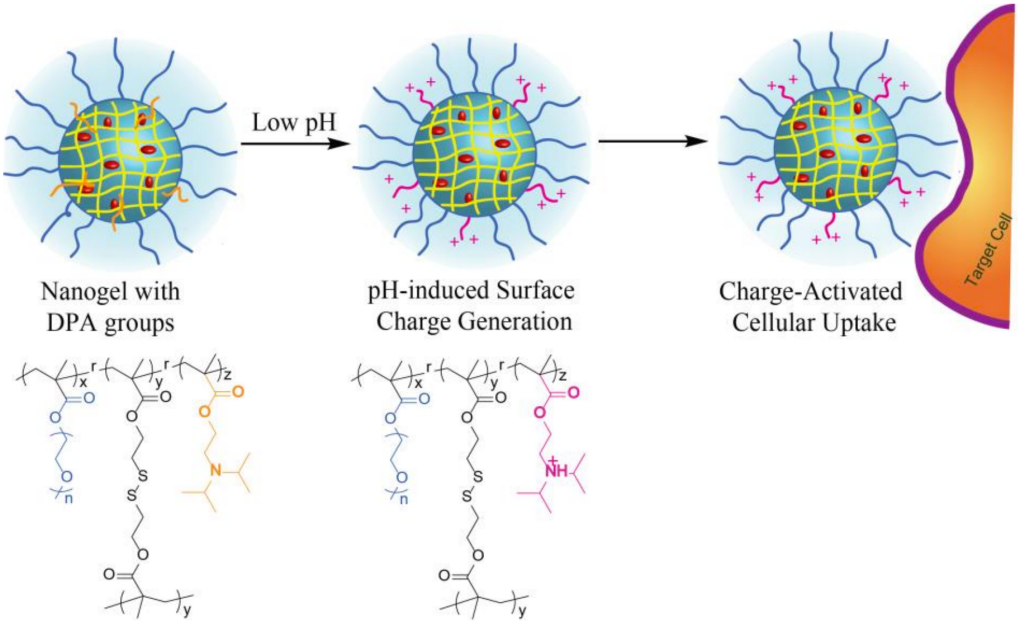

Figure 6. Schematic illustration of nanogel and corresponding chemical structure of polymer for pH-induced cationic surface generation for enhanced cellular uptake (reprinted with permission from reference[120]. Copyright 2013 Royal Society of Chemistry).

Further subcellular specificity can also be achieved with responsive materials due to the varied pH of compartments such as the endosomes and lysosomes (pH 5 or lower) compared to the cytosol (pH 7.4) extracellular regions.[133] Polymers that contain imidazole and poly(amidoamine) or poly(ethyleneimine) with pH responsivity are capable of buffering endosomal pH and have been demonstrated to improve endosomal escape for cytosolic delivery.[134]

1.6.3 Enzyme-Responsive Polymeric Nanoparticles

Nanomaterials that respond to biochemical stimuli such as enzymes can be advantageous for delivery of therapeutics, sensing, diagnostics, imagining, and bio-mimicry applications. Responses such as surface modifications, supramolecular assembly or disassembly, and sol-gel transitions can occur in response to enzymes.[135] The advantage of exploiting enzymes as stimuli is their specificity for biomedical function, particularly in disease states. Enzyme dysregulation is common in different cancers, for instance, and can be unique to the tumor environment. The advantage of incorporating biochemical stimuli-induced responses to a molecular design is that they have the potential to be specific for a biomedical function.[136, 137] Due to their upregulation in cancer cells, several protease-responsive systems have been investigated. Those of immense interest include matrix metalloproteinases (MMPs), which are zinc-dependent proteases that degrade the extracellular matrix. MMPs are associated with tumor invasiveness, metastasis, and angiogenesis, and are observed in many solid tumor types.[138] MMPs have been demonstrated to induce nanoparticle size[139] or morphological changes[140] or disassembly[141, 142] to result in therapeutic release specifically in the extracellular milieu. In the interest in site-selective cell uptake, several reports have pursued MMP-activation through changes in nanoassembly surface chemistry.[143-149]

1.6.4 Temperature-Responsive Polymeric Nanoparticles

Temperature changes can also impact the solubility or confirmation of some polymers leading to changes in their hydrophobic-hydrophilic balance. The polymer poly(*N*-isopropyl acrylamide), for instance, is thermoresponsive and exists as hydrated swollen expanded coil below its lower critical solution temperature (LCST), but collapses

into a hydrophobic globular state when heated above its LCST (32 °C), which is close to biological temperature.[150, 151] Poly(2-dimethyamino)ethyl methacrylate is also commonly employed in temperature responsive systems due to its hydrophobic transition when heated to its LCST (40-50 °C).[152] Upper critical solution temperature (UCST), the temperature above which components of a mixture are miscible, is also employed in thermoresponsive systems using polymers such as polyoxazolines or poly(sulfobetaine)s.

The LCST of poly(ethylene glycol) is commonly employed in such temperature responsive systems. The reduced solubility at elevated temperatures is attributed to the reduced hydrogen bonding between the polymer and water.[153] In the context of OEG containing polymeric nanogels, temperature has been used to manipulate their aggregation characteristics to achieve particles of different sizes.[108] The fine-tuning of nanogel size was further investigated by the use of Hofmeister inorganic salts.[154] Salts have been observed to enhance or hinder the solubility of proteins, according to the Hofmeister series.[155-157] Likewise, it has been shown that salts can affect the LCST of water soluble polymers according to the identity of Hofmeister salt.[158-161] In investigation of salts effects on nanogel aggregation characteristics, it was found that Hofmeister anions could systematically cause aggregation of the polymer. Kosmotropic "salting out" sulfate systematically tuned particle size with concentration, while chaotropic "salting in" thiocyanate led to a loose nature of aggregates and lessened encapsulation stability of guest. This fine tuning was attributed to the relative hydration of OEG units, causing aggregation behavior when less water soluble, and leaky character when loose inter-aggregate crosslinking occurred.

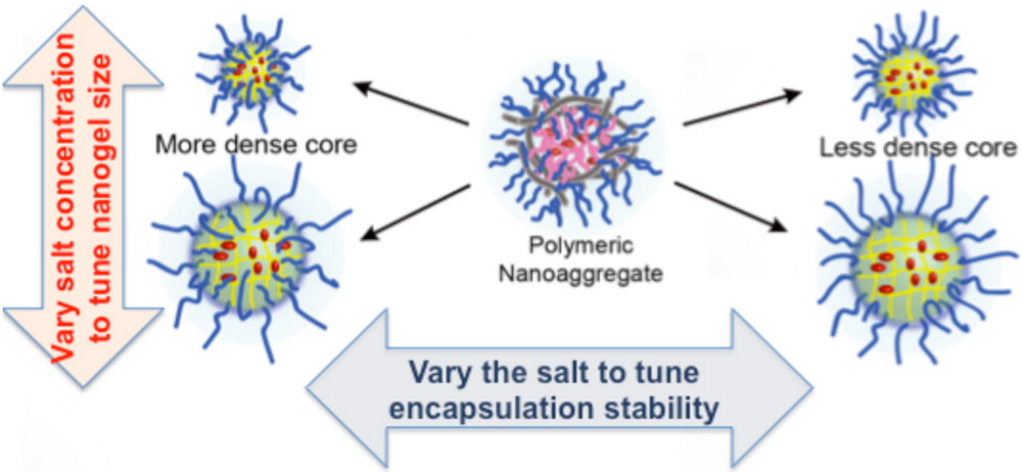

Figure 7. Schematic illustration of the use of Hofmeister ions to vary size and guest encapsulation stability in polymeric nanogels (reprinted with permission from reference[154]. Copyright 2013 American Chemical Society).

1.7 Post-Modification of Nanogels Through Thiol-Disulfide Exchange

The activated disulfide PDS moiety in the polymer can also serve as a functional handle with free thiol molecules by thiol-disulfide exchange, and this has been shown to modify the nanogel with targeting ligands.[109] The random copolymer nature of the aggregate means that some percentage of PDS units will be surface exposed accessible for surface conjugation. Nanogels were post modified with ligands including folic acid, cell-penetrating peptide tri-arginine, and cyclic arginine-glycine-aspartic acid (cRGD) peptide by installing cysteine as a thiol handle on the ligand. Their conjugation processes could be monitored and quantified by the release of PDS byproduct pyridinethione. Tri-arginine ligand-modified nanogels were shown to be rapidly internalized in cells regardless of cell type. RGD and folic acid modified nanogels were shown to selectively internalize in cells overexpressing integrin and folate receptor, respectively.

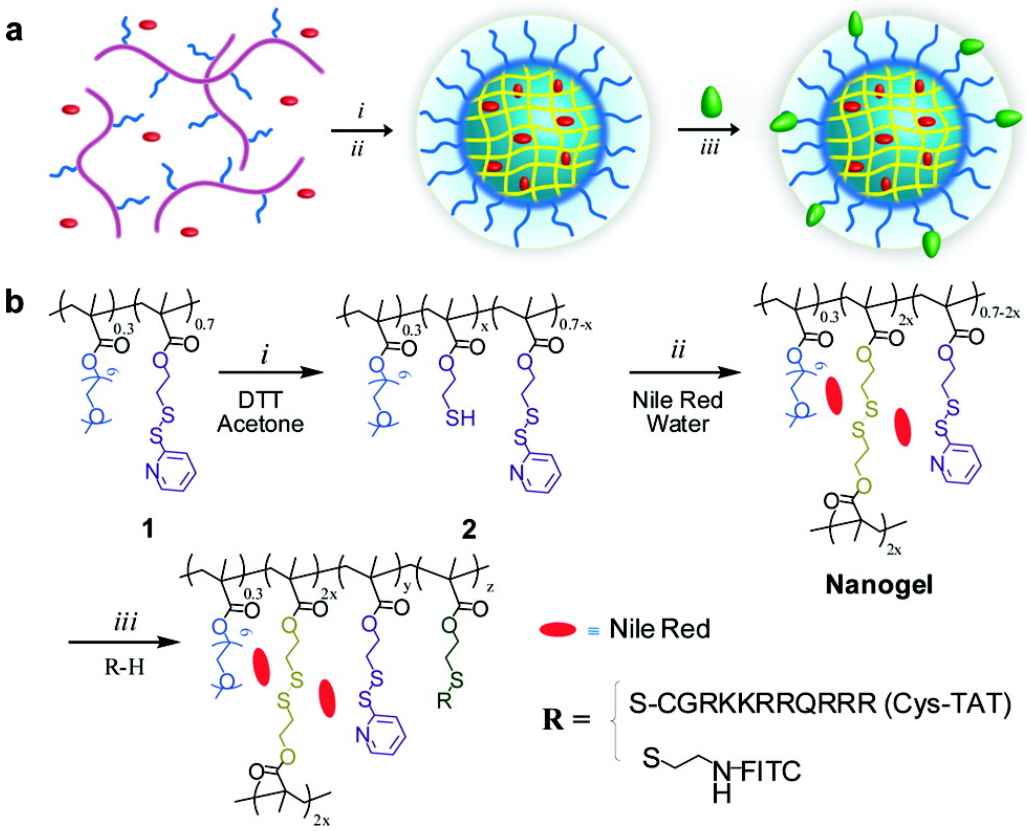

Figure 8. (a) Schematic representation of synthesis of targeting nanogels, (b) Polymer and targeting nanogel structures, and (c) Cysteine-modified targeting ligands (reprinted with permission from reference [109]. Copyright 2010 American Chemical Society).

1.8 Considerations of Polymeric Nanoparticle Biocompatibility

An additional caveat to therapeutic translation of polymeric nanomaterials is their biocompatibility. Polymers, and any byproducts that result from biological degradation or metabolism, should by non-toxic and non-immunogenic.[162] In contrast to time-release systems, stimuli-release systems should evade biological degradation until the intended therapeutic function is achieved. Polymeric nanocarriers achieved through radical polymerization methods are generally not biodegradable.[163] Various hydrolytically labile and enzymatically labile groups can be incorporated in polymers using ring opening polymerization and condensation polymerization methods, including esters, anhydrides, carbonates, amides, imines, and ureas.[164] Several of such biodegradable polymers have

appropriate lack of toxicity in biological use, yet suffer from rapid degradation and clearance limit their versatility in drug delivery. However, the ability to chemically and structurally modify these polymers to influence their self-assembly characteristics and particle surface properties may alter their degradation susceptibility for use in therapeutics.

1.9 Thesis Overview

In this chapter, we discussed the merits and applications of polymeric nanoparticles to encapsulate therapeutic contents, be structurally of chemically modified according to application, and respond to appropriate stimuli of the local environment. Design principles that satisfy figures of merit as delivery vehicles were outlined by discussing specific examples. The amphiphilic random copolymer-based nanogels developed in our group have been highlighted. In this dissertation, we expand upon this platform to address some unmet needs including 1) understanding the biodistribution pattern of these nanogels, 2) compromising the passive and active targeting features of these nanogels, and 3) considerations of nanomaterials' nanotoxicity. We address these points by through specific structural manipulations in size and surface composition, incorporation of extracellular and intracellular stimuli responsivity, and biocompatible polymeric design for applications in delivery of therapeutics. In Chapter 2 we systematically manipulated the size and surface composition of nanogels to determine their impact on biodistribution in triple negative human mammary carcinoma bearing mice. In Chapter 3 we further expanded the polymer nanogel design and strategy of surface chemistry modification to investigate the safety and efficacy of these nanogels loaded with docetaxel in mice bearing triple negative breast cancer models. In Chapter 4 we describe a novel abridged strategy to achieve enhanced cellular uptake from activation with disease-relevant extracellular MMP-9. In Chapter 5

we investigated the application of amphiphilic random copolymer design to polymer comprised biocompatible poly(L-glutamic) acid as the backbone. Similar aggregation characteristics to traditional poly(methacrylate)-based amphiphiles were achieved. Summaries of findings and future research directions will be discussed in Chapter 6.

1.10 References

1. Mu, J.; Zhang, L.; Zhao, M.; Wang, Y. Catalase Mimic Property of Co_3O_4 Nanomaterials with Different Morphology and Its Application as a Calcium Sensor. *ACS Appl. Mater. Interfaces* **2014**, *6*, 7090–7098.

2. Huang, X.; Zheng, B.; Liu, Z.; Tan, C.; Liu, J.; Chen, B.; Li, H.; Chen, J.; Zhang, X.; Fan, Z.; Zhang, W.; Guo, Z.; Huo, F.; Yang, Y.; Xie, L.; Huang, W.; Zhang, H. Coating Two-Dimensional Nanomaterials with Metal–Organic Frameworks. *ACS Nano* **2014**, *8*, 8695–8701.

3. Li, Q.; Zeng, L.; Wang, J.; Tang, D.; Liu, B.; Chen, G.; Wei, M. Magnetic Mesoporous Organic−Inorganic $NiCo_2O_4$ Hybrid Nanomaterials for Electrochemical Immunosensors. *ACS Appl. Mater. Interfaces* **2011**, *3*, 1366–1373.

4. Peng, F.; Su, Y.; Zhong, Y.; Fan, C.; Lee, S.-T.; He, Y. Silicon Nanomaterials Platform for Bioimaging, Biosensing, and Cancer Therapy. *Acc. Chem. Res.* **2014**, *47*, 612–623.

5. Feng, X.; Lv, F.; Liu, L.; Tang, H.; Xing, C.; Yang, Q.; Wang, S. Conjugated Polymer Nanoparticles for Drug Delivery and Imaging. *ACS Appl. Mater. Interfaces* **2010**, *2*, 2429–2435.

6. Kozielski, K. L.; Tzeng, S. Y.; Hurtado De Mendoza, B. A.; Green, J. J. Bioreducible Cationic Polymer-Based Nanoparticles for Efficient and Environmentally Triggered Cytoplasmic siRNA Delivery to Primary Human Brain Cancer Cells. *ACS Nano* **2014**, *8*, 3232–3241.

7. Ge, J.; Lei, J.; Zare, R. N. Bovine Serum Albumin–Poly(methyl methacrylate) Nanoparticles: An Example of Frustrated Phase Separation. *Nano Lett*. **2011**, *11*, 2551–2554.

8. Kim, J.-H.; Bryan, W. W.; Chung, H.-W.; Park, C. Y.; Jacobson, A. J.; Lee, T. R. Gold, Palladium, and Gold−Palladium Alloy Nanoshells on Silica Nanoparticle Cores. *ACS Appl. Mater. Interfaces* **2009**, *1*, 1063–1069.

9. Bartczak, D.; Muskens, O. L.; Sanchez-elsner, T.; Kanaras, A. G.; Millar, T. M. Manipulation of *in Vitro* Angiogenesis Using Peptide-Coated Gold Nanoparticles. *ACS Nano* **2013**, *7*, 5628–5636.

10. Gold, A. A.; Ghosh, P. S.; Kim, C.; Han, G.; Forbes, N. S.; Rotello, V. M. Efficient Gene Delivery Vectors by Tuning the Surface Charge Density of Amino Acid-Functionalized Gold Nanoparticles. *ACS Nano* **2008**, *2*, 2213–2218.

11. Rosenholm, J. M.; Meinander, A.; Peuhu, E.; Niemi, R.; Eriksson, J. E.; Sahlgren, C.; Linde, M. Targeting of Porous Hybrid Silica Nanoparticles to Cancer Cells. *ACS Nano* **2009**, *3*, 197–206.

12. Luo, M.; Liu, Y.; Hu, J.; Liu, H.; Li, J. One-Pot Synthesis of CdS and Ni-Doped CdS Hollow Spheres with Enhanced Photocatalytic Activity and Durability. *ACS Appl. Mater. Interfaces* **2012**, *4*, 1813– 1821.

13. Yang, G.; Gai, S.; Qu, F.; Yang, P. SiO_2@YBO_3:Eu^{3+} Hollow Mesoporous Spheres for Drug Delivery Vehicle. *ACS Appl. Mater. Interfaces* **2013**, *5*, 5788– 5796.

14. Ge, G.; Brus, L. E. Fast Surface Diffusion of Large Disk-Shaped Nanocrystal Aggregates. *Nano Lett.* **2001**, *1*, 219–222.

15. Jana, S.; Cooper, A.; Ohuchi, F.; Zhang, M. Uniaxially Aligned Nanofibrous Cylinders by Electrospinning. *ACS Appl. Mater. Interfaces* **2012**, *4*, 4817–4824.

16. Petzetakis, N.; Robin, M. P.; Patterson, J. P.; Kelley, E. G.; Cotanda, P.; Bomans, P. H. H.; Sommerdijk, N. A. J. M.; Dove, A. P.; Epps, T. H.; O'Reilly, R. K. Hollow Block Copolymer Nanoparticles through a Spontaneous One-step Structural Reorganization. *ACS Nano* **2013**, *7*, 1120–1128.

17. Ikkala, O.; ten Brinke, G. Functional materials based on self-assembly of polymeric supramolecules. *Science* **2002**, *295*, 2407–2409.

18. Janata, J.; Josowicz, M. Conducting polymers in electronic chemical sensors. *Nat. Mater*. **2003**, *2*, 19–24.

19. Zotti, G.; Vercelli, B.; Berlin, A. Monolayers and multilayers of conjugated polymers as nanosized electronic components. *Acc. Chem. Res.* **2008**, *41*, 1098–1109.

20. Aida, T.; Meijer, E. W.; Stupp, S. I. Functional supramolecular polymers. *Science*, **2012**, *335*, 813–817.

21. Rösler, A.; Vandermeulen, G. W. M.; Klok, H.-A. Advanced drug delivery devices via selfassembly of amphiphilic block copolymers. *Adv. Drug Delivery Rev*. **2012**, *64*, 270–279.

22. Shokeen, M.; Pressly, E. D.; Hagooly, A.; Zheleznyak, A.; Ramos, N.; Fiamengo, A. L.; Welch, M. J.; Hawker, C. J.; Anderson, C. J. Evaluation of Multivalent, Functional Polymeric Nanoparticles for Imaging Applications. *ACS Nano* **2011**, *5*, 738–747.

23. Acharya, S.; Sahoo, S. K. PLGA nanoparticles containing various anticancer agents and tumour delivery by EPR effect. *Adv. Drug Deliv. Rev*. **2011**, *63*, 170–183.

24. Owens, D. E. III; Peppas, N. A. Opsonization, biodistribution, and pharmacokinetics of polymeric nanoparticles. *Int. J. Pharm*. **2006**, *307*, 93–102.

25. Yan, Z.; Yang, Y.; Wei, X.; Zhong, J.; Wei, D.; Liu, L.; Xie, C.; Wang, F.; Zhang, L.; Lu, W.; He, D. Tumor-Penetrating Peptide Mediation: An Effective Strategy for Improving the Transport of Liposomes in Tumor Tissue. *Mol. Pharm*. **2014**, *11*, 218–225.

26. Nahire, R.; Hossain, R.; Patel, R.; Paul, S.; Meghnani, V.; Ambre, A. H.; Gange, K. N.; Katti, K. S.; Leclerc, E.; Srivastava, D. K.; Sarkar, K.; Mallik, S. pH-Triggered Echogenicity and Contents Release from Liposomes. *Mol. Pharm*. **2014**, *11*, 4059–4068.

27. Lee, S.; Koo, H.; Na, J. H.; Lee, K. E.; Jeong, S. Y.; Choi, K.; Kim, S. H.; Kwon, I. C.; Kim, K. DNA Amplification in Neutral Liposomes for Safe and Efficient Gene Delivery. *ACS Nano* **2014**, *8*, 4257–4267.

28. Alexander, C. M.; Hamner, K. L.; Maye, M. M.; Dabrowiak, J. C. Multifunctional DNA-Gold Nanoparticles for Targeted Doxorubicin Delivery. *Bioconjug. Chem*. **2014**, *25*, 1261–1271.

29. Shi, Y.; Goodisman, J.; Dabrowiak, J. C. Cyclodextrin Capped Gold Nanoparticles as a Delivery Vehicle for a Prodrug of Cisplatin. *Inorg. Chem*. **2013**, *52*, 9418–9426.

30. Wu, Y.; Phillips, J. A.; Liu, H.; Yang, R.; Tan, W. Carbon Nanotubes Protect DNA Strands during Cellular Delivery. *ACS Nano* **2008**, *2*, 2023–2028.

31. Das, M.; Singh, R. P.; Datir, S. R.; Jain, S. Intranuclear Drug Delivery and Effective in Vivo Cancer Therapy via Estradiol–PEG-Appended Multiwalled Carbon Nanotubes. *Mol. Pharm.* **2013**, *10*, 3404–3416.

32. Jiang, S.; Eltoukhy, A. A.; Love, K. T.; Langer, R.; Anderson, D. G. Lipidoid-Coated Iron Oxide Nanoparticles for Efficient DNA and siRNA delivery. *Nano Lett*. **2013**, *13*, 1059–1064.

33. Jain, T. K.; Morales, M. A.; Sahoo, S. K.; Leslie-Pelecky, D. L.; Labhasetwar, V. Iron Oxide Nanoparticles for Sustained Delivery of Anticancer Agents. *Mol. Pharm*. **2005**, *2*, 194–205.

34. Quan, Q.; Xie, J.; Gao, H.; Yang, M.; Zhang, F.; Liu, G.; Lin, X.; Wang, A.; Eden, H. S.; Lee, S.; Zhang, G.; Chen, X. HSA Coated Iron Oxide Nanoparticles as Drug Delivery Vehicles for Cancer Therapy. *Mol. Pharm*. **2011**, *8*, 1669–1676.

35. Medina, S. H.; El-sayed, M. E. H. Dendrimers as Carriers for Delivery of Chemotherapeutic Agents. *Chem. Rev*. **2009**, *109*, 3141–3157.

36. Ma, X.; Zhou, Z.; Jin, E.; Sun, Q.; Zhang, B.; Tang, J.; Shen, Y. Facile Synthesis of Polyester Dendrimers as Drug Delivery Carriers. *Macromolecules* **2013**, *46*, 37–42.

37. Evans, D. F.; Wennerstrom, H. The Colloidal Domain, 2nd ed.; Wiley-VCH: New York, 1999.

38. Menger, F. M. The Structure of Micelles. *Acc. Chem. Res*. **1979**, *12*, 111–117.

39. Miyake, M.; Yamada, K.; Oyama, N. Self-Assembling of Guanidine-Type Surfactant. *Langmuir* **2008**, *24*, 8527–8532.

40. Tung, S. H.; Lee, H. Y.; Raghavan, S. R. A Facile Route for Creating "Reverse" Vesicles: Insights into "Reverse" Self-Assembly in Organic Liquids. *J. Am. Chem. Soc*. **2008**, *130*, 8813– 8817.

41. Vauthey, S.; Santoso, S.; Gong, H.; Watson, N.; Zhang, S. Molecular Self- Assembly of Surfactant-like Peptides to Form Nanotubes and Nanovesicles. *Proc. Natl. Acad. Sci. U.S.A.* **2002**, *99*, 5355–5360.

42. Torchilin, V. P. Structure and Design of Polymeric Surfactant-based Drug Delivery Systems. *J. Control. Release* **2001**, *73*, 137−172.

43. Cabral, H.; Nishiyama, N.; Kataoka, K. Supramolecular Nanodevices: From Design Validation to Theranostic Nanomedicine. *Acc. Chem. Res*. **2011**, *44*, 999−1008.

44. Soussan, E.; Cassel, S.; Blanzat, M.; Rico-Lattes, I. Drug Delivery by Soft Matter: Matrix and Vesicular Carriers. *Angew. Chem., Int. Ed*. **2009**, *48*, 274−288.

45. Hartgerink, J. D.; Beniash, E.; Stupp, S. I. Self-Assembly and Mineralization of Peptide-Amphiphile Nanofibers. *Science* **2001**, *294*, 1684−1688.

46. Israelachvili, J. N.; Mitchell, D. J.; Ninham, B. W. Theory of Self-Assembly of Hydrocarbon Amphiphiles into Micelles and Bilayers. *J. Chem. Soc., Faraday Trans II*. **1976**, *72*, 1525−1568.

47. Evans, D. F.; Ninham, B. W. Molecular Forces in the Self-Organization of Amphiphiles. *J. Phys. Chem*. **1986**, *90*, 226−234.

48. Nagarajan, R. Molecular Packing Parameter and Surfactant Self-assembly: The Neglected Role of the Surfactant Tail. *Langmuir* **2002**, *18*, 31−38.

49. Brunsveld, L.; Folmer, B. J. B.; Meijer, E. W.; Sijbesma, R. P. Supramolecular Polymers. *Chem. Rev*. **2001**, *101*, 4071–4098.

50. Discher, B. M.; Won, Y. Y.; Ege, D. S.; Lee, J. C.-M.; Bates, F. S.; Discher, D. E.; Hammer, D. A. Polymersomes: Tough Vesicles Made from Diblock Copolymers. *Science* **1999**, *284*, 1143–1146.

51. Fuhrhop, J.-H.; Wang, T. Bolaamphiphiles. *Chem. Rev*. **2004,** *104*, 2901–2937.

52. Lee, M.; Cho, B.-K.; Zin, W.-C. Supramolecular Structures from Rod−Coil Block Copolymers. *Chem. Rev*. **2001**, *101*, 3869–3892.

53. Moffitt, M.; Khougaz, K.; Eisenberg, A. Micellization of Ionic Block Copolymers. *Acc. Chem. Res*. **1996**, *29*, 95–102.

54. Neiser, M. W.; Muth, S.; Kolb, U.; Harris, J. R.; Okuda, J.; Schmidt, M. Micelle Formation from Amphiphilic "Cylindrical Brush"–Coil Block Copolymers Prepared by Metallocene Catalysis. *Angew. Chem., Int. Ed*. **2004**, *43*, 3192–3195.

55. Zhang, L.; Yu, K.; Eisenberg, A. Ion-Induced Morphological Changes in "Crew- Cut" Aggregates of Amphiphilic Block Copolymers. *Science* **1996**, *272*, 1777– 1779.

56. Nakatani, K.; Ogura, Y.; Koda, Y.; Terashima, T.; Sawamoto, M. Sequence-regulated copolymers via tandem catalysis of living radical polymerization and in situ transesterification. *J. Am. Chem. Soc*. **2012**, *134*, 4373–4383.

57. Hawker, C. J.; Bosman, A. W.; Harth, E. New polymer synthesis by nitroxide mediated living radical polymerizations. *Chem. Rev*. **2001**, *101*, 3661–3688.

58. Moad, G.; Rizzardo, E.; Thang, S. H. Living radical polymerization by the RAFT process–a third update. *Aust. J. Chem*. **2012**, *65*, 985–1076.

59. Hilf, S.; Kilbinger, A. F. M. Functional end groups for polymers prepared using ring-opening metathesis polymerization. *Nat. Chem*. **2009**, *1*, 537–546.

60. Matyjaszewski, K.; Tsarevsky, N. V. Macromolecular engineering by atom transfer radical polymerization. *J. Am. Chem. Soc*. **2014**, *136*, 6513–6533.

61. Rosebrugh, L. E.; Marx, V. M.; Keitz, B. K.; Grubbs, R. H. Synthesis of highly cis, syndiotactic polymers via ring-opening metathesis polymerization using ruthenium metathesis catalysts. *J. Am. Chem. Soc*. **2013**, *135*, 10032–10035.

62. Kim, J. K.; Yang, S. Y.; Lee, Y.; Kim, Y. Functional nanomaterials based on block copolymer self-assembly. *Prog. Polym. Sci*. **2010**, *35*, 1325–1349.

63. Zhang, Q.; Ko, N. R.; Oh, J. K. Recent advances in stimuli-responsive degradable block copolymer micelles: synthesis and controlled drug delivery applications. *Chem. Commun*. **2012**, *48*, 7542–7552.

64. Mai, Y.; Eisenberg, A. Self-assembly of block copolymers. *Chem. Soc. Rev*. **2012**, *41*, 5969– 5985.

65. Quémener, D.; Davis, T. P.; Barner-Kowollik, C.; Stenzel, M. H. RAFT and click chemistry: A versatile approach to well-defined block copolymers. *Chem. Commun*. **2006**, *42*, 5051–5053.

66. Wong, C. -H.; Zimmerman, S. C. Orthogonality in organic, polymer, and supramolecular chemistry: from Merrifield to click chemistry. *Chem. Commun*. **2013**, *49*, 1679–1695.

67. Johnson, J. A.; Lu, Y. Y.; Burts, A. O.; Lim, Y. -H.; Finn, M. G.; Koberstein, J. T.; Turro, N. J.; Tirrell, D. A.; Grubbs, R. H. Core-clickable PEG-branch-azide bivalent-bottle-brush polymers by ROMP: grafting-through and clicking-to. *J. Am. Chem. Soc*. **2010**, *133*, 559–566.

68. Safra, T.; Muggia, F.; Jeffers, S.; Tsao-Wei, D. D.; Groshen, S.; Lyass, O.; Henderson, R.; Berry, G.; Gabizon, A. Pegylated liposomal doxorubicin (doxil): Reduced clinical cardiotoxicity in patients reaching or exceeding cumulative doses of 500 mg/m^2. *Ann. Oncol*. **2000**, *11*, 1029–1033.

69. Fassas, A.; Buffels, R.; Kaloyannidis, P.; Anagnostopoulos, A. Safety of high-dose liposomal daunorubicin (daunoxome) for refractory or relapsed acute myeloblastic leukaemia. *Br. Jo. Haematol*. **2003**, *122*, 161–163.

70. Matsumura, Y.; Maeda, H. A new concept for macromolecular therapeutics in cancer chemotherapy: mechanism of tumoritropic accumulation of proteins and the antitumor agent smancs. *Cancer Res*. **1986**, *46*, 6387–6392.

71. Maeda, H.; Nakamura, H.; Fang, J. The EPR effect for macromolecular drug delivery to solid tumors: Improvement of tumor uptake, lowering of systemic toxicity, and distinct tumor imaging in vivo. *Adv. Drug Deliv. Rev*. **2013**, *65*, 71–79.

72. Bae, Y. H.; Park, K. Targeted drug delivery to tumors: myths, reality and possibility. *J. Controlled Release* **2011**, *153*, 198.

73. Li, S.-D.; Huang, L. Pharmacokinetics and Biodistribution of Nanoparticles. *Mol. Pharmaceutics*, **2008**, *5 (4)*, 496–504.

74. Venturoli, D.; Rippe, B. Ficoll and dextran vs. globular proteins as probes for testing glomerular permselectivity: effects of molecular size, shape, charge and deformability. *Am. J. Physiol*. **2005**, *288*, F605–F613.

75. Romberg, B.; Hennink, W. E.; Storm, G. Sheddable coatings for long-circulating nanoparticles. *Pharm. Res*. **2008**, *25*, 55–71.

76. Moghimi, S. M.; Hunter, A. C.; Murray, J. C. Long-circulating and target-specific nanoparticles: Theory to practice. *Pharmacol. ReV*. **2001**, *53*, 283–318.

77. Vittaz, M.; Bazile, D.; Spenlehauer, G.; Verrecchia, T.; Veillard, M.; Puisieux, F.; Labarre, D. Effect of PEO surface density on long-circulating PLA-PEO nanoparticles which are very low complement activators. *Biomaterials* **1996**, *17*, 1575–1581

78. Molineux, G. PEGylation: engineering improved pharmaceuticals for enhanced therapy. *Cancer Treat Rev*. **2002**, *28* (Suppl. A), 13−16.

79. Moribe, K.; Maruyama, K. Reviews on PEG coated liposomal drug carriers. *Drug Delivery Syst*. **2001**, *16 (3)*, 165−171.

80. Verbaan, F. J.; Oussoren, C.; Snel, C. J.; Crommelin, D. J.; Hennink, W. E.; Storm, G. Steric stabilization of poly(2-(dimethylamino)ethyl methacrylate)-based polyplexes mediates prolonged circulation and tumor targeting in mice. *J. Gene Med*. **2004**, *6*, 64-75.

81. Vader, P.; van der Aa, L. J.; Engbersen, J. F.; Storm, G.; Schiffelers, R. M. Physicochemical and Biological Evaluation of siRNA Polyplexes Based on PEGylated Poly(amido amine)s. *Pharm. Res.* **2012**, *29(2)*, 352–361.

82. Crownover, E.; Duvall, C. L.; Convertine, A.; Hoffman, A. S.; Stayton, P. S. RAFT-synthesized Graft Copolymers that Enhance pH-dependent Membrane Destabilization and Protein Circulation Times. *J. Controlled Release* **2011**, *155*, 167-174.

83. Chaudhari, K. R.; Ukawala, M.; Manjappa, A. S.; Kumar, A.; Mundada, P. K.; Mishra, A. K. Mathur, R.; Monkkonen, J.; Murthy, R.S. Opsonization, biodistribution, cellular uptake and apoptosis study of PEGylated PBCA nanoparticle as potential drug delivery carrier. *Pharm. Res*. **2012**, *29*, 53-68.

84. Murthy, N.; Campbell, J.; Fausto, N.; Hoffman, A. S.; Stayton, P. S. Design and synthesis of pH-responsive polymeric carriers that target uptake and enhance the intracellular delivery of oligonucleotides. *J. Control. Release* **2003**, *89*, 365-374.

85. Guo, M.; Que, C.; Wang, C.; Liu, X.; Yan, H.; Liu, K. Multifunctional superparamagnetic nanocarriers with folate-mediated and pH-responsive targeting properties for anticancer drug delivery. *Biomaterials* **2011**, *32*, 185-194.

86. Sarko, D.; Beijer, B.; Boy, R. G.; Nothelfer, E.-M.; Leotta, K.; Eisenhut, M.; Altmann, A.; Haberkorn, U.; Mier, W. The Pharmacokinetics of Cell-Penetrating Peptides. *Mol. Pharmaceutics* **2010**, *7*, 2224−2231.

87. Ruoslahti, E. RGD and Other Recognition Sequences for Integrins. *Annu. Rev. Cell. Dev. Biol*. **1996**, *12*, 697–715.

88. Friden, P. M.; Walus, L. R.; Musso, G. F.; Taylor, M. A.; Malfroy, B.; Starzyk, R. M. Anti-Transferrin Receptor Antibody and Antibody Drug Conjugates Cross the Blood Brain Barrier. *Proc. Natl. Acad. Sci. U.S.A*. **1991**, *88*, 4771–4775.

89. Gabizon, A.; Horowitz, A. T.; Goren, D.; Tzemach, D.; Mandelbaum-Shavit, F.; Qazen, M. M.; Zalipsky, S. Targeting Folate Receptor with Folate Linked to Extremities of Poly(ethylene glycol)-Grafted Liposomes: In Vitro Studies. *Bioconjugate Chem*. **1999**, *10*, 289–298.

90. Phillips, M. A.; Gran, M. L.; Peppas, N. A. Targeted Nanodelivery of Drugs and Diagnostics. *Nano Today*, **2010,** *5(2),*143-159.

91. Alarcon, C. d. l. H.; Pennadam, S.; Alexander, C. Stimuli Responsive Polymers for Biomedical Applications. *Chem. Soc. Rev*. **2005**, *34*, 276–285.

92. Langer, R. New Methods of Drug delivery. *Science* **1990**, *249*, 1527–1533.

93. Meng, F.; Zhong, Z.; Feijen, J. Stimuli-Responsive Polymersomes for Programmed Drug Delivery. *Biomacromolecules* **2009**, *10*, 197–209.

94. Stuart, M. A. C.; Huck, W. T. S.; Genzer, J.; Muller, M.; Ober, C.; Stamm, M.; Sukhorukov, G. B.; Szleifer, I.; Tsukruk, V. V.; Urban, M.; Winnik, F.; Zauscher, S.; Luzinov, I.; Minko, S. Emerging Applications of Stimuli-Responsive Polymer Materials. *Nat. Mater.* **2010**, *9*, 101–113.

95. Chung, H. J.; Park, T. G. Self-Assembled and Nanostructured Hydrogels for Drug Delivery and Tissue Engineering. *Nano Today* **2009**, *4*, 429–437.

96. Shchukin, D. G.; Grigoriev, D. O.; Mohwald, H. Application of Smart Organic Nanocontainers in Feedback Active Coatings. *Soft Matter* **2010**, *6*, 720–725.

97. Diaz D. D.; Kuhbeck, D.; Koopmans, R. J. Stimuli-Responsive Gels as Reaction Vessels and Reusable Catalysts. *Chem. Soc. Rev*. **2011**, *40*, 427–448.

98. Zhuang, J.; Gordon, M. R.; Ventura, J.; Li, L. Thayumanavan, S. Multi-Stimuli Responsive Macromolecules and Their Assemblies. *Chem. Soc. Rev*. **2013**, *42*, 7421–7435.

99. Quesada, M.; Muniesa, C.; Botella, P. Hybrid PLGA-Organosilica Nanoparticles with Redox-Sensitive Molecular Gates. *Chem. Mater*. **2013**, *25*, 2597–2602.

100. Jiang, G.; Wang, Y.; Zhang, R.; Wang, R.; Wang, X.; Zhang, M.; Sun, X.; Bao, S.; Wang, T.; Wang, S. Preparation of Redox-Sensitive Shell Cross-Linked Nanoparticles for Controlled Release of Bioactive Agents. *ACS Macro Lett*. **2012**, *1*, 489–493.

101. Ranucci, E.; Suardi, M. a; Annunziata, R.; Ferruti, P.; Chiellini, F.; Bartoli, C. Poly(amidoamine) Conjugates with Disulfide-Linked Cholesterol Pendants Self-Assembling into Redox-Sensitive Nanoparticles. *Biomacromolecules* **2008**, *9*, 2693–2704.

102. Shao, Y.; Shi, C.; Xu, G.; Guo, D.; Luo, J. Photo and Redox Dual Responsive Reversibly Cross-Linked Nanocarrier for Efficient Tumor-Targeted Drug Delivery. *ACS Appl. Mater. Interfaces* **2014**, *6*, 10381–10392.

103. Bao, Y.; Guo, Y.; Zhuang, X.; Li, D.; Cheng, B.; Tan, S.; Zhang, Z. d-α-Tocopherol Polyethylene Glycol Succinate-Based Redox-Sensitive Paclitaxel Prodrug for Overcoming Multidrug Resistance in Cancer Cells. *Mol. Pharm*. **2014**, *11*, 3196–3209.

104. Wang, Y.-C.; Wang, F.; Sun, T.-M.; Wang, J. Redox-Responsive Nanoparticles from the Single Disulfide Bond-Bridged Block Copolymer as Drug Carriers for Overcoming Multidrug Resistance in Cancer Cells. Bioconjug. Chem. 2011, 22, 1939–1945.

105. Ghosh, S.; Irvin, K.; Thayumanavan, S. Tunable Disassembly of Micelles Using a Redox Trigger. *Langmuir* **2007**, *23*, 7916–7919.

106. Ryu, J.-H.; Roy, R.; Ventura, J.; Thayumanavan, S. Redox-Sensitive Disassembly of Amphiphilic Copolymer Based Micelles. *Langmuir* **2010**, *26*, 7086–7092.

107. Guo, X.; Shi, C.; Yang, G.; Wang, J.; Cai, Z.; Zhou, S. Dual-Responsive Polymer Micelles for Target-Cell-Specific Anticancer Drug Delivery. *Chem. Mater*. **2014**, *26*, 4405–4418.

108. Ryu, J. -H.; Chacko, R. T.; Jiwpanich, S.; Bickerton, S.; Babu R. P.; Thayumanavan, S. Self-cross-linked polymer nanogels: a versatile nanoscopic drug delivery platform. *J. Am. Chem. Soc*. **2010**, *132*, 17227–17235.

109. Ryu, J. -H.; Jiwpanich, S.; Chacko, R.; Bickerton S.; Thayumanavan, S. Surface functionalizable polymer nanogels with facile hydrophobic guest encapsulation capabilities. J. *Am. Chem. Soc*. **2010**, *132*, 8246–8247.

110. Jiwpanich, S.; Ryu, J. -H.; Bickerton, S.; Thayumanavan, S. Noncovalent encapsulation stabilities in supramolecular nanoassemblies. *J. Am. Chem. Soc*. **2010**, *132*, 10683-10685.

111. Li, L.; Thayumanavan, S. Environment-dependent guest exchange in supramolecular hosts. *Langmuir* **2014**, *30*, 12384-12390.

112. Gao, W.; Chan, J. M.; Farokhzad, O. C. pH-Responsive Nanoparticles for Drug Delivery. *Mol. Pharm*. **2010**, *7*, 1913–1920.

113. Kararli, T. T. Comparison of the gastrointestinal anatomy, physiology, and biochemistry of humans and commonly used laboratory animals. *Biopharm. Drug Dispos*. **1995**, *16*, 351–380.

114. Dressman, J. B.; Berardi, R. R.; Dermentzoglou, L. C.; Rusell, T. L.; Schmaltz, S. P.; Barnett, J. L.; Jarvenpaa, K. M. Upper gastrointestinal (GI) pH in young, healthy men and women. *Pharm. Res.* **1990**, *7*, 756–761.

115. Colombo, P.; Sonvico, F.; Colombo, G.; Bettini, R. Novel platforms for oral ddrug delivery. *Pharm. Res*. **2009**, *26*, 601– 611.

116. Yasumasa Kato, Shigeyuki Ozawa, Chihiro Miyamoto, Yojiro Maehata, Atsuko Suzuki, Toyonobu Maeda, and Yuh Baba, Acidic extracellular microenvironment and cancer, *Cancer Cell Int*. **2013**, *13*, 89.

117. Wu, X. L.; Kim, J. H.; Koo, H.; Bae, S. M.; Shin, H.; Kim, M. S.; Lee, B.-H.; Park, R.-W.; Kim, I.-S.; Choi, K.; Kwon, I. C.; Kim, K.; Lee, D. S. Tumor-Targeting Peptide Conjugated pH-Responsive Micelles as a Potential Drug Carrier for Cancer Therapy. *Bioconjug. Chem*. **2010**, *21*, 208–213.

118. Criscione, J. M.; Le, B. L.; Stern, E.; Brennan, M.; Rahner, C.; Papademetris, X.; Fahmy, T. M. Self-assembly of pH-responsive fluorinated dendrimer-based particulates for drug delivery and noninvasive imaging. *Biomaterials* **2009**, *30*, 3946–3955.

119. Zhuang, J.; Chacko, R. T.; Amado Torres, D. F.; Wang, H.; Thayumanavan, S. Dual Stimuli-Dual Response Nanoassemblies Prepared from a Simple Homopolymer. *ACS Macro Lett*. **2014**, *3*, 1−5.

120. Li, L.; Raghupathi, K.; Yuan, C.; Thayumanavan, S. Surface charge generation in nanogels for activated cellular uptake at tumor-relevant pH. *Chem. Sci*. **2013**, *4*, 3654-3360.

121. Gu, J.; Cheng, W. P.; Liu, J.; Lo, S. Y.; Smith, D.; Qu X.; Yang, Z. pH-Triggered Reversible “Stealth” Polycationic Micelles, *Biomacromolecules*, **2008**, *9*, 255–262.

122. Gao, Y.; Yang, C.; Liu, X.; Ma, R.; Kong D.; Shi, L. A Multifunctional Nanocarrier Based on Nanogated Mesoporous Silica for Enhanced Tumor-Specific Uptake and Intracellular Delivery. *Macromol. Biosci*. **2011**, *12*, 251–259.

123. Ding, C. X.; Gu, J. X.; Qu, X. Z.; Yang, Z. Z. Preparation of Multifunctional Drug Carrier for Tumor-Specific Uptake and Enhanced Intracellular Delivery through the Conjugation of Weak Acid Labile Linker. *Bioconjugate Chem*. **2009**, *20*, 1163–1170.

124. Ding, D.; Kwok, R. T. K.; Yuan, Y.; Feng, G.; Tang, B. Z.; Liu, B. A Fluorescent Light-up Nanoparticle Probe with Aggregation-induced Emission Characteristics and Tumor-acidity Responsiveness for Targeted Imaging and Selective Suppression of Cancer Cells. *Mater. Horiz.* **2015**, *2*, 100−105.

125. Sun, C.-Y.; Shen, S.; Xu, C.-F.; Li, H.-J.; Liu, Y.; Cao, Z.-T.; Yang, X.-Z.; Xia, J.-X.; Wang, J. Tumor Acidity-Sensitive Polymeric Vector for Active Targeted siRNA Delivery. *J. Am. Chem. Soc*. **2015**, *137*, 15217−15224.

126. Mizuhara, T.; Saha, K.; Moyano, D. F.; Kim, C. S.; Yan, B.; Kim, Y.-K.; Rotello, V. M. Acylsulfonamide-Functionalized Zwitterionic Gold Nanoparticles for Enhanced Cellular Uptake at Tumor pH. *Angew. Chem., Int. Ed*. **2015**, *54*, 6567−6570.

127. Mutsaers, S. E.; Papadimitriou, J. M. Surface charge of macrophages and their interaction with charged particles. *J. Leukocyte Biol*. **1988**, *44*, 17–26.

128. Richard, J. P.; Melikov, K.; Vives, E.; Ramos, C.; Verbeure, B.; Gait, M. J.; Chernomordik, L. V.; Lebleu, B. Cell-penetrating peptides. A reevaluation of the mechanism of cellular uptake. *J. Biol. Chem*. **2003**, *278*, 585–590.

129. Ulbrich, K.; Subr, V. Polymeric anticancer drugs with pH-controlled activation. *Adv. Drug Delivery Rev*. **2004**, *56*, 1023–1050.

130. Lee, H. J.; Pardridge, W. M. Monoclonal Antibody Radiopharmaceuticals: Cationization, Pegylation, Radiometal Chelation, Pharmacokinetics, and Tumor Imaging. *Bioconjugate Chem*. **2003**, *14*, 546–553.

131. Li, W.; Nakayama, M.; Akimoto, J.; Okano, T. Effect of block compositions of amphiphilic block copolymers on the physicochemical properties of polymeric micelles. *Polymer* **2011**, *52*, 3783-3790.

132. Dobrovolskaia, M. A.; Patri, A. K.; Simak, J.; Hall, J. B.; Semberova, J.; De Paoli Lacerda, S. H.; McNeil, S. E. Nanoparticle size and surface charge determine effects of PAMAM dendrimers on human platelets in vitro. *Mol. Pharm*. **2012**, *9*, 382.

133. Geisow, M. J.; Evans, W. H. pH in the endosome. Measurements during pinocytosis and receptor-mediated endocytosis. *Exp. Cell Res*. **1984**, *150*, 36–46.

134. Varkouhi, A. K.; Scholte, M.; Storm, G.; Haisma, H. J. Endosomal escape pathways for delivery of biologicals. *J. Control. Release* **2011**, *151*, 220–228.

135. Hu, J.; Zhang, G.; Liu, S. Enzyme-responsive polymeric assemblies, nanoparticles and hydrogels. *Chem. Soc. Rev*. **2012**, *41*, 5933-5949.

136. Choi, K. Y.; Swierczewska, M.; Lee, S.; Chen, X. Y. Protease- Activated Drug Development. *Theranostics* **2012**, *2*, 156−178.

137. de la Rica, R.; Aili, D.; Stevens, M. M. Enzyme-responsive nanoparticles for drug release and diagnostics. *Adv. Drug Delivery Rev*. **2012**, *64*, 967−978.

138. Coleman, J. D.; Thompson, J. T.; Smith, R. W., 3rd; Prokopczyk, B.; Vanden, H. J. P. Role of Peroxisome Proliferator-Activated Receptor β/δ and B-Cell Lymphoma-6

in Regulation of Genes Involved in Metastasis and Migration in Pancreatic Cancer Cells. *PPAR Res*. **2013**, *2013*, 121956.

139. Yu, S. S.; Lau, C. M.; Thomas, S. N.; Jerome, W. G.; Maron, D. J.; Dickerson, J. H.; Hubbell, J. A.; Giorgio, T. D. Size- and charge-dependent non-specific uptake of PEGylated nanoparticles by macrophages. *Int. J. Nanomed*. **2012**, *7*, 799-813.

140. Callmann, C. E.; Barback, C.V.; Thompson, M. P.; Hall, D. J.; Mattrey, R. F.; Gianneschi, N. C. Therapeutic Enzyme-Responsive Nanoparticles for Targeted Delivery and Accumulation in Tumors. *Adv. Mater*. **2015**, *27*, 4611–4615.

141. Kulkarni, P. S.; Haldar, M. K.; Nahire, R. R.; Katti, P.; Ambre, A. H.; Muhonen, W. W.; Shabb, J. B.; Padi, S. K. R.; Singh, R. K.; Borowicz, P. P.; Shrivastava, D. K.; Katti, K. S.; Reindl, K.; Guo, B.; Mallik, S. MMP-9 Responsive PEG Cleavable Nanovesicles for Efficient Delivery of Chemotherapeutics to Pancreatic Cancer. *Mol. Pharmaceutics*. **2014**, *11*, 2390−2399.

142. Liu, Y.; Ding, X.; Li, J.; Luo, Z.; Hu, Y.; Liu, J.; Dai, L.; Zhou, J.; Hou, C.; Cai, K. Enzyme responsive drug delivery system based on mesoporous silica nanoparticles for tumor therapy in vivo. *Nanotechnology* **2015**, *26*, 145102-145116.

143. Li, H.; Yu, S. S.; Miteva, M.; Nelson, C. E.; Werfel, T.; Giorgio, T. D.; Duvall, C. L. Matrix Metalloproteinase Responsive, Proximity-Activated Polymeric Nanoparticles for siRNA Delivery. *Adv. Funct. Mater*. **2013**, *23*, 3040–3052.

144. Li, J.; Ge, Z.; Liu, S. PEG-sheddable polyplex micelles as smart gene carriers based on MMP-cleavable peptide-linked block copolymers. *Chem. Commun*. **2013**, *49*, 6974−6976.

145. Wu, J.; Han, H.; Jin, Q.; Li, Z.; Li, H.; Ji, J. Design and Proof of Programmed 5-Aminolevulinic Acid Prodrug Nanocarriers for Targeted Photodynamic Cancer Therapy. *ACS Appl. Mater. Interfaces* **2017**, *9 (17)*, 14596–14605.

146. Harris, T. J.; von Maltzahn, G.; Lord, M. E.; Park, J. H.; Agrawal, A.; Min, D. H.; Sailor, M. J.; Bhatia, S. N. Protease-Triggered Unveiling of Bioactive Nanoparticles. *Small* **2008**, *4*, 1307-1312.

147. Zhu, L.; Kate, P.; Torchilin, V. P. Matrix Metalloprotease 2-Responsive Multifunctional Liposomal Nanocarrier for Enhanced Tumor Targeting. *ACS Nano*, **2012**, *6(4)*, 3491-3498.

148. Fay, F.; Hansen, L.; Hectors, S. J. C. G.; Sanchez-Gaytan, B. L.; Zhao, Y.; Tang, J.; Munitz, J.; Alaarg, A.; Braza, M. S.; Gianella, A.; Aaronson, S. A.; Reiner, T.; Kjems, J.; Langer, F. J. M. Hoeben, H. M. Janssen, C. Calcagno, G. J. Strijkers, Z. A. Fayad, C. Peŕez-Medina, R.; Mulder. W. J. M. Investigating the Cellular Specificity in Tumors of a Surface-Converting Nanoparticle by Multimodal Imaging. *Bioconjugate Chem*. **2017**, *28*, 1413−1421.

149. Zhang, J.; Yuan, Z. F.; Wang, Y.; Chen, W. H.; Luo, G. F.; Cheng, S. X.; Zhuo, R. X.; Zhang, X. Z. Multifunctional Envelope- Type Mesoporous Silica Nanoparticles for Tumor-Triggered Targeting Drug Delivery. *J. Am. Chem. Soc*. **2013**, *135*, 5068−5073.

150. Schild, H. G. Poly(*N*-isopropylacrylamide): experiment, theory and application. *Prog. Polym. Sci.* **1992**, *17*, 163–249.

151. Zhang, Y.; Cremer, P. S. Interactions between macromolecules and ions: the Hofmeister series. *Curr. Opin. Chem. Biol*. **2006**, *10*, 658–663.

152. Klaikherd, A.; Nagamani, C.; Thayumanavan, S. Multi-Stimuli Sensitive Amphiphilic Block Copolymer Assemblies. *J. Am. Chem. Soc*. **2009**, *131*, 4830–4838.

153. Saeki, S.; Kuwahara, N.; Nakata, M.; Kaneko, M. Upper and lower critical solution temperature in poly (ethylene glycol) solutions. *Polymer* **1976**, *17*, 685–689.

154. Li, L.; Ryu, J. -H.; Thayumanavan, S. Effect of Hofmeister ions on the size and encapsulation stability of polymer nanogels. *Langmuir* **2013**, *29*, 50-55.

155. Hofmeister, F. On the understanding of the effects of salts, second report. On irregularities in the precipitating effect of salts and their relationship to their physical behavior. *Arch. Exp. Pathol. Pharmocol.* **1888**, *24*, 247-260.

156. Von Hippel, P. H.; Wong. K. Y. Neutral salts: the generality of their effects on the stability of macromolecular conformations. *Science* **1964**, *145*, 577-580.

157. Baldwin, R. L. How Hofmeister ion interactions affect protein stability. *Biophys. J.* **1996**, *71*, 2056-2063.

158. Zhang, Y. J.; Furyk, S.; Bergbreiter, D. E.; Cremer, P. S. Specific ion effects on the water solubility of macromolecules: PNIPAM and the Hofmeister Series. *J. Am. Chem. Soc.* **2005**, *127*, 14505–14510.

159. Magnusson, J. P.; Khan, A.; Pasparakis, G.; Saeed, A. O.; Wang, W. X.; Alexander, C. Ionsensitive isothermal responsive polymers prepared in water. *J. Am. Chem. Soc*. **2008**, *130*, 10852– 10853.

160. Suwa, K.; Yamamoto, K.; Akashi, M.; Takano, K.; Tanaka, N.; Kunugi, S. Effects of salt on the temperature and pressure responsive properties of poly(N-vinylisobutyramide) aqueous solutions. *Colloid Polym. Sci*. **1998**, *276*, 529-533.

161. Zhang, Y.; Furyk, S.; Sagle, L. B.; Cho, Y.; Bergbreiter, D. E.; Cremer, P. S. Effects of Hofmeister anions on the LCST of PNIPAM as a function of molecular weight. *J. Phys. Chem. C*. **2007**, *111*, 8916-8924.

162. Lloyd, A. W. Interfacial bioengineering to enhance surface biocompatibility. *Med. Device Technol*. 2002, *13*, 18–21.

163. Nair, L. S.; Laurencin, C. T. Biodegradable polymers as biomaterials. *Prog. Polym. Sci*. **2007**, *32*, 762-789.

164. Li. S. Hydrolytic degradation characteristics of aliphatic polyesters derived from lactic and glycolic acids. *J. Biomed. Mater. Res*. **1999**, *48*, 342–353.

CHAPTER 2

BIODISTRIBUTION ANALYSIS OF NIR-LABELED NANOGELS USING IN VIVO FMT IMAGING IN TRIPLE NEGATIVE HUMAN MAMMARY CARCINOMA MODELS

2.1 Introduction

In recent years, the advancements in polymeric nanoparticle synthesis, formulation, and modification chemistries have advanced their use for applications including diagnostics and therapeutics for various diseases, particularly cancer. Nanoparticles have the potential to improve the solubility, stability, and clearance profiles and weaken side effects of therapeutics which are otherwise plagued with short half-life, low efficacy, and poor tissue selectivity, requiring frequent administration.[1,2] Parameters such as their morphology, polymer composition, size, and surface chemistry can all impact their extent of nonspecific interaction and circulation residence time to substantially influence their biodistribution. A more detailed understanding of these features relation to *in vivo* performance is required to improve the effectiveness of delivery to the region of interest, specifically solid tumors.

Nanoparticles have been under investigation following the discovery of the enhanced permeability and retention (EPR) effect, which showed increased tumoral accumulation of macromolecules by extravasation through fenestrated blood vessels from 100 nm to 2 μM, depending on tumor type.[3, 4] The poor lymphatic drainage of tumors also aids extracellular retention of contents.[5] There are many biological features that can impact biodistribution, including the propensity of nano-sized materials to accumulate in specific tissues with leaky endothelial walls, including the liver, spleen, and bone marrow.[6] The kidneys are also capable of filtering particles smaller than 10 nm, while the liver is capable of capturing particles larger than 100 nm.[7] A large obstacle facing nanocarriers is clearance

through the reticuloendothelial system (RES), also known mononuclear phagocyte system (MPS), which is the body's natural immune response to destroy foreign material. Immune cells in the blood stream by monocytes, platelets, leukocytes, and dendritic cells, and in phagocytes present in the liver (Kupffer cells), lymph nodes (dendritic cells), and in the spleen (B cells) can all clear nanoparticles from circulation.[8-11] A common pathway for uptake by these immune cells is opsonization, which is facilitated by the adsorption of plasma proteins, or opsonins, on the particle surface.[9] Currently, it is not clear that the binding of specific proteins, or a combination or conformation thereof, impact the extent of phagocytosis.[12]

Coating the nanocarrier surface with poly(ethylene glycol) (PEG), a method referred to as PEGylation, through grafting, conjugation, or adsorption has been shown to reduce their filtration and achieve extended blood circulation half-lives.[13-15] The favorable results due to its inherent physiochemical properties of PEG to impart a hydrated corona which generates steric stabilization and reduces non-specific interactions with proteins and compliment activation. [16, 17] PEG also has low toxicity and non-immunogenicity, and is approved for clinical use by the Food and Drug Administration (FDA). Long PEG chains and high surface density have been shown as optimal conditions for protein resistance by mathematical modeling.[18, 19] Investigations of PEG length and density effect on either protein absorption or biodistribution has led to some varied conclusion, likely heavily dependent on specific nanomaterial investigated and is also particle size. A significant correlation between size and protein absorption was found, with 80, 171, and 243 nm poly(cyanoacrylate-*co*-*n*-hexadecyl) cyanoacrylate (PHDCA) nanoparticles with PEG block of 5000 M_n, having 6%, 23% and 34% protein absorption, respectively.[20] The *in vivo*

blood clearance was twice as slow with the small compared to larger particles, which allowed smaller particles to accumulate in tumors twice greater than larger particles. One study systematically varied the PEG length and percentage in PLA-*b*-PEG diblock copolymer-based nanoparticles and found PEG between 2000 and 5000 M_n were able to most reduce surface protein adsorption, with maximum reduction at 5 wt. % PEG.[12] Additional advantage weren't obtained at higher weight percentages, and protein adsorption could not be completely prevented, potentially because PEG chains could not fully cover the surface.[21] Investigation of protein absorption of PEG5K-*b*-PLA and PEG2K-*b*-PLA diblock copolymer nanoparticles found no detectable differences in albumin adsorption could be detected.[22] Alternatively, investigation of PEG reduction of albumin and fibrinogen absorption on poly(ethylene terephthalate) found 3500 to be the critical M_n in reducing absorption.[21] A threshold of PEG M_n 1500 was found for restriction of protein absorption on planar polystyrene surfaces, with no improved effect up to 20000 M_n.[23, 24] A minimum PEG length producing a protein absorption benefit is thought to be due to a loss in flexibility in shorter chains. It is expected that a threshold benefit of PEG is that at a certain length the chains fold leading to coils with loosely bound water molecules. A more heavily hydrated random conformation of PEG chains is expected to best inhibit protein absorption due to the unfavorable entropy change from compressing this coating.[21, 24]

Currently the relationship between size and biodistribution of nanoparticles has some contrasting trends in results, likely due to nanomaterial differences. It is generally thought that the high curvature of smaller particles can reduce opsonization reactions and subsequent clearance by macrophages, however smaller particles have not always

performed better *in vivo*. For instance, one study investigated the tumor accumulation of 20, 30 and 60 nm nanolatex polymeric core-crosslinked nanoparticles, comprised of amphiphilic block copolymer poly(PEG-methacrylate-*b*-methoxyethylmethacrylate, and found a correlation between tumor accumulation and an increase in particle size.[25] The tissue which primarily removed the nanolatex polymers was the liver, and the size trend of localization was converse to tumor accumulation, with smaller particles resulting in higher %ID/g liver. Although they have different surface composition, liposome size-dependence on biodistribution was also investigated, and found that smaller particles (50 nm) more heavily accumulated in the liver, while larger particles (400 nm) more heavily accumulated in the spleen.[26] Liposomes of 100-200 nm achieved 4-fold tumoral accumulation compared to those that were larger or smaller. However, biodistribution investigation of polystyrene particles that were coated with d-α-tocopheryl poly(ethylene glycol) (1,000 M_n) succinate that ranged in size from 50-500 nm showed higher levels in both the liver spleen and for larger particles compared to smaller particles.[27] Further, the first polymeric micellar nanoparticle that has reached phase II clinical trials in the unites states is Genexol-PM [methoxy-PEG-poly(D,L-lactide)Taxol], comprised of a core containing Taxol-modified poly(lactide) and a corona of mPEG of 2000 M_n and sizes ranging 20-50 nm.[28, 29]

The purpose of this study is to the effect of nanogel size and surface poly(ethylene glycol) content on whole body residence times and tumor tissue extravasation in mice bearing triple negative human mammary carcinomas. Our group has developed a versatile amphiphilic random copolymer-based nanogel that encompasses many of the desirable features of a drug delivery vehicle including particle size control, guest encapsulation, and cytosolic release.[30-32] The copolymer forms micelle-type assemblies, encapsulating

hydrophobic guest molecules in aqueous media, which can then be core-crosslinked particle and quantifiably post-modified with PEG. While extensive work has investigated biodistribution profiles using PEG containing block copolymers, to our knowledge relatively little work has investigated random copolymers that are extensively post-modified with PEG on their coronas. With the expectation that minor physicochemical differences can greatly impact the *in vivo* performance and profile, we aim to systematically modify polymer size (20-135 nm), length of PEG conjugated to the surface (1000, 2000, and 5000 M_n), and amount of PEG conjugated to the surface (0-50 mole %) to determine the parameters that can most significantly direct a nanogel to the desired tumor target.

2.2 Results and Discussion

2.2.1 Nanogel Synthesis and Characterization

To afford nanogels with defined size and surface composition we utilized our reported self-crosslinking disulfide-based nanogels as the scaffold.[30-32] We aimed to formulate nanogels of different sizes (28-135 nm), crosslink density (20-100%), corona PEG length (M_n 1000, 2000, and 5000), and extent of PEG functionalization (up to 50 mol %). Our polymeric nanogels were achieved using amphiphilic random copolymers that self-assemble into nanoscale aggregates with disulfide functionality that allows for both controlled guest entrapment and stimuli-responsive release. Redox-responsive guest release of nanoassemblies are of significant interest due to the relative concentrations of glutathione (GSH) in blood plasma (10 μM) compared to the cytosol (10 mM).[33, 34] While stable encapsulation is observed at extracellular concentrations of GSH, these nanogels can release their therapeutic cargo following cellular internalization upon exposure to cytosolic

concentration of GSH. Further, fine control in particle size has been demonstrated using polymer molecular weight[30], as well as both temperature[30] and Hofmeister ions[35] due to the lower critical solution temperature (LCST) and relative hydration or dehydration behavior of PEG. In our current work, we expanded on this platform to include surface post-conjugation with PEGs of different length in a controlled and quantifiable manner.

Table 1. Characteristics of polymers prepared for nanogel formulation.

Polymer	Mn[a]	Đ[a]	OEG[b] (Mole%)	PDS[b] (Mole%)	AE[b] (Mole%)
P1	6.0 K	1.5	29	68	3
P2	13 K	1.2	28	70	2
P3	22 K	1.3	27	69	4

[a] Estimated by GPC (THF) using PMMA as a standard. [b] Determined by NMR.

The p(OEGMA-*co*-PDSMA-*co*-AEMA) random copolymers were synthesized by a reversible addition–fragmentation chain transfer (RAFT) copolymerization of monomers poly(ethylene glycol) methyl ether methacrylate (OEGMA), pyridyl disulfide ethyl methacrylate (PDSMA), 2-aminoethyl methacrylate hydrochloride (AEMA) (**Scheme 1**). After polymerization, the polymers were purified by dialysis against dichloromethane to remove unreacted monomers, then characterized by NMR and GPC (**Table 1**). We used the characteristic resonances of the 2-pyridylthio moieties of PDS (δH_a = 8.42, δH_b = 7.63, δH_c = 7.07 ppm), methoxy moieties of OEG (δH = 3.34, ppm), and methylene moieties of AE (δH = 3.78-3.46 ppm) to calculate the relative ratios of the monomer ratios for OEG:PDS:AE, which were similar for all copolymers. A range of different molecular weights were prepared, similar to those previously published, to access nanogels of various sizes.[30] The number-average molecular weight (M_n) and dispersity ($Đ = M_w/M_n$) of the copolymers was evaluated by GPC. The AE moieties were then used as a handle to

covalently conjugate the near IR probe, NHS ester functionalized cyanine 7. The reaction extent was determined to be nearly complete by evaluation of free amine using fluorescamine assay, suggesting the p(OEGMA-*co*-PDSMA-*co*-Cy7) random copolymers contains ~3 mole % near IR dye (**Figure 18**).

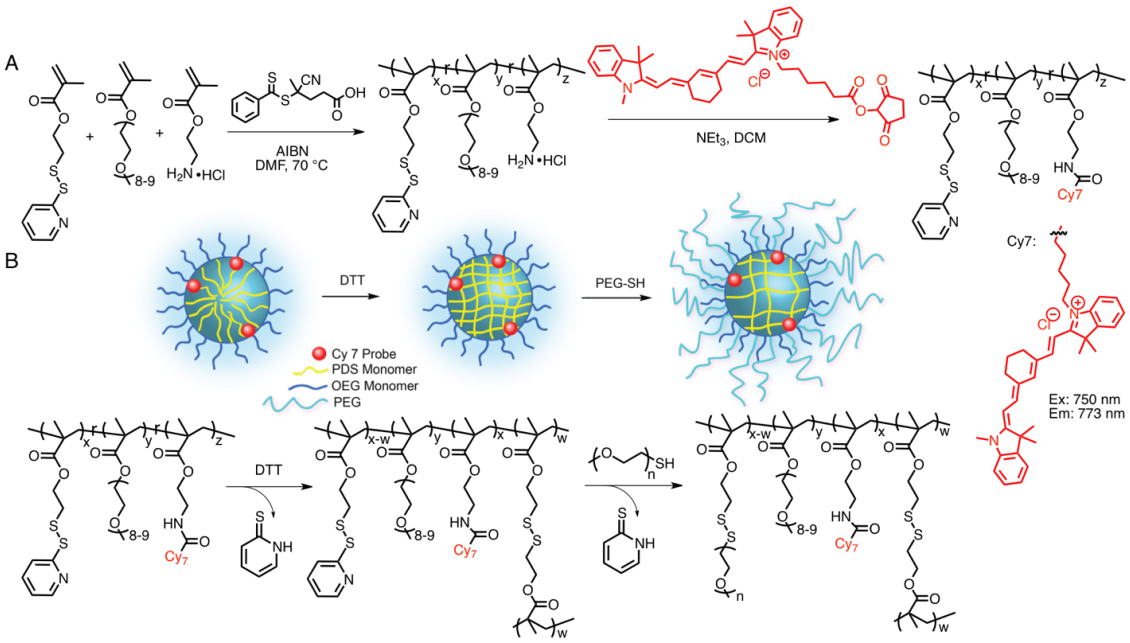

Scheme 1. (A) Synthetic scheme of p(OEGMA-*co*-PDSMA-*co*-Cy7) nanogel precursors; (B) schematic representation and corresponding reaction scheme of nanogel formulation by first crosslinking of PDS group by reducing agent DTT, then post-modification with poly(ethylene glycol) methyl ether thiol through thiol-disulfide exchange.

The NIR-labeled nanogels were formulated by first dispersing the p(OEGMA-*co*-PDSMA-*co*-Cy7) random copolymers (**P1, P2 or P3**) in the aqueous phase (10 mg/mL), then either diluting, heating, or mixing with sodium sulfate or sodium carbonate and monitored by DLS to manipulate the size of the self-assembled aggregates (**Table 3**). Once the desired size was achieved, the aggregates were locked under those specific solution conditions through intra-aggregate disulfide crosslink formation. The covalent crosslinking is achieved by addition of a stoichiometric amount of reducing agent DL-dithiothreitol (DTT), which generates the corresponding quantity of free thiols on PDS moieties in the

aggregate interior, which then react with the remaining PDS moieties in the polymer chain. For these nanogels, crosslink densities were quantified using the reaction byproduct 2-pyridinethione's characteristic absorption peak at 343 nm (**Figure 19**). The nanogel solution can then be manipulated (i.e. dilution, concentration, mild salt or heat treatment) without any consequence to the particle's size.

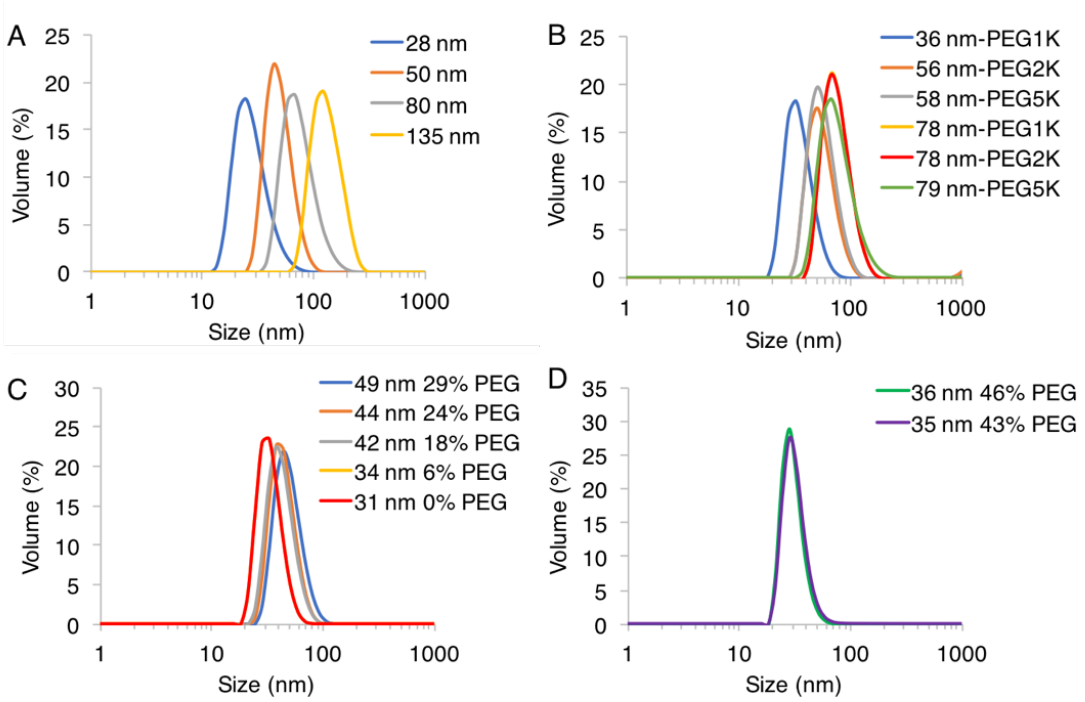

Figure 9. Size distribution of (A) Size Series (B) Length PEG Series (C) Percent PEG Series (D) Small Size High PEG Series nanogels obtained by DLS measurements in water.

Next, the remaining PDS handles of the nanogels were modified with mPEG thiols of M_n 1000, 2000, or 5000 through thiol-disulfide exchange reaction (**Table 3**). This post-modification was quantified by absorbance using the reaction byproduct 2-pyridinethione as previously demonstrated with post-modification with thiol ligands (**Figure 19**).[31, 36] A high reaction extent was achievable with PEG M_n 1000 and 2000, ranging from ~80-97% remaining PDS groups, however it was more limited at ~68-72% with PEG M_n 5000. Additional excess PEG 5000 did not increase the conjugation extent, likely due to steric

congestion, as these nanogels still contained the highest total surface ethylene glycol. Final sizes of nanogels were obtained using DLS (**Figure 9**). Post-modification to the nanogels, particularly with M_n 5000, often increased smaller particles by as much as 10-20 nm in diameter, leading to some unavoidable size discrepancy in comparing smaller particles with differing PEG length. Five series of nanogels were prepared chronologically based on *in vivo* findings: size, length PEG, percent PEG, and small size high PEG (**Table 2**).

Table 2. Size and corona properties of p(OEGMA-co-PDSMA-co-Cy7) nanogels.

Series	Name	Diameter (nm)	PEG (M_n)	PEG (mole%)
Size	28 nm	28 ± 9	1000	27
Size	50 nm	50 ± 14	1000	40
Size	80 nm	80 ± 20	1000	45
Size	135 nm	135 ± 31	1000	45
Length PEG	36 nm-PEG1K	36 ± 10	1000	51
Length PEG	56 nm-PEG2K	56 ± 16	2000	49
Length PEG	58 nm-PEG5K	58 ± 17	5000	37
Length PEG	78 nm-PEG1K	78 ± 23	1000	53
Length PEG	78 nm-PEG2K	78 ± 22	2000	51
Length PEG	79 nm-PEG5K	79 ± 28	5000	40
Percent PEG	49 nm 29% PEG	49 ± 13	2000	29
Percent PEG	44 nm 24% PEG	44 ± 11	2000	24
Percent PEG	42 nm 18% PEG	42 ± 12	2000	18
Percent PEG	34 nm 6% PEG	34 ± 8	2000	6
Percent PEG	31 nm 0% PEG	31 ± 9	2000	0
Small Size High PEG	36 nm 46% PEG	36 ± 11	2000	46
Small Size High PEG	35 nm 43% PEG	35 ± 12	2000	43

2.2.2 Tumor Cell Implantation and Growth

Triple negative breast cancer does not express the genes for estrogen receptor (ER), progesterone receptor (PRE), or human epidermal growth factor receptor 2 (Her2/neu).[37] Aside from surgery and radiation, patient treatment commonly uses combinatorial chemotherapeutics including anthracyclines, taxanes, and platinum agents. Also, these patients are not candidates for endocrine therapies used to treat other more common forms of breast cancer.[38] Triple negative breast cancers comprise 15-25% of breast cancer cases,

and have shorter median relapses and lower survival times. Nanoparticle-based therapeutics are attractive for treatment of triple negative breast cancer since they have the potential to increase target-specific delivery, weaken side effects, and are compatible with combinatorial therapy.

Cultured triple negative breast cancer cell line MDA-MB-231-luc-D3H2LN were implanted ($5x10^6$ cells, 50% Matrigel®) subcutaneously low in the right flank of each 6-7 week old animal on Day 0 and tumors grown until they reach the size of ~200-400 mg (target 300 mg). On Day 19-21, depending on tumor growth progress of mice model, the body weights were obtained and tumor burdens were determined from caliper measurements. The average weights and estimated tumor burdens were in a well-matched range for the first day of treatment and imaging for each series. Mice were triaged into groups (n=5 mice per group) with tumor burden within 10% overall mean, then dosed once with a 100 µL nanogel by intravenous injection for imaging on Day 0.

2.2.3 *In Vivo* FMT Tissue Distribution

Fluorescence Molecular Tomography (FMT) is an *in vivo* whole body quantitative imaging modality that uses red to near-infrared (NIR) light in a wavelength range of 700–900 nm. The deep tissue penetration of light up to 5 cm thick allows for time-dependent and non-invasive characterization of small animal subjects treated with NIR fluorescent probes in a 3-dimensional manner with a resolution of 1-2 mm.[39, 40] The minimal NIR autofluorescence from biological tissue allows for quantitative information and sub-picomolar sensitivity with the appropriate choice of probe with NIR excitation wavelength, high molar absorption coefficient and fluorescence quantum yield. Cyanine 7 probe was chosen for covalent conjugation to nanogels for its NIR excitation (λmax: 750 nm, ε:

199000) and emission (773 nm).

In FMT imaging for nanogel samples, the total whole body fluorescence was obtained at time 0, when signal distribution is attributed to the animal vasculature, and then monitored over time to assess both clearance and changes in the tissue distribution, including extravasation into specific tissues. For all nanogels, the total body probe decreased over time, but was still detectable at 72 hours after administration (**Figure 10, 12, and 14**). The fluorescence values at the 0-hour imaging time point for each nanogel sample were normalized in their group average total whole body probe, which scanned shoulders to base of the tail, as 100% (**Figure 11, 13, and 15**). The normalized percentages were calculated at each imaging time point, so that the percent retention of total body probe signal over 0-72 hours could be compared between nanogel samples, despite minor variation of fluorophore concentration between nanogel samples. Tissue-based quantification of fluorophore concentration was obtained by manual positioning and scanning over the regions of interest (ROI). Fluorescence signals were significant and localized to the various tissues, allowing for quantification in the tumor, liver, spleen, intestines, lung and heart. To normalize the obtained fluorescence values, the percent injected dose (%ID) in the tissue of the total body probe signal per imaging time point were reported. For the tumor ROI, the primary endpoints were the percent injected dose per gram (%ID/g) tumor and used as an indicator for percentage of nanogel that accumulates in the tumor.

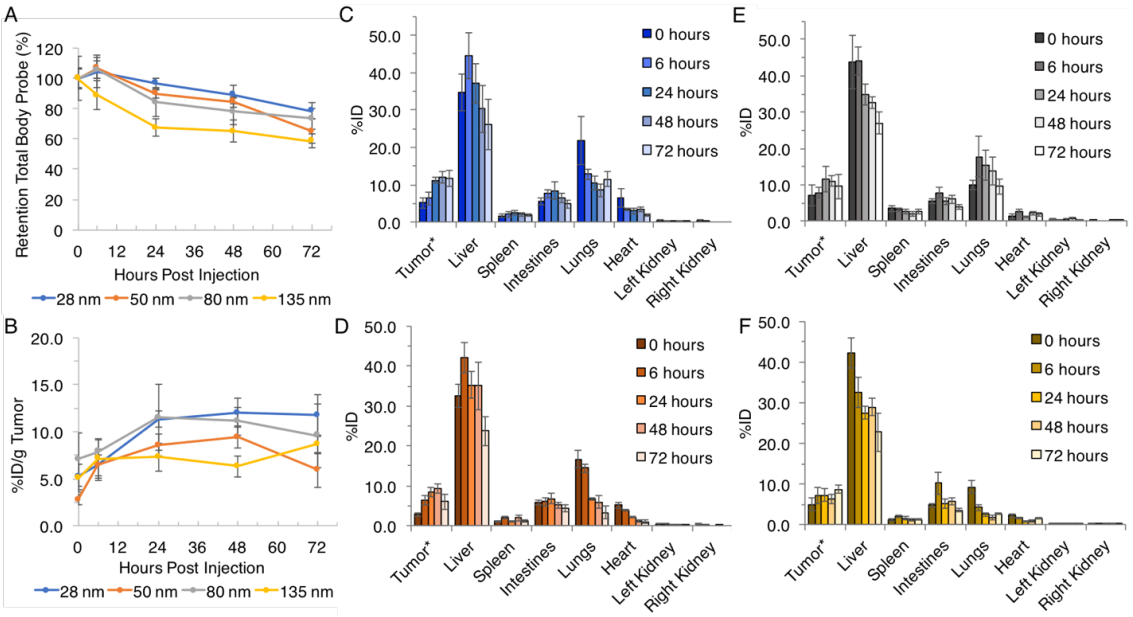

Figure 10. Size series quantitative *in vivo* (A) retention of total body probe over 72 hours; (B) %ID/g tumor over 72 hours; (C) tissue distribution for tumor, liver, spleen, intestines, lungs, heart, left and right kidney of 28 nm nanogel, (D) 50 nm nanogel, (E) 80 nm nanogel and (F) 135 nm nanogel following intravenous administration obtained by FMT imaging. Data are given as mean ± standard deviation (n = 5). *Tumor values are given %ID/g tumor to normalize for any variations in mass (all group mean estimated tumor burden: 343 mg, range: 312-396 mg).

2.2.3.1 Size Series

The 28, 50, and 80 nm nanogels showed a pattern of accumulation following injection over time to a maximum %ID/g tumor at 24 to 48 hours, followed by a decrease at 72 hours (**Figure 10**). The 135 nm nanogel had a generally constant %ID/g tumor observed from 0-48 hours followed by an increase at 72 hours. From initial injection to nanogels peak maximum %ID/g, the group average tumor percent increased 7, 7, 5, and 4% for the 28, 50, 80, and 135 nm nanogel, respectively. In general, the observed accumulation trend correlated to a decrease in nanogel size, which all had a measurable, but non-significant, overall increase in %ID/g. This accumulation over time was observed despite a contrasting monotonic decrease in the whole body, liver, lungs, intestines, spleen, and heart (**Figure 10, 11**). This suggests that the nanogels exhibit a selective behavior

towards accumulation the tumor compared to normal tissues. The peak maximum %ID/g tumor was 12% (48 hours), 9% (48 hours) and 12% (24 hours), and 9% (72 hours) for nanogels 28nm, 50nm, 80nm, and 135 nm, respectively.

The retention of total body probe for all nanogels decreased over time, with generally the smaller particles achieving higher retention, which is similar to the tumor accumulation trends (**Figure 10**). The 28 nm nanogel had the highest percentage retention in total body probe over time, with 79% of total signal retained at 72 hours. The second, third, and fourth highest retention in probe at 72 hours was the 80, 50, and 135 nm nanogels with 73, 65, and 59% of total signal retained, respectively.

The liver was consistently the tissue with the highest localization (**Figure 10, 11**). For the 28 nm nanogel the liver %ID was at a maximum of 45% at 6 hours post injection, which deceased to 26% at 72 hours (**Figure 11**). For the 50 nm nanogel, the liver %ID was at a maximum of 42% at 6 hours post injection, which deceased to 24% at 72 hours. The 80 nm nanogel was at a maximum liver %ID of 44% at 6 hours post injection, which deceased to 27% at 72 hours. Lastly, the 135 nm nanogel liver %ID was at a maximum of 42% 0 hours post injection, which deceased to 23% at 72 hours, which was the highest rate of decreasing liver concentration. For all nanogels, the intestines, lungs, heart, and spleen showed a much lower %ID and similar general monotonic decrease over the time studied. The kidneys, showed minimal and virtually non-detectable %ID with < 1% for all nanogels and all imaging time points.

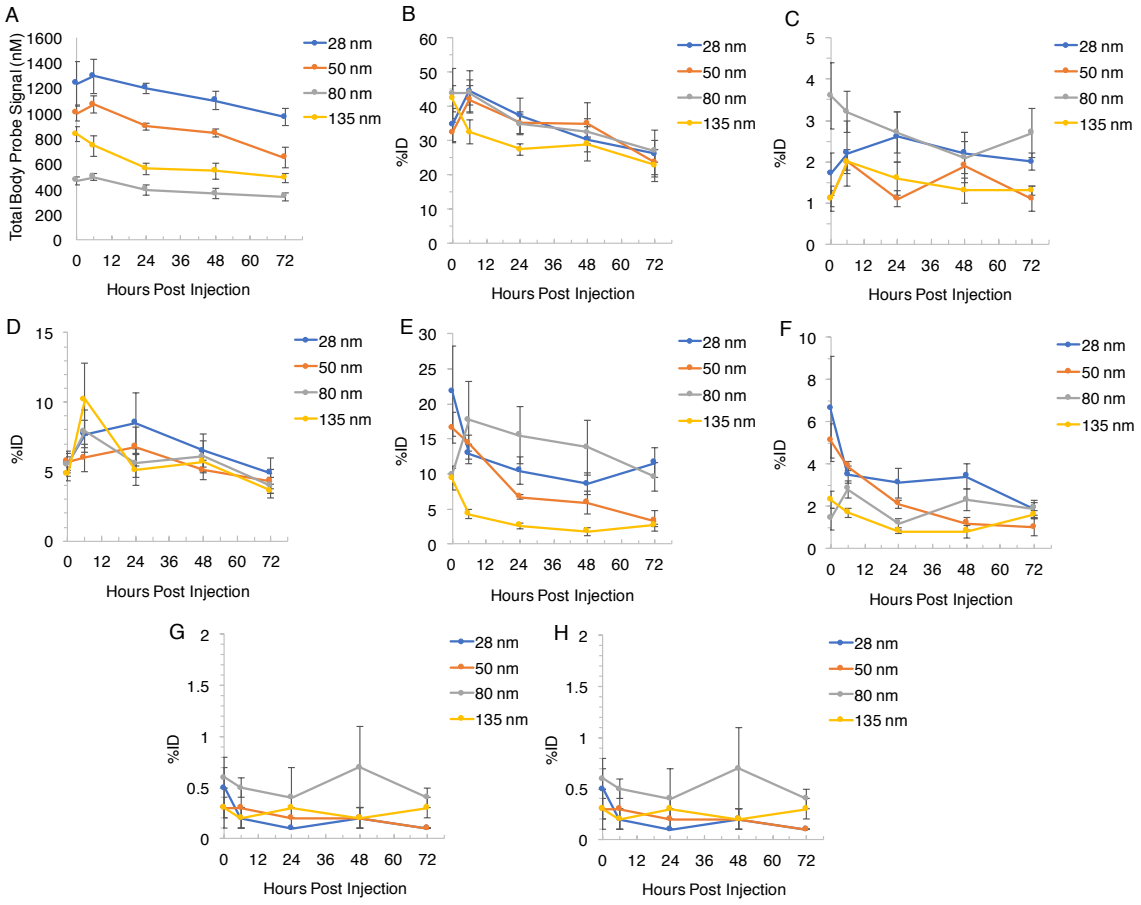

Figure 11. Size series quantitative *in vivo* (A) whole body probe signal, (B) %ID liver, (C) %ID spleen, (D) %ID intestine, (E) %ID lungs, (F) %ID heart, (G) %ID left kidney, and (H) %ID right kidney over 72 hours following intravenous administration obtained by FMT imaging. Data are given as mean ± standard deviation (n = 5).

General results from this series suggest that smaller nanogels gave measurably greater tumor specificity with higher %ID/g, a greater tumoral accumulation over time, and had higher total body retention over the time studied. However, the we were cautious to make far-reaching conclusions in this preliminary series due to sample variability (**Table 3**) and the statistical significance of differences in values of tumor accumulation were not deemed sufficient. These findings, however, motivated the further investigation of the 28 nm and 80 nm nanogels. Therefore, nanogels of a smaller and larger size were made, then decorated with different lengths of PEG: M_n 1000, 2000, and 5000, to obtain nanogels 36

nm-PEG1K, 56 nm-PEG2K, 58 nm-PEG5K, 78 nm-PEG1K, 78 nm-PEG2K, and 79 nm-PEG5K (**Table 2**). Notice that PEGylation of the smaller size particles caused a considerable diameter increase from M_n 1000 to M_n 5000, while understandably not appreciably affecting the larger sized particles (**Figure 9**).

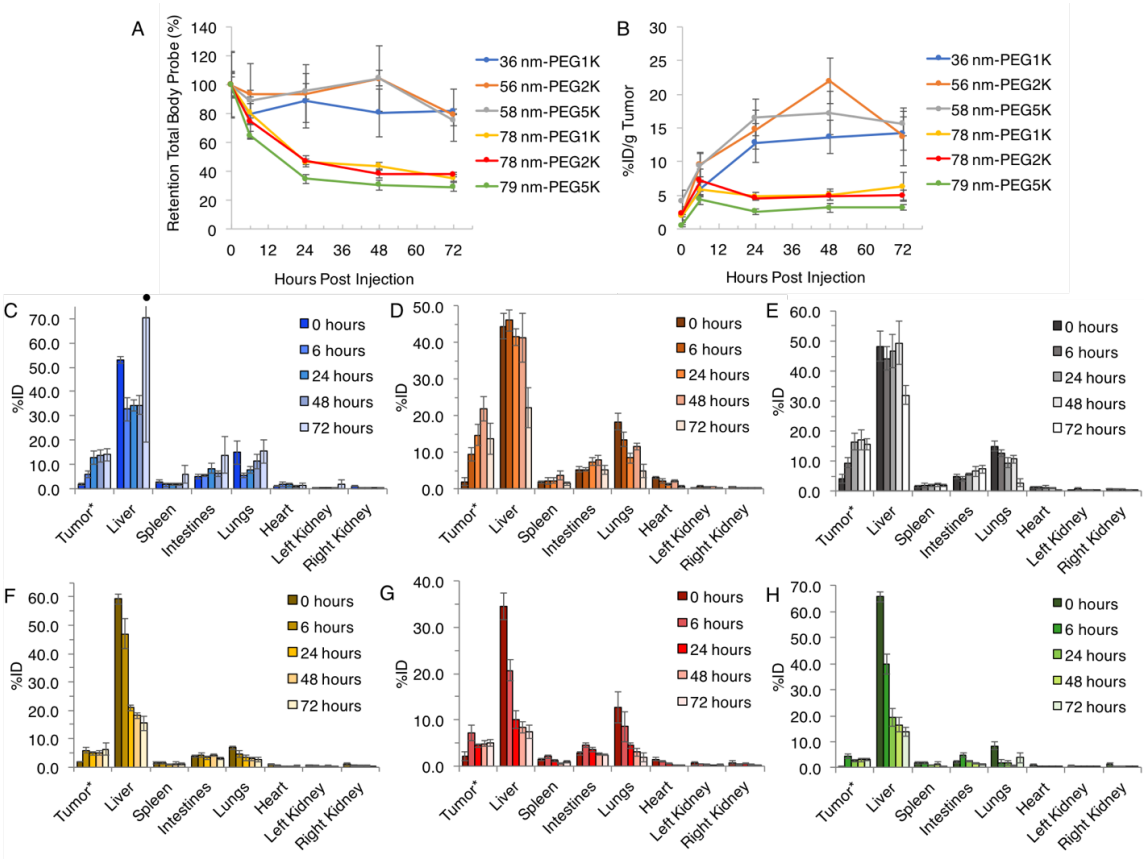

Figure 12. Length PEG series quantitative in vivo (A) retention of total body probe over 72 hours; (B) %ID/g tumor over 72 hours; (C) tissue distribution for tumor, liver, spleen, intestines, lungs, heart, left and right kidney of 36 nm-PEG1K nanogel, (D) 56 nm-PEG2K nanogel, (E) 58 nm-PEG5K nanogel, (F) 78 nm-PEG1K nanogel, (G) 78 nm-PEG2K nanogel and (H) 79 nm-PEG5K nanogel following intravenous administration obtained by FMT imaging. Data are given as mean ± standard deviation (n = 5). •%ID is 70 ± 51, with high error due to values from one mouse in group. *Tumor values are given %ID/g tumor to normalize for any variations in mass (all group mean estimated tumor burden: 316 mg, range: 312-323 mg).

2.2.3.2 Length PEG Series

Smaller nanogels showed a pattern of accumulation over time to a maximum %ID/g

tumor at 48 hours, except the 36 nm-PEG1K nanogel which increased up to 72 hours, exhibiting a selective behavior towards accumulation the tumor (**Figure 12**). This accumulation over time was observed despite a contrasting monotonic decrease in the whole body, liver, lungs, intestines, spleen, and heart (**Figure 12, 13**). An exception would be a small increase in the intestines in the smaller nanogels (36 nm-PEG1K, 56 nm-PEG2K, and 58 nm-PEG5K). Larger nanogel patterns were less clear, with maximum %ID/g tumor occurring at 72 hours for 78 nm-PEG1K and 6 hours for both 78 nm-PEG2K and 79 nm-PEG5K.

In general, the observed accumulation trend correlated to a decrease in nanogel size. The tumors showed a measurable, but non-significant, overall increase in %ID/g at variable times post-injection, followed by monotonic decreases to 72 hours. Over the time studied, the group average tumor percentage increased 12, 20, 13, 4, 5, and 4% for the nanogels 36 nm-PEG1K, 56 nm-PEG2K, 58 nm-PEG5K, 78 nm-PEG1K, 78 nm-PEG2K, and 79 nm-PEG5K, respectively (**Figure 12**). The peak maximum %ID/g tumor was 14% (72 hours), 22% (48 hours), 17% (48 hours), 6% (72 hours), 7% (6 hours), and 4% (6 hours) for nanogels 36 nm-PEG1K, 56 nm-PEG2K, 58 nm-PEG5K, 78 nm-PEG1K, 78 nm-PEG2K, 79 nm-PEG5K respectively. This generally also suggests that smaller nanogels (originally 28 nm) gave higher tumor specificity, with 2-3-fold the peak %ID/g obtained compared to larger nanogels.

The retention of total body probe for all nanogels decreased over time, with the smaller particles achieving nearly 2-fold the percent retention in total body probe compared to the larger particles, regardless of PEG length (**Figure 12**). This was well-matched with tumor accumulation trends amongst nanogels. The 36 nm-PEG1K had the highest

percentage retention in total body probe over time, with 82% of total signal retained at 72 hours. The 56 nm-PEG2K nanogel had the second highest percentage retention in total body probe over time, with 79% of total signal retained at 72 hours, and the 58 nm-PEG5K nanogel also had high retention with 75% of total signal retained at 72 hours. The 78 nm-PEG1K, 78 nm-PEG2K, and 79 nm-PEG5K nanogel had 35, 38, and 29% of total signal retained at 72 hours, respectively.

The tissue accumulation for these nanogels were slightly more variable. Generally, the liver showed the highest %ID, followed by the lungs (**Figure 12, 13**). Of the smaller nanogels, the 36 nm-PEG1K nanogel had a liver %ID of 53% 0 hours post injection, which deceased to 34% at 48 hours. The variability at the 72-hour time point is due to one mouse in its group having a high liver intensity. The spleen, intestines, and left kidney also had one mouse introducing variability at the 72-hour measurement, impacting the general pattern of decrease over time (**Figure 13**), while %ID values were generally low. Amongst all nanogels the kidneys again showed minimal and virtually non-detectable (< 1) %ID. The 56 nm-PEG2K nanogel had a liver %ID of 46% at 6 hours post injection, which deceased monotonically to 22% at 72 hours. Some tissues did not show the same pattern of decrease over time. The lungs had an elevated percentage to 48 hours at 12%, and the intestines and spleen showed some increase (8% and 4%, respectively) to 48 hours. The 58 nm-PEG5K nanogel had a liver %ID of 49% at 48 hours post injection, and decreased to 32% at 72 hours, a greater decrease than other nanogels. The lungs for this nanogel also had an elevated percentage to 48 hours at 11%, as did the spleen (2%) to 48 hours, and the intestines (7%) to 72 hours.

For the larger nanogels, regardless of PEG length, the liver had considerable %ID

decrease over time suggesting rapid clearance of these nanogels (**Figure 12**). The 78 nm-PEG1K nanogel had a liver %ID of 59% 0 hours post injection and deceased to 16% at 72 hours (**Figure 13**). The intestines showed consistently low values over 72 hours, while the spleen showed generally low and decreasing %ID over the time studied. The 78 nm-PEG2K nanogel had a liver %ID of 34% at 0 hours post injection, and decreased to 8% at 72 hours. The intestines showed some increase to 6 hours followed by decrease over 72 hours, the spleen was relatively constant. The 79 nm-PEG5K nanogel had a liver %ID of 66% at 0 hours post injection, which deceased to 14% at 72 hours. The intestines showed some increase to 6 hours followed by decrease over 72 hours. These nanogels also showed generally low and decreasing %ID for the lungs, heart, and kidney.

The results suggested that smaller nanogels had greater tumor specificity with higher %ID/g tumor, propensity to accumulate over time, and retention of total body probe over the time studied. The PEG2K decorated nanogels of both sizes performed slightly better with higher peak %ID/g compared to their 1k and 5k counterparts. We were therefore interested in further evaluating smaller particles decorated with different mole percent of PEG2K, to evaluate if a threshold advantage could be identified. Nanogels of 31 nm were made then decorated with PEG2K (0-29 mole percent) (**Table 2**) to achieve sizes ranging 31 to 49 nm (**Figure 9**).

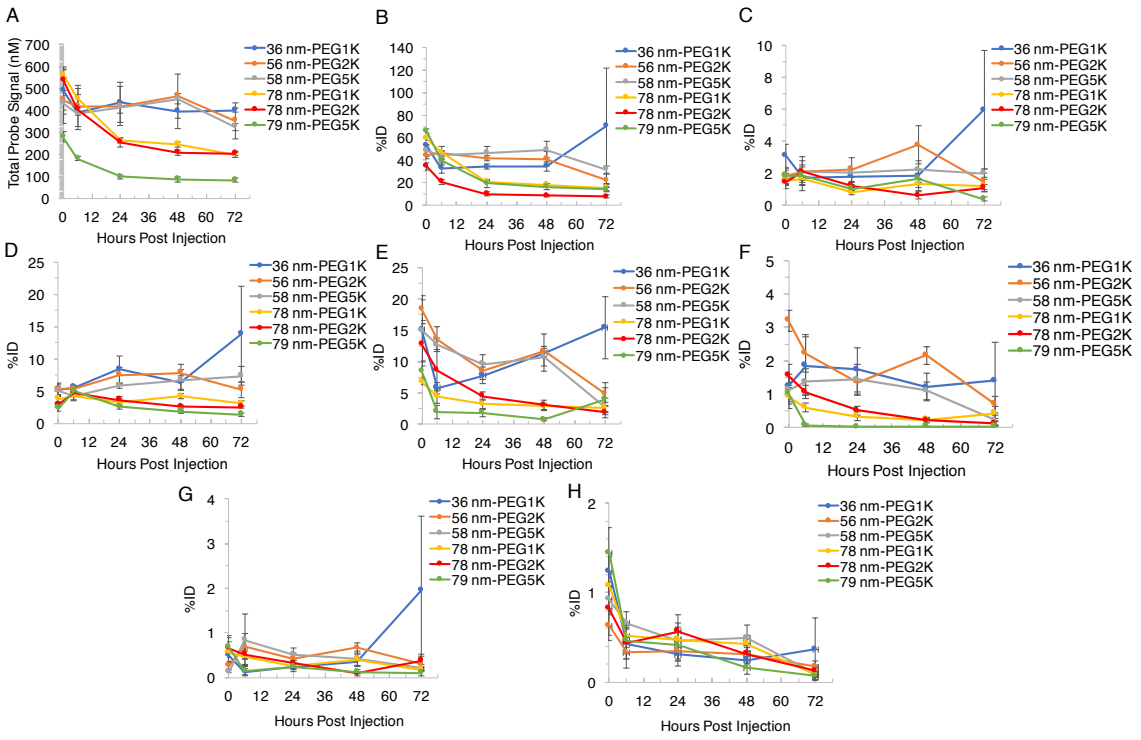

Figure 13. Length PEG series quantitative in vivo (A) whole body probe signal, (B) %ID liver, (C) %ID spleen, (D) %ID intestine, (E) %ID lungs, (F) %ID heart, (G) %ID left kidney, and (H) %ID right kidney over 72 hours following intravenous administration obtained by FMT imaging. Data are given as mean ± standard deviation (n = 5).

2.2.3.3 Percent PEG Series

Based on the general consistency of tissue profiles for previous nanogels, for this series only the total body probe and %ID/g tumor were obtained and calculated to establish relative nanogel performance. In this series, the whole total body fluorophore concentration was readily detected following administration, which then had 50% clearance and decrease to near-background levels by 24-48 hours (**Figure 14, 15**). With one nanogel, 34 nm 6% PEG, the whole-body fluorophore concentration reached background levels at 6 hours. The retention in total body probe over 72 hours was low, with 15, 15, 14, 3, and 15% observed for nanogels 49 nm 29% PEG, 44 nm 24% PEG, 42 nm 18% PEG, 34 nm 6% PEG, and 31 nm 0% PEG, respectively. Such a detrimental effect was attributed to these lower PEG

percentages compared to previous systems.

Compared to previous nanogels tested, these nanogels had a highest %ID/g tumor immediately after injection and decreased over 72 hours post-administration (**Figure 14**). This suggested no propensity towards tumor specificity or accumulation. The 49 nm 29% PEG nanogel had the peak %ID/g tumor at 0 hours with 15%, however one mouse introduced large variability in this time point measurement which normalized at subsequent time points. The %ID/g tumor then had a monotonic decrease to 3% at 72 hours. The peak %ID/g tumor then followed the trend in decrease in percent PEG, with nanogels 44 nm 24% PEG, 42 nm 18% PEG, 34 nm 6% PEG, and 31 nm 0% PEG obtaining peak %ID/g of 4, 3, 2, and 2%, respectively.

We expect these very rapidly cleared and low tumor accumulating samples are highly correlated to their lower PEG percentages which are conjugated on their surface compared to previously tested samples. It was surprising to see a decrease of 10-20 mole% PEG could impart such a detrimental effect to these nanogels. Based on observed animal excretions this result is expected to be due to clearance through the renal system. We therefore wanted to reexamine these smaller nanogels that would be comprised of even higher percentages of PEG2K conjugated to their surface. Two nanogels were prepared: 36 nm 46% PEG and 35 nm 43% PEG for FMT analysis (**Table 2, Figure 9**).

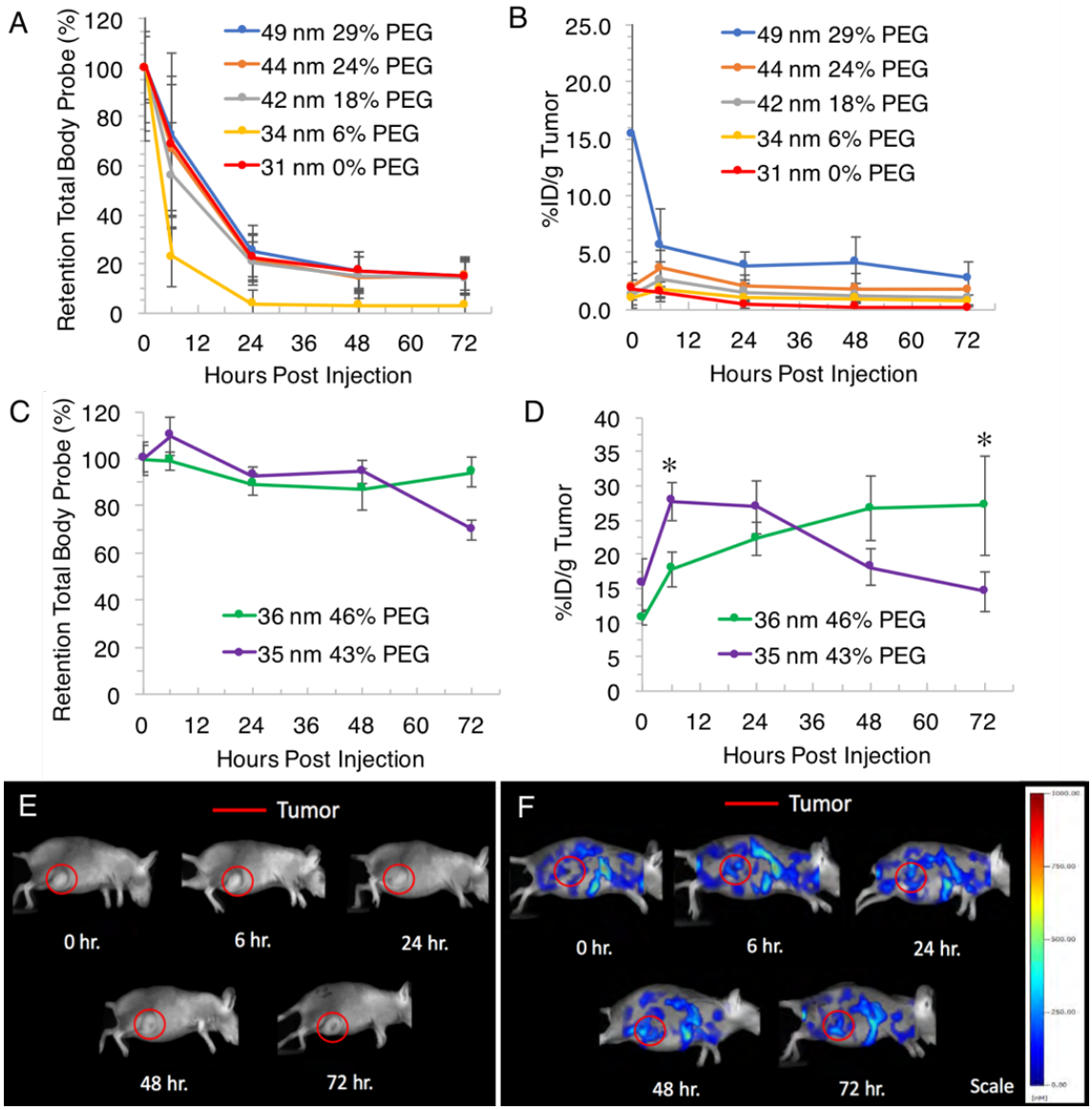

Figure 14. Quantitative in vivo (A) retention of total body probe and (B) %ID/g tumor of Percent PEG series (tumor burden all groups means: 377 mg, n = 5, range: 363-404 mg) and (C) retention of total body probe and (D) %ID/g tumor of Small Size High PEG series (tumor burden all groups means: 294 mg, n = 5, range: 283-301 mg) following intravenous administration. *Statistically significant ($P<0.05$) increase in tumor %ID/g from 0 hour of administration. Representative 2D fluorescent images (lateral view) of female Harlan Beige Nude XID mice with subcutaneously implanted MDA-MB-231-luc-D3H2LN cell line in the right flank injected with (E) 100 µL saline and (F) 100 µL 36 nm 46% PEG nanogel.

2.2.3.4 Small Size Higher PEG

The 36 nm 46% nanogel PEG had the peak %ID/g tumor at 72 hours with 27%

(**Figure 14**). This nanogel had a statistically significant ($P<0.05$), monotonic increase in the tumor %ID/g from 11-27% from 0-72 hours post-administration, an additional accumulation of 17% over the study, which constitutes a 1.5-fold increase compared to the 0-hour tumor signal. Representative 2D fluorescent images of a mouse injected with saline and a mouse injected with the 36 nm 46% nanogel this group showed the increase in fluorescence intensity in the tumor ROI over time when treated with nanogel. This nanogel also had the highest retention in total body probe throughout the study, with 94% of total signal retained at 72 hours. This signifies only 6% of the injected dose was lost through elimination.

The 35 nm 43% PEG nanogel had a peak %ID/g tumor at 6 hours with 28%, the highest maximum percentage achieved throughout this whole study (**Figure 14**). This nanogel had a statistically significant ($P<0.05$), monotonic increase in the tumor %ID/g from 16-28% from 0-6 hours post-administration, an additional accumulation of 12% over 6 hours, which constitutes a 0.8-fold increase compared to the 0-hour tumor signal. The %ID/g tumor then monotonically decreased to a final 15% at 72 hours. This nanogel had less retention over the test period, with 70% of total whole body probe remaining at 72 hours.

The results again suggested smaller nanogels performed better in both tumor specificity with high %ID/g, accumulation over time, and retention of total body probe over time, with prerequisite that is contains extensive PEGylation. These results again suggest that nanogel surface PEG modification can dramatically impact the tumor accumulation and circulation retention. These results were consistent with general conclusions from the size series and the PEG length series, and suggests that a PEG2K-

modification has thus far imparted the greatest advantage in tumor specificity.

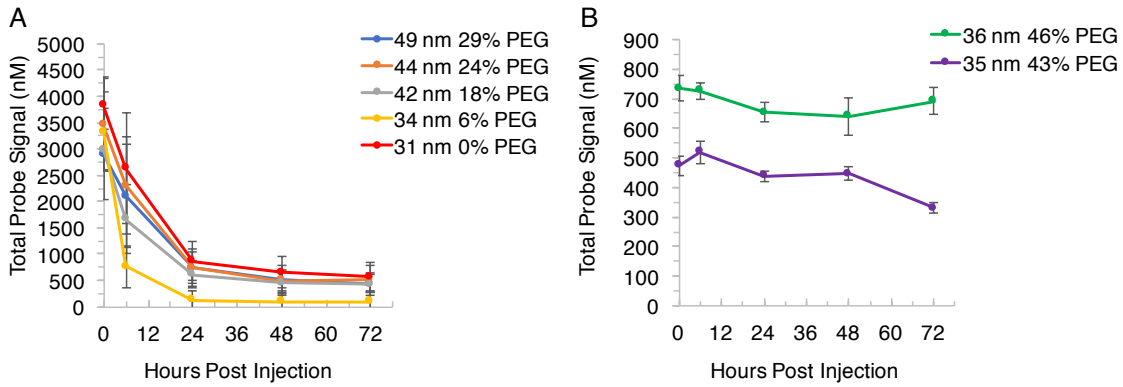

Figure 15. FMT imaging *in vivo* whole body probe signal of (A) Percent PEG series nanogels and (B) Small Size High PEG series nanogels 72 hours following intravenous. Data are given as mean ± standard deviation (n = 5).

2.2.3.5 Liver Localization

The nanogels evaluated for full tissue profiles (size series and length PEG series) had the highest %ID in the liver. For all nanogels, throughout 72 hours the liver displayed a monotonic decrease in probe concentration over time. In all cases the liver localization at initial injection was frequently above 40% (**Figure 10, 12**). In the case of smaller particles, the %ID in the liver decreased to ~20-30% over 72 hours, however with larger particles they decreased to as little as ~10% (**Figure 11, 13**). The pattern of highest accumulation in the liver with slow monotonic decrease suggests that the nanogels are being cleared through the liver through hepatic uptake and not through kidney filtration. Nanoparticles can become sequestered in one of the RES organs following surface absorption of proteins leading to opsonization and removal from the blood stream. Despite PEG improvements on circulation, it has been shown that RES clearance is often significant even in optimized PEGylated systems, with >50% of the ID residing in the liver and spleen after 48 hours.[41-44] An additional contributor to this observation is that the

noncontiguous vasculature in the liver with fenestrae pore size (50-100 nm) allows nanoparticles to penetrate their endothelial wall and nonspecifically accumulate.[26]

2.2.3.6 Other Tissue Localization

The second highest tissue of localization at initial imaging was the lungs, while the spleen, intestines, and heart showed less though detectable and resolvable %ID (**Figure 10, 12**). The kidneys, however, showed minimal and virtually non-detectable %ID with < 1% for all nanogels and all imagining time points. Very little observed kidney localization indicates hepatic metabolism and not renal elimination as the mechanism of clearance. Also, relatively little spleen localization was observed, which is not always the case in polymeric nanoparticles.[25] The considerable lung localization and low splenic accumulation may indicate that lung macrophages may contribute to particle uptake,[45] but also may be a result of the mechanical deformability of these heavily PEGylated particles.[46] "Softer" deformation-prone nanoparticles and hydrogels with high water content have been shown to reduce accumulation in the spleen compared to those with hydrophobic or tightly crosslinked cores.[25, 47, 48] Further, recent microfluidic blood capillary models have shown that deformability of particles may aid in transport through small capillaries like those in the lung.[46] The tissue profile obtained with these nanogels may likewise be impacted by the deformable parameter of these particles.

2.2.4 Toxicity

Injection of 100 μL of all samples were well-tolerated and throughout imaging no abnormal side effects were observed. For one mouse treated with the 28 nm nanogel sample (size series), during necropsy an edema in the abdominal cavity was observed. One mouse

treated with 36 nm-PEG1K nanogel and one mouse treated with 56 nm-PEG2K nanogel had an enlarged spleen and tumor-like growth on the pancreas (PEG length series). Separate mice treated with 56 nm-PEG2K, 78 nm-PEG1K, and 78 nm-PEG2K also had enlarged spleens. During necropsy, one mouse treated with 36 nm 46% PEG nanogel (small size high PEG series) was observed as having an enlarged spleen. For all other mice used throughout this study, no unusual observations were made during necropsy.

2.2.5 *Ex Vivo* Tissue Distribution

The *ex vivo* quantification of the fluorescence signal in individual tissue homogenates from gross necropsy 72 hours post injection was reasonably consistent with the *in vivo* FMT analysis (**Figure 16**). Comparing across tissues of mice treated with the PEG length nanogel series, *ex vivo* homogenates showed the highest intensity in the liver in all groups, followed by the tumor and intestines. The smallest nanogel in this series had considerable error in the FMT values at the 72-hour time point due to irregular values obtained for one mouse, which was not observed in tissue homogenates. Plots of *in vivo* versus *ex vivo* results for tissues gave variable correlation, with R^2 values of 0.90, 0.89, 0.70, 0.76 and 0.34, for nanogels 56 nm-PEG2K, 58 nm-PEG5K, 78 nm-PEG1K, 78 nm-PEG2K, and 79 nm-PEG5K, respectively (**Figure 17**). The tissue introducing the greatest correlation deviation is the intestines, which gave higher efficiency values for homogenates than FMT. *Ex vivo* results gave slightly lower florescence values for the lungs than expected, while the liver, tumor, spleen, lungs, heart, and kidney fluorescence intensities were in reasonable agreement. Further, a similar trend between nanogels was observed in the tumor at this time-point for both *in vivo* and *ex vivo* results. Aside from minor discrepancies in intestine signals, *ex vivo* findings provided additional confidence in the

reliability of tissue signal segmentation by *in vivo* FMT. FMT distribution has been shown to well correlated with *ex vivo* results,[49, 50] however performance can be impacted by tissue optical properties and depth.[51, 52] Live imaging can be used in combination with X-ray computed tomography, magnetic resonance imaging, or diffuse optical tomography to improve either structural imaging or optical property accuracy.[53-55]

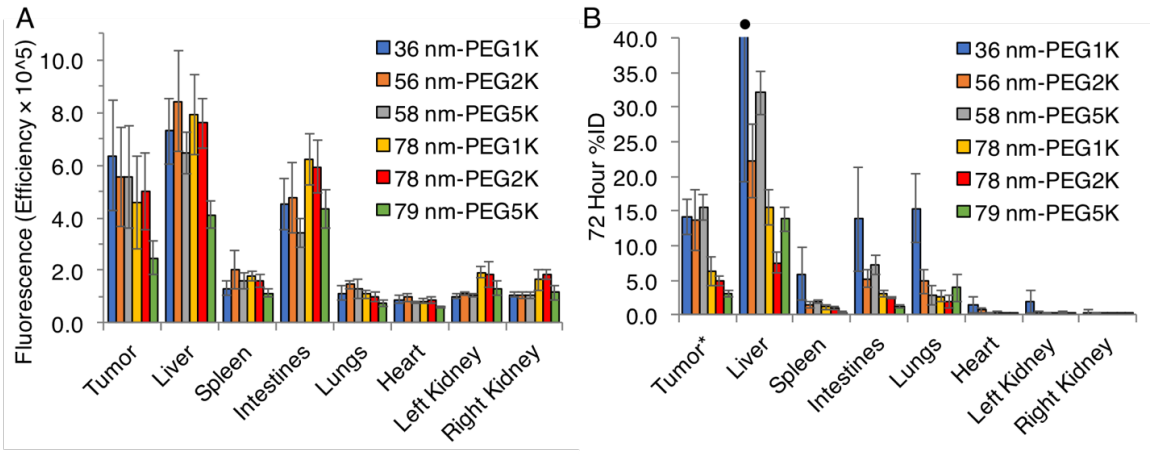

Figure 16. Length PEG series nanogels (A) ex vivo quantification of tissue fluorescence efficiency (radiance of subject/illumination intensity) following final imaging and gross necropsy at 72 hours, quantified using filter set: ex: 710-760 nm, em: 810-875 nm, and (B) in vivo FMT comparison at 72 hours. •%ID is 70 ± 51, with high error due to values from one mouse in group. Data are given as mean ± standard deviation (n = 5).

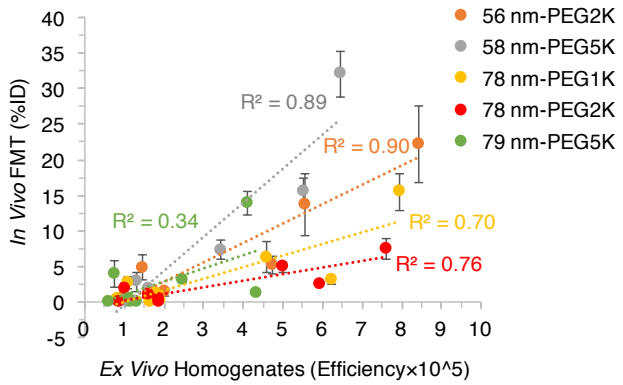

Figure 17. Comparison between in vivo FMT and ex vivo homogenate results of biodistribution values for tumor, liver, lung, spleen, intestine, heart, left kidney, and right kidney tissues using mean value of nanogels (n=5 in group) 56 nm-PEG2K, 58 nm-PEG5K, 78 nm-PEG1K, 78 nm-PEG2K, and 79 nm-PEG5K**.**

2.3 Conclusion

In summary, NIR-labeled nanogels of various size and PEG content were formulated and exhibited discernable performance trends by *in vivo* FMT imaging. Using the model of triple negative human mammary carcinomas (cell line MDA-MB-231-luc-D3H2LN), we determined that smaller nanogels (~30 nm) with a high PEG conjugation (~50 mole %) of M_n 2000 length performed better in both tumor specificity with highest maximum %ID/g, a greater accumulation over time, and greater retention of total body probe. These conclusions were supported by the consistency of smaller particles with extensive PEG conjugation outperforming those that were larger or less PEGylated. Nanogels without extensive PEGylation were excreted faster, even at similar sizes to PEGylated nanogels which achieved greater total body retention and tumor specificity. Nanogels had the highest %ID in the liver throughout the time studied, however like other tissues displayed a monotonic decrease over time suggesting the nanogels are being cleared by hepatic metabolism and not through the kidneys. The %IDs observed in RES organs are consistent with reported findings on other optimized PEGylated nanomaterials.[41-44] The *ex vivo* quantification of individual tissues from gross necropsy at 72 hours post injection generally showed trends that correlated with the FMT analysis, providing additional confidence in the reliability of tissue signal segmentation *in vivo*. Injection of all samples were well-tolerated and throughout imaging no abnormal side effects were observed. During necropsy, among the 85 mice used throughout this study, some observations included one mice with an edema in the abdominal cavity, five mice with enlarged spleens, two mice with a tumor-like growth on the pancreas. For all other mice, no unusual observations were made during necropsy. Overall, we determine here that minor physical

and chemical differences in these nanogels greatly impacted *in vivo* performance. Given that the key versatility of these nanogels arises from the fact that the self-assembly strategy offers enormous tunability in the nanoparticle, these findings will guide the design of next generation of nanogels as therapeutic delivery vehicles for cancer therapy.

2.4 Experimental

2.4.1 Materials and Methods

Poly(ethylene glycol) methyl ether methacrylate (MW 475 g/mol, OEGMA), 2-aminoethyl methacrylate hydrochloride (AEMA), D,L-dithiothreitol (DTT), 4-cyano-4-(phenylcarbonothioylthio)pentanoic, cyanine 7 NHS ester (Cy7), poly(ethylene glycol) methyl ether thiol (average M_n 1000, 2000, and 5000), and other conventional reagents were obtained from commercial sources and without further purification, unless otherwise mentioned. AIBN (2,2'-azobis(2-methylpropionitrile) was purchased from Sigma Aldrich and purified by recrystallization. MDA-MB-231-luc-D3H2LN cells were obtained from Xenogen Corporation (Caliper Life Sciences). Pyridyl disulfide ethyl methacrylate (PDSMA) was prepared as previously reported.[56] Polymers were synthesized using RAFT polymerization and purified by dialysis using a membrane with 3500 MWCO. ^{1}H-NMR spectra were recorded on a 400 MHz Bruker NMR spectrometer using the residual proton resonance of the deuterated solvent as the internal standard. Polymer molecular weights were estimated by gel permeation chromatography (GPC, Waters) using THF as eluent at a flow rate of 1 mL/min by a refractive index detector compared to PMMA standard. Dynamic light scattering (DLS) measurements were conducted using a Malvern Nano Zetasizer. UV-visible absorption spectra were recorded on a Varian spectrophotometer

(model EL 0112047). Near-IR probe was quantified using a NanoDrop 2000C spectrophotometer.

2.4.2 Experimental Procedures

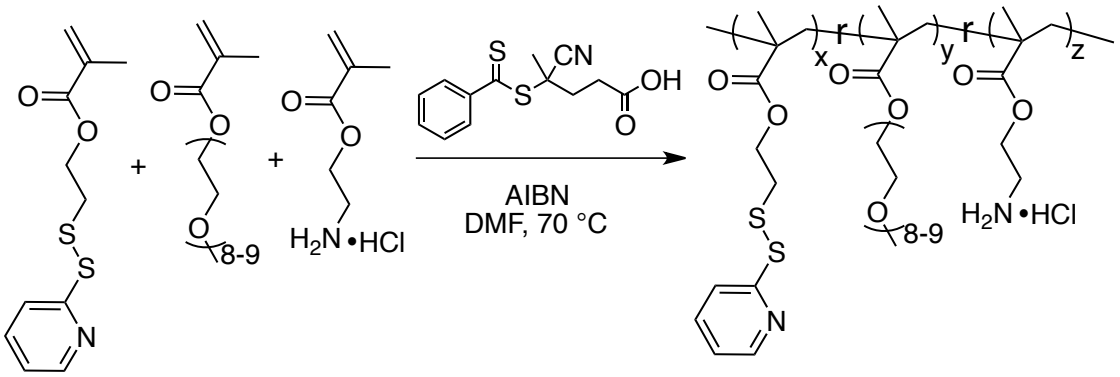

Scheme 2. Synthetic reaction scheme of p(OEGMA-*co*-PDSMA-*co*-AEMA).

Synthesis of random copolymer p(OEGMA-*co*-PDSMA-*co*-AEMA) P1: To a Schlenk-flask, monomers PDSMA (1.160 g, 4.54 mmol), OEGMA (800 mg, 1.68 mmol), AEMA (23.6 mg, 0.20 mmol), chain transfer agent 4-cyano-4-(phenylcarbonothioylthio)pentanoic acid (47.2 mg, 0.17 mmol), and AIBN (5.6 mg, 0.034 mmol) were dissolved in DMF (4 mL). The mixture was degassed by performing three freeze-pump-thaw cycles and filled with argon. The reaction mixture was then sealed and transferred into a pre-heated oil bath at 70 °C and stirred for 24 h. The reaction flask was submerged in an ice bath to quench the polymerization, then dialyzed against dichloromethane in MWCO 3500 membrane for 48 hours to remove unreactive monomers. The solution was dried to yield the random copolymer **P1** as a waxy oil. GPC (THF) M_n: 6 kDa. Đ: 1.5. ^{1}H NMR (400 MHz, $CDCl_3$) δ (ppm): 8.49, 7.71, 7.15, 4.35-4.01, 3.76-3.51, 3.39, 3.05, 2.26-1.73, 1.18-0.78. The molar ratio of the three monomers in the polymer were determined by relative integrations of the aromatic protons of PDS, methoxy protons of PEG, and methylene protons of AE to give 29:68:3 (OEG:PDS:AE).

Synthesis of random copolymer p(OEGMA-*co*-PDSMA-*co*-AEMA) P2: To a Schlenk-flask, monomers PDSMA (510 mg, 2 mmol), OEGMA (352 mg, 0.74 mmol), AEMA (14.7 mg, 0.089 mmol), chain transfer agent 4-cyano-4-(phenylcarbonothioylthio)pentanoic acid (10.3 mg, 0.037 mmol), and AIBN (1.2 mg, 0.0037 mmol) were dissolved in DMF (1.8 mL). The mixture was degassed by performing three freeze-pump-thaw cycles and filled with argon. The reaction mixture was then sealed and transferred into a pre-heated oil bath at 65 °C and stirred for 18 h. The reaction flask was submerged in an ice bath to quench the polymerization, then dialyzed against dichloromethane in MWCO 3500 membrane for 48 hours to remove unreactive monomers. The solution was dried to yield the random copolymer **P2** as a waxy oil. GPC (THF) M_n: 13 kDa. Đ: 1.2. ^{1}H NMR (400 MHz, Acetone-D_6) δ (ppm): 8.45, 7.66, 7.10, 4.35-3.97, 3.77-3.49, 3.34, 2.95, 2.12-1.67, 1.14-0.77. The molar ratio of the three monomers in the polymer were determined by relative integrations of the aromatic protons of PDS, methoxy protons of PEG, and methylene protons of AE to give 28:70:2 (OEG:PDS:AE).

Synthesis of random copolymer p(OEGMA-*co*-PDSMA-*co*-AEMA) P3: To a Schlenk-flask, monomers PDSMA (402 mg, 1.57 mmol), OEGMA (269 mg, 0.57 mmol), AEMA (11.4 mg, 0.07 mmol), chain transfer agent 4-cyano-4-(phenylcarbonothioylthio)pentanoic acid (6.9 mg, 0.025 mmol), and AIBN (0.8 mg, 0.005 mmol) were dissolved in DMF (1.2 mL). The mixture was degassed by performing three freeze-pump-thaw cycles and filled with argon. The reaction mixture was then sealed and transferred into a pre-heated oil bath at 65 °C and stirred for 18 h. The reaction flask was submerged in an ice bath to quench

the polymerization, then dialyzed against dichloromethane in MWCO 3500 membrane for 48 hours to remove unreactive monomers. The solution was dried to yield the random copolymer **P3** as a waxy oil. GPC (THF) M_n: 22 kDa. Đ: 1.3. ^{1}H NMR (400 MHz, Acetone-D_6) δ (ppm): 8.42, 7.63, 7.07, 4.37-3.93, 3.78-3.46, 3.34, 2.99, 2.10-1.60, 1.13-0.74. The molar ratio of the three monomers in the polymer were determined by relative integrations of the aromatic protons of PDS, methoxy protons of PEG, and methylene protons of AE to give 27:69:4 (OEG:PDS:AE).

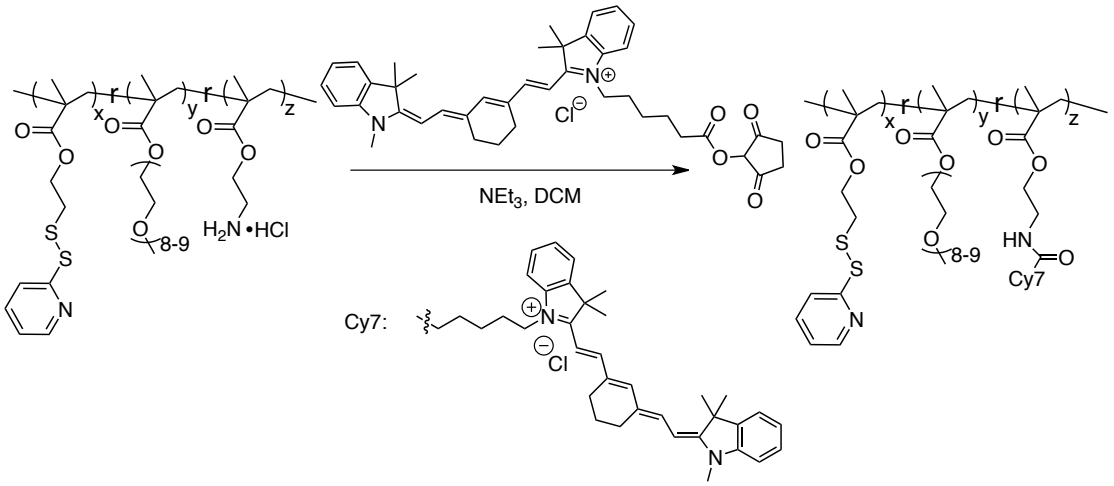

Scheme 3. Synthetic reaction scheme of p(OEGMA-*co*-PDSMA-*co*-Cy7).

Synthesis of p(OEGMA-*co*-PDSMA-*co*-Cy7) P1-P3: To round bottom flasks, the p(OEGMA-*co*-PDSMA-*co*-AEMA) polymers **P1-P3** (200 mg, 0.022 mmol AE) separately, each with Cy7 NHS ester (22.2 mg, 0.032 mmol), were dissolved in DCM (3 mL) and purged with argon. Then triethylamine (6.14 μL, 0.044 mmol) was added and the mixtures were stirred for 12 hours at ambient temperature. Mixtures were purified by dialysis against dichloromethane in a MWCO 3500 regenerated cellulose membrane for 48 hours. The solutions were dried to yield the Cy7-labeled polymers p(OEGMA-*co*-PDSMA-*co*-Cy7) **P1-P3** as waxy oils.

Cy7 Conjugation Quantification of p(OEGMA-*co*-PDSMA-*co*-Cy7): The presence of unreacted amine of AEMA monomer was evaluated by using the Fluorescamine reaction. Nanogels solutions (1 mg/mL, 93 nM amine/AE monomer) of precursor polymer p(OEGMA-*co*-PDSMA- *co*-AEMA), or NG-AE, and Cy7 reacted polymer p(OEGMA-*co*-PDSMA-*co*-Cy7), or NG-Cy7, were prepared in PBS buffer pH 7.4. In a 96 well (flat-bottomed) plate PBS buffer pH 7.4 (150 μL) and sample solutions NG-AE or NG-Cy7 (20 uL) were added to each well. A blank control was prepared containing PBS buffer pH 7.4 (170 μL). Then, fluorescamine solution in DMSO (12 μL, 465 nM) was added to each well and the fluorescence was obtained using a Molecular Devices Spectramax M5 plate reader (excitation: 390 nm; emission 465 nm). Average fluorescence values and deviation were obtained from replicate readings (n=3). The background fluorescence values from the blank solution was subtracted from values fluorescence intensity obtained for NG-AE and NG-Cy7 and normalized. Assuming complete fluorescamine reaction with free amines, there are was about 12.8% the fluorescence for NG-Cy7 compared to of NG-AE, indicating about 12.8% remaining amines of the NG-Cy7 sample (**Figure 18**). Of a polymer containing 3 mole percent polymer, this is only 04% or negligible, so we considered the conjugation sufficient.

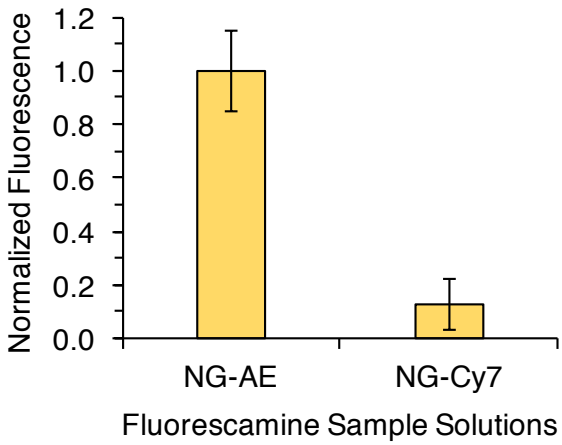

Figure 18. Fluorescamine normalized fluorescence of free amine reaction of nanogel NG-AE from precursor polymer p(OEGMA-*co*-PDSMA- *co*-AEMA) and NG-Cy7 of polymer p(OEGMA-*co*-PDSMA-*co*-Cy7), or NG-Cy7.

Synthesis and Formulation of NIR-labeled Nanogels: Random copolymers p(OEGMA-*co*-PDSMA-*co*-AEMA) were synthesized by reversible addition-fragmentation chain-transfer (RAFT) polymerization to yield three polymers of *Mn*: 6.0 kDa with Đ: 1.5, *Mn*: 13 kDa with Đ: 1.2, and *Mn*:22 kDa with Đ: 1.3, with monomer ratios for OEG:PDS:AE of 29:68:3, 28:70:2, and 27:69:4, respectively (see Supporting Information). The polymer was reacted with NIR probe, Cy7 NHS ester, to give covalently labeled polymer p(OEGMA-*co*-PDSMA-*co*-Cy7). The polymer was made into an aqueous particle suspension (10 mg/mL) using repeated cool and sonicate cycles until the solution appeared dissolved. Smaller aggregates (20-30 nm) were achieved at 25 °C sometimes requiring dilution (**Table 3**). To achieve aggregates, the polymer solutions were heated (to 40-50 °C), requiring the presence of sodium sulfate or sodium carbonate (1-15 mM) in some cases, until desired sizes of aggregate were obtained, similar to conditions previously reported.[30, 35] The crosslinking density was determined using the previously reported procedure by calculating the amount of 2-pyridinethione byproduct using its molar extinction coefficient (8.08 x 10^3 M^{-1} cm^{-1} at 343 nm).[30, 31, 34] UV-vis absorption

measurements were performed on 1000-fold dilutions of crosslinking reaction solutions. Crosslinking percentage was calculating by assumption that cleavage of two PDS units would produce two pyridinethione byproduct and one disulfide bond. Nanogels were then post-modified with poly(ethylene glycol)monomethyl ether thiol (mPEG thiol) (average M_n 1000, 2000, and 5000) using simple thiol-disulfide exchange using the remaining PDS groups of the nanogels. Typically, mPEG thiol was dissolved in a minimum volume water then reacted with crosslinked nanogel solution at PDS molar equivalencies of 1, 1.2, and 2, for M_n 1000, 2000 and 5000, respectively, and stirred for 24 hours. For example, PEG(1000)-SH (27.5 mg, 0.0275 mmol) was dissolved in a minimum volume of water (170 μL) then added to the crosslinked nanogel solution (11.55 mg, 0.0275 mmol) and stirred for 24 hours. Pyridinethione concentration calculations using its molar extinction coefficient was supported by comparison with addition of excess DTT, to obtain 100% pyridinethione generation. The conjugation extent was then determined using UV-vis absorption by quantification of pyridinethione absorbance at 343 nm as previously described.[30, 31, 36] Dynamic light scattering experiments to obtain particle size were performed by using a digital correlator and goniometer with a light source operating at 514 nm. Final nanogel size measurements were obtained at 25 °C at a correlation time of 30 seconds. Dust was removed by filtering the solution through 0.45 μm polycarbonate filter. Final polymeric nanogel concentrations were calculated using initial feed, and final probe concentrations were determined using a NanoDrop 2000C spectrophotometer to obtain the absorbance of Cy7 (λmax: 750, ε: 199000).

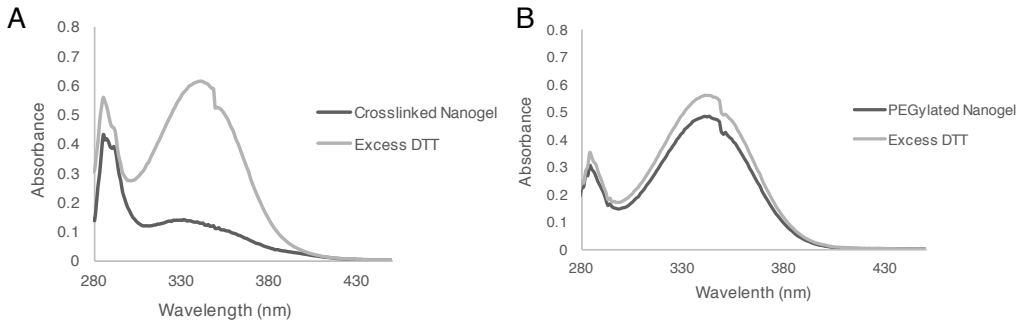

Figure 19. UV-vis absorption Spectra of pyridinethione byproduct at 343 nm (A) crosslinking reaction with DTT and (B) PEG conjugation with poly(ethylene glycol) methyl ether thiol M_n 2000, each with comparison to 100% pyridinethione from reaction with excess DTT.

Table 3. Nanogel formulation, crosslink (CL) and mPEG-thiol conjugation information.

Name	Polymer	Formulation Conditions	CL (mole%)	PEG (M_n)	PEG % (PDS)	PEG (mole%)
28 nm	P2	5 mg/mL, 25 ºC	42	1000	97	27
50 nm	P1	10 mg/mL, 15 mM Na_2SO_4, 25 ºC	28	1000	95	40
80 nm	P2	5 mg/mL, 1 mM Na_2CO_3 50 ºC	14	1000	80	45
135 nm	P2	5 mg/mL, 2.5 mM Na_2CO_3, 50 ºC	14	1000	80	45
36 nm PEG-1K	P1	10 mg/mL, 1.5 mM Na_2SO_4, 25 ºC	16	1000	94	51
56 nm PEG-2K	P1	10 mg/mL, 1.5 mM Na_2SO_4, 25 ºC	16	2000	91	49
58 nm PEG-5K	P1	10 mg/mL, 1.5 mM Na_2SO_4, 25 ºC	16	5000	68	37
78 nm PEG-1K	P1	5 mg/ml, 1 mM Na_2CO_3, 50 ºC	14	1000	94	53
78 nm PEG-2K	P1	5 mg/ml, 1 mM Na_2CO_3, 50 ºC	14	2000	91	51
79 nm PEG-5K	P1	5 mg/ml, 1 mM Na_2CO_3, 50 ºC	14	5000	72	40
49 nm 29% PEG	P2	10 mg/mL, 40 ºC	21	2000	63	29
44 nm 24% PEG	P2	10 mg/mL, 40 ºC	26	2000	48	24
42 nm 18% PEG	P2	10 mg/mL, 40 ºC	36	2000	54	18
34 nm 6% PEG	P2	10 mg/mL, 40 ºC	58	2000	43	6
31 nm 0% PEG	P2	10 mg/mL, 40 ºC	68	2000	N/A	0
36 nm 46% PEG	P3	10 mg/mL, 2 mM Na_2CO_3, 25 ºC	14	2000	82	46
35 nm 43% PEG	P3	10 mg/mL, 2 mM Na_2CO_3, 25 ºC	21	2000	88	43

Final Nanogel Cy7 Probe Concentration: The Cy7 probe concentration in final nanogel solutions were obtained by UV-vis absorption measurements using its molar extinction coefficient (199000 M^{-1} cm^{-1} at 759 nm) at Near-IR probe was quantified using a NanoDrop 2000C spectrophotometer. Concentrations were calculated assuming a path length of 1 mm.

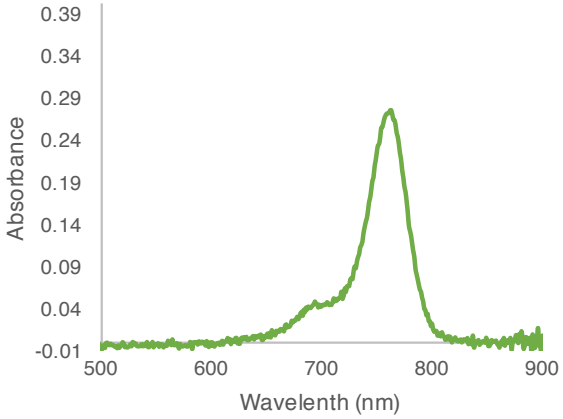

Figure 20. UV-vis absorption Spectra of Cy7-conjugated nanogel obtained using a NanoDrop spectrophotometer.

Table 4. Nanogel formulation conditions and final Cy7 and polymer concentrations for *in vivo* injection.

Series	Name	Polymer (mg/mL)	Cy7 (μM)
Size	28 nm	5.1	38
Size	50 nm	4	18
Size	80 nm	4.5	13
Size	135 nm	2.2	27
Length PEG	36 nm-PEG1K	0.69	45
Length PEG	56 nm-PEG2K	0.69	23
Length PEG	58 nm-PEG5K	0.69	16.8
Length PEG	78 nm-PEG1K	0.69	127
Length PEG	78 nm-PEG2K	0.69	50
Length PEG	79 nm-PEG5K	0.69	26.9
Percent PEG	49 nm 29% PEG	2.5	88
Percent PEG	44 nm 24% PEG	2.5	100
Percent PEG	42 nm 18% PEG	2.5	96
Percent PEG	34 nm 6% PEG	2.5	100
Percent PEG	31 nm 0% PEG	2.5	150
Small Size High PEG	36 nm 46% PEG	2.2	112
Small Size High PEG	35 nm 43% PEG	2.2	727

Animals and Husbandry: All animal work was conducted by Molecular Imaging, Inc. This experiment used female Harlan Beige SCID mice (Hsd:NIHS-Lyst^{bg}Foxn1^{nu}Btk^{xid}), which lack T, B, and NK cells, for size and length PEG series nanogels, female Harlan Nude mice (Hsd:AthymicNude-Fox1^{nu}), which lack T cells, for percent PEG series nanogels, and female Harlan Beige Nude XID mice (Hsd:NIHS-Lyst$^{bg\text{-}J}$Fox1^{nu}Btk^{xid}) for small sixe high PEG series nanogels that were all 6-7 weeks old at the time of implantation. Animals were fed *ad libitum* (water and irradiated Harlan 2918.15 Rodent Diet) and housed inside Biobubble® Clean Rooms with Bed-O'Cobs^{TM} bedding with an environment of 70±2 °F and 30-70% humidity. All measurements and imaging were conducted in the bubble environment with filtered high efficiency particulate air and 100 air changes per hour. All animal procedures were carried out under compliance with National Institutes of Health (NIH) guidelines and with Molecular Imaging, Inc.'s (AAALAC accredited and PHS assured facility) Animal Care and Use Committee approval.

Cell Preparation: MDA-MB-231-luc-D3H2LN cells were grown in Minimal Essential Media (MEM) with Earle's Balanced Salt Solution (EBSS) supplemented with 10% Fetal Bovine Serum (FBS), 1% penicillin-streptomycin-glutamine (PSG), 1% L-glutamine, 1% non-essential amino acids, and 1% sodium pyruvate. Cells were grown at 5% CO_2 and 37 °C and, after expansion, cells (passage 5) were suspended using trypsin 0.25% and 2.21 mM EDTA in *Hank's Balanced Salt Solution* (HBSS) then trypsin was deactivated with complete growth media. Cells were counted using Trypan Blue exclusion and a hemacytometer then centrifuged (1,374 rpm, 8 min), decanted, then resuspended in serum-

free media ($2.5x10^7$ cells/ml). On day 0, cells ($5x10^6$, 200 μL) with 50% Matrigel® were implanted subcutaneously low in the right flank of each animal using a 27-guage needle in the animals. Three thioglycolate cultures of tumor cells tested negative for gross bacterial contamination. Daily clinical observations were made and moribund or distressed animals or those bearing ulcerated, weeping, or excessive (>1 gram) tumors were euthanized.

Measurements and Endpoints: Measurements were conducted using reported general principles.[57-63] At the initiation of imaging (sample injection Day 0), animal body weights were recorded and tumor burden determined from caliper measurements of orthogonal length (L) and width (W) in mm, and using the prolate ellipsoid formula: $(L \times W^2)/2$ = tumor burden (mg). The primary endpoints for evaluation are total whole body probe signal and percent injected dose per gram of the tumor region of interest (%ID/g), and secondary endpoint are percent injected dose (%ID) for heart, lungs, liver, kidneys, spleen, and intestines. Percent injected dose is defined by the probe signal in the tissue divided by 1.15-fold the total whole body probe signal [%ID/(1.15× total whole probe signal)] to account for head mass, a common assumption.[57] The percent injected dose per gram (%ID/g) is defined by %ID for the tumor region of interest (ROI) divided by the tumor weight in grams.

Treatment: Following tumor implantation at Day 0, on Day 21 body weights were obtained and tumor burdens were determined from caliper measurements. For size series nanogels, the average SCID Beige mice weights (range of group means: 20.6- 21.2 g, all ≥18.0 g) and estimated tumor burden (all groups means: 343 mg, range: 312-396 mg) were

in a well-matched range for the first day of treatment and imaging. For PEG length series nanogels, on Day 21 the average SCID Beige weights (range of group means: 19.4-20.4 g, all ≥17.8 g) and estimated tumor burden (all groups means: 316 mg, range: 312-323 mg) were in a well-matched range for the first day of treatment and imaging. For percent PEG series nanogels, the growth rate of tumors in the nude mice was slightly faster, with animal weights (range of group means: 20.9-22.6 g, all ≥19.0 g) and estimated tumor burden (all groups means: 377 mg, range: 363-404 mg) were in a well-matched range and, still within the historical norms for this model, ready for treatment and imaging at Day 19. Similarly, for small size high PEG series nanogels the beige nude mice on Day 19 were a little larger (range of group means: 20.6-22.4 g, all ≥19.3 g) and estimated tumor burden (all groups means: 294 mg, range: 283-301 mg) were in a well-matched range for the first day of treatment and imaging. Mice were triaged into groups so that the tumor burden was within 10% of the overall mean. Following weight and tumor burden measurements, mice were dosed once with a single injection of 100 μL nanogel solution in endotoxin free water for imaging on Day 0 (n=5 mice per nanogel solution were treated in each group).

Fluorescence Molecular Tomography: Following sample injection, mice were individually imaged *in vivo* at 0, 6, 24, 48 and 72 hours by 3D FMT using the Perkin-Elmer FMT 2500TM LX Quantitative Tomography Imaging System. Just prior and throughout imaging mice were anesthetized with 2% isoflurane gas, then placed in the supine position in the imaging cassette, which was then was inserted to the heated (37 °C) docking system in the FMT imaging chamber. Prior to scanning the fluorescence scan region was manually positioned from the shoulders to base of tail for full body imaging (representative images

Figure 14). Total whole body signal was increased by 15% to account for body mass from non-imaged head.[57] Specific regions of interest were scanned by manual positioning over the regions of interest using a medium source density (3 mm). Obtained images were analyzed using Perkin-Elmer TrueQuant software.

***Ex Vivo* Imaging:** Following final imaging at 72 hours, gross necropsy was performed and *ex vivo* images were acquired. On an IVIS 50 2D reflectance fluorescence images were obtained using the Indocyanine Green (ICG) filter set (ex:710-760 nm, em: 810-875 nm). Several hundred counts from each tissue were observable without saturation using 20 seconds of exposure and large binning off CCD camera chip, and image analysis was performed using Living Image software (Caliper Life Sciences, Hopkinton, MA). The signal intensities of each tissue were quantified by efficiency (radiance of subject/illumination intensity).

Assessment of Side Effects: Throughout tumor growth and sample treatment animals were observed for clinical signs daily. Following treatment and euthanasia, or in the case of any inadvertent death, animals were necropsied for general assessment and specific organ toxicity including edema or enlargement. For each animal, the existence or absence of tumor metastases was recorded.

Statistics: Data are expressed as mean ± standard deviation of the five mice tested per sample. Significance of data was analyzed using one-way analysis of variance (ANOVA), and post-hoc analysis by the method of Holm-Sidak. A Kruskall-Wallace ANOVA by

ranks with post-hoc analysis was performed if the data did not pass normality or equal variance testing, by the method of Tukey. Statistical comparisons were performed for the total body probe between time points within each group, and between groups at each time point. Statistical comparisons of %ID/g tumor were performed between time points within each group, and between groups at each time point. Likewise, statistical comparisons of %ID of individual tissues were performed between time points within each group, and between groups at each time point. Statistically significant differences were set at p values ≤ 0.05, and calculated using SigmaPlot 12.0 software.

2.5 References

1. Safra, T.; Muggia, F.; Jeffers, S.; Tsao-Wei, D. D.; Groshen, S.; Lyass, O.; Henderson, R.; Berry, G.; Gabizon, A. Pegylated liposomal doxorubicin (doxil): Reduced clinical cardiotoxicity in patients reaching or exceeding cumulative doses of 500 mg/m^2. *Ann. Oncol.* **2000**, *11*, 1029–1033.

2. Fassas, A.; Buffels, R.; Kaloyannidis, P.; Anagnostopoulos, A. Safety of high-dose liposomal daunorubicin (daunoxome) for refractory or relapsed acute myeloblastic leukaemia. *Br. Jo. Haematol.* **2003**, *122*, 161–163.

3. Matsumura, Y.; Maeda, H. A new concept for macromolecular therapeutics in cancer chemotherapy: mechanism of tumoritropic accumulation of proteins and the antitumor agent smancs. *Cancer Res.* **1986**, *46*, 6387–6392.

4. Maeda, H.; Nakamura, H.; Fang, J. The EPR effect for macromolecular drug delivery to solid tumors: Improvement of tumor uptake, lowering of systemic toxicity, and distinct tumor imaging in vivo. *Adv. Drug Deliv. Rev.* **2013**, *65*, 71–79.

5. Bae, Y. H.; Park, K. Targeted drug delivery to tumors: myths, reality and possibility. *J. Controlled Release* 2011, *153*, 198.

6. Li, S.-D.; Huang, L. Pharmacokinetics and Biodistribution of Nanoparticles. *Mol. Pharmaceutics*, **2008**, *5* (4), 496–504.

7. Venturoli, D.; Rippe, B. Ficoll and dextran vs. globular proteins as probes for testing glomerular permselectivity: effects of molecular size, shape, charge and deformability. *Am. J. Physiol*. **2005**, *288*, F605–F613.

8. Romberg, B.; Hennink, W. E.; Storm, G. Sheddable coatings for long-circulating nanoparticles. *Pharm. Res*. **2008**, *25*, 55–71.

9. Moghimi, S. M.; Hunter, A. C.; Murray, J. C. Long-circulating and target-specific nanoparticles: Theory to practice. *Pharmacol. Re*V. **2001**, *53*, 283–318.

10. Vittaz, M.; Bazile, D.; Spenlehauer, G.; Verrecchia, T.; Veillard, M.; Puisieux, F.; Labarre, D. Effect of PEO surface density on long-circulating PLA-PEO nanoparticles which are very low complement activators. *Biomaterials* **1996**, *17*, 1575–1581

11. Owens, D. E. III; Peppas, N. A. Opsonization, biodistribution, and pharmacokinetics of polymeric nanoparticles. *Int. J. Pharm*. **2006**, *307*, 93–102.

12. Gref, R.; Lück, M.; Quellec, P.; Marchand, M.; Dellacherie, E.; Harnisch, S.; Blunk, T.; Müller, R. H. 'Stealth' corona-core nanoparticles surface modified by polyethylene glycol (PEG): Influences of the corona (PEG chain length and surface density) and of the core composition on phagocytic uptake and plasma protein adsorption. *Colloids Surf.* **2000**, *18*, 301–313.

13. Verbaan, F. J.; Oussoren, C.; Snel, C. J.; Crommelin, D. J.; Hennink, W. E.; Storm, G. Steric stabilization of poly(2-(dimethylamino)ethyl methacrylate)-based polyplexes mediates prolonged circulation and tumor targeting in mice. *J. Gene Med.* **2004**, *6*, 64-75.

14. Vader, P.; van der Aa, L. J.; Engbersen, J. F.; Storm, G.; Schiffelers, R. M. Physicochemical and Biological Evaluation of siRNA Polyplexes Based on PEGylated Poly(amido amine)s. *Pharm. Res.* 2012, 29(2), 352–361.

15. Crownover, E.; Duvall, C. L.; Convertine, A.; Hoffman, A. S.; Stayton, P. S. RAFT-synthesized Graft Copolymers that Enhance pH-dependent Membrane Destabilization and Protein Circulation Times. *J. Controlled Release* 2011, *155*, 167-174.

16. Molineux, G. PEGylation: engineering improved pharmaceuticals for enhanced therapy. Cancer Treat Rev. **2002**, *28* (Suppl. A), 13−16.

17. Moribe, K.; Maruyama, K. Reviews on PEG coated liposomal drug carriers. *Drug Delivery Syst*. **2001**, *16 (3)*, 165−171.

18. Jeon, S. I.; Andrade, J. D. Protein-surface interactions in the presence of olyethylene oxide: Effect of protein size. *J. Colloid Interf. Sci*. **1991**, *142*, 159-166.

19. Jeon, S. I.; Lee, J. H.; Andrade, J. D.; De Gennes, P. G. Protein-surface interactions in the presence of olyethylene oxide: Simplified theory. *J. Colloid Interf. Sci*. **1991**, 142, 149-158.

20. Fang, C.; Shi, B.; Pei, Y. Y.; Hong, M. H.; Wu, J.; Chen, H. Z. In vivo tumor targeting of tumor necrosis factor-R-loaded stealth nanoparticles: Effect of MePEG molecular weight and particle size. *Eur. J. Pharm. Sci.* **2006**, *27*, 27–36.

21. Gombotz, W. R.; Guanghui, W.; Horbett, T. A.; Hoffman, A. S. Protein adsorption to poly(ethylene oxide) surfaces. *J. Biomed. Mater. Res*. 1991, *25*, 1547–1562.

22. Stolnik, S.; Dunn, S. E.; Garnett, M. C.; Davies, M. C.; Coombes, A. G. A.; Taylor, D. C.; Irving, M. P.; Purkiss, S. C.; Tadros, T. F.; Davis, S. S.; Illum, L. Surface Modification of Poly(lactide-co-glycolide) Nanospheres by Biodegradable Poly(lactide)-Poly(ethylene glycol) Copolymers. *Pharm. Res.* 1994, *11(12),* 1800–1808.

23. Bergström, K.; Holmberg, K.; Safranj, A.; Hoffman, A. S.; Edgell, M. J.; Kozlowski, A.; Hovanes, B. A.; Harris, J. M. Reduction of fibrinogen adsorption on PEG-coated polystyrene surfaces. *J. Biomed. Mater. Res*. 1992, *26(6),* 779–790.

24. Bergström, K.; Osterberg, E.; Holmberg, K.; Hoffman, A. S.; Schuman, T. P.; Kozlowski, A.; Harris, J. M. Effects of branching and molecular weight of surface-bound poly(ethylene oxide) on protein rejection. *J Biomater Sci Polymer Edn*. **1994**, *6*, 123–132.

25. Yang, Z.; Leon, J.; Martin, M.; Harder, J. W.; Zhang, R.; Liang, D.; Lu, W.; Tian, M., Gelovani, J. G.; Qiao, A.; Li, C. Pharmacokinetics and biodistribution of near-infrared fluorescence polymeric nanoparticles. *Nanotechnology* **2009**, *20*, 165101-16511.

26. Liu, D.; Mori, A.; Huang, L. Role of liposome size and RES blockade in controlling biodistribution and tumor uptake of GM1- containing liposomes. *Biochim. Biophys. Acta* **1992**, *1104*, 95– 101.

27. Nagayama, S.; Ogawara, K.; Fukuoka, Y.; Higaki, K.; Kimura, T. Time-dependent changes in opsonin amount associated on nanoparticles alter their hepatic uptake characteristics. *Int. J. Pharm.* **2007**, *342*, 215–221.

28. Kim D. W.; Kim S. Y.; Kim, H. K.; Kim, S. W.; Shin, S. W.; Kim, J. S.; Park, K.; Lee, M. Y. Heo, D. S. Multicenter phase II trial of Genexol-PM, a novel Cremophor-free, polymeric micelle formulation of paclitaxel, with cisplatin in patients with advanced non-small-cell lung cancer. *Ann. Oncol*. **2007**, *18*, 2009–2014.

29. Lee K. S.; Chung, H. C.; Im, S. A.; Park, Y. H.; Kim, C. S.; Kim, S. B.; Rha, S. Y.; Lee, M. Y.; Ro, J. Multicenter phase II trial of Genexol-PM, a Cremophor-free, polymeric micelle formulation of paclitaxel, in patients with metastatic breast cancer. *Breast Cancer Res. Treat*. **2008**, *108*, 241–250.

30. Ryu, J. H.; Chacko, R. T.; Jiwpanich, S.; Bickerton, S.; Babu, R. P.; Thayumanavan, S. Self-Cross-Linked Polymer Nanogels: A Versatile Nanoscopic Drug Delivery Platform. *J. Am. Chem. Soc*. **2010**, *132*, 17227–17235.

31. Ryu, J. H.; Jiwpanich, S.; Chacko, R.; Bickerton, S.; Thayumanavan, S. Surface-Functionalizable Polymer Nanogels with Facile Hydrophobic Guest Encapsulation Capabilities. *J. Am. Chem. Soc*. **2010**, *132*, 8246–8247.

32. Jiwpanich, S.; Ryu, J. H.; Bickerton, S.; Thayumanavan, S. Noncovalent Encapsulation Stabilities in Supramolecular Nanoassemblies, *J. Am. Chem. Soc*. **2010**, *132*, 10683–10685.

33. Saito, G.; Swanson, J. A.; Lee, K. D. Drug delivery strategy utilizing conjugation via reversible disulfide linkages: role and site of cellular reducing activities. *Adv. Drug Delivery Rev*. **2003**, *55*, 199-215.

34. Meister, A.; Anderson, M. E. Glutathione. *Ann. Rev. Biochem*. **1983**, *52*, 711-760.

35. Li, L.; Ryu, J. H.; Thayumanavan, S. Effect of Hofmeister Ions on the Size and Encapsulation Stability of Polymer Nanogels. *Langmuir*, **2013**, *29* (1), 50–55.

36. Ventura, J. Eron, S. J. González-Toro, D. C.; Raghupathi, K.; Wang, F.; Hardy, J. A.; Thayumanavan, S. Reactive Self-Assembly of Polymers and Proteins to Reversibly Silence a Killer Protein. *Biomacromolecules*, **2015**, *16(10)*, 3161–3171.

37. Foulkes, W. D.; Smith, I. E.; and Reis-Filho, J. S. Triple-negative breast cancer. *N. Engl. J. Med*. **2010**, *363*, 1938-1948.

38. Hudis, C. A.; Gianni, L. Triple-Negative Breast Cancer: An Unmet Medical Need. *The Oncologist*. **2011**, *16*, 1–11.

39. Kovar, J. L.; Simpson, M. A.; Schutz-Geschwender, A.; Olive, D. M. A systematic approach to the development of fluorescent contrast agents for optical imaging of mouse cancer models. *Anal Biochem.* **2007**, *367*, 1–12.

40. Weissleder, R. A clearer vision for in vivo imaging. *Nat Biotechnol*. **2001**, *19*, 316–317.

41. Perrault, S. D.; Walkey, C.; Jennings, T.; Fischer, H. C.; Chan, W. C. Mediating tumor targeting efficiency of nanoparticles through design. *Nano letters*. **2009**, *9*, 1909–1915.

42. Alexis, F.; Pridgen, E.; Molnar, L. K.; Farokhzad, O. C. Factors affecting the clearance and biodistribution of polymeric nanoparticles. *Mol Pharm*. **2008**, *5*, 505–515.

43. Nahrendorf, M.; Keliher, E.; Marinelli, B.; Waterman, P.; Feruglio, P. F,; Fexon, L.; Pivovarov, M.; Swirski, F. K,; Pittet, M. J.; Vinegoni, C.; Weissleder, R. Hybrid PET-optical imaging using targeted probes. *Proc. Natl. Acad. Sci. U. S. A*. **2010**, *107*, 7910–7915.

44. Choi, C. H.; Alabi, C. A.; Webster, P.; Davis, M. E. Mechanism of active targeting in solid tumors with transferrin-containing gold nanoparticles. *Proc. Natl. Acad. Sci. U. S. A*. **2010**, *107*, 1235–1240.

45. Blanco, E.; Shen, H.; Ferrari, M. Principles of nanoparticle design for overcoming biological barriers to drug delivery. *Nature Biotechnology*, 2015, *33*, 941-951.

46. Cui, J.; Björnmalm, M.; Liang, K.; Xu, C.; Best, J. P.; Zhang, X.; Caruso F. Super-soft hydrogel particles with tunable elasticity in a microfluidic blood capillary model. *Adv. Mater*. 2014, *26*, 7295–7299.

47. Zhang, L.; Cao, Z.; Li, Y.; Ella-Menye, J.-R.; Bai, T.; Jiang, S. Softer zwitterionic nanogels for longer circulation and lower splenic accumulation. *ACS Nano*, 2012, *6*, 6681–6686.

48. Merkel, T. J.; Chen, K.; Jones, S. W.; Pandya, A. A.; Tian, S.; Napier, M. E.; Zamboni, W. E.; DeSimone, J. M. The effect of particle size on the biodistribution of low-modulus hydrogel PRINT particles. *J. Control. Release*, **2012**, *162*, 37–44.

49. Hage, C.; Gremse, F.; Griessinger, C. M.; Maurer, A.; Hoffmann, S. H. L.; Osl, F.; Pichler, B. J.; Kiessling, F.; Scheuer, W.; Pöschinger, T. Comparison of the Accuracy of FMT/CT and PET/MRI for the Assessment of Antibody Biodistribution in Squamous Cell Carcinoma Xenografts. *J. Nucl. Med*. 2017.

50. Vasquez, K. O.; Casavant, C.; Peterson, J. D. Quantitative Whole Body Biodistribution of Fluorescent-Labeled Agents by Non-Invasive Tomographic Imaging. *PLoS One*, **2011**, *6*, e20594.

51. Ale, A.; Ermolayev, V.; Herzog, E.; Cohrs, C.; de Angelis, M. H.; Ntziachristos, V. FMT-XCT: in vivo animal studies with hybrid fluorescence molecular tomography–X-ray computed tomography. *Nature Methods*, **2012**, *9*, 613-622.

52. Jacques, S.L.; Pogue, B.W. Tutorial on diffuse light transport. *J. Biomed. Opt*. **2008**, 13, 041302.

53. Stuker, F.; Ripoll, J.; Rudin, M. Fluorescence Molecular Tomography: Principles and Potential for Pharmaceutical Research. *Pharmaceutics*, **2011**, *3*, 229-274.

54. Tan, Y.; Jiang, H. Diffuse optical tomography guided quantitative fluorescence molecular tomography. *Appl Opt*. **2008**, *47*, 2011–2016.

55. Tan, Y.; Jiang, H. DOT guided fluorescence molecular tomography of arbitrarily shaped objects. *Med. Phys*. **2008**, *35*, 5703–5707.

56. Ghosh, S.; Basu, S.; Thayumanavan, S. Simultaneous and Reversible Functionalization of Copolymers for Biological Applications. *Macromolecules* 2006, *39*, 5595-5597.

57. Vasquez, K. O.; Casavant, C.; Peterson, J. D. Quantitative Whole Body Biodistribution of Fluorescent-Labeled Agents by Non-Invasive Tomographic Imaging. *PLoS ONE*, **2011**, *6(6),* e20594.

58. Schabel, F.; Griswold, D.; Laster, W.; Corbett, T.; Lloyd, H. Quantitative evaluation of anticancer agent activity in experimental animals. *Pharmac. Ther. A*. **1977**, *1*, 411-435.

59. Corbett, T.; Griswold, D.; Roberts, B.; Peckham, J.; Schabel, F.; Evaluation of single agents and combinations of chemotherapeutic agents in mouse colon carcinomas. *Cancer*, **1977**, *40(5)*, 2660-2690.

60. Schabel, F.; Griswold, D.; Corbett, T.; Laster, R.; Mayo, J.; Lloyd, H. Testing therapeutic hypotheses in mice and man: Observations on the therapeutic activity against advanced solid tumors of mice treated with anticancer drugs that have demonstrated or potential clinical utility for treatment of advanced solid tumors of man. *Methods in Cancer Research* **1979**, *17*, 3-51.

61. Plowman, J, Dykes D, Hollingshead M, Simpson-Herren L, and Alley M. Human tumor xenograft models in NCI drug development. In: Anticancer drug development guide: preclinical screening, clinical trials, and approval. Teicher (ed) Humana Press Inc. 1993.

62. Corbett, T.; Valeriote, F.; LoRusso, P.; Polin, L.; Panchapor, C.; Pugh, S.; White, K.; Knight, J.; Demchik, L.; Jones, J.; Jones, L.; Lowichik, N.; Biernat, L.; Foster. B.; Wozniak, A.; Lisow, L.; Valdivieso, M.; Baker, L.; Leopold, W.; Sebolt, J.; Bissery, M.; Mattes, K.; Dzubow, J.; Rake, J.; Perni, R.; Wentland, M.; Coughlin, S.; Shaw, J. M.; Liversidge, G.; Liversidge, E.; Bruno, J.; Sarpotdar, P.; Moore, R.; Patterson, G. Tumor models and the discovery and secondary evaluation of solid tumor active agents. *Int. J. Pharmacognosy*, **1995**, *33*, 102-122.

63. Corbett, T.; Polin, L.; Roberts, B. J.; Lawson, A. J.; Wilbur, R.; Leopold, W. R.; White, K.; Kushner, J.; Paluch, J.; Hazeldine, S.; Moore, R.; Rake, J.; Horwitz, J. P. Transplantable Syngeneic Rodent Tumors: Solid Tumors of Mice. Tumor Models in Cancer Research, **2002**, Humana Press, 41-71.

CHAPTER 3

EVALUATION OF EFFICACY AND SAFETY OF DOCETAXEL-LOADED NANOGELS IN MICE BEARING TRIPLE NEGATIVE HUMAN MAMMARY CARCINOMA

3.1 Introduction

Hydrophobic therapeutic molecules can suffer from poor bioavailability, hydrolytic or enzymatic instability, and non-specific treatment leading to side effects, low efficacy, short half-life, and frequent administration.[1,2] Many therapeutic candidates fail during development due to poor tolerability or efficacy from these complications. Formulation of drugs through encapsulation, conjugation, emulsion, or nanocrystalline methods can enhance their pharmacokinetic and pharmacodynamics properties through aqueous suspension and shielding the active compound during transport.[3] However, development of drug delivery systems that satisfy a multitude of criteria remains a technical challenge.[4] Several factors can diminish the performance of therapeutic formulations, including non-specific accumulation in healthy tissues, clearance, protein binding, and degradation.[5-7]

Nano-scale formulations have attracted increased attention in the treatment of solid tumor type cancers due to the discovery of the enhanced permeability and retention (EPR) effect.[8, 9] Nanoparticles can migrate through fenestrated neovasculature and accumulate in tumors, and content retention is aided by poor lymphatic drainage.[10] To this end, a variety of nano-scale morphologies have been explored to enhance tumor delivery and protect therapeutic contents, including micelles, liposomes, and polymeric nanoparticles. Some examples of chemotherapeutic formulations include protein complexes such as Abraxane,[11] micelle formulations such as NK105 and Genexol,[12,13] and polymer conjugates such as Opaxio and Cellax.[14-18]

Taxane chemotherapeutics such as such as paclitaxel (PTX) and docetaxel (Doc)

are frequently used to treat a common cancer indications including breast, non-small cell lung cancer, and prostate cancer.[19] However, their solvent-based formulations induce systemic side effects from non-specificity, including neuropathy and neutropenia. Commonly used formulations such as solubilizing agent Cremophor EL can induce hypersensitivity responses in patients. Docetaxel has received increased interest from the Polysorbate 80 formulation, which has reduced toxicity and improved clinical results, but can still cause hypersensitivity responses.[19-21]

For hydrophobic drugs, liposomes can be limited by their lipid bilayer capacity, and can be loaded to a higher extent with aqueously soluble or amphiphilic drugs, such as doxorubicin.[22-25] Further, stability in serum is a concern because encapsulated hydrophobic contents can be subject to burst release in liposomal structures.[22] Micelles, formed through self-assembly of small molecule amphiphiles or detergents, are better candidates for suspension of hydrophobic contents, however they often suffer from high critical aggregation concentrations (CACs) and poor mechanical stability. Polymeric nanoparticles that form micelle-type aggregates, however, generally have greater stability and low CAC values, making them good candidates for use as nano-containers.[26]

Genexol and NK105 are polymeric micelle-type formulations that non-covalently encapsulate PTX and have shown improved pharmacokinetics and efficacy compared to free PTX in preclinical models.[12, 13, 27] However, in clinical trials, drug release in plasma and adsorption to proteins such as serum albumin and alpha-1-glycoprotein led to reduced tumor efficacy and pharmacokinetic profiles like those of free PTX. Non-covalent systems have also been explored with Doc, including encapsulation in PLA-PEG block copolymer assemblies, with surface ligand decoration for the binding of prostate-specific membrane

antigen on prostate cancer cells as well as non-prostate solid tumor neovasculature.[28] In preclinical evaluation, this system demonstrated enhanced accumulation and tumor growth suppression after 12 hours in tumor bearing mice, compared to solvent-based Doc formulations. Further, the plasma concentrations of the Doc-loaded targeted nanoparticle after 24 hours were 100-fold compared to solvent based Doc formulations.

Alternatively, the covalent conjugation of taxanes to polymeric delivery vehicles has been explored in efforts to limit drug partitioning and avoid side effects.[6,29] Some drug-conjugate systems have suffered lower efficacy compared to solubilizing agent-based taxanes administered at the same dose.[30] One system, Opaxio, a conjugate of PTX and polyglutamate, was well tolerated and showed improved efficacy over PTX, but ultimately suffered from degradation in serum, non-specific distribution to the liver, spleen, kidney, and heart, and did not exhibit improvement over classic chemotherapy.[14-16] A taxane-polymer conjugate comprised PEGylated cellulose-Doc has also been explored for antitumor efficacy.[17] This amphiphilic micelle-type aggregate, Cellax, exhibited 5.5-fold tumor uptake and improved efficacy compared to Taxotere, a Polysorbate 80 formulation, and exhibited tumor retention for several days. Cellax demonstrated greater safety with less non-specific accumulation in the kidney, lung and heart compared to Taxotere. The formulation was then evaluated in different tumor models (EMT-6, B16F10, PC3, and MDA-MB-231), and variability in efficacy was observed, which was directly associated with extent of tumor uptake of each model.[18]

We have developed a drug delivery platform based on an amphiphilic random copolymer capable of self-assembly, encapsulation of hydrophobic contents, and core chemical crosslinking. This nanogel design can address limitations of existing systems due

to its highly tailorable size, crosslink percentage, and post-formulation surface PEGylation. We have previously shown that the circulation time and tumor accumulation of these particles can be improved by PEGylation of their surfaces. Here, we aimed to evaluate the preclinical *in vivo* therapeutic efficacy of Doc loaded nanogels in triple negative breast cancer models MDA-MB-231 xenograft, PDX BR1458, PDX BR1474, and PDX BR1282 in BALB/c nude mice. Triple negative breast cancer is often treated with combinatorial chemotherapeutics including anthracyclines, taxanes, and platinum agents. [31] Triple negative breast cancer does not express the genes for estrogen receptor (ER), progesterone receptor (PRE), or human epidermal growth factor receptor 2 (Her2/neu), and is not a candidate for endocrine therapies used to treat other more common forms of breast cancer.[32] Triple negative breast cancers comprise 15-25% of breast cancer cases, and have shorter median relapses and lower survival times. Therefore, nanoparticle-based therapeutics are attractive for treatment of triple negative breast cancer due to their potential to increase target-specific delivery, weaken side effects, and compatibility with combinatorial therapy.

3.2 Results and Discussion

The objective of this study was to evaluate the *in vivo* efficacy of Doc loaded nanogels in triple negative human breast cancer models in BALB/c nude mice. The therapeutic efficacy of two nanogels (NG1 and NG2) loaded with Doc was studied in four triple negative breast cancer models: MDA-MB-231 xenograft, PDX BR1458, PDX BR1474, and PDX BR1282. Efficacy nanogels were studied in the four models, where each model uses 3 arms with 10 mice each. The three arms include: 1.) dose of compound (Doc loaded nanogel), 2.) negative control, and 3.) Doc positive control. The desirable Doc

dosage schedule was 10 mg/kg/week. The dosing will be 4 injections/week for up to 3 weeks, or 10 mg/kG QWx3, where QW = once a week.

3.2.1 Synthesis and Formulation of Docetaxel-Loaded Nanogels

All nanogel characteristics (polymer Mn and monomer composition, as well as particle size, crosslink density, PEG post-modification) were motivated on previously obtained biodistribution results. Previously, the biodistribution nanogels were comprised of a 21.6 K polymer with, monomer ratio PDS:OEG:Cy7 near IR tag of 69:28:3. Aqueous polymer solutions were used to generate 30 nm precursor nanogels, covalently crosslinked 20-30% then post modified with PEG thiols (Mn 2,000) to reach sizes ranging from approximately 30-40 nm. Among other nanogels tested, these samples obtained the highest maximum %ID/g tumor over a 72-hour period. Encapsulation efforts in these nanogels, however, yielded poor Doc loading, with 0.4-0.5 weight percent achieved. Extensive precipitation of the drug was observed during the PEGylation step of formulation, which severely compromised the hydrophobicity of the particle core. Therefore, alternative designs were pursued to with the aim to compromise particle size and PEG content parameters with higher guest encapsulation.

To achieve this, a strategy for post-modification with PEG on the hydrophilic OEG moieties of the polymer assembly, rather than on hydrophobic PDS moieties, was pursued. Orthogonal NHS ester-amine coupling chemistry was chosen as the method to post functionalize the polymer with PEG due to its aqueous phase compatibility. To this end, a random copolymer was synthesized with amine functionality on the terminus of OEG units in the polymer (**Scheme 4**). To optimize aggregation characteristics, random copolymers with various amine composition were made from synthesis of precursors p[(BocNH-OEG_8-

MA)-*co*-PDSMA] by RAFT polymerization, and characterized by ^{1}H NMR spectroscopy. Monomer ratios were determined by relative integrations of the aromatic protons of PDS and ethylene protons of BocNH-OEG to give 28:72, 34:66, and 46:54 BocNH-OEG:PDS for the three polymers. The polymers were determined to have similar molecular weights by GPC with M*n* 14.7 kDa Đ:1.29, M*n* 15.8 kDa Đ:1.4, and M*n* 18.7 kDa Đ:1.3, respectively. The Boc groups were removed by TFA to yield random copolymers p[(NH_2-OEG_8-MA)-*co*-PDSMA 28:72, 34:66, and 46:54. The polymers were then post modified with alkane thiol to substitute half of remaining PDS groups that would not be used for crosslinking, to generate random copolymers p[(NH_2-OEG_8-MA)-*co*-PDSMA-*co*-Dodecyl] 28:36:36, 24:33:33, 46:27:27 for NH_2-OEG:PDS:Dodecyl, as determined by relative integrations of the aromatic protons of PDS, ethylene protons of NH_2-OEG, and ethylene protons of dodecyl.

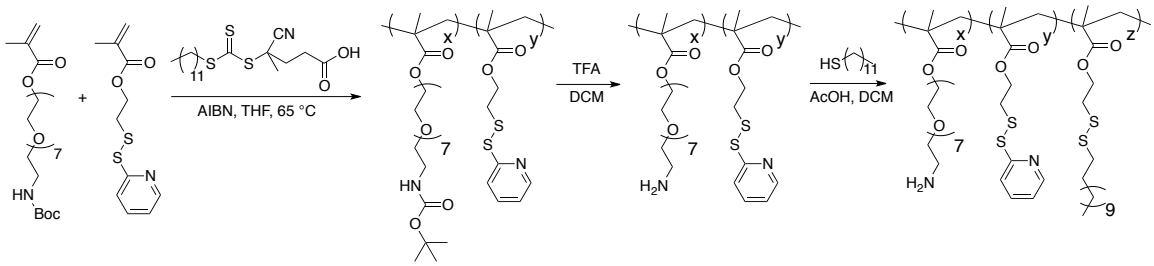

Scheme 4. Synthesis of surface functionalizable amphiphilic random copolymer p[(NH_2-OEG_8-MA)-*co*-PDSMA-*co*-Dodecyl].

The aggregation characteristics of polymers where then monitored by DLS. The polymers were made into an aqueous particle suspension (10 mg/mL) using repeated chill and sonicate cycles. Doc was loaded by dissolving 5 weight % in acetone and adding it to the polymer solution at a 1:1 volume ratio for acetone:water and left stirring open to atmosphere until the acetone evaporated. Aggregates of ~20 nm were achieved at 25 °C with polymer containing 46% NH_2-OEG, but less than 10 nm for 28 and 34% NH_2-OEG

(**Figure 21**). Upon heating the solutions to 45 °C, 46% NH_2-OEG aggregates did not increase above 20 nm while 28 and 34% NH_2-OEG increased slightly to ~10 nm, so crosslinking with DTT was performed at 45 °C. Following crosslinking, post-conjugation was achieved with PEG(2000)-NHS ester (**Scheme 5**). Nanogel were standardized to 1× PBS pH 7.4 by addition of 10× PBS buffer, then brought to pH 8-8.5, and poly(ethylene glycol) methyl ether N-hydroxy succinimide ester (average M_n 2000) was added. The solution was stirred for 48 hours at ambient temperature, and, following dialysis purification, was characterized to be 31, 32, and 25 nm for polymers 28, 34% 46% NH_2-OEG.

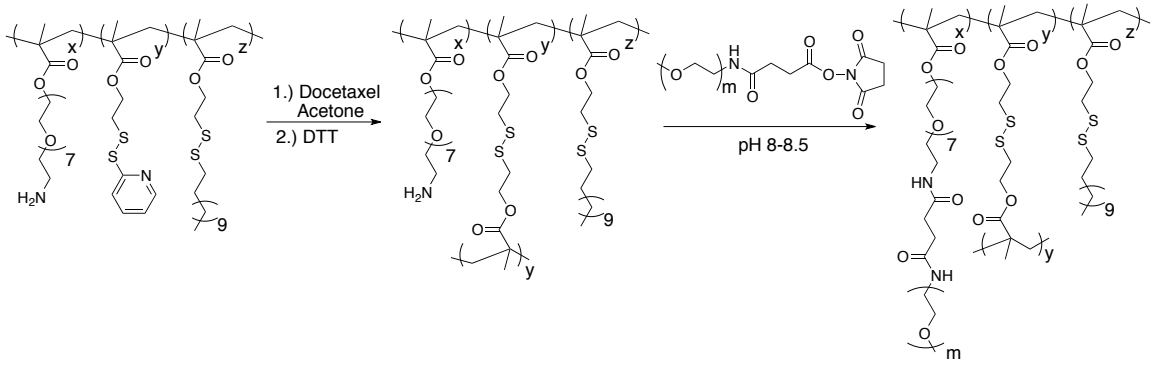

Scheme 5. Synthesis of surface functionalizable amphiphilic random copolymer p[(NH_2-OEG_8-MA)-*co*-PDSMA-*co*-Dodecyl].

Table 5. Characteristics of amine monomer variation random copolymers p[(NH_2-OEG_8-MA)-*co*-PDSMA-*co*-Dodecyl] and resultant nanogel.

NH_2-OEG	PDS	Dodecyl	Mn	Đ	Conditions	Size (nm)
28	36	36	14744 K	1.29	10 mg/mL, 45°C	31
34	33	33	15839 K	1.35	10 mg/mL, 45°C	32
46	27	27	18711 K	1.38	10 mg/mL, 45°C	25

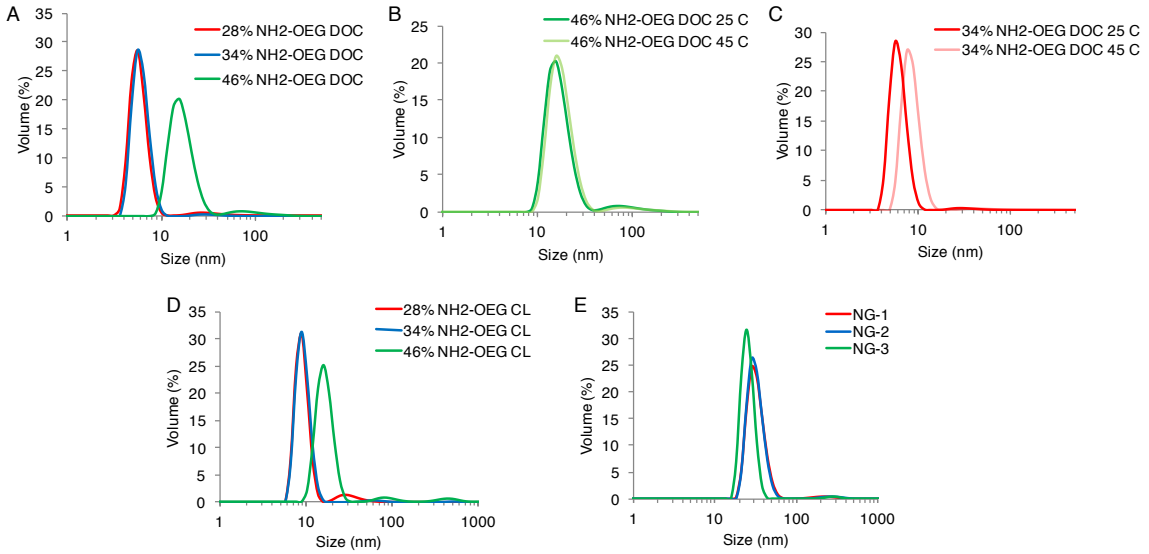

Figure 21. DLS sizes of amine monomer (NH_2-OEG) variation aggregates A) Docetaxel-loaded aggregates, B) temperature responsiveness of 46% NH_2-OEG, C) temperature responsiveness of 34% NH_2-OEG, D) crosslinked aggregates, and E) PEGylated final nanogel sizes, with NG1, NG2, NG3 representing 28% NH_2-OEG, 34% NH_2-OEG and 46% NH_2-OEG polymers, respectively.

From this amine monomer variation, we established that any of these NH_2-OEG ratios could achieve appropriate target sizes with temperature manipulation. Moving forward we aimed to vary the crosslink to dodecyl ratio to investigate any effects on encapsulation efficiency, with ~34% NH_2-OEG polymer. Precursor polymer p[(BocNH-OEG_8-MA)-*co*-PDSMA] of M*n* 16 kDa Đ:1.2, and monomer ratio 36:64 BocNH-OEG:PDS was synthesized, then post modified with 2-dodecanethiol to various extents. Polymers p[(BocNH-OEG_8-MA)-*co*-PDSMA-*co*-Dodecyl] were determined to be 36:64:0, 36:51:13, 36:42:22, and 36:37:27 for BocNH-OEG:PDS:Dodecyl. TFA removal of Boc groups then yielded p[(NH_2-OEG_8-MA)-*co*-PDSMA-*co*-Dodecyl] polymers of the same respective ratios. After aggregate suspension and Doc loading (5 weight %), the two polymers containing 0 and 13% Dodecyl could not be manipulated with temperature or Hoffmeister salts to achieve target sizes. However, ~20 nm aggregates were achieved with

10 mg/mL at 40 °C and 13 or 22 mM Na_2CO_3 for 22 and 27% Dodecyl, respectively (**Figure 22, Table 6**).

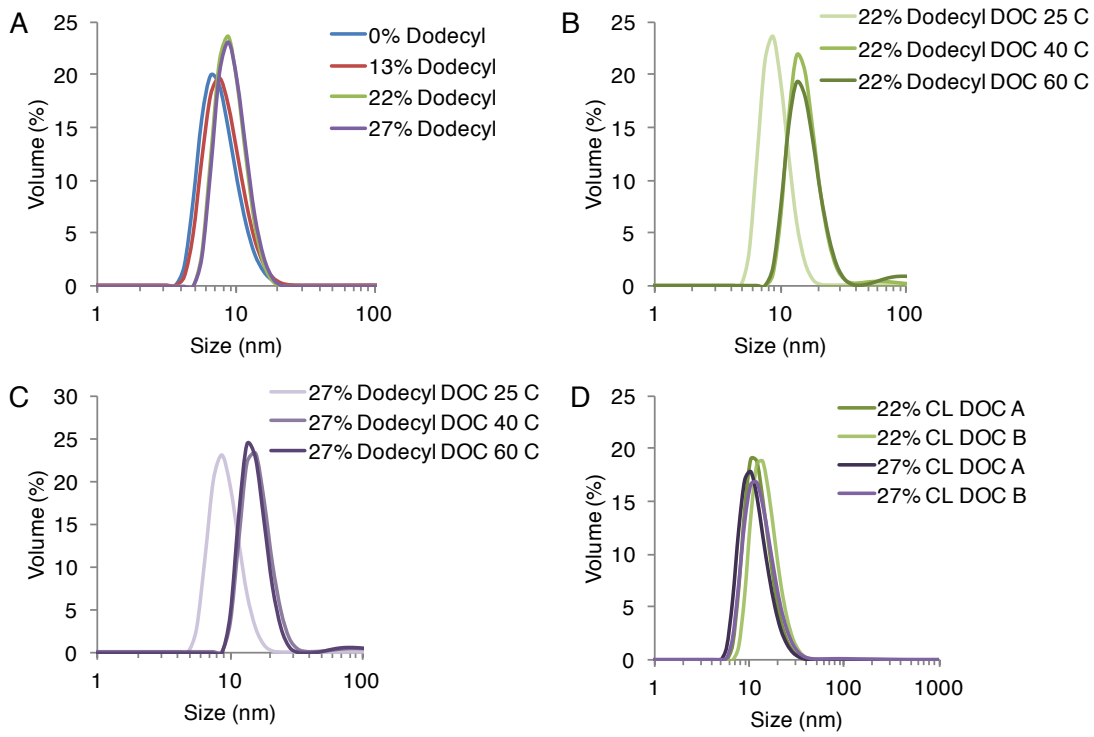

Figure 22. DLS sizes of A) 10 mg/mL aggregates, B) temperature responsiveness of DOC-loaded 22% Dodecyl, C) temperature responsiveness of DOC-loaded 27% Dodecyl, D) replicates of crosslinked 22% DOC Dodecyl and 27% DOC Dodecyl.

Table 6. Characteristics of dodecyl monomer variation random copolymers p[(NH_2-OEG_8-MA)-*co*-PDSMA-*co*-Dodecyl].

NH_2-OEG	PDS	Dodecyl	Mn	Đ	Conditions	Size (nm)
36	64	0	16.2 K	1.2	N/A	N/A
36	15	16.2	16.2 K	1.2	N/A	N/A
36	42	22	16.2 K	1.2	10 mg/mL, 40 °C, 13 mM Na_2CO_3	20 nm
36	37	27	16.2 K	1.2	10 mg/mL, 40 °C, 22 mM Na_2CO_3	20 nm

The Doc loading in these nanogels were then evaluated by HPLC. To do this, a calibration curve of area under the curve (AUC) of absorbance at 214 nm of various Doc concentrations was prepared (**Figure 23**). Docetaxel solutions in methanol were injected at a set volume (20 µL) to and characterized by HPLC using a C18 column (4.6 mm × 10 cm, 2.7 µm particle size) using a gradient mobile phase of acetonitrile 0% to 70%

acetonitrile in water, both containing 0.05% (v/v) trifluoroacetic acid, monitoring absorbance of 214 nm at a flow rate of 1 mL/min. Docetaxel showed consistent retention time of 16.6 min so that AUC for 214 absorbance could be compared for different concentrations of injections. The linear fit for 0.01-1 mg/mL Doc, performed in triplicate, gave R^2=0.99. Thus, concentrations of Doc could be calculated for unknown samples using obtained AUC for absorbance of 214 nm at 16.6 min. These values were obtained by disrupting aggregate encapsulation integrity by adding acetone (1:1 volume %) to nanogel solutions, then characterizing HPLC results of 20 µL of this solution. Nanogels with 22 and 27% dodecyl, prepared in duplicate, achieved average Doc loads of 0.9 and 1.23%, respectively (**Table 7**). With feeds or 5 weight %, this suggests that efficiency was low, with 18 and 25% for nanogels with 22 and 27% dodecyl, respectively.

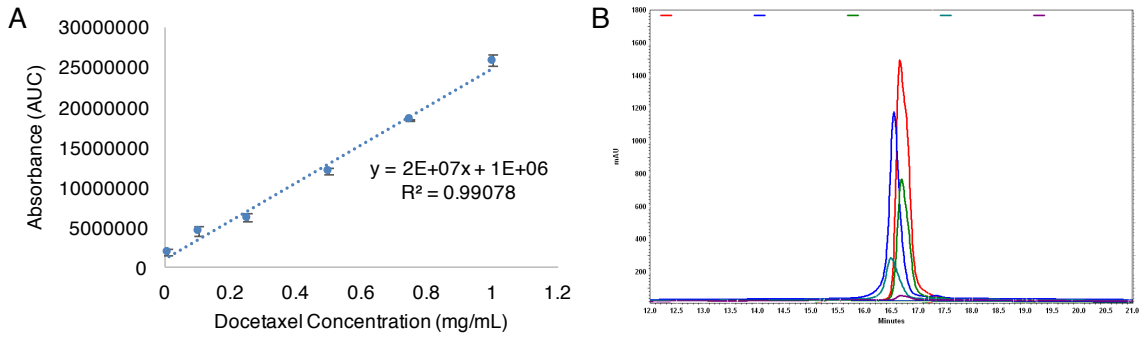

Figure 23. HPLC A) calibration curve of docetaxel from absorbance at 214 nm and B) chromatogram overlays of 0.01-1 mg/mL docetaxel injection with retention time of 16.6 min.

Table 7. Docetaxel loading in dodecyl monomer variation random copolymers p[(NH_2-OEG_8-MA)-*co*-PDSMA-*co*-Dodecyl].

Dodecyl (%)	Doc Feed (wt %)	Doc Load (wt %)	Efficiency (%)
22	5	0.90 ± 0.07	18 ± 1
27	5	1.55 ± 0.46	25 ± 9

From these findings, we estimated encapsulation would be approximately 1 weight % for nanogels of this composition. With the efficacy plan of four models, with 10 mice

each at docetaxel doses desired was 10 mg/kg/week (mouse is approximately 20 g), and two test nanogels, we estimated 2.5 g of polymer would be required for each nanogel to encapsulate sufficient Doc. Larger scale random copolymer p[(BocNH-OEG_8-MA)-*co*-PDSMA] was synthesized by reversible addition-fragmentation chain-transfer (RAFT) polymerization to yield a M*n* of 20.7 kDa. Đ: 1.2 and monomer ratio of 39:61 (BocNH-OEG_8:PDS). The polymer was then post modified with alkane thiol to substitute PDS groups that would not be used for crosslinking, to generate random copolymers p[(BocNH-OEG_8-MA)-*co*-PDSMA-*co*-Dodecyl] 1 and p[(BocNH-OEG_8-MA)-*co*-PDSMA-*co*-Dodecyl] 2, The molar ratio of the three monomers was determined by relative integrations of the aromatic protons of PDS, methoxy protons of OEG, and ethylene protons of dodecyl to give 39:37:24 (BocNH-OEG_8-MA:PDS:Dodecyl) and 36:22:36 (BocNH-OEG_8-MA:PDS:Dodecyl), for 1 and 2 respectively. Then Boc groups were removed by using TFA, to yield random copolymer p[(NH_2-OEG_8-MA)-*co*-PDSMA-*co*-Dodecyl] 1 and p[(NH_2-OEG_8-MA)-*co*-PDSMA-*co*-Dodecyl] 2 with ratios 39:37:24 (NH_2-OEG:PDS:Dodecyl) and 36:22:36 (NH_2-OEG:PDS:Dodecyl), for 1 and 2 respectively.

Table 8. Characteristics of random copolymers p[(NH_2-OEG_8-MA)-*co*-PDSMA-*co*-Dodecyl] and aggregates for efficacy studies.

NH_2-OEG	PDS	Dodecyl	Mn	Đ	Conditions	Size (nm)
36	22	36	20.7 K	1.1	40 mg/mL, 70 °C, 20 mM Na_2CO_3	18 nm

The random copolymer p[(NH_2-OEG_8-MA)-*co*-PDSMA-*co*-Dodecyl] were made into an aqueous particle suspension (40 mg/mL) using repeated chill and sonicate cycles (**Figure 24, Table 8**). Docetaxel was loaded into sample NG1 by dissolving 5 weight % in acetone and adding it to the polymer solution at a 1:1 volume ratio for acetone:water and left stirring open to atmosphere until the acetone evaporated. Control C1 was not loaded with docetaxel. Aggregates of ~20 nm were achieved at 40 mg/mL, 70 °C, and 20 mM

Na_2CO_3 and crosslinked at that size with DTT, and quantified as 100% by UV-vis spectroscopy by release of 2-pyridinethione at 343 nm. Nanogels were standardized to 1× PBS pH 7.4 by addition of 10× PBS buffer, then brought to pH 8-8.5, and poly(ethylene glycol) methyl ether N-hydroxy succinimide ester (average M_n 2000) was added. The solution was stirred for 72 hours at ambient temperature, and, following dialysis purification, was characterized to be 35 nm and 43 nm for nanogels NG1 and C1, respectively. The Doc load in NG1 was characterized by HPLC as described above, and determined to by 1.1 weight %, and efficiency of 22%. NG1 was concentrated using Spectra/Gel Absorbent to 0.5 mg/mL drug (44.3 mg/mL polymer) so that a 100 µL animal injection would be the appropriate dosage. C1, empty nanogel control, was then concentrated to the same polymer concentration for continuity.

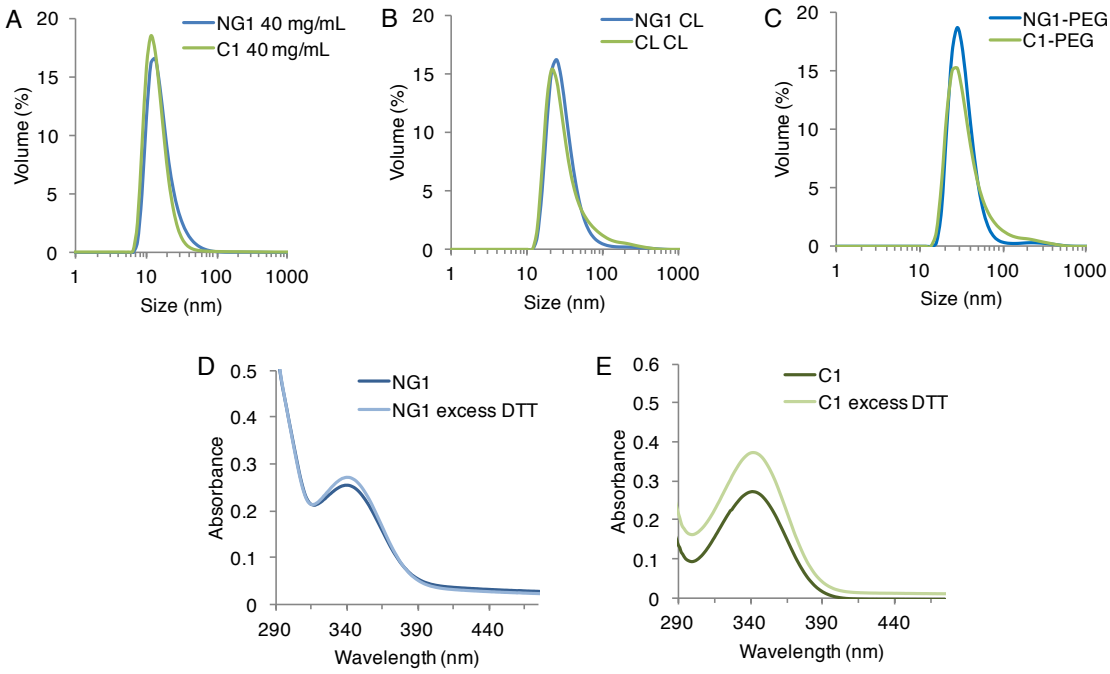

Figure 24. DLS sizes of A) 40 mg/mL Doc-loaded NG1 and empty C1, B) crosslinked NG1 and C1, and C) PEG-conjugated NG1 and C1. UV-vis absorbance spectra of crosslink reaction for D) NG1 and E) C1.

The formulation of a second nanogel with slightly varied dodecyl:PDS (i.e. dodecyl:crosslink), gave aggregates that were larger than 100 nm and highly disperse, and manipulations to concentration and temperature of assembly could not achieve target aggregate sizes. An alternative non-PEGylated nanogel was quickly prepared for testing. Random copolymer p(OEGMA-*co*-PDSMA) was synthesized by reversible addition-fragmentation chain-transfer (RAFT) polymerization to yield a *Mn* of 21.7 kDa. Đ: 1.2, and monomer ratio of 34:66 (OEG:PDS) (**Scheme 6**). The polymer was then post modified with alkane thiol to substitute PDS groups that would not be used for crosslinking, to generate random copolymer p(OEGMA-*co*-PDSMA-*co*-Dodecyl). The molar ratio of the three monomers was determined by relative integrations of the aromatic protons of PDS, methoxy protons of OEG, and ethylene protons of dodecyl to give 34:34:32 (OEG:PDS:Dodecyl). The polymer was made into an aqueous particle suspension (40 mg/mL) using repeated chill and sonicate cycles until the solution appeared dissolved. Aggregates of around 20 nm were achieved at 25 °C, then docetaxel was loaded by dissolving 5 weight % in acetone and adding it to the polymer solution at a 1:1 volume ratio for acetone:water and left stirring open to atmosphere until the acetone evaporated to create NG2 (**Figure 25, Table 9**). Following evaporation, Nanogels NG2 was crosslinked using reducing agent DTT to lock their nanogel size. Crosslink was quantified by release of byproduct 2-pyridinethione by its absorption at 343 nm by UV-vis spectroscopy. Following dialysis, Doc loading was quantified by HPLC against the obtained calibration curve loading of 0.59 weight percent, a 12% loading efficiency, was achieved for nanogel NG2. This nanogel was concentrated using Spectra/Gel Absorbent to 0.5 mg/mL drug (84.6

mg/mL polymer) so that a 100 μL animal injection would be the appropriate dosage (**Table 10**).

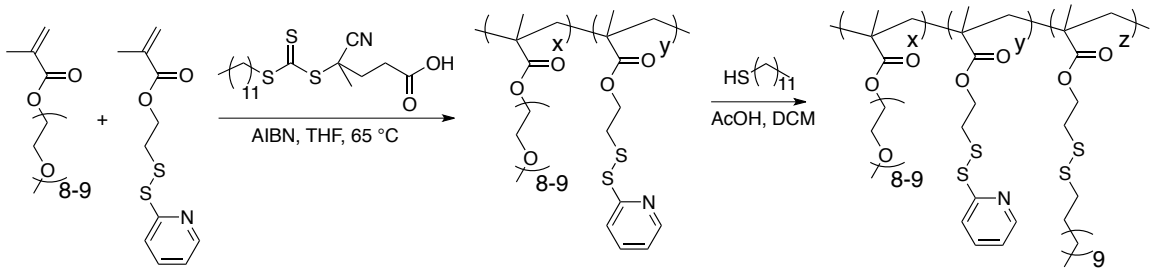

Scheme 6. Synthesis of amphiphilic random copolymer p(OEGMA-*co*-PDSMA-*co*-Dodecyl).

Table 9. Characteristics of random copolymers p(OEGMA-*co*-PDSMA-*co*-Dodecyl) and aggregates for efficacy studies.

OEG	PDS	Dodecyl	Mn	Đ	Conditions	Size (nm)
34	34	32	21.7 K	1.2	40 mg/mL, 25 °C	24 nm

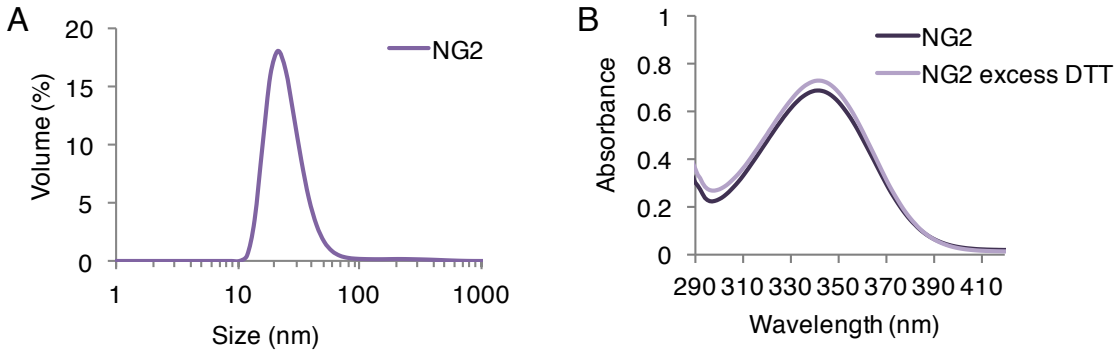

Figure 25. Sample NG2 A) DLS size and B) crosslinking quantification by UV-vis absorbance.

Table 10. Sample information of Nanogels NG1, C1, and NG2 for *in vivo* efficacy studies.

Nanogel	Size (nm)	Doc Load (wt %)	Doc (mg/mL)	Doc (mM)	Nanogel (mg/mL)	Volume (mL)	Drug (total mg)	Nanogel (total g)
NG1	35	1.1	0.5	0.62	44.3	57.6	28.8	2.552
C1	43	0	0	0	44.3	57.6	0	2.552
NG2	24	0.59	0.5	0.62	84.6	33.6	16.7	2.841

3.2.2 Efficacy Study Results Model MDA-MB-231

Due to sample limitations, dosages of docetaxel were adjusted. For model MDA-MB-231 only NG1 and its negative control C1 were tested at a dosage of 8 mg/kg/week

for up to 3 weeks. Treatments with nanogel were initiated when the mean tumor size reached 152 mm^3. The sample administration for model MDA-MB-231 is shown in experimental (**Table 19**). Mice were treated with 100 µL of nanogel sample per injection, 2 mg/kg per injection, and their tumor growth, inhibition, and total body weights were monitored over the treatment period. From the tumor growth curves and tumor growth curves (**Figure 26, Table 11**), NG1 did not demonstrate any significant anti-tumor activity against the orthotopic MDA-MB-231 human breast cancer xenograft model. Free docetaxel inhibited tumor growth by 25% at 24 days of treatment. No adverse effects on body weight was observed with NG1 or C1, however (**Figure 26**).

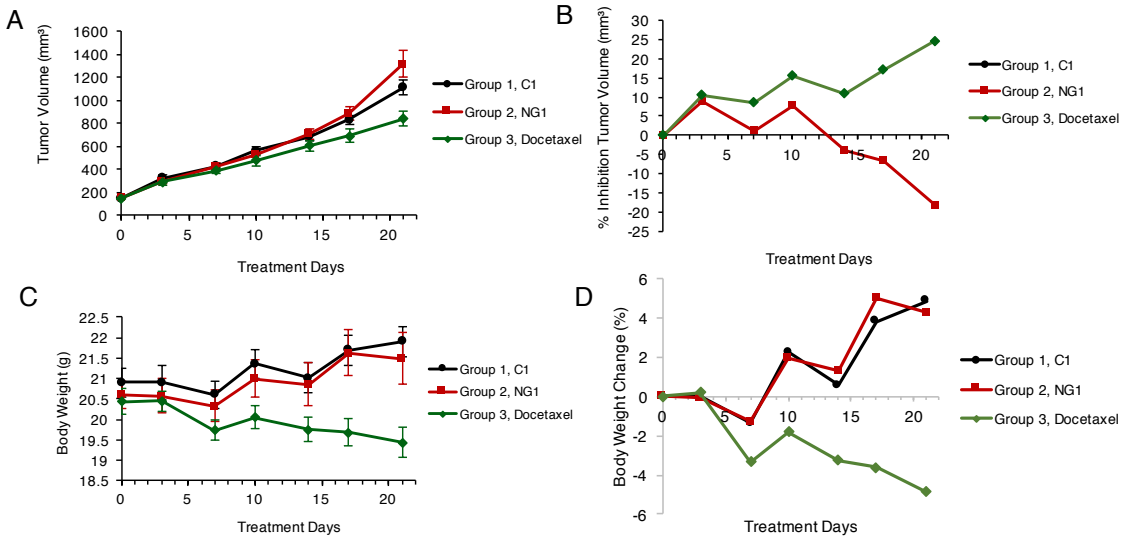

Figure 26. Treatment with C1, NG1, and Docetaxel on orthotopic MDA-MB-231 xenograft model groups A) mean tumor volume B) % inhibition tumor volume C) mean body weight, and D) percent change body weight over 21 days (Mean ± SEM, n = 10 female Musculus BALB/c nude mice).

Table 11. Antitumor Activity on the Treatment of Orthotopic MDA-MB-231 Human Breast Cancer Xenograft Model

Treatment	Tumor size (mm^3)[a] on day 0 of treatment	Tumor size (mm^3)[a] at termination	T/C (%)	*P* value[b]
G1 C1 (0 mg/kg)	151.5 ± 6.5	1111 ± 60	--	--
G2 NG1 (2 mg/kg)	151.5 ± 7.2	1317 ± 114	118.5	0.130
G3 Docetaxel **(**2 mg/kg**)**	151.5 ± 7.1	838 ± 63	75.4	0.006

Note: a. Mean ± SEM; b. Inhibition of test (T) NG1 or Docetaxel compared with the control (C1) at termination; c. compared to control (C1) at termination.

3.2.3 Efficacy Study Results Model BR1474

For model BR1474 also, only NG1 and its negative control C1 were tested at the same dosage of 8 mg/kg/week for up to 3 weeks. Once the mean tumor size reached 150 mm^3, nanogel treatment was initiated. The sample administration for model BR1474 is shown in experimental (**Table 20**). Mice were treated with 100 μL of nanogel sample per injection, 2 mg/kg/week, and their tumor growth, inhibition, and total body weights were monitored over the treatment period. From the tumor growth curves and tumor growth curves (**Figure 27, Table 12**), NG1 did not demonstrate any significant anti-tumor activity against the subcutaneous PDX BR1474 human breast cancer model. Free docetaxel inhibited tumor growth by 25% at 24 days of treatment. No adverse effects on body weight was observed with NG1 or C1, however (**Figure 27**).

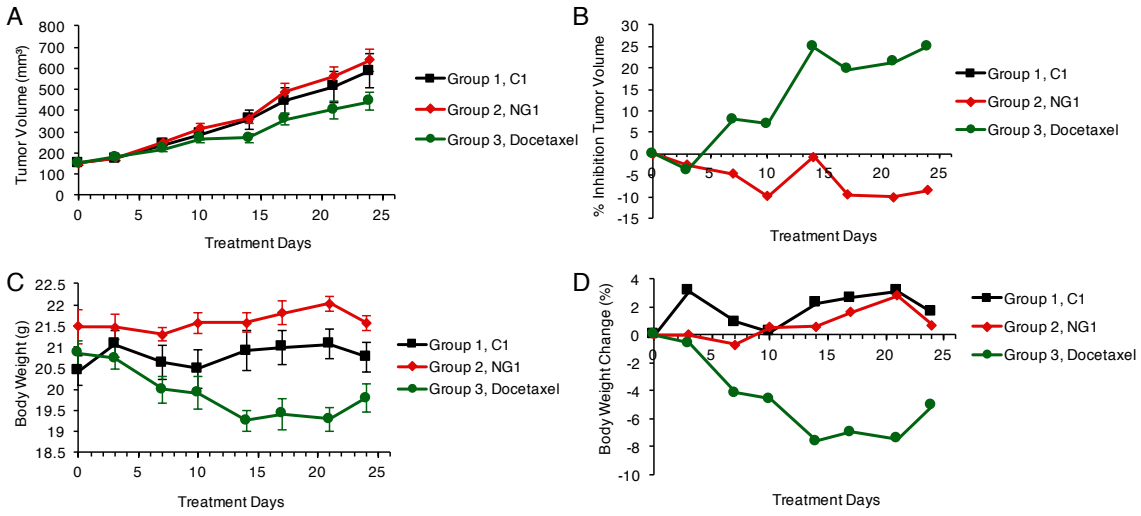

Figure 27. Treatment with C1, NG1, and Docetaxel on subcutaneous PDX BR1474 model groups A) mean tumor volume B) % inhibition tumor volume C) mean body weight, and D) percent change body weight over 24 days (Mean ± SEM, n = 10 female Musculus BALB/c nude mice).

Table 12. Antitumor Activity of in the Treatment of Breast PDX Model BR1474

Treatment	Tumor size (mm^3)[a] on day 0 of treatment	Tumor size (mm^3)[a] on day 24 of treatment	T/C (%)[b]	*P* value[c]
G1 C1 (0 mg/kg)	149.7 ± 9.1	588.0 ± 83.3	-	-
G2 NG1 (2 mg/kg)	149.7 ± 8.8	637.5 ± 50.6	108.42	0.836
G3 Docetaxel (2 mg/kg)	149.7 ± 9.2	441.4 ± 42.3	75.07	0.228

Note: a. Mean ± SEM; b. Inhibition of test (T) NG1 or Docetaxel compared with the control (C1) at termination; c. compared to control (C1) at termination.

3.2.4 Efficacy Study Results Model BR1282

Dosages were then increased to 12 mg/kg/week for model BR1282 in an effort to improve antitumor activity. Both NG1 and NG2 were tested for this model. Once the mean tumor size reached 150 mm^3, nanogel treatment was initiated. The sample administration for model BR1282 is shown in experimental (**Table 21**). Mice were treated with 100 µL of nanogel sample per injection, 3 mg/kg/week, and their tumor growth, inhibition, and total body weights were monitored over the treatment period (**Figure 28, Table 13**). After 2 weeks of dosing no significant tumor inhibition was observed for NG1 (about 3%)

compared to free docetaxel (95%). However, tumor inhibition of about 17% was observed with NG2. The test compound NG2 at 3 mg/kg therefore showed minor antitumor activity in subcutaneous breast PDX models BR1282. The study was terminated at 2 weeks due to adverse effects to body mass observed in free Docetaxel samples, however this dosage in the nanogels were well tolerated (**Figure 28**).

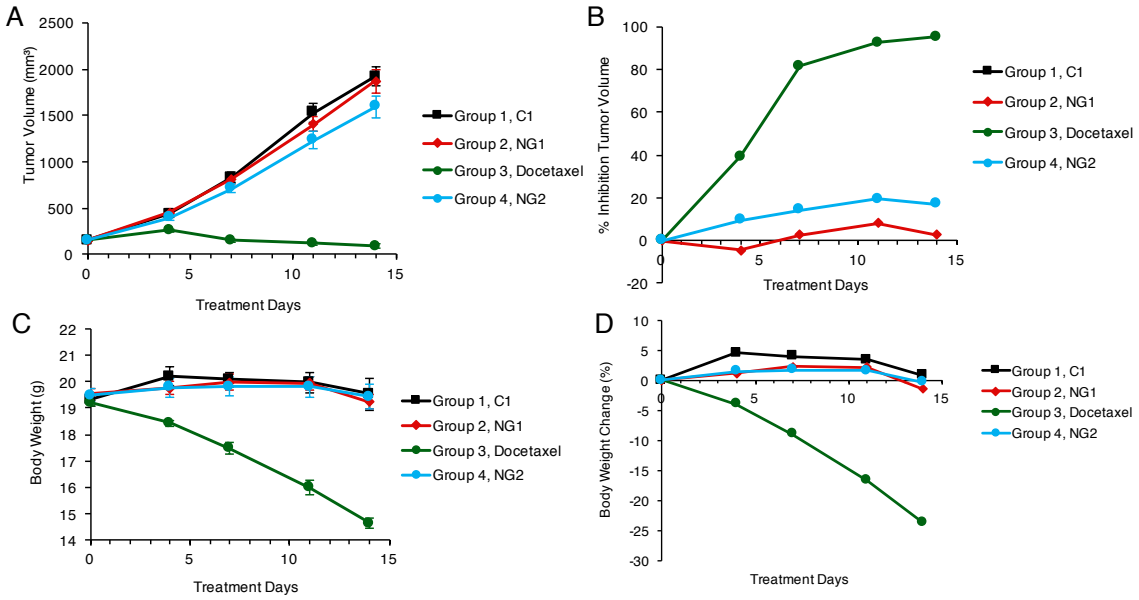

Figure 28. Treatment with C1, NG1, NG2, and Docetaxel on subcutaneous PDX BR1282 model groups A) mean tumor volume B) % inhibition tumor volume C) mean body weight, and D) percent change body weight over 14 days (Mean ± SEM, n = 10 female Musculus BALB/c nude mice).

Table 13. Antitumor Activity of in the Treatment of Breast PDX Model BR1282

Treatment	Tumor size (mm^3)[a] on day 0 of treatment	Tumor size (mm^3)[a] on day 14 of treatment	T/C (%)[b]	*P* value[c]
G1 C1 (0 mg/kg)	150.2 ± 8.0	1917.7 ± 101.2	-	-
G2 NG1 (3 mg/kg)	150.2 ± 7.8	1869.2 ± 124.1	97.47	0.990
G3 Docetaxel (3 mg/kg)	150.2 ± 8.9	92.3 ± 20.0	4.81	<0.001
G4 NG2 (3 mg/kg)	150.2 ± 8.4	1593.6 ± 120.3	83.10	0.206

Note: a. Mean ± SEM; b. Inhibition of test (T) NG1 or Docetaxel compared with the control (C1) at termination; c. compared to control (C1) at termination

3.2.5 Efficacy Study Results Model BR1458

For model BR1458 dosing was returned to 8 mg/kg/week for up to 3 weeks due to sample limitations. Both NG1 and NG2 were tested for this model. Once the mean tumor size reached 153 mm^3, nanogel treatment was initiated. The sample administration for model BR1458 is shown in experimental (**Table 22**). Mice were treated with 100 µL of nanogel sample per injection, 2 mg/kg/week, and their tumor growth, inhibition, and total body weights were monitored over the treatment period (**Figure 29, Table 14**). For this model, both NG1 and NG2 exhibited some antitumor effect (**Figure 29**). At day 24 the percent tumor inhibition was approximately 31% for NG1 and 44% for NG2, compared to 76% for free docetaxel. The efficacy of these nanogels was observed without any adverse effects observed for body weight, however was not an improvement in tumor inhibition compared to free docetaxel (Figure X).

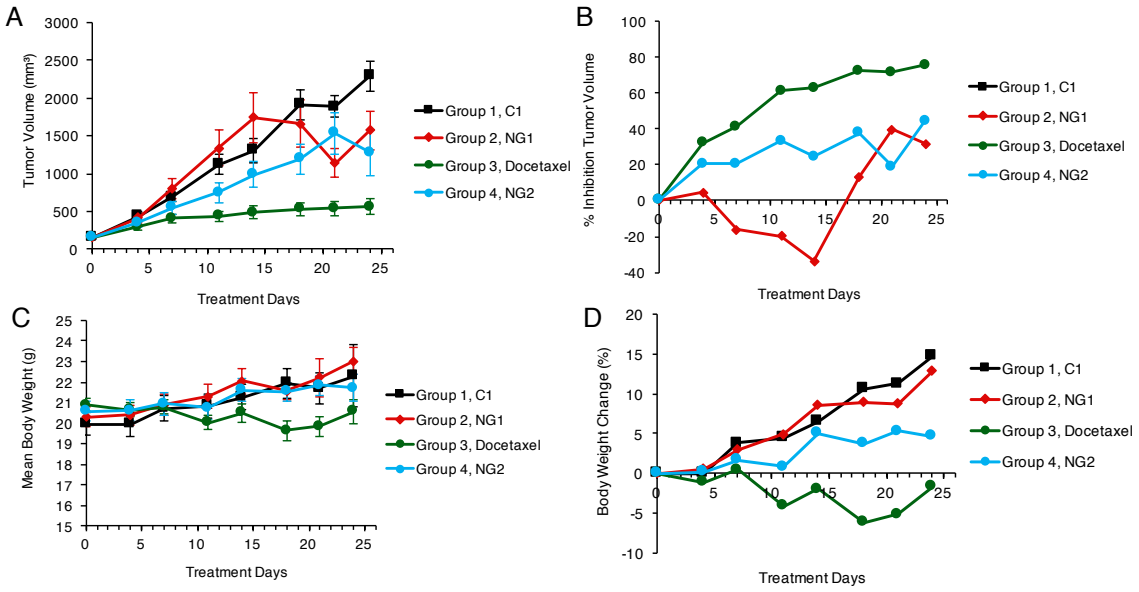

Figure 29. Treatment with C1, NG1, NG2, and Docetaxel on subcutaneous PDX BR1458 model groups A) mean tumor volume B) % inhibition tumor volume C) mean body weight, and D) percent change body weight over 24 days (Mean ± SEM, n = 10 female Musculus BALB/c nude mice).

Table 14. Antitumor Activity of in the Treatment of Breast PDX Model BR1458

Treatment	Tumor size (mm^3)[a] on day 0 of treatment	Tumor size (mm^3)[a] on day 14 of treatment	T/C (%)[b]	*P* value[c]
G1 C1 (0 mg/kg)	153.2 ± 21.5	1305.5 ± 155.2	-	-
G2 NG1 (2 mg/kg)	153.0 ± 21.1	1744.1 ± 331.8	133.60	0.913
G3 Docetaxel (2 mg/kg)	153.1 ± 20.8	484.2 ± 80.8	37.09	0.001
G4 NG2 **(**2 mg/kg**)**	153.0 ± 20.9	987.8 ± 166.5	75.66	0.467

Note: a. Mean ± SEM; b. Inhibition of test (T) NG1 or Docetaxel compared with the control (C1) at termination; c. compared to control (C1) at termination.

3.3 Conclusion

In this study, the therapeutic efficacy of docetaxel-loaded nanogels were evaluated in the treatment of human mammary orthotopic MDA-MB-231 xenograft model, and subcutaneous PDX models BR1474 BR1282 and BR1458. Polymeric nanogels were synthesized, optimized in terms of monomer composition and particle size, and docetaxel load was quantified by HPLC. Tumor-bearing mice were then treated with regimens of nanogels and any tumor inhibition or adverse effects were monitored. The results of these studies showed some anti-tumor activity for NG2 in model BR1282 and anti-tumor activity both NG1 and NG2 for model BR1458. These initial results obtained for these particles may have several opportunities for improvement in the future. The tunability in particle size, surface composition, and guest encapsulation allows for greater optimization in investigation of tumor inhibition. Furthermore, the opportunity for active targeting may further improve the tumor cell uptake and tumor inhibition with these docetaxel-loaded particles.

3.4 Experimental

3.4.1 Materials and Methods

Methacryloyl chloride, O-(hydroxyl)-O′-[2-(Boc-amino)ethyl]heptaethylene glycol (BocNH-OEG$_8$-OH), D,L-dithiothreitol (DTT), 1-dodecanethiol, poly(ethylene glycol) methyl ether N-hydroxy succinimide ester (average M_n 2000), 4-cyano-4-[(dodecylsulfanylthiocarbonyl)sulfanyl]pentanoic acid, trifluoroacetic acid, and other conventional reagents were obtained from commercial sources and without further purification, unless otherwise mentioned. AIBN (2,2'-azobis(2-methylpropionitrile) was purchased from Sigma Aldrich and purified by recrystallization. Pyridyl disulfide ethyl methacrylate (PDSMA) was prepared as previously reported.[44] Docetaxel was for nanogel encapsulation was obtained by TCI, while free docetaxel was obtained by Jiang Su Heng Rui Medicine Co. Ltd, Lot no.: 15081816 (light yellow-yellow clear viscous liquid, 20 mg in 0.5ml/vial, stored at 4 ºC). Polymers were synthesized using RAFT polymerization and purified by dialysis using a membrane with 3500 MWCO. ^{1}H-NMR spectra were recorded on a 400 MHz Bruker NMR spectrometer using the residual proton resonance of the deuterated solvent as the internal standard. Polymer molecular weights were estimated by gel permeation chromatography (GPC, Waters) using THF as eluent at a flow rate of 1 mL/min by a refractive index detector compared to PMMA standard. Dynamic light scattering (DLS) measurements were conducted using a Malvern Nanozetasizer. UV-visible absorption spectra were recorded on a PerkinElmer Lambda 35 UV/Vis Spectrophotometer. Docetaxel calibration was conducted by High performance liquid chromatography was conducted using a Shimadzu Prominence Modular HPLC. Separations were performed using a C18 column (4.6 mm × 10 cm, 2.7 μm particle size)

using a gradient mobile phase of acetonitrile, both containing 0.05% (v/v) trifluoroacetic acid, monitoring absorbance of 214 nm at a flow rate of 1 mL/min.

3.4.2 Experimental Procedures

Synthesis of monomer BocNH-OEG$_8$-MA: To a round bottom flask BocNH-OEG$_8$-OH (3.0 g, 6.38 mmol) and triethylamine (1.08 mL, 7.67 mmol) were dissolved in DCM and under argon at ambient temperature. Then methacryloyl chloride (0.749, 7.67 mmol) was added dropwise and allowed to stir for 10 hours. The crude reaction was dried under reduced pressure, then purified by Combiflash column chromatography using ethyl acetate: methanol 95:5 as eluent. The pure product BocNH-OEG$_8$-MA was isolated as a clear oil (90% yield) and analyzed by ^{1}H NMR (400 MHz, $CDCl_3$) δ (ppm): 6.11 (s, 1H, CH), 5.56 (s, 1H, CH), 5.04 (s, 1H, NH), 4.29 (t, J = 4.84 Hz, 2H, CH_2), 3.37 (t, J = 4.84 Hz, 2H, CH_2), 3.64 (m, 24H, 12×CH_2), 3.52 (t, J = 4.72 Hz, 2H, CH_2), 3.31 (q, J = 5.04 Hz, 2H, CH_2), 1.94 (s, 3H, CH_3), 1.43 (s, 9H, 3×CH_3).

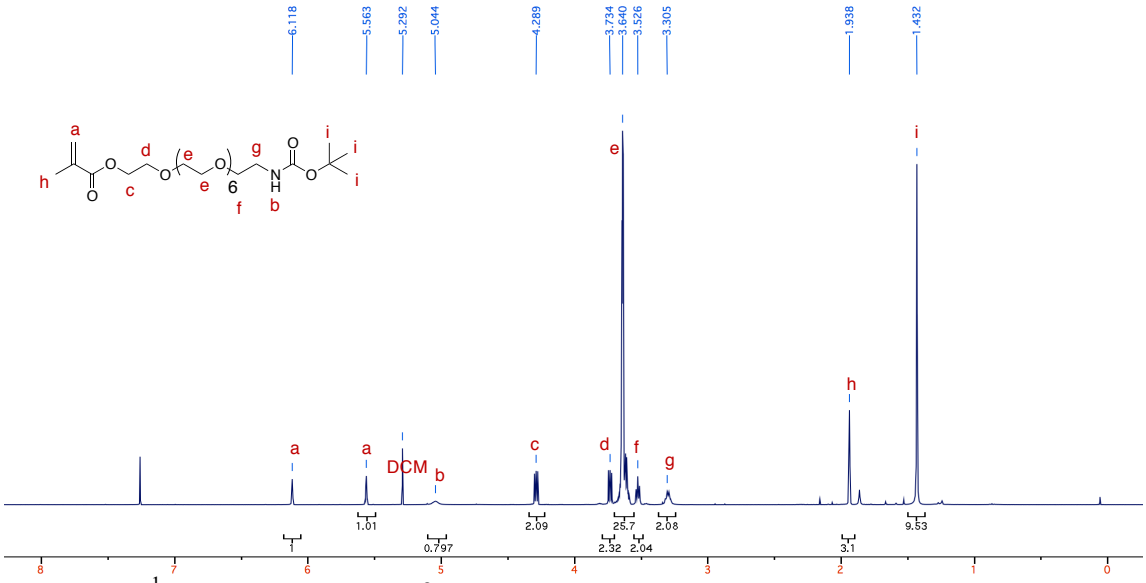

Figure 30. ^{1}H-NMR spectrum of monomer BocNH-OEG$_8$-MA.

Synthesis of random copolymer p[(BocNH-OEG$_8$-MA)-*co*-PDSMA] A (28:72): To a Schlenk-flask, monomers PDSMA (203 mg, 0.79 mmol), BocNH-OEG$_8$-MA (183 mg, 0.34 mmol), chain transfer agent 4-cyano-4-[(dodecylsulfanylthiocarbonyl)sulfanyl]pentanoic acid (6.2 mg, 0.015 mmol), and AIBN (0.5 mg, 0.003 mmol) were dissolved in THF (0.5 mL). The mixture was degassed by performing three freeze-pump-thaw cycles and filled with argon. The reaction mixture was then sealed and transferred into a pre-heated oil bath at 65 °C and stirred for 24 h. The reaction flask was submerged in an ice bath to quench the polymerization, then dialyzed against dichloromethane in MWCO 3500 membrane for 48 hours to remove unreacted monomers. The solution was dried to yield the random copolymer as an oil. GPC (THF) *Mn*: 14.7 kDa. Đ: 1.3. ^{1}H NMR (400 MHz, CDCl3) δ: 8.38, 7.60, 7.03, 5.03, 4.46-3.88, 3.87-3.32, 3.23, 2.96, 2.20-1.58, 1.37, 1.27-0.63 ppm. The molar ratio of the two monomers in the polymer were determined by relative integrations of the aromatic protons of PDS and methylene protons of OEG to give 28:72 (BocNH-OEG$_8$-MA:PDS).

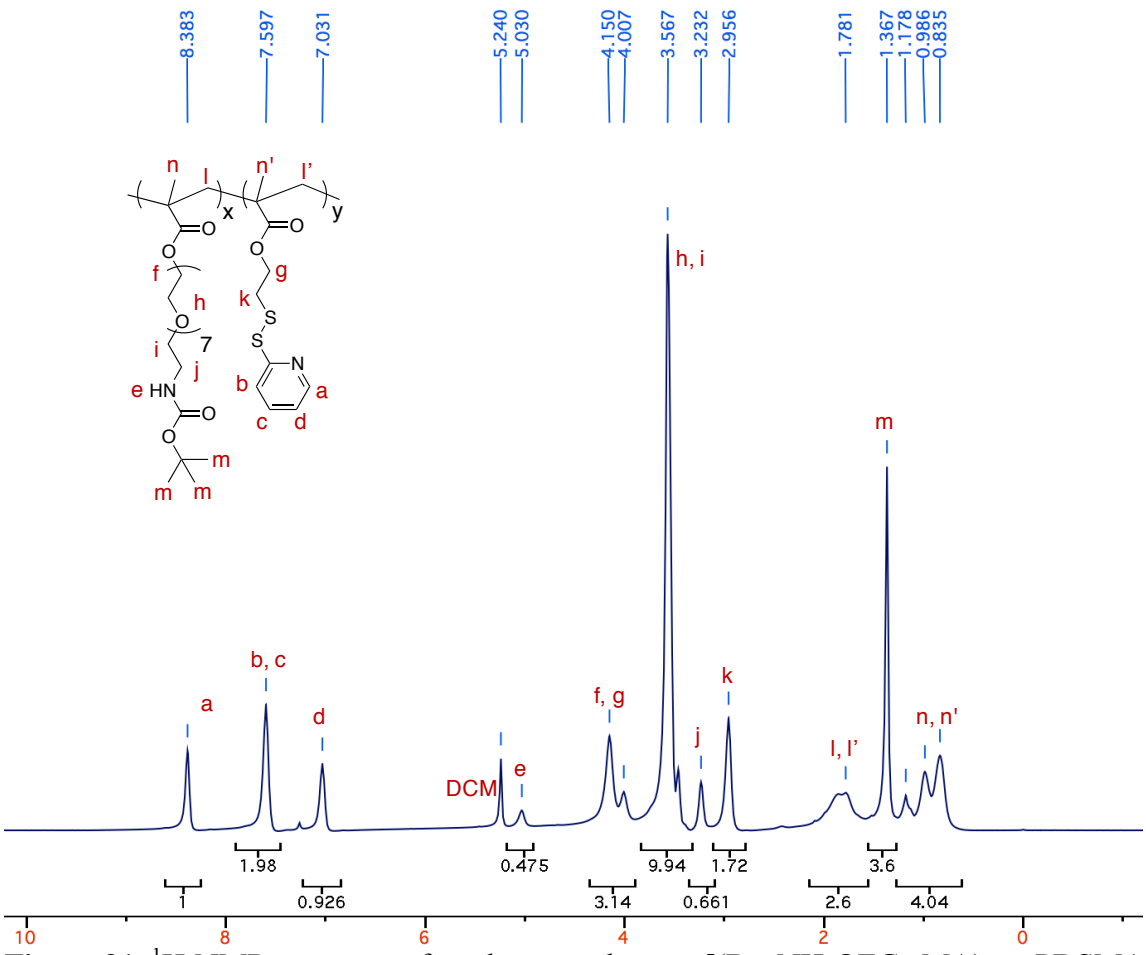

Figure 31. ^{1}H-NMR spectrum of random copolymer p[(BocNH-OEG$_8$-MA)-*co*-PDSMA] A (28:72).

Synthesis of random copolymer p[(BocNH-OEG$_8$-MA)-*co*-PDSMA] B (34:66): To a Schlenk-flask, monomers PDSMA (134 mg, 0.52 mmol), BocNH-OEG$_8$-MA (188 mg, 0.33 mmol), chain transfer agent 4-cyano-4-[(dodecylsulfanylthiocarbonyl)sulfanyl]pentanoic acid (4.8 mg, 0.012 mmol), and AIBN (0.4 mg, 0.0024 mmol) were dissolved in THF (0.5 mL). The mixture was degassed by performing three freeze-pump-thaw cycles and filled with argon. The reaction mixture was then sealed and transferred into a pre-heated oil bath at 65 °C and stirred for 24 h. The reaction flask was submerged in an ice bath to quench the polymerization, then dialyzed against dichloromethane in MWCO 3500 membrane for 48 hours to remove unreacted

monomers. The solution was dried to yield the random copolymer as an oil. GPC (THF) *Mn*: 15.8 kDa. Đ: 1.4. ^{1}H NMR (400 MHz, $CDCl_3$) δ: 8.40, 7.61, 7.05, 5.04, 4.33-3.87, 3.82-3.33, 3.24, 2.97, 2.09-1.51, 1.38, 1.09-0.64 ppm. The molar ratio of the two monomers in the polymer were determined by relative integrations of the aromatic protons of PDS and methylene protons of OEG to give 34:66 (BocNH-OEG$_8$-MA:PDS).

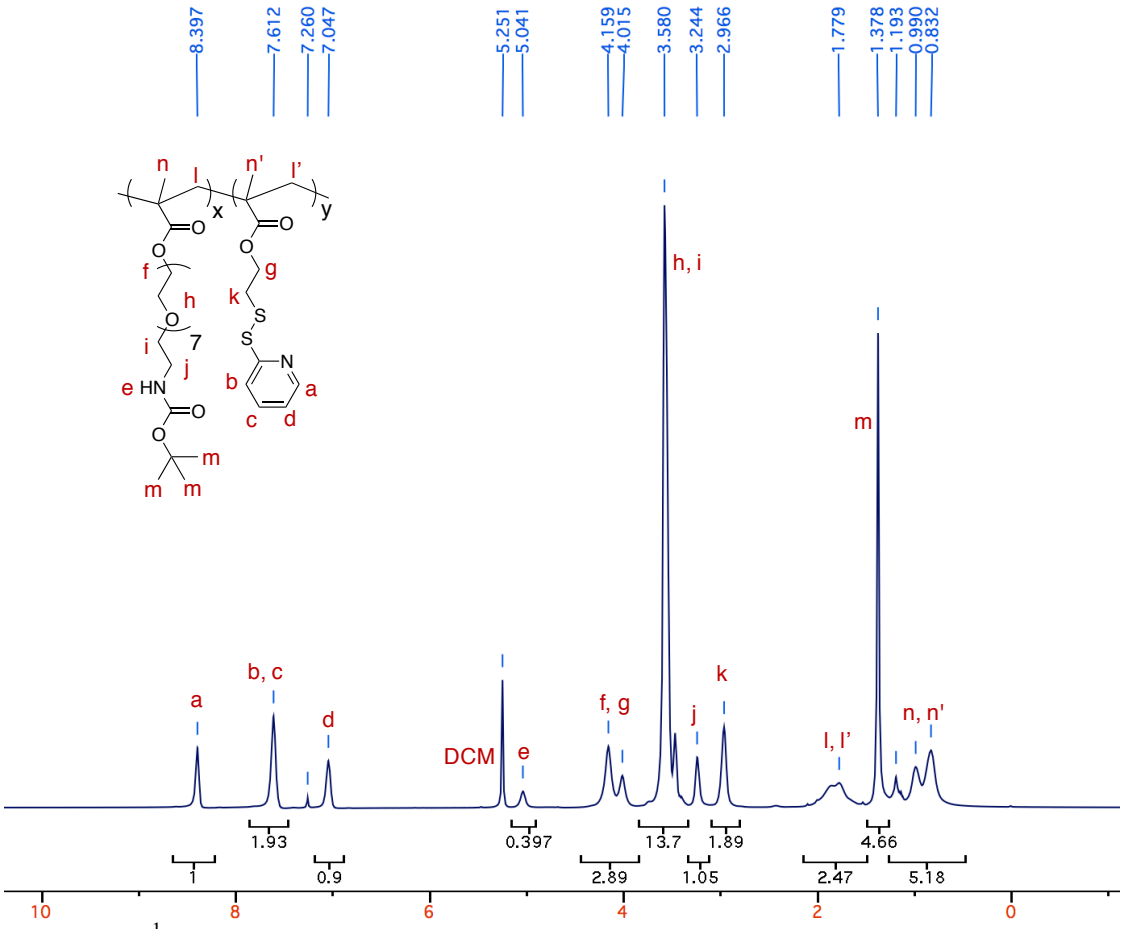

Figure 32. ^{1}H-NMR spectrum of random copolymer p[(BocNH-OEG$_8$-MA)-*co*-PDSMA] B (34:66).

Synthesis of random copolymer p[(BocNH-OEG$_8$-MA)-*co*-PDSMA] C (46:54): To a Schlenk-flask, monomers PDSMA (95 mg, 0.37 mmol), BocNH-OEG$_8$-MA (200 mg, 0.37 mmol), chain transfer agent 4-cyano-4-[(dodecylsulfanylthiocarbonyl)sulfanyl]pentanoic acid (4.1 mg, 0.010 mmol), and AIBN (0.33 mg, 0.002 mmol) were dissolved in THF (0.5

mL). The mixture was degassed by performing three freeze-pump-thaw cycles and filled with argon. The reaction mixture was then sealed and transferred into a pre-heated oil bath at 65 °C and stirred for 24 h. The reaction flask was submerged in an ice bath to quench the polymerization, then dialyzed against dichloromethane in MWCO 3500 membrane for 48 hours to remove unreacted monomers. The solution was dried to yield the random copolymer as an oil. GPC (THF) *Mn*: 18.7 kDa. Đ: 1.3. ^{1}H NMR (400 MHz, $CDCl_3$) δ: 8.44, 7.65, 7.09, 5.07, 4.37-3.93, 3.85-3.37, 3.28, 3.00, 2.12-1.59, 1.41, 1.29-0.70 ppm. The molar ratio of the two monomers in the polymer were determined by relative integrations of the aromatic protons of PDS and methylene protons of OEG to give 46:54 (BocNH-OEG_8-MA:PDS).

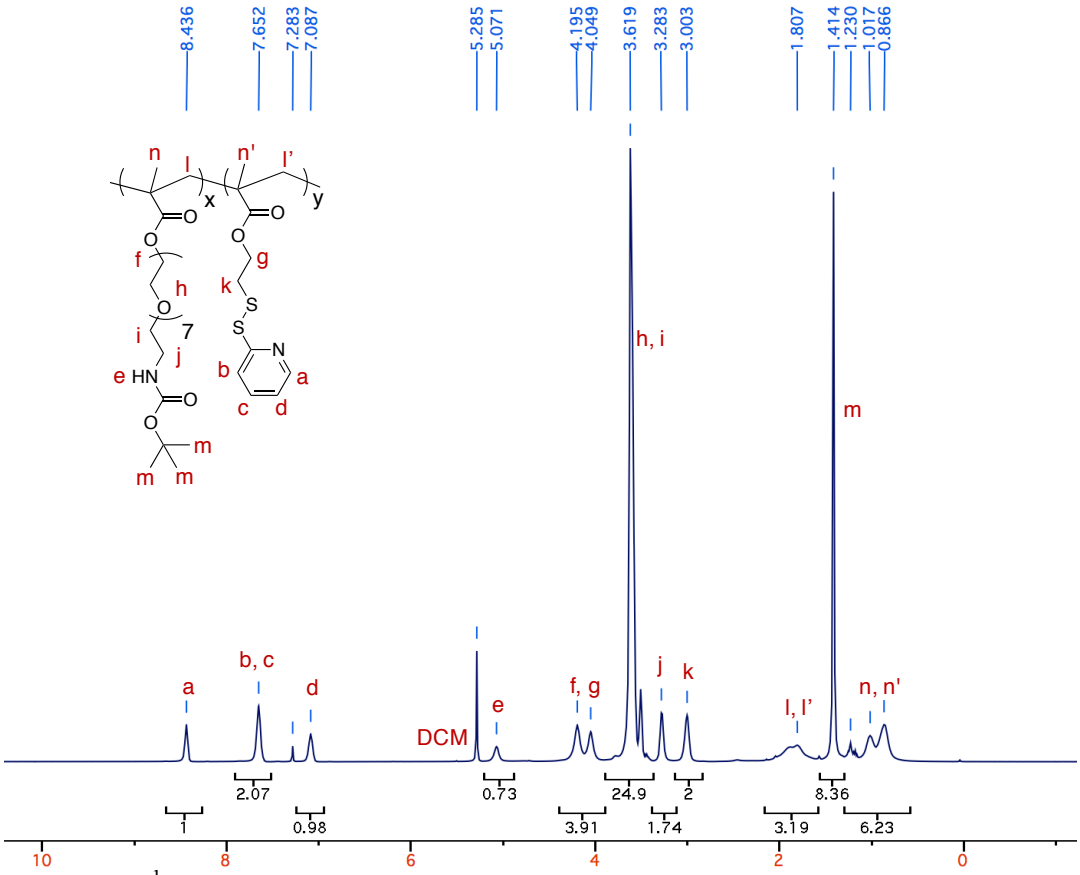

Figure 33. ^{1}H-NMR spectrum of random copolymer p[(BocNH-OEG_8-MA)-*co*-PDSMA] C (46:54).

Synthesis of random copolymer p[(NH_2-OEG_8-MA)-*co*-PDSMA] A (28:72): To a round bottom flask polymer p[(BocNH-OEG_8-MA)-*co*-PDSMA] A (300 mg) was dissolved in DCM (1.5 mL) and purged with argon. Then trifluoroacetic acid (1.5 mL) was added and the mixture was stirred for 12 hours at ambient temperature. The mixture was evaporated under reduced pressure, then purified by dialysis against dichloromethane then acetone in a MWCO 3500 regenerated cellulose membrane for 48 hours. The solution was dried to yield p[(NH_2-OEG_8-MA)-*co*-PDSMA] as a waxy oil. ^{1}H NMR (400 MHz, $CDCl_3$) δ: 8.45, 7.69, 7.12, 4.42-3.94, 3.87-3.37, 3.15, 3.09, 2.12-1.58, 1.32-0.62 ppm. The reaction completion was confirmed by the disappearance of Boc group (δ: 1.38 ppm).

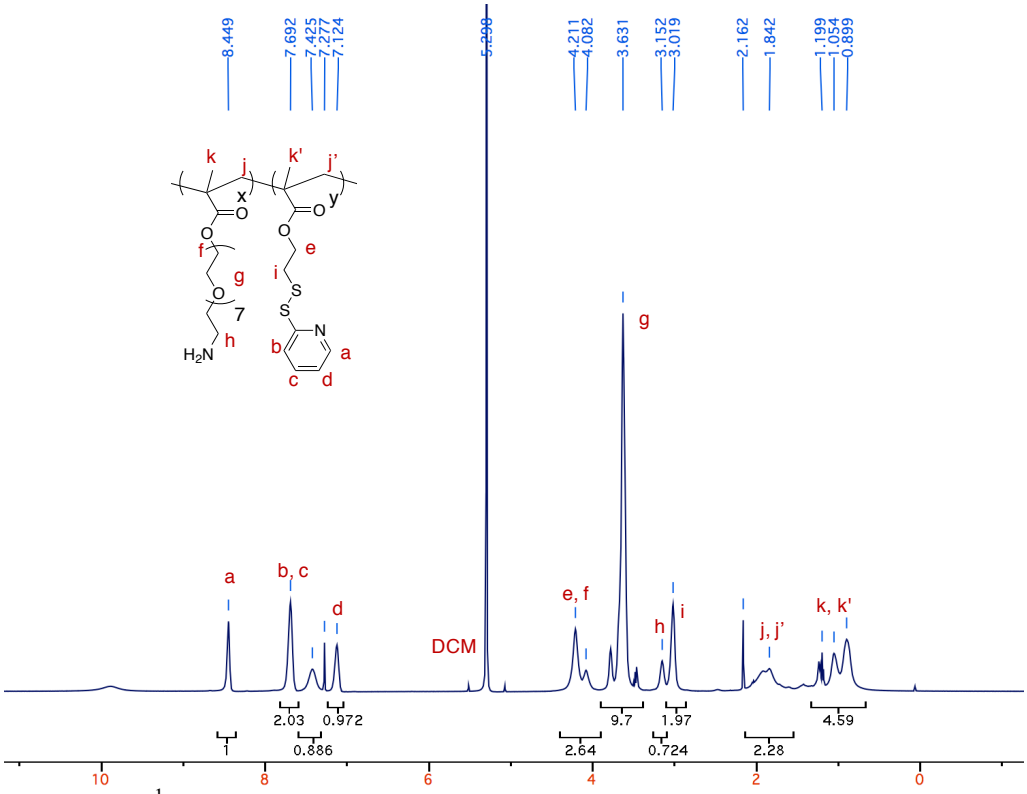

Figure 34. ^{1}H-NMR spectrum of random copolymer p[(NH_2-OEG_8-MA)-*co*-PDSMA] A (28:72).

Synthesis of random copolymer p[(NH_2-OEG_8-MA)-*co*-PDSMA] B (34:66): To a round bottom flask polymer p[(BocNH-OEG_8-MA)-*co*-PDSMA] B (180 mg) was

dissolved in DCM (1.5 mL) and purged with argon. Then trifluoroacetic acid (1.5 mL) was added and the mixture was stirred for 12 hours at ambient temperature. The mixture was evaporated under reduced pressure, then purified by dialysis against dichloromethane then acetone in a MWCO 3500 regenerated cellulose membrane for 48 hours. The solution was dried to yield p[(NH_2-OEG_8-MA)-*co*-PDSMA] as a waxy oil. ^{1}H NMR (400 MHz, $CDCl_3$) δ: 8.46, 7.67, 7.12, 4.37-3.97, 4.85-3.41, 3.17, 3.03, 2.11-1.71, 1.20-0.75 ppm. The reaction completion was confirmed by the disappearance of Boc group (δ: 1.21 ppm).

Synthesis of random copolymer p[(NH_2-OEG_8-MA)-*co*-PDSMA] C (46:54): To a round bottom flask polymer p[(BocNH-OEG_8-MA)-*co*-PDSMA] C (160 mg) was dissolved in DCM (1.5 mL) and purged with argon. Then trifluoroacetic acid (1.5 mL) was added and the mixture was stirred for 12 hours at ambient temperature. The mixture was evaporated under reduced pressure, then purified by dialysis against dichloromethane then acetone in a MWCO 3500 regenerated cellulose membrane for 48 hours. The solution was dried to yield p[(NH_2-OEG_8-MA)-*co*-PDSMA] as a waxy oil. ^{1}H NMR (400 MHz, $CDCl_3$) δ: 8.45, 7.69, 7.12, 4.36-3.94, 3.87-3.40, 3.24-2.92, 2.11-1.54, 1.13-0.71 ppm. The reaction completion was confirmed by the disappearance of Boc group (δ: 1.21 ppm).

Synthesis of random copolymer p[(NH_2-OEG_8-MA)-*co*-PDSMA-*co*-Dodecyl] A (28:36:36): To a round bottom flask polymer p[(NH_2-OEG_8-MA)-*co*-PDSMA-*co*-Dodecyl] A (40 mg, 0.09 mmol PDS) and 1-dodecanethiol (6.2 μL, 0.045 mmol) was dissolved in DCM (2 mL) and purged with argon. Then glacial acetic acid (3 μL) was added and the mixture was stirred for 12 hours at ambient temperature. The mixture was

purified by dialysis against dichloromethane in a MWCO 3500 regenerated cellulose membrane for 72 hours. The solution was dried to yield p[(NH_2-OEG_8-MA)-*co*-PDSMA-*co*-Dodecyl] as a waxy oil. ^{1}H NMR (400 MHz, CDCl3) δ: 8.48, 7.79, 7.27, 4.43-4.07, 3.91-3.56, 3.29, 3.21, 3.06, 2.85, 1.94, 1.79, 1.36, 1.24-0.80 ppm. The molar ratio of the three monomers in the polymer were determined by relative integrations of the aromatic protons of PDS, methylene protons of OEG, and methylene protons of dodecyl to give 28:36:36 (NH_2-OEG_8-MA:PDS:Dodecyl).

Synthesis of random copolymer p[(NH_2-OEG_8-MA)-*co*-PDSMA-*co*-Dodecyl] B (34:33:33): To a round bottom flask polymer p[(NH_2-OEG_8-MA)-*co*-PDSMA-*co*-Dodecyl] B (40 mg, 0.083 mmol PDS) and 1-dodecanethiol (5.7 μL, 0.041 mmol) was dissolved in DCM (2 mL) and purged with argon. Then glacial acetic acid (3 μL) was added and the mixture was stirred for 12 hours at ambient temperature. The mixture was purified by dialysis against dichloromethane in a MWCO 3500 regenerated cellulose membrane for 72 hours. The solution was dried to yield p[(NH_2-OEG_8-MA)-*co*-PDSMA-*co*-Dodecyl] as a waxy oil. ^{1}H NMR (400 MHz, CDCl3) δ: 8.46, 7.83, 7.21, 4.46-4.07, 3.94-3.57, 3.29, 3.23, 3.06, 2.86, 1.79, 1.36, 1.22-0.82 ppm. The molar ratio of the three monomers in the polymer were determined by relative integrations of the aromatic protons of PDS, methylene protons of OEG, and methylene protons of dodecyl to give 34:33:33 (NH_2-OEG_8-MA:PDS:Dodecyl).

Synthesis of random copolymer p[(NH_2-OEG_8-MA)-*co*-PDSMA-*co*-Dodecyl] C (46:27:26): To a round bottom flask polymer p[(NH_2-OEG_8-MA)-*co*-PDSMA-*co*-

Dodecyl] C (40 mg, 0.068 mmol PDS) and 1-dodecanethiol (4.7 μL, 0.034 mmol) was dissolved in DCM (2 mL) and purged with argon. Then glacial acetic acid (3 μL) was added and the mixture was stirred for 12 hours at ambient temperature. The mixture was purified by dialysis against dichloromethane in a MWCO 3500 regenerated cellulose membrane for 72 hours. The solution was dried to yield p[(NH_2-OEG_8-MA)-*co*-PDSMA-*co*-Dodecyl] as a waxy oil. ^{1}H NMR (400 MHz, CDCl3) δ: 8.46, 7.83, 721, 4.43-4.08, 3.94-3.56, 3.30, 3.23, 3.06, 2.85, 1.78, 1.36, 1.23-0.80 ppm. The molar ratio of the three monomers in the polymer were determined by relative integrations of the aromatic protons of PDS, methylene protons of OEG, and methylene protons of dodecyl to give 46:27:26 (NH_2-OEG_8-MA:PDS:Dodecyl).

Synthesis of random copolymer p[(BocNH-OEG_8-MA)-*co*-PDSMA] (36:64): To a Schlenk-flask, monomers PDSMA (1.005 g, 3.93 mmol), BocNH-OEG_8-MA (1.411 g, 2.62 mmol), chain transfer agent 4-cyano-4-[(dodecylsulfanylthiocarbonyl)sulfanyl]pentanoic acid (48.5 mg, 0.12 mmol), and AIBN (3.9 mg, 0.023 mmol) were dissolved in THF (4 mL). The mixture was degassed by performing three freeze-pump-thaw cycles and filled with argon. The reaction mixture was then sealed and transferred into a pre-heated oil bath at 65 °C and stirred for 24 h. The reaction flask was submerged in an ice bath to quench the polymerization, then dialyzed against dichloromethane in MWCO 3500 membrane for 48 hours to remove unreacted monomers. The solution was dried to yield the random copolymer as an oil. GPC (THF) *Mn*: 16.0 kDa. Đ: 1.3. ^{1}H NMR (400 MHz, CDCl3) δ: 8.44, 7.65, 7.09, 5.08, 4.34-3.92, 3.89-3.36, 3.29, 3.00, 2.08-1.57, 1.42, 1.31-0.67 ppm. The molar ratio of the two monomers

in the polymer were determined by relative integrations of the aromatic protons of PDS and methylene protons of OEG to give 36:64 (BocNH-OEG$_8$-MA:PDS).

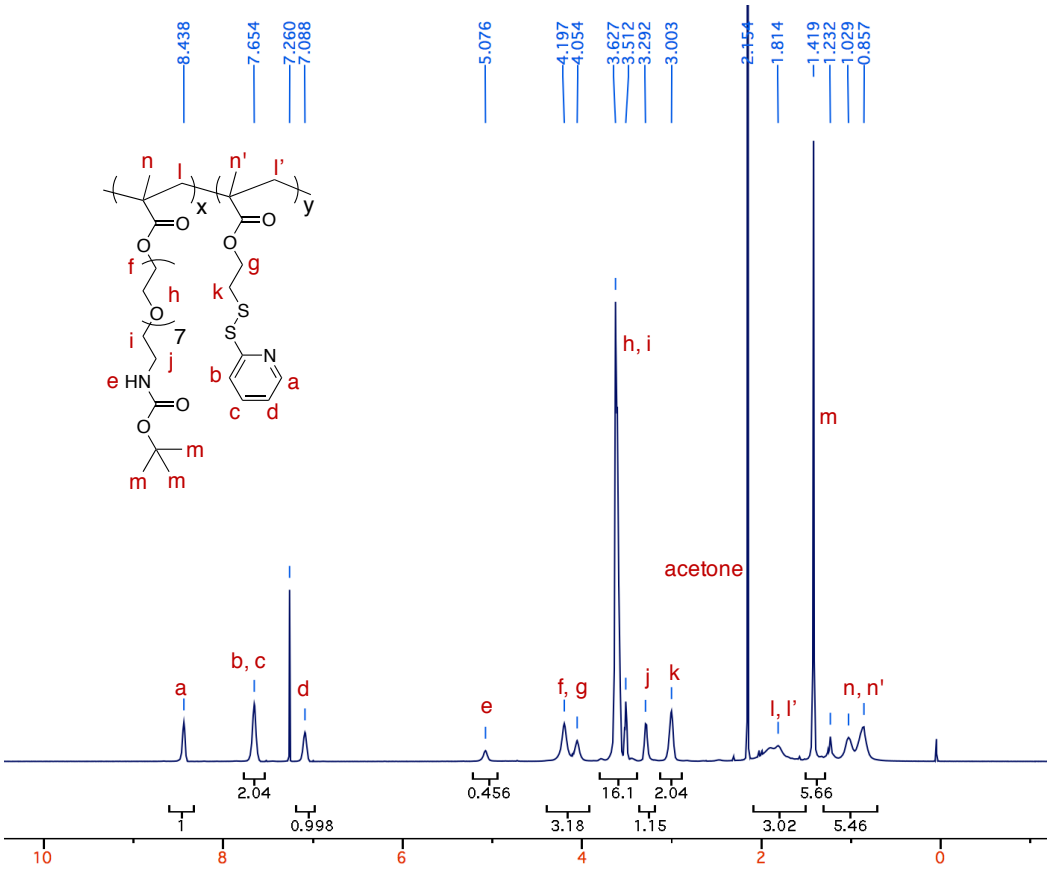

Figure 35. ^{1}H-NMR spectrum of random copolymer p[(BocNH-OEG$_8$-MA)-*co*-PDSMA] (36:64).

Synthesis of random copolymers p[(BocNH-OEG$_8$-MA)-*co*-PDSMA-*co*-Dodecyl] 13-27: To a round bottom flask polymer each p[(BocNH-OEG$_8$-MA)-*co*-PDSMA] 36:34 (160 mg, 2.8 mmol PDS) and separately 1-dodecanethiol (14.3 µL, 0.59 mmol; 27.8 µL, 1.1 mmol; 40.9 µL, 1.7 mmol) was dissolved in DCM (3 mL) and purged with argon. Then glacial acetic acid (15 µL) was added to each and the mixtures were stirred for 48 hours at ambient temperature. The mixture was purified by dialysis against dichloromethane in a MWCO 3500 regenerated cellulose membrane for 48 hours. The solutions were dried to yield p[(BocNH-OEG$_8$-MA)-*co*-PDSMA-*co*-Dodecyl] polymers as a waxy oils. ^{1}H NMR

Dodecyl 13% (400 MHz, $CDCl_3$) δ: 8.44, 7.66, 7.09, 5.07, 4.36-3.95, 3.84-3.41, 3.29, 3.00, 2.83, 2.65, 2.10-1.51, 1.42, 1.23, 1.13-0.68 ppm. ^{1}H NMR Dodecyl 22% (400 MHz, $CDCl_3$) δ: 8.44, 7.66, 7.09, 5.07, 4.34-3.93, 3.77-3.42, 3.28, 3.00, 2.83, 2.65, 2.05-1.51, 1.41, 1.23, 1.15-0.66 ppm. ^{1}H NMR Dodecyl 27% (400 MHz, $CDCl_3$) δ: 8.45, 7.66, 7.10, 5.06, 4.38-3.94, 3.80-3.43, 3.29, 3.01, 2.83, 2.66, 2.05-1.50, 1.42, 1.23, 1.14-0.64 ppm. The molar ratio of the three monomers in each polymer were determined by relative integrations of the aromatic protons of PDS, methylene protons of OEG, and methylene protons of dodecyl to give each 36:51:13, 36:42:22, and 36:37:27 (BocNH-OEG$_8$-MA:PDS:Dodecyl).

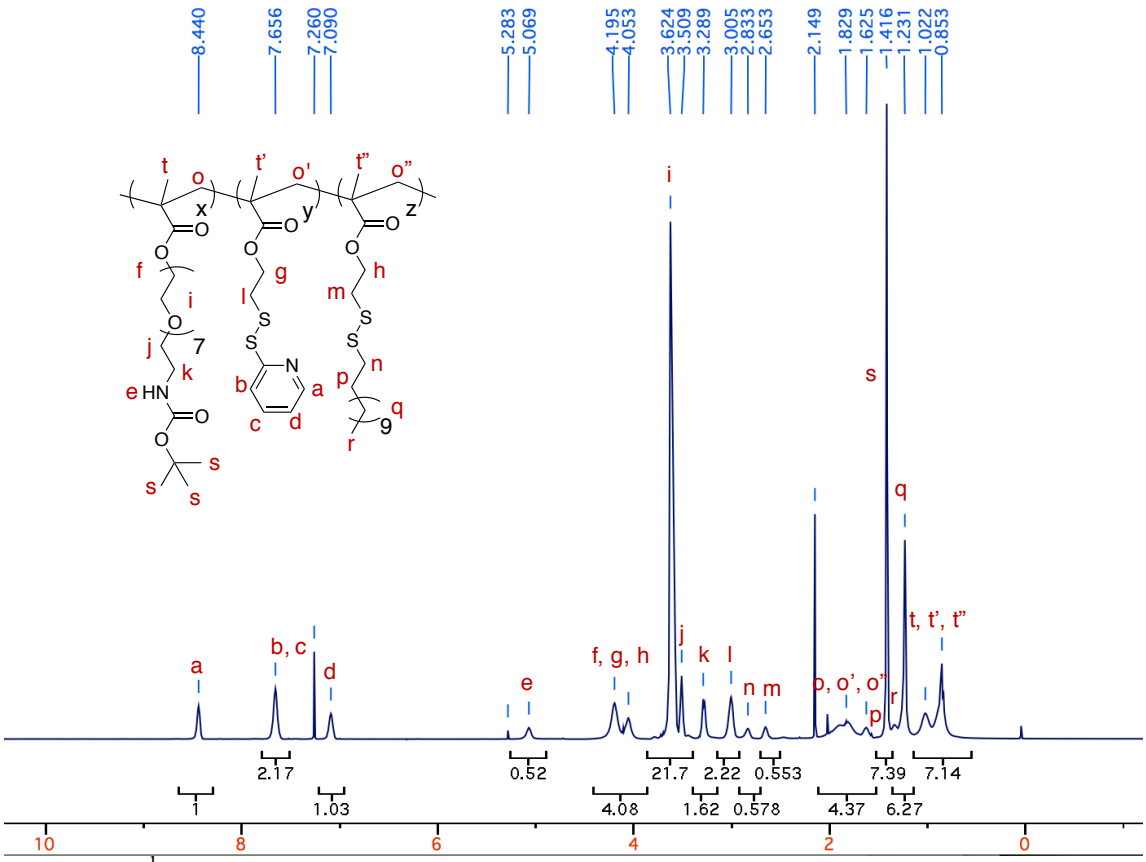

Figure 36. ^{1}H-NMR spectrum of random copolymers p[(BocNH-OEG$_8$-MA)-*co*-PDSMA-*co*-Dodecyl] (36:51:13).

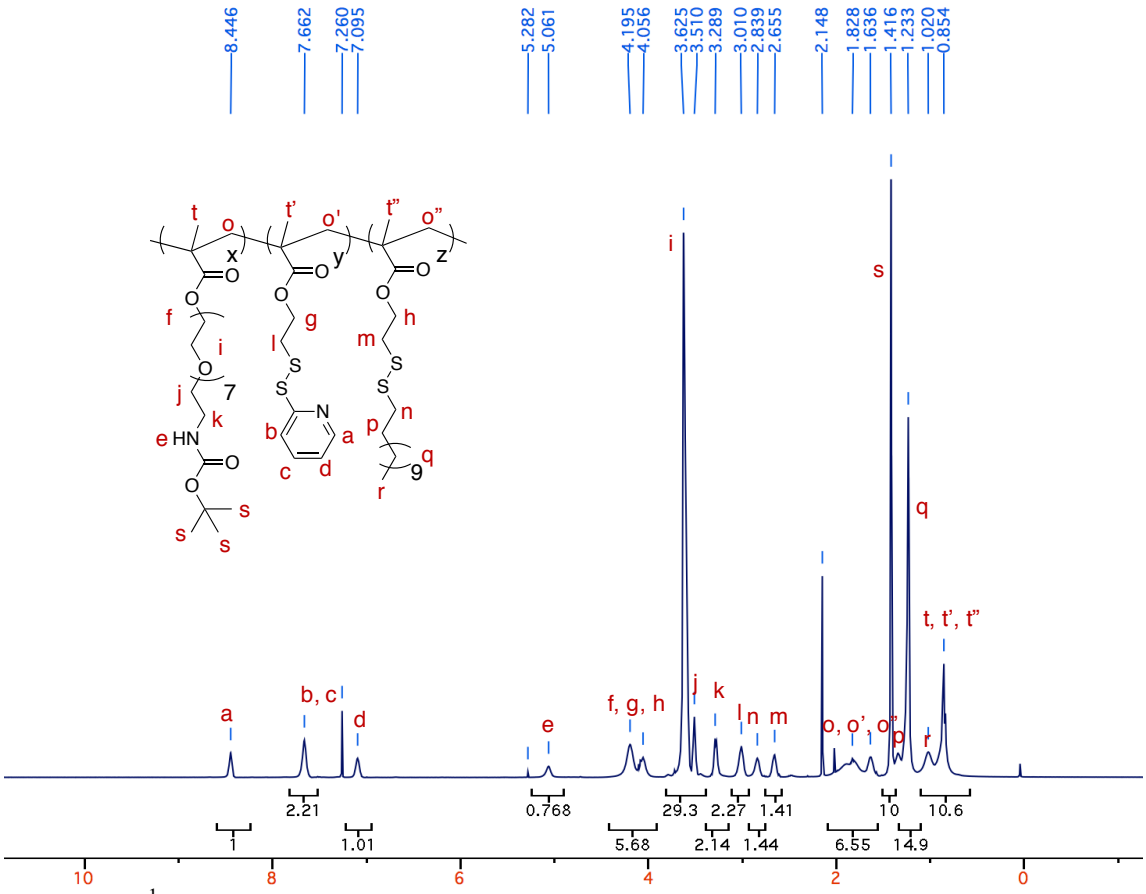

Figure 37. ^{1}H-NMR spectrum of random copolymers p[(BocNH-OEG$_8$-MA)-*co*-PDSMA-*co*-Dodecyl] (36:42:22).

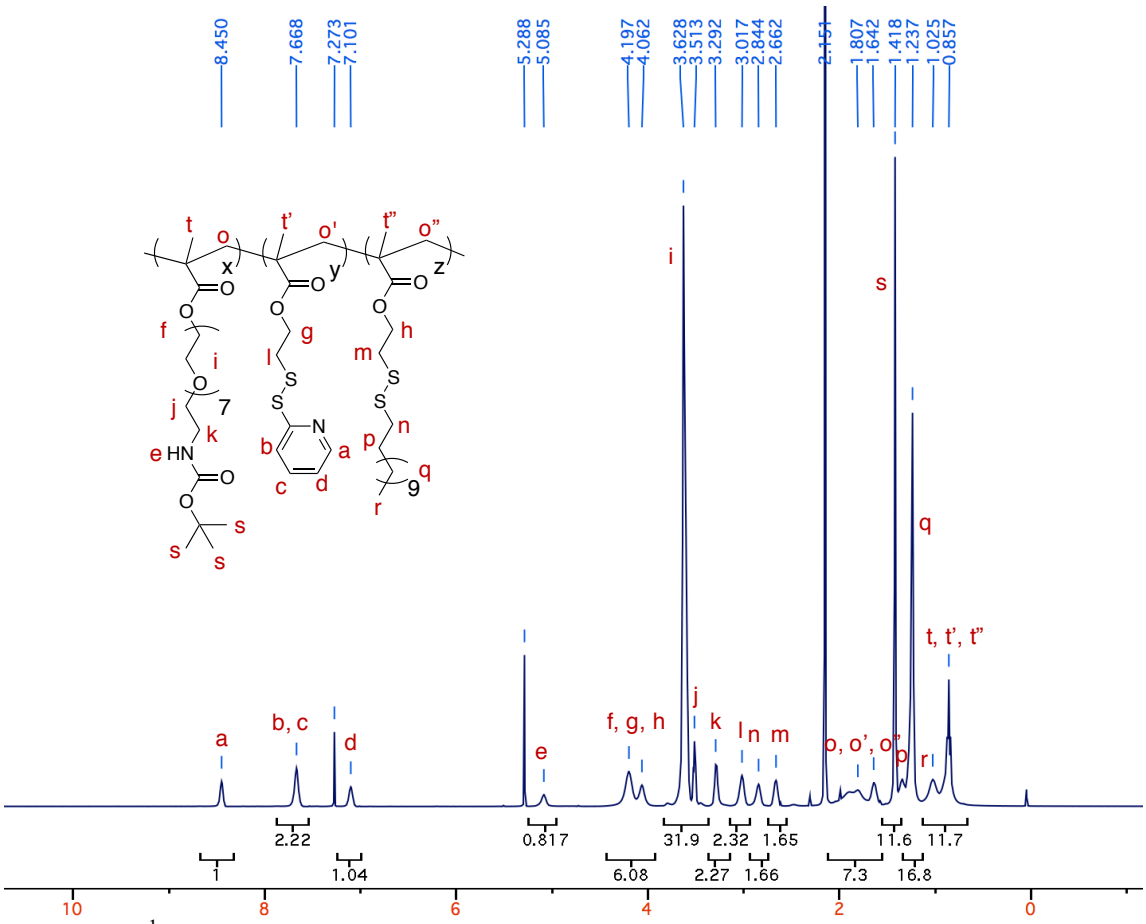

Figure 38. ^{1}H-NMR spectrum of random copolymers p[(BocNH-OEG$_8$-MA)-*co*-PDSMA-*co*-Dodecyl] (36:37:27).

Synthesis of random copolymer p[(NH_2-OEG_8-MA)-*co*-PDSMA-*co*-Dodecyl] 13-27:

To a round bottom flask polymers p[(BocNH-OEG$_8$-MA)-*co*-PDSMA-*co*-Dodecyl] Dodecyl 0, 13, 22, and 27% (140 mg) were each dissolved in DCM (3 mL) and purged with argon. Then trifluoroacetic acid (3 mL) was added and the mixtures were stirred for 12 hours at ambient temperature. The mixtures were evaporated under reduced pressure, then purified by dialysis against dichloromethane then acetone in a MWCO 3500 regenerated cellulose membrane for 48 hours. The solutions were dried to yield polymers p[(NH_2-OEG_8-MA)-*co*-PDSMA-*co*-Dodecyl] as waxy oils. ^{1}H NMR Dodecyl 0% (400 MHz, Methanol-D4) δ: 8.46, 7.84, 7.26, 4.43-4.03, 3.91-3.51, 3.34, 3.18, 2.3-1.77, 1.45-0.79 ppm. ^{1}H NMR Dodecyl 13% (400 MHz, Methanol-D4) δ: 8.45, 7.83, 7.25, 4.50-4.00,

3.90-3.43, 3.17, 3.98, 2.75, 2.28-1.54, 1.29, 1.21-0.73 ppm. ^{1}H NMR Dodecyl 22% (400 MHz, Acetone-D6) δ: 8.52, 7.86, 7.28, 4.49-4.07, 3.82-3.54, 3.30, 3.21, 3.03, 2.80, 2.28-1.54, 1.72, 1.31, 1.22-0.82 ppm. ^{1}H NMR Dodecyl 27% (400 MHz, Acetone-D6) δ: 8.51, 7.85, 7.27, 4.50-4.05, 3.97, 3.87, 3.70, 3.62, 3.29, 3.21, 3.02, 2.79,1.72, 1.30, 1.20-0.78 ppm. The reaction completions were confirmed by the disappearance of Boc group (δ: 1.21 ppm).

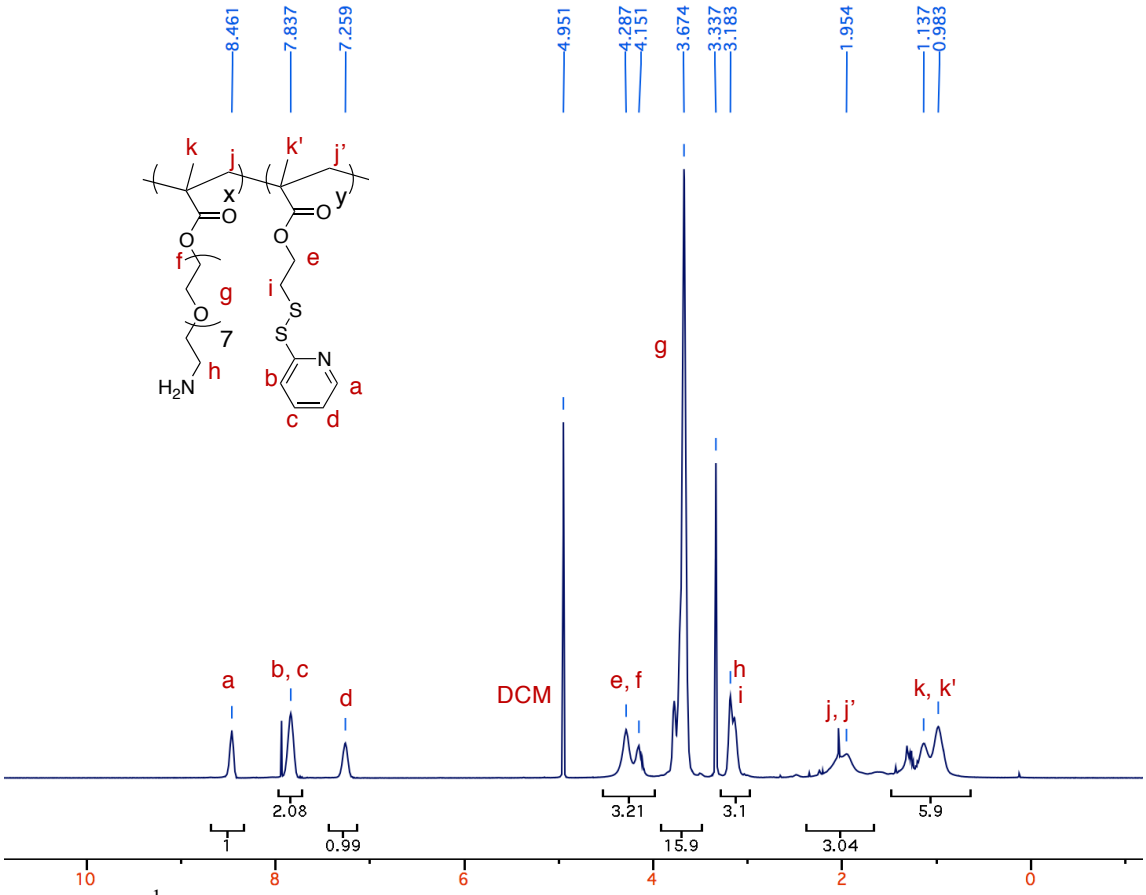

Figure 39. ^{1}H-NMR spectrum of random copolymer p[(NH_2-OEG_8-MA)-*co*-PDSMA-*co*-Dodecyl] (36:64).

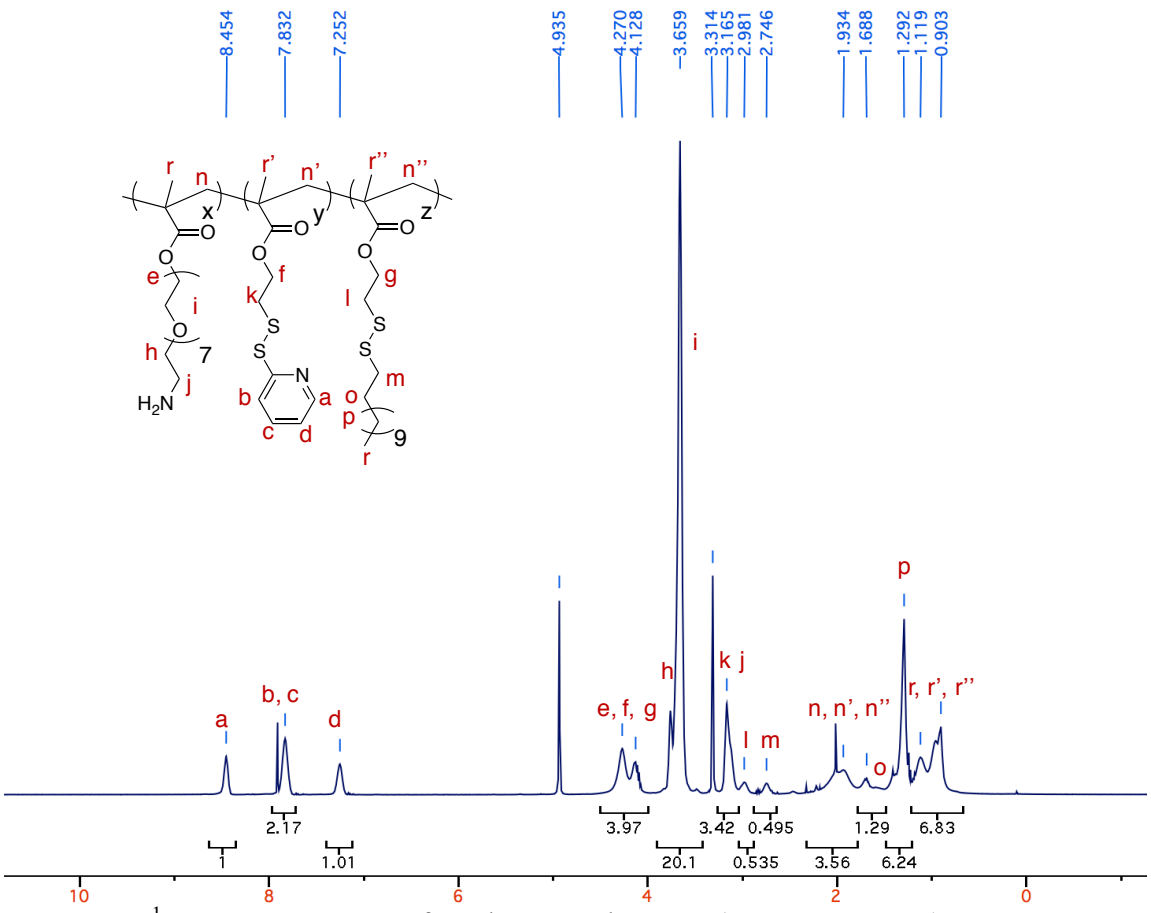

Figure 40. ^{1}H-NMR spectrum of random copolymer p[(NH_2-OEG_8-MA)-*co*-PDSMA-*co*-Dodecyl] (36:51:13).

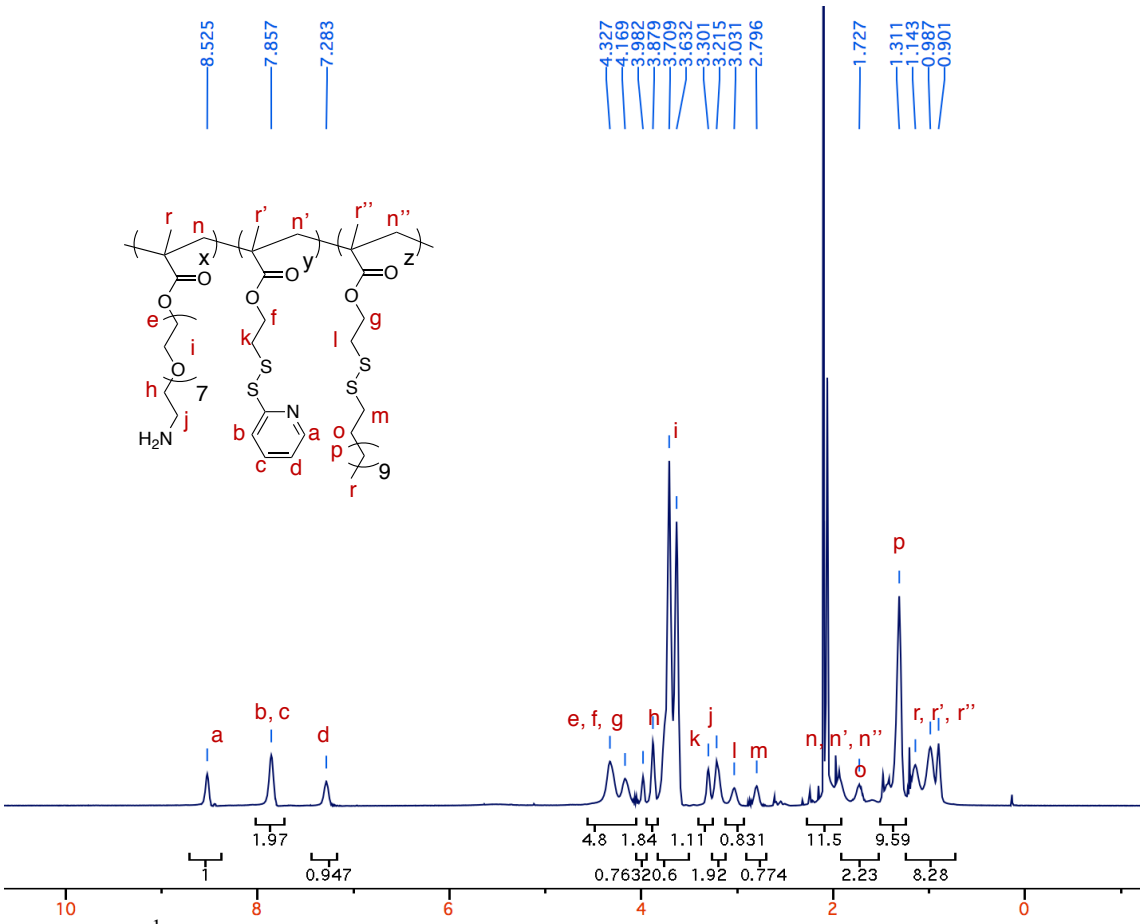

Figure 41. ^{1}H-NMR spectrum of random copolymer p[(NH_2-OEG_8-MA)-*co*-PDSMA-*co*-Dodecyl] (36:42:22).

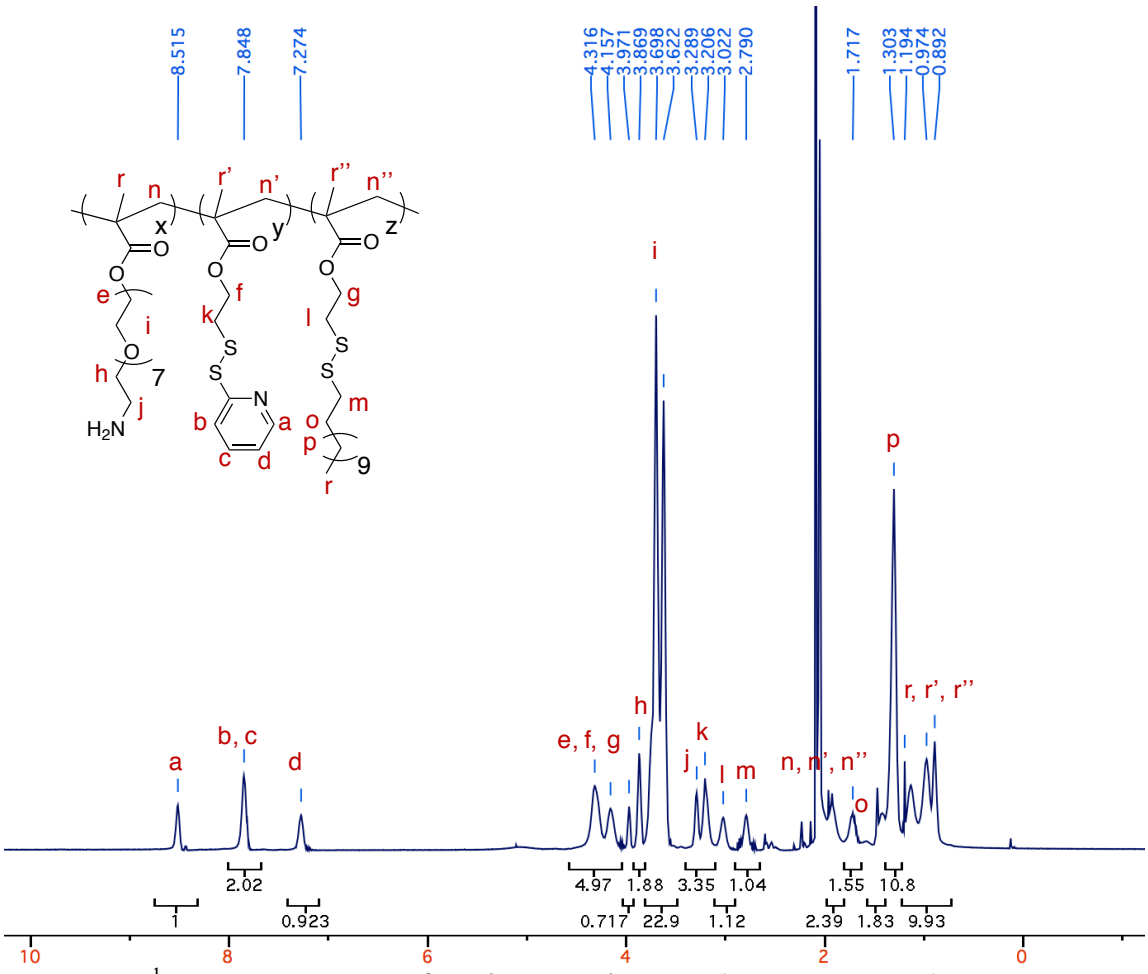

Figure 42. ^{1}H-NMR spectrum of random copolymer p[(NH_2-OEG_8-MA)-*co*-PDSMA-*co*-Dodecyl] (36:42:22). (36:37:27).

Synthesis of random copolymer p[(BocNH-OEG_8-MA)-*co*-PDSMA] (39:61) large scale: To a Schlenk-flask, monomers PDSMA (3.678 g, 14.4 mmol), BocNH-OEG_8-MA (5.161 g, 9.60 mmol), chain transfer agent 4-cyano-4-[(dodecylsulfanylthiocarbonyl)sulfanyl]pentanoic acid (108 mg, 0.268 mmol), and AIBN (8.8 mg, 0.054 mmol) were dissolved in THF (12 mL). The mixture was degassed by performing three freeze-pump-thaw cycles and filled with argon. The reaction mixture was then sealed and transferred into a pre-heated oil bath at 65 °C and stirred for 24 h. The reaction flask was submerged in an ice bath to quench the polymerization, then dialyzed against dichloromethane in MWCO 3500 membrane for 48 hours to remove unreacted

monomers. The solution was dried to yield the random copolymer as an oil. GPC (THF) *Mn*: 20.7 kDa. Đ: 1.2. ^{1}H NMR (400 MHz, CDCl3) δ: 8.43, 7.65, 7.09, 5.05, 4.32-3.93, 3.73-3.42, 3.28, 3.00, 2.11-1.62, 1.41, 1.17-0.70 ppm. The molar ratio of the two monomers in the polymer were determined by relative integrations of the aromatic protons of PDS and methylene protons of OEG to give 39:61 (BocNH-OEG$_8$-MA:PDS).

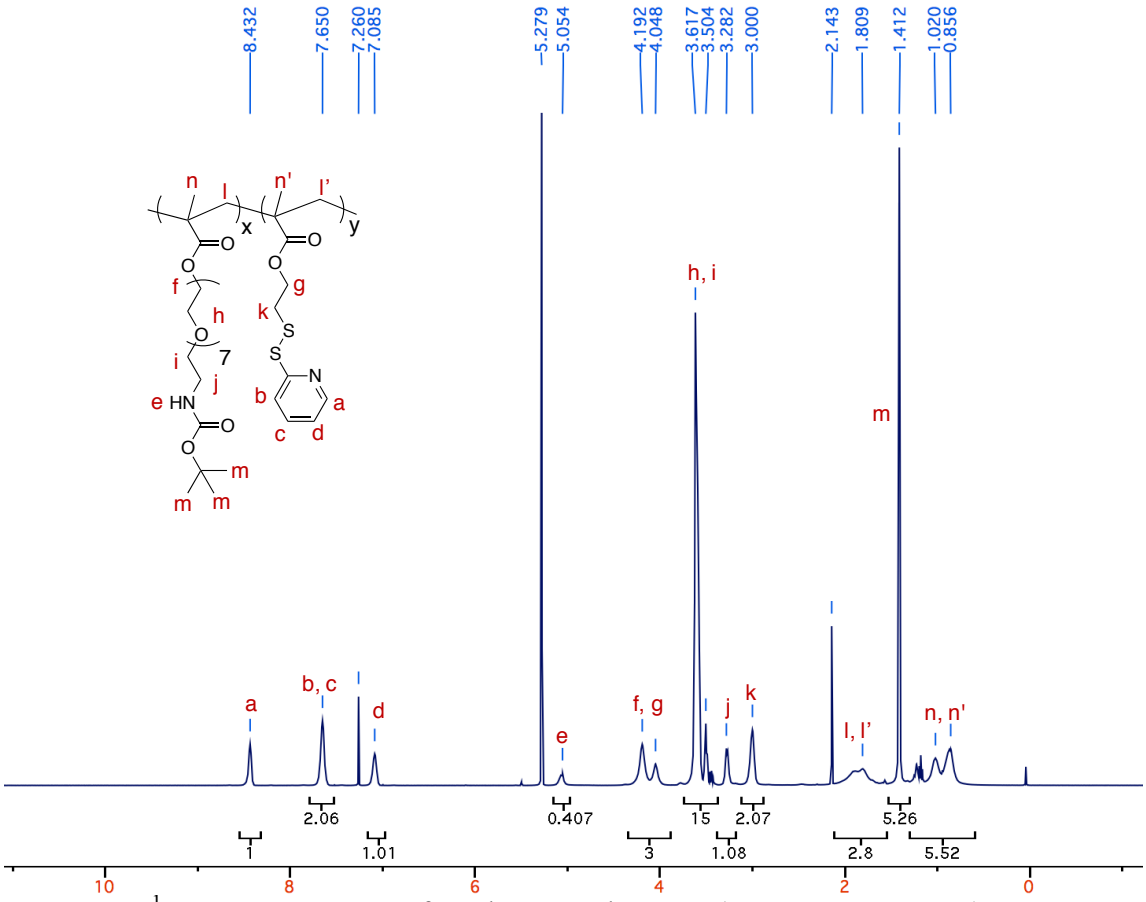

Figure 43. ^{1}H-NMR spectrum of random copolymer p[(BocNH-OEG$_8$-MA)-*co*-PDSMA] (39:61) large scale.

Synthesis of random copolymer p[(BocNH-OEG$_8$-MA)-*co*-PDSMA-*co*-Dodecyl] 1 (39:37:24): To a round bottom flask polymer p[(BocNH-OEG$_8$-MA)-*co*-PDSMA] (3.67 g, 6.8 mmol PDS) and 1-dodecanethiol (0.656 mL, 2.7 mmol) was dissolved in DCM (3 mL) and purged with argon. Then glacial acetic acid (332 µL) was added and the mixture was stirred for 48 hours at ambient temperature. The mixture was purified by dialysis against

dichloromethane in a MWCO 3500 regenerated cellulose membrane for 72 hours. The solution was dried to yield p[(BocNH-OEG$_8$-MA)-*co*-PDSMA-*co*-Dodecyl] as a waxy oil. ^{1}H NMR (400 MHz, CDCl3) δ: 8.48, 7.69, 7.13, 5.11, 4.36-3.98, 3.78-3.42, 3.32, 3.05, 2.87, 2.69, 2.10-1.72, 1.66, 1.44, 1.26, 1.16-0.70 ppm. The molar ratio of the three monomers in the polymer were determined by relative integrations of the aromatic protons of PDS, methylene protons of OEG, and methylene protons of dodecyl to give 39:37:24 (BocNH-OEG$_8$-MA:PDS:Dodecyl).

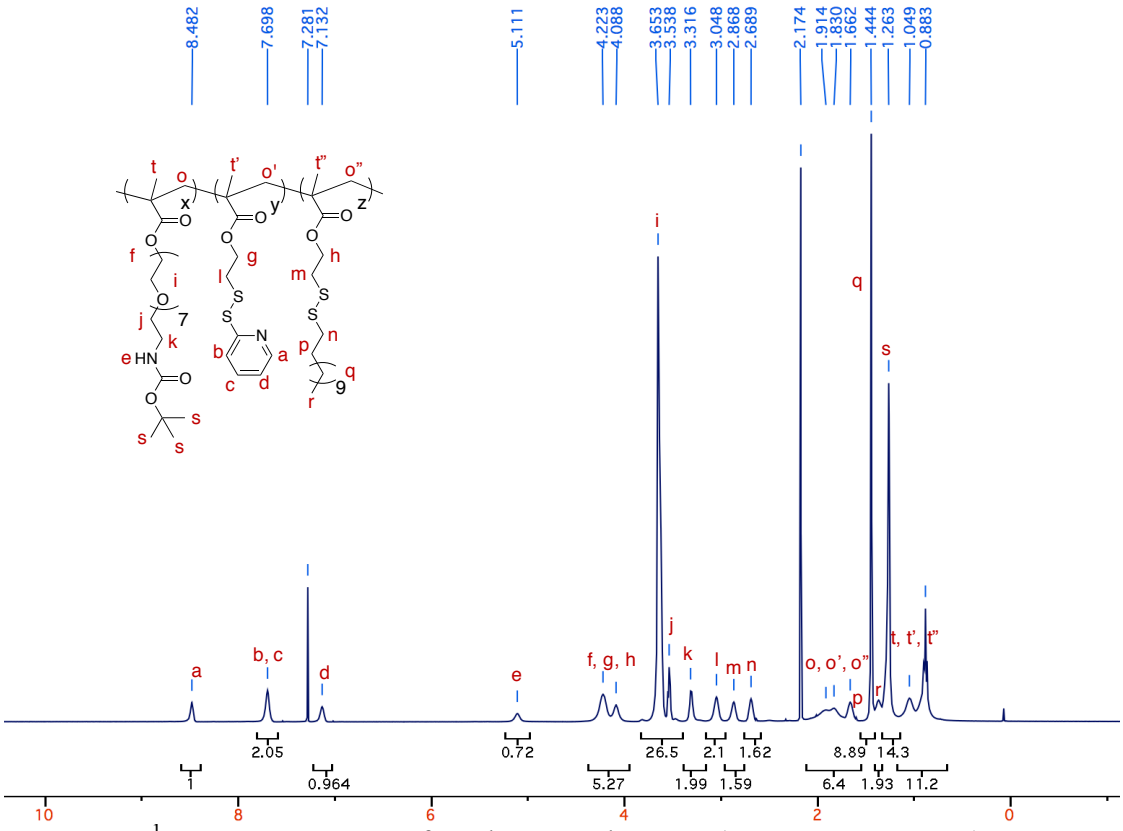

Figure 44. ^{1}H-NMR spectrum of random copolymer p[(BocNH-OEG$_8$-MA)-*co*-PDSMA-*co*-Dodecyl] 1 (39:37:24).

Synthesis of random copolymer p[(BocNH-OEG$_8$-MA)-*co*-PDSMA-*co*-Dodecyl] 2 (36:22:36): To a round bottom flask polymer p[(BocNH-OEG$_8$-MA)-*co*-PDSMA] (3.67 g, 6.8 mmol PDS) and 1-dodecanethiol (0.984 mL, 4.1 mmol) was dissolved in DCM (25 mL) and purged with argon. Then glacial acetic acid (332 µL) was added and the mixture

was stirred for 48 hours at ambient temperature. The mixture was purified by dialysis against dichloromethane in a MWCO 3500 regenerated cellulose membrane for 72 hours. The solution was dried to yield p[(BocNH-OEG$_8$-MA)-*co*-PDSMA-*co*-Dodecyl] as a waxy oil. ^{1}H NMR (400 MHz, CDCl3) δ: 8.43, 7.65, 7.09, 5.09, 4.34-3.90, 3.82-3.37, 3.25, 2.99, 2.82, 2.64, 2.05-1.50, 1.39, 1.21, 1.10-0.60 ppm. The molar ratio of the three monomers in the polymer were determined by relative integrations of the aromatic protons of PDS, methylene protons of OEG, and methylene protons of dodecyl to give 36:22:36 (BocNH-OEG$_8$-MA:PDS:Dodecyl).

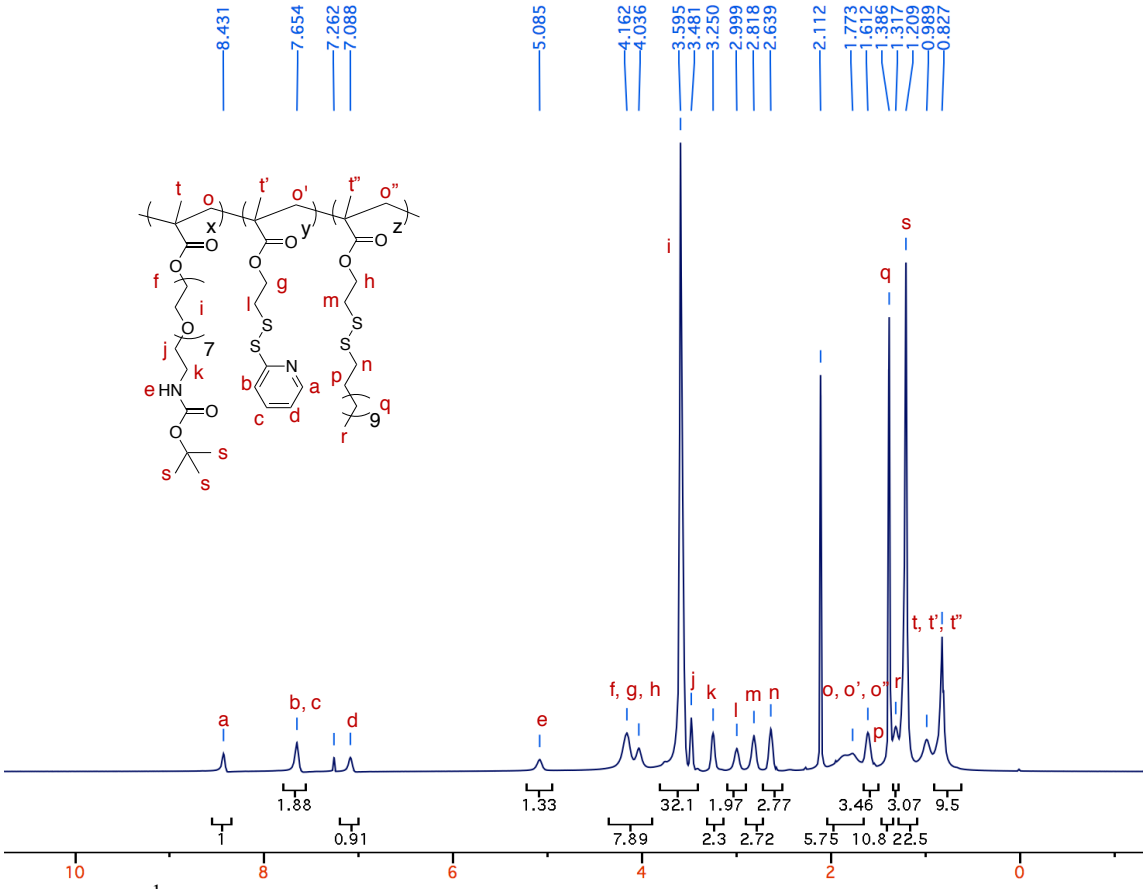

Figure 45. ^{1}H-NMR spectrum of random copolymer p[(BocNH-OEG$_8$-MA)-*co*-PDSMA-*co*-Dodecyl] 2 (36:22:36).

Synthesis of random copolymer p[(NH_2-OEG$_8$-MA)-*co*-PDSMA-*co*-Dodecyl] 1 (39:37:24): To a round bottom flask polymer p[(BocNH-OEG$_8$-MA)-*co*-PDSMA-*co*-

Dodecyl] 1 (4.366 g) was dissolved in DCM (16 mL) and purged with argon. Then trifluoroacetic acid (6 mL) was added and the mixture was stirred for 12 hours at ambient temperature. The mixture was evaporated under reduced pressure, then purified by dialysis against dichloromethane then acetone in a MWCO 3500 regenerated cellulose membrane for 48 hours. The solution was dried to yield p[(NH_2-OEG_8-MA)-*co*-PDSMA-*co*-Dodecyl] as a waxy oil. ^{1}H NMR (400 MHz, Acetone-D6) δ: 8.52, 7.86, 7.28, 4.55-4.05, 4.03-3.53, 3.30, 3.20, 3.03, 2.80, 2.0-1.52, 1.31, 1.21-0.77 ppm. The reaction completion was confirmed by the disappearance of Boc group (δ: 1.21 ppm).

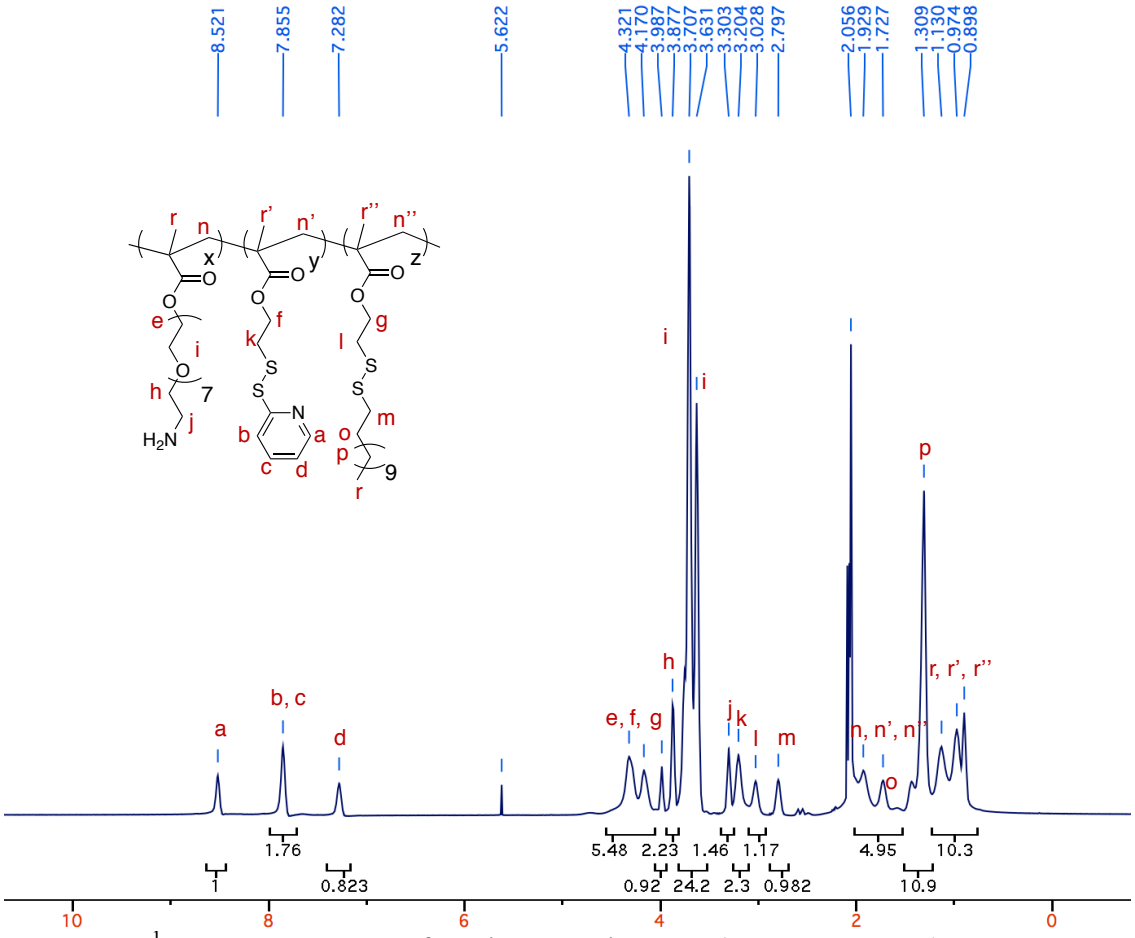

Figure 46. ^{1}H-NMR spectrum of random copolymer p[(NH_2-OEG_8-MA)-*co*-PDSMA-*co*-Dodecyl] 1 (39:37:24).

Synthesis of random copolymer p[(NH_2-OEG_8-MA)-*co*-PDSMA-*co*-Dodecyl] 2 (36:22:36): To a round bottom flask polymer p[(BocNH-OEG_8-MA)-*co*-PDSMA-*co*-Dodecyl] 2 (4.4 g) was dissolved in DCM (16 mL) and purged with argon. Then trifluoroacetic acid (6 mL) was added and the mixture was stirred for 12 hours at ambient temperature. The mixture was evaporated under reduced pressure, then purified by dialysis against dichloromethane then acetone in a MWCO 3500 regenerated cellulose membrane for 48 hours. The solution was dried to yield p[(NH_2-OEG_8-MA)-*co*-PDSMA-*co*-Dodecyl] as a waxy oil. ^{1}H NMR (400 MHz, Acetone-D6) δ: 8.52, 7.85, 7.28, 4.46-4.04, 4.00-3.53, 3.29, 3.20, 3.02, 2.80, 2.04-1.81, 1.73, 1.31, 1.21-0.77 ppm. The reaction completion was confirmed by the disappearance of Boc group (δ: 1.21 ppm).

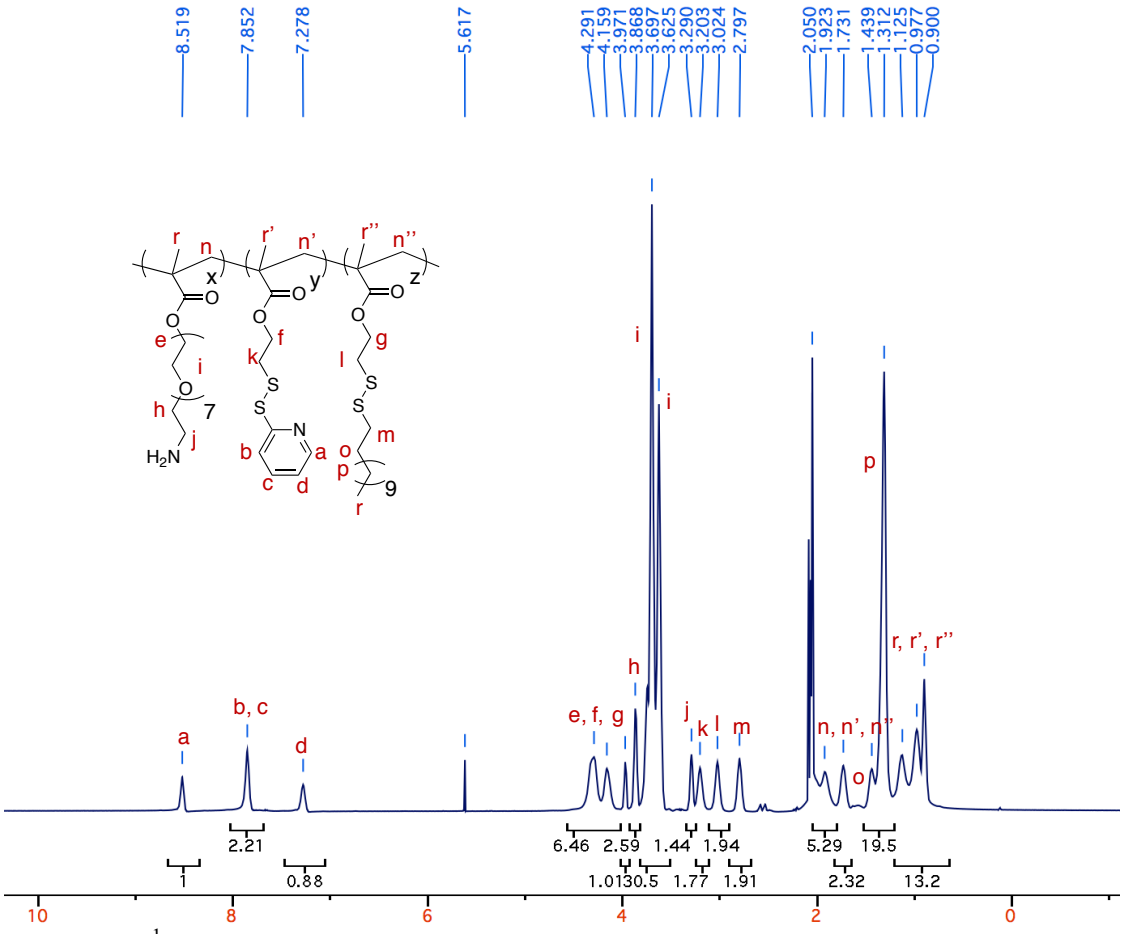

Figure 47. ^{1}H-NMR spectrum of random copolymer p[(NH_2-OEG_8-MA)-*co*-PDSMA-*co*-Dodecyl] 2 (36:22:36).

Synthesis of random copolymer p(OEGMA-*co*-PDSMA): To a Schlenk-flask, monomers PDSMA (3.8 g, 14.9 mmol), OEGMA (2.76 g, 5.5 mmol), chain transfer agent 4-cyano-4-[(dodecylsulfanylthiocarbonyl)sulfanyl]pentanoic acid (111 mg, 0.276 mmol), and AIBN (9.1 mg, 0.055 mmol) were dissolved in THF (10 mL). The mixture was degassed by performing three freeze-pump-thaw cycles and filled with argon. The reaction mixture was then sealed and transferred into a pre-heated oil bath at 65 °C and stirred for 24 h. The reaction flask was submerged in an ice bath to quench the polymerization, then dialyzed against dichloromethane in MWCO 3500 membrane for 48 hours to remove unreactive monomers. The solution was dried to yield the random copolymer as an oil.

GPC (THF) *Mn*: 21.7 kDa. Đ: 1.2. ^{1}H NMR (400 MHz, Acetone-D6) δ: 8.47, 7.79, 7.20, 4.37-4.00, 3.72-3.41, 3.34, 3.13, 2.14-1.77, 1.36-0.82 ppm. The molar ratio of the two monomers in the polymer were determined by relative integrations of the aromatic protons of PDS and methoxy protons of OEG to give 34:66 (OEG:PDS).

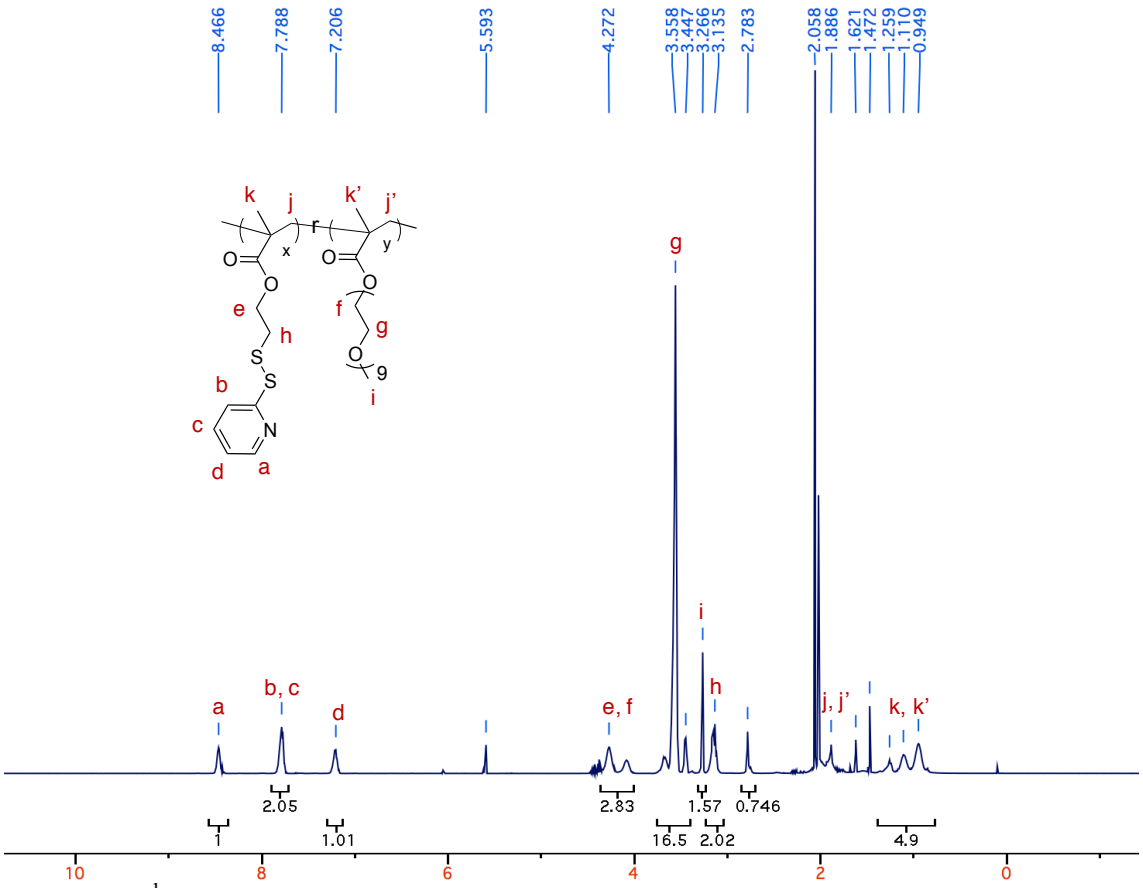

Figure 48. ^{1}H-NMR spectrum of random copolymer p(OEGMA-*co*-PDSMA).

Synthesis of random copolymer p(OEGMA-*co*-PDSMA-*co*-Dodecyl): To a round bottom flask polymer p(OEGMA-*co*-PDSMA) (6.121 g, 12.6 mmol PDS) and 1-dodecanethiol (1.825 mL, 7.56 mmol) was dissolved in DCM (100 mL) and purged with argon. Then glacial acetic acid (600 μL) was added and the mixture was stirred for 48 hours at ambient temperature. The mixture was purified by dialysis against dichloromethane then acetone in a MWCO 3500 regenerated cellulose membrane for 48 hours. The solution was

dried to yield p(OEGMA-*co*-PDSMA-*co*-Dodecyl) as a waxy oil. ^{1}H NMR (400 MHz, Acetone-D6) δ: 8.52, 7.87, 7.29, 4.43-4.03, 3.82-3.45, 3.32, 3.22, 4.04, 2.82, 1.95, 1.75, 1.337. 1.25-0.85. The molar ratio of the three monomers in the polymer were determined by relative integrations of the aromatic protons of PDS, methoxy protons of OEG, and ethylene protons of dodecyl to give 34:34:32 (OEG:PDS:Dodecyl).

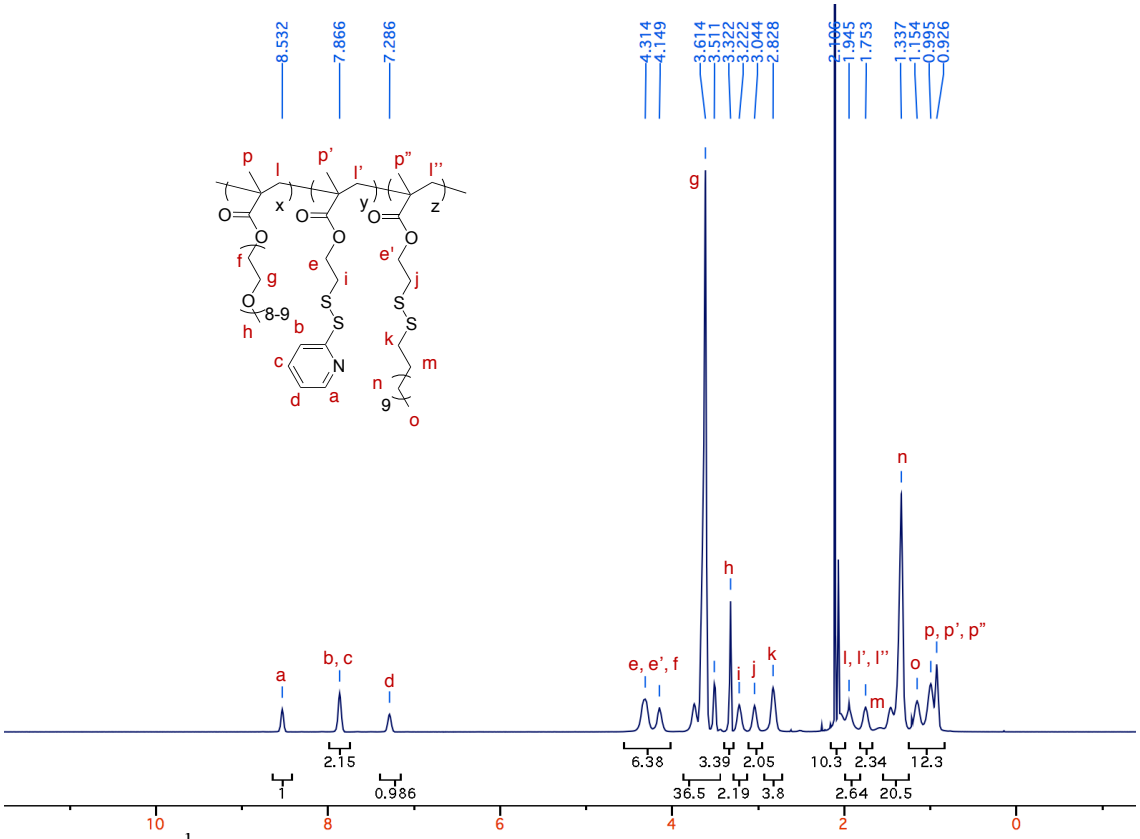

Figure 49. ^{1}H-NMR spectrum of random copolymer p(OEGMA-*co*-PDSMA-*co*-Dodecyl).

Formulation of Nanogels: Dynamic light scattering experiments to obtain particle size were performed by using a digital correlator and goniometer with a light source operating at 514 nm. Final nanogel size measurements were obtained at 25 °C at a correlation time of 30 seconds. Dust was removed by filtering the solution through 0.45 µm polycarbonate filter. Final polymeric nanogel concentrations were calculated using initial feed, and final docetaxel concentrations were determined HPLC.

PEG-NHS ester Conjugation: Nanogel in aqueous solution were standardized to 1× PBS pH 7.4 by addition of 10× PBS buffer, then brought to pH 8-8.5 with 1 M NaOH. To this solution, poly(ethylene glycol) methyl ether N-hydroxy succinimide ester (average M_n 2000) (g, mmol, 5 equivalents to nanogel NH_2-OEG monomer) was added, and stirred for 48 hours at ambient temperature. Nanogels were purified by dialysis against a cellulose membrane with 8-10 kDa MWCO.

Nanogel Crosslinking: The crosslinking was quantified using the previously reported procedure[34] by monitoring the amount of 2-pyridinethione byproduct produced from DTT addition using its molar extinction coefficient (8.08 x 10^3 M^{-1} cm^{-1} at 343 nm).[35] UV-vis absorption measurements were obtained on 1000-fold crosslinking reaction dilutions. The assumption that cleavage of two PDS units would produce two pyridinethione byproduct and one disulfide bond was made to calculate crosslink density.

Quantification of Docetaxel Load: Docetaxel loads were determined by analytical HPLC, using a C18 column (4.6 mm × 10 cm, 2.7 μm particle size) using a gradient mobile phase of acetonitrile 0% to 70% acetonitrile in water, both containing 0.05% (v/v) trifluoroacetic acid, monitoring absorbance of 214 nm at a flow rate of 1 mL/min. A calibration curve was prepared by Docetaxel by obtaining AUC for 214 absorbance at consistent retention time of 16.6 min for the drug, for 0.01-1 mg/mL doc, performed in triplicate. The linear fit for AUC vs Doc concentration gave R^2=0.99. Thus, concentrations of Doc could be calculated for unknown samples using obtained AUC for absorbance of 214 nm at 16.6 min. These

values were obtained by disrupting aggregate encapsulation integrity by adding acetone (1:1 volume %) to nanogel solutions, then characterizing HPLC results of 20 μL of this solution.

Animals and Husbandry: All animal work was conducted by Crown Biosciences, Inc. All experiments used female Musculus BALB/c nude mice supplied by Shanghai Lingchang Bio-Technology Co. Ltd (LC, Shanghai, China). At the time of inoculation animals were 7-8 weeks for MDA-MB-231 model, 9-10 weeks old for BR1282 model, 11-12 weeks old for BR1458 model, and 13-14 weeks old for BR 1474 model. Their body weights were 17-22 g. Animals were fed *ad libitum* (reverse osmosis autoclaved water and Co^{60} irradiation sterilized dry granule food) and housed inside individually ventilated cage (IVC) systems with corn cob bedding, 5 animals in each cage, and an environment of 21-26 °C and 30-70% humidity. All procedures involving use and care of animals were performed in compliance with the Institutional Animal Care and Use Committee (IACUC) of CrownBio, Inc. and in accordance with regulations of the Association for Assessment and Accreditation of Laboratory Animal Care (AAALAC).

Cell Preparation and Tumor Inoculation: MDA-MB-231 cells were grown and maintained in *in vitro* culture in L-15 medium supplemented with 10% fetal bovine serum (heat inactivated) at 37 ºC in 100% air. Tumor cells were subcultured twice per week, and cells in exponential growth phase were harvested and for tumor inoculation. On day 0, MDA-MB-231 tumor cells (1×10^7) in PBS with 50% Matrigel® (100 μL) were inoculated subcutaneously at right mammary pad of each animal for tumor development. Fragments

of tumor tissues (2-3 mm in diameter) were harvested from stock mice inoculated with breast PDX model BR1282, BR1458 or BR1474 and inoculated subcutaneously at the right flank into each BALB/c nude for tumor development

Measurements and Endpoints: Following tumor inoculation, all animals body weights were obtained and tumor volumes calculated using caliper measurements. Throughout treatment tumor volumes were measured twice weekly and expressed in mm^3 using the formula: $V = 0.5\ a \times b^2$ where *a* and *b* are the length and width of the tumor, respectively. Systematic error was minimized by randomizing animals prior to treatment into specified groups by minimal variation in tumor volume using StudyDirector™ software (Studylog Systems, Inc. CA, USA). The primary endpoints for the study is tumor growth inhibition (TGI), which is an indication of antitumor effectiveness. The inhibition is expressed as TGI (%) =100 × (1-T/C), where the mean tumor volume (or weight) for the treated (T) and control (C) were obtained on a given day. Tumor sizes are given in **Tables 15-18**.

Table 15. Tumor Sizes in the Different Treatment Groups in MDA-MB-231 Study

Days	Tumor Volume (mm^3)		
	C1 (0 mg/kg)	NG1 (2 mg/kg)	Docetaxel (2 mg/kg)
0	151.5 ± 6.5	151.5 ± 7.2	151.5 ± 7.1
3	326.1 ± 24.2	297.5 ± 19.0	292.0 ± 25.7
7	426.9 ± 23.3	422.0 ± 31.1	390.6 ± 29.7
10	562.6 ± 28.8	520.2 ± 39.3	475.0 ± 46.4
14	680.7 ± 35.9	707.6 ± 48.0	606.4 ± 44.9
17	831.0 ± 40.6	885.5 ± 58.0	688.9 ± 58.0
21	1111.5 ± 60.1	1316.6 ± 114.5	838.1 ± 63.0

Note: data expressed as Mean ± SEM

Table 16. Tumor Sizes in the Different Treatment Groups in BR1282 Study.

Days	Tumor Volume (mm^3)			
	C1 (0 mg/kg)	NG1 (3 mg/kg)	Docetaxel (3 mg/kg)	NG2 (3 mg/kg)
0	150.2 ± 8.0	150.2 ± 7.8	150.2 ± 8.9	150.2 ± 8.4
4	433.3 ± 32.8	453.6 ± 33.5	263.5 ± 17.9	392.9 ± 18.0
7	832.2 ± 50.1	810.0 ± 54.1	153.6 ± 15.4	714.7 ± 45.7
11	1527.3 ± 98.0	1403.6 ± 81.0	116.5 ± 20.8	1230.3 ± 97.1
14	1917.7 ± 101.2	1869.2 ± 124.1	92.3 ± 20.0	1593.6 ± 120.3

Note: data expressed as Mean ± SEM. *One animal in C1 group was sacrificed on Day 12 after the first treatment due to tumor volume >2000mm^3.

Table 17. Tumor Sizes in the Different Treatment Groups in BR1458 Study.

Days	Tumor Volume (mm^3)			
	C1 (0 mg/kg)	NG1 (2 mg/kg)	Docetaxel (2 mg/kg)	NG2 (2 mg/kg)
0	153.2 ± 21.5	153.0 ± 21.1	153.1 ± 20.8	153.0 ± 20.9
4	437.5 ± 57.5	417.3 ± 67.5	297.2 ± 39.9	348.7 ± 51.5
7	689.2 ± 63.8	801.5 ± 136.5	405.1 ± 55.8	546.6 ± 84.3
11	1117.4 ± 133.6	1339.8 ± 230.8	433.2 ± 70.9	746.8 ± 125.7
14	1305.5 ± 155.2	1744.1 ± 331.8	484.2 ± 80.8	987.8 ± 166.5
18	1916.2 ± 199.6	1661.7 ± 310.0	530.3 ± 86.3	1195.7 ± 201.5
21	1886.2 ± 142.4	1140.7 ± 192.1	538.2 ± 89.7	1530.4 ± 267.5
24	2294.0 ± 198.7	1571.7 ± 258.5	562.1 ± 97.8	1278.2 ± 301.3

Note: data expressed as Mean ± SEM

*There were animals being sacrificed from day 18 after the first treatment due to tumor volume >2000mm^3.

Table 18. Tumor Sizes in the Different Treatment Groups in BR1474 Study.

Days	Tumor Volume (mm^3)		
	C1 (0 mg/kg)	NG1 (2 mg/kg)	Docetaxel (2 mg/kg)
0	149.7 ± 9.1	149.7 ± 8.8	149.7 ± 9.2
3	172.5 ± 11.3	177.0 ± 10.7	179.0 ± 12.9
7	237.7 ± 17.5	248.9 ± 18.1	218.8 ± 16.4
10	288.5 ± 26.0	316.9 ± 21.3	268.4 ± 19.8
14	357.9 ± 44.3	360.4 ± 21.8	269.1 ± 23.5
17	445.1 ± 62.0	487.2 ± 40.7	358.1 ± 29.5
21	512.2 ± 73.1	563.5 ± 45.6	403.1 ± 39.8
24	588.0 ± 83.3	637.5 ± 50.6	441.4 ± 42.3

Note: data expressed as Mean ± SEM

Treatment: Treatment was initiated with the group mean tumor size reached 152, 150, 153, and 150 mm^3 for tumor models MDA-MB-231, BR1282, BR1458, and BR1474 respectively. Nanogels and docetaxel solutions were administered to the tumor-bearing

mice according to the regimens in **Tables 19-22**. Stock docetaxel (0.02 mL, 40 mg/mL) was diluted to 0.06 mL with 13% ethanol solution, then 1.52 mL saline to make a final 1.6 mL of 0.5 mg/mL dosing solution, same as test nanogel concentrations. All dosing, tumor measurements, and body weight measurement were conducted in a Laminar Flow Cabinet. The MDA-MB-231, BR1474, BR1282, and BR1458 studies were terminated after dosing on Day 21, Day 24, Day 14, and Day 24, respectively.

Table 19. Treatment administration schedule for MDA-MB-231 bearing mice.

Group	N	Treatment	Dose (mg/kg)	Dosing Volume (mL/kg)	Dosing Route	Schedule
1	10	C1	0	4	*i.v.*	4 days on 3 days off/week x 3 weeks
2	10	NG1	2	4	*i.v.*	4 days on 3 days off/week x 3 weeks
3	10	Docetaxel	2	4	*i.v.*	4 days on 3 days off/week x 3 weeks

Table 20. Treatment administration schedule for BR1474 bearing mice.

Group	N	Treatment	Dose (mg/kg)	Dosing Volume (mL/kg)	Dosing Route	Schedule
1	10	C1	0	4	*i.v.*	4 days on 3 days off/week x 3 weeks
2	10	NG1	2	4	*i.v.*	4 days on 3 days off/week x 3 weeks
3	10	Docetaxel	2	4	*i.v.*	4 days on 3 days off/week x 3 weeks

Table 21. Treatment administration schedule for BR1282 bearing mice.

Group	N	Treatment	Dose (mg/kg)	Dosing Volume (mL/kg)	Dosing Route	Schedule
1	10	C1	0	6	*i.v.*	4 days on 3 days off/week x 2 weeks
2	10	NG1	3	6	*i.v.*	4 days on 3 days off/week x 2 weeks
3	10	Docetaxel	3	6	*i.v.*	4 days on 3 days off/week x 2 weeks
4	10	NG2	3	6	*i.v.*	4 days on 3 days off/week x 2 weeks

Table 22. Treatment administration schedule for BR1458 bearing mice.

Group	N	Treatment	Dose (mg/kg)	Dosing Volume (mL/kg)	Dosing Route	Schedule
1	10	C1	0	4	*i.v.*	4 days on 3 days off/week x 3 weeks
2	10	NG1	2	4	*i.v.*	4 days on 3 days off/week x 3 weeks
3	10	Docetaxel	2	4	*i.v.*	4 days on 3 days off/week x 3 weeks
4	10	NG2	2	4	*i.v.*	4 days on 3 days off/week x 3 weeks

Assessment of Side Effects: Throughout tumor growth animals were observed for morbidity and mortality daily. Throughout the study the animals were routinely checked for clinical signs of tumor growth or treatment effects on mobility, food and water consumption, body weight gain or loss (measured twice weekly), eye/hair matting and any other unusual observations. Any observed clinical signs and death were recorded.

Statistics: Statistical analysis of MDA-MB-231 was evaluated using Independent-Samples T Test. All data were analyzed in SPSS (Statistical Product and Service Solutions) version 18.0 (IBM, Armonk, NY, U.S.). Analysis of BR1282 (day 14 TV) was conducted using a one-way ANOVA and comparisons using Games-Howell. Statistical analysis of BR1458 (day 14 TV) and BR1474 (day 28 TV) was conducted using a one-way ANOVA and Tukey HSD. Log transformation was performed for homogeneity of variances when necessary. Statistically significant differences were set at p values ≤ 0.05.

3.5 References

1. Safra, T.; Muggia, F.; Jeffers, S.; Tsao-Wei, D. D.; Groshen, S.; Lyass, O.; Henderson, R.; Berry, G.; Gabizon, A. Pegylated liposomal doxorubicin (doxil): Reduced clinical cardiotoxicity in patients reaching or exceeding cumulative doses of 500 mg/m^2. *Ann. Oncol.* **2000**, *11*, 1029–1033.

2. Fassas, A.; Buffels, R.; Kaloyannidis, P.; Anagnostopoulos, A. Safety of high-dose liposomal daunorubicin (daunoxome) for refractory or relapsed acute myeloblastic leukaemia. *Br. Jo. Haematol.* **2003**, *122*, 161–163.

3. Danhier, F.; Feron, O.; Preat, V. To exploit the tumor microenvironment: passive and active tumor targeting of nanocarriers for anti-cancer drug delivery. *J. Control Release* **2010**, *148*, 135-146.

4. Lipinski, C. A. Drug-like properties and the causes of poor solubility and poor permeability. *J. Pharmacol. Toxicol. Methods* **2000**, *44*, 235-249.

5. Shou, M. Prediction of pharmacokinetics and drug-drug interactions from in vitro metabolism data. *Curr. Opin. Drug Discov. Devel*. **2005**, *8*, 66-77.

6. Fang, J.; Nakamura, H.; Maeda, H. The EPR effect: unique features of tumor blood vessels for drug delivery, factors involved, and limitations and augmentation of the effect. *Adv. Drug Deliv. Rev*. **2011**, *63*, 136-151.

7. Urien, S.; Barre, J.; Morin, C.; Paccaly, A.; Montay, G.; Tillement, J. P. Docetaxel serum protein binding with high affinity to alpha 1-acid glycoprotein. *Invest New Drugs* **1996**, *14*, 147-151.

8. Matsumura, Y.; Maeda, H. A new concept for macromolecular therapeutics in cancer chemotherapy: mechanism of tumoritropic accumulation of proteins and the antitumor agent smancs. *Cancer Res.* **1986**, *46*, 6387–6392.

9. Maeda, H.; Nakamura, H.; Fang, J. The EPR effect for macromolecular drug delivery to solid tumors: Improvement of tumor uptake, lowering of systemic toxicity, and distinct tumor imaging in vivo. *Adv. Drug Deliv. Rev.* **2013**, *65*, 71–79.

10. Bae, Y. H.; Park, K. Targeted drug delivery to tumors: myths, reality and possibility. *J. Controlled Release* **2011**, *153*, 198.

11. Gradishar, W. J. Albumin-bound paclitaxel: a next-generation taxane. *Expert Opin. Pharmacother*. **2006**, *7*, 1041-1053.

12. Letchford. K.; Liggins, R.; Wasan, K. M.; Burt, H. In vitro human plasma distribution of nanoparticulate paclitaxel is dependent on the physicochemical properties of poly(ethylene glycol)-block-poly(caprolactone) nanoparticles. *Eur. J. Pharm Biopharm*. **2009**, *71*, 196-206.

13. Lim, W. T.; Tan, E. H.; Toh, C. K.; Hee, S. W.; Leong, S. S.; Ang, P. C.; Wong, N. S., Chowbay, B. Phase I pharmacokinetic study of a weekly liposomal paclitaxel formulation (Genexol-PM) in patients with solid tumors. *Ann. Oncol*. **2010**, *21*, 382-388.

14. Li, C. Poly(L-glutamic acid)-anticancer drug conjugates. *Adv. Drug Deliv. Rev.* **2002**, *54*, 695-713.

15. O'Brien, M. E.; Socinski, M. A.; Popovich, A. Y.; Bondarenko, I. N.; Tomova, A.; Bilynsky, B. T.; Hotko, Y. S.; Ganul, V. L.; Kostinsky, I. Y.; Eisenfeld, A. J.; Sandalic, L.; Oldham, F. B.; Bandstra, B.; Sandler, A. B.; Singer, J. W. Randomized phase III trial comparing single-agent paclitaxel Poliglumex (CT-2103, PPX) with single-agent gemcitabine or vinorelbine for the treatment of PS 2 patients with chemotherapy-naive advanced non-small cell lung cancer. *J. Thorac. Oncol*. **2008**, *3*, 728-734.

16. Li, C.; Newman, R. A.; Wu, Q. P.; Ke, S.; Chen, W.; Hutto, T.; Kan, Z.; Brannan, M. D.; Charnsangavej, C.; Wallace, S. Biodistribution of paclitaxel and poly(L-glutamic acid)-paclitaxel conjugate in mice with ovarian OCa-1 tumor. *Cancer Chemother. Pharmacol.* **2000**, *46*, 416-422.

17. Ernsting, M. J.; Tang, W. L.; Maccallum, N. W.; Li, S. D. Preclinical pharmacokinetic, biodistribution, and anti-cancer efficacy studies of a docetaxel-carboxymethylcellulose nanoparticle in mouse models. *Biomaterials* **2012**, *33*, 1445–1454.

18. Ernsting, M. J.; Foltz, W. D.; Undzys, E,; Tagami, T.; Li, S. D. Tumor-targeted drug delivery using MR- contrasted docetaxel - carboxymethylcellulose nanoparticles. *Biomaterials* **2012**, *33*, 3931–3941.

19. Shelley, W. B.; Talanin, N.; Shelley, E. D. Polysorbate 80 hypersensitivity. *Lancet* **1995**, *345*, 1312-1313.

20. Gelderblom, H.; Verweij, J.; Nooter, K.; Sparreboom, A. Cremophor EL: the drawbacks and advantages of vehicle selection for drug formulation. *Eur. J. Cancer* **2001**, *37*, 1590-1598.

21. Jones S. Head-to-head: docetaxel challenges paclitaxel. *EJC Supplements* **2006**, *4*, 4-8.

22. Zhigaltsev, I. V.; Winters, G.; Srinivasulu, M.; Crawford, J.; Wong, M.; Amankwa, L.; Waterhouse, D.; Masin, D.; Webb, M.; Harasym, N.; Heller, L.; Bally, M. B.; Ciufolini, M. A.; Cullis, P. R.; Maurer, N. Development of a weak-base docetaxel derivative that can be loaded into lipid nanoparticles. *J Control Release* **2010**, *144*, 332-340.

23. Tagami, T.; Ernsting, M. J.; Li, S. D. Efficient tumor regression by a single and low dose treatment with a novel and enhanced formulation of thermosensitive liposomal doxorubicin. *J. Control Release* **2011**, *152*, 303-309.

24. Tagami, T.; Foltz, W. D.; Ernsting, M. J.; Lee, C. M.; Tannock, I. F.; May, J. P.; Li, S. P. MRI monitoring of intratumoral drug delivery and prediction of the therapeutic effect with a multifunctional thermosensitive liposome. *Biomaterials* **2011**, *32*, 6570-6578.

25. Tagami, T.; Ernsting, M. J.; Li, S. D. Optimization of a novel and improved thermosensitive liposome formulated with DPPC and a brij surfactant using a robust in vitro system. *J. Control Release* **2011**, *154*, 290-297.

26. Brunsveld, L.; Folmer, B. J. B.; Meijer, E. W.; Sijbesma, R. P. Supramolecular Polymers. *Chem. Rev*. **2001**, *101*, 4071–4098.

27. Gaucher, G.; Marchessault, R. H.; Leroux, J. C. Polyester-based micelles and nanoparticles for the parenteral delivery of taxanes. *J. Control Release* **2010**, *143*, 2-12.

28. Hrkach, J.; Von Hoff, D.; Ali, M. M.; Andrianova, E.; Auer, J.; Campbell, T.; De Witt, D.; Figa, M.; Figueiredo, M.; Horhota, A.; Low, S.; McDonnell, K.; Peeke, E.; Retnarajan, B.; Sabnis, A.; Schnipper, E.; Song, J. J.; Song, Y. H.; Summa, J.; Tompsett, D.; Troiano, G.; Van Geen Hoven, T.; Wright, J.; Lorusso, P.; Kantoff, P. W.; Bander, N. H.; Sweeney, C.; Farokhzad, O. C.; Langer, R.; Zale, S. Preclinical Development and Clinical Translation of a PSMA-Targeted Docetaxel Nanoparticle with a Differentiated Pharmacological Profile. *Sci. Transl. Med*. **2012**, *4*, 128-139.

29. Duncan R. Polymer conjugates as anticancer nanomedicines. *Nat. Rev. Cancer* **2006**, *6*, 688-701.

30. Auzenne, E.; Ghosh, S. C.; Khodadadian, M.; Rivera, B.; Farquhar, D.; Price, R. E.; Ravoori, M.; Kundra, V.; Freedman, R. S.; Klostergaard, J. Hyaluronic acid-paclitaxel: antitumor efficacy against CD44(þ) human ovarian carcinoma xenografts. *Neoplasia* **2007**, *9*, 479-486.

31. Hudis, C. A.; Gianni, L. Triple-Negative Breast Cancer: An Unmet Medical Need. *The Oncologist*. **2011**, *16*, 1–11.

32. Foulkes, W. D.; Smith, I. E.; and Reis-Filho, J. S. Triple-negative breast cancer. *N. Engl. J. Med*. **2010**, *363*, 1938-1948.

33. Ryu, J. -H.; Chacko, R. T.; Jiwpanich, S.; Bickerton, S.; Babu R. P.; Thayumanavan, S. Self-cross-linked polymer nanogels: a versatile nanoscopic drug delivery platform. *J. Am. Chem. Soc*. **2010**, *132*, 17227–17235.

34. González-Toro, D. C.; Ryu, J.-H.; Chacko, R. T.; Zhuang, J.; Thayumanavan, S. Concurrent Binding and Delivery of Proteins and Lipophilic Small Molecules Using Polymeric Nanogels. *J. Am. Chem. Soc*., **2012**, *134*, 6964-6967.

35. Kavimandan, N. J.; Losi, E.; Wilson, J. J.; Brodbelt, J. S.; Peppas, N. A.; Synthesis and Characterization of Insulin-Transferrin Conjugates. *Bioconjug Chem*. **2006**, *17*, 1376-1384

CHAPTER 4

MATRIX METALLOPROTEINASE-9 RESPONSIVE NANOGELS FOR PROXIMAL SURFACE CONVERSION AND ACTIVATED CELLULAR UPTAKE

4.1 Introduction

A nanoscopic drug delivery platform that can maintain long blood circulation times without compromising selective and rapid target tissue internalization is still a big challenge in obtaining desired therapeutic profiles for clinical applications. The passive mechanism by which nanoscale systems diffuse and accumulate in tumor tissue is a result of fenestrated hypervasculature from angiogenesis and a deficient lymphatic drainage. [1] Albeit somewhat controversial, [2-4] this enhanced permeation and retention (EPR) effect drives the development of particles with long circulation characteristics. In the development of passive nanocarriers, poly(ethylene glycol) polymers (PEG) have been shown to achieve non-fouling characteristics for nanoparticles by reducing non-specific interactions and protein adsorption to their surfaces.[5, 6] The grafting, conjugation, or adsorption of PEG on the surface of macromolecules has been shown to reduce the extent of phagocytic elimination by the reticular endothelial system (RES) and achieve extended blood circulation half-lives. [7-13]

Passive nanogels inherently lack the ability to distinguish healthy tissues from diseased ones, and their stealth surface properties can inhibit cellular interaction resulting in reduced endosomolytic activity.[14, 15] Active targeting aims to address these points through enhancement or specificity of cellular internalization. Active uptake is often pursued through one of two ways: *i)* targeting of unique cell-surface receptors or *ii)* enhanced cellular interaction with cationic materials. The former aims to improve specificity of receptor-mediated endocytosis through cancer cell surface receptors and

antigens.[16-20] Various systems have been explored for active targeting including the incorporation of cell-penetrating peptides,[21,22] targeting peptides,[23] monoclonal antibodies,[24,25,26] or small molecules.[27,28,29] Concerns for *in vivo* surface decoration of such ligands is that they can limit their stealth surface, resulting in RES recognition and clearance,[30] and their tumor penetration.[31] Further, internalization through receptor mediated endocytosis can lead to therapeutic decomposition in the lysosome.[32] The later cationic strategy is due to enhanced charge-charge interaction with the anionic phospholipid bilayer of cell membranes, resulting in adsorptive endocytosis at a higher rate than neutral or anionic formulations.[33,34] Many polycationic nanocarriers have been developed with the aim of improved cellular internalization of therapeutic contents, particularly with anionic nucleotide-based or nucleic acid therapeutics such as siRNA, mRNA, and DNA.[35] Systemic administration of cationic nanomaterials however, result in indiscriminate cellular internalizations, nonspecific adsorption of serum proteins, and short circulation half-lives due to rapid RES clearance.[36-38]

This dilemma can be addressed by developing passive "smart" nanocarriers that become "active" in response to specific stimulus proximal to the disease site. Many externally applied stimuli have been explored (e.g. light, temperature),[39] however tumor-specific endogenous stimuli can exploit inherent physiological biochemical differences in cancerous tissues.[40] Such stimuli that are intrinsic to the extracellular tumor microenvironment include decreased pH and enzyme dysregulation. Nanocarriers with pH-sensitivity have been well explored because lactate production from anerobic glycolysis under hypoxic conditions in tumors causes a pH decrease (6.2-6.9).[42] Nanoscopic systems that can generate positive charge or shed surface PEG in response to mildly acidic

conditions have been demonstrated to facilitate phagocytosis.[42-48] One disadvantage of pH dependent strategies is that inflammatory regions also have mildly acidic hypoxic environments. Further, hypoxia can be variable in incidence and severity, in some cases irregularly affecting regions distant from the nutritive vasculature where oxygen diffusion is limited and the tumor outgrows its blood supply.[49, 50]

The dysregulation of enzymes however, is common to many tumor types and can be highly specific to the local microenvironment.[51,52] The overexpression of matrix metalloproteinases (MMPs), zinc-dependent proteases that degrade the extracellular matrix, has been observed in various cancers and are associated with tumor invasiveness, metastasis, and angiogenesis.[53] Furthermore, these tumor-associated proteases are expressed at the angiogenic invasive anterior of tumors where nanoparticles may more easily access and accumulate, supporting their candidacy as proximal activators of nanoparticles. Variable supramolecular designs in the protease-induced activation of nanoparticles have been pursued.[54-64] Extracellularly overexpressed MMPs have been used to improve cell uptake through exposure of cationic polymeric block[54,55], cationic cell penetrating peptide[56, 57], or through revealing underlying ligands[58-60]. Other approaches have used MMPs to decrease particle hydrodynamic radius[61], or induce nanoparticle morphological changes[62] and disassembly[63, 64] to result in extracellular therapeutic release.

Here, we investigate an abridged protease activation strategy that explores the generation of peptide N-termini on the particle surface to enhance cellular uptake. This strategy can be achieved by simply installing a protease-cleavable substrate to a particle at its C-terminus that is shielded by PEG at its N-terminus (**Scheme 7**). Therefore, peptide hydrolysis by a relevant enzyme, here MMP-9, removes the PEG shield to reveal a

polyamine-type surface from N-termini. The resultant "active" nanogel is expected to internalize more rapidly than its PEGylated parent "passive" nanogel due to charge conversion, reduced steric stabilization, and resultant enhanced membrane interactions. Such a design is versatile and flexible in that the peptide substrate can dictate the sensitivity and specificity of MMP cleavage, or be adapted to the known MMP types in a target tissue of interest. Further, the formulation is modular in nature such that the enzyme-responsive feature is post-conjugated to the pre-formed nanogel surface, allowing for facile substrate amendment and versatility in molecular design. This study focuses on proof-of-concept formulation and characterization of an MMP-9-responsive nanogel delivery platform that offers potential for tumor-specific delivery of chemotherapeutics.

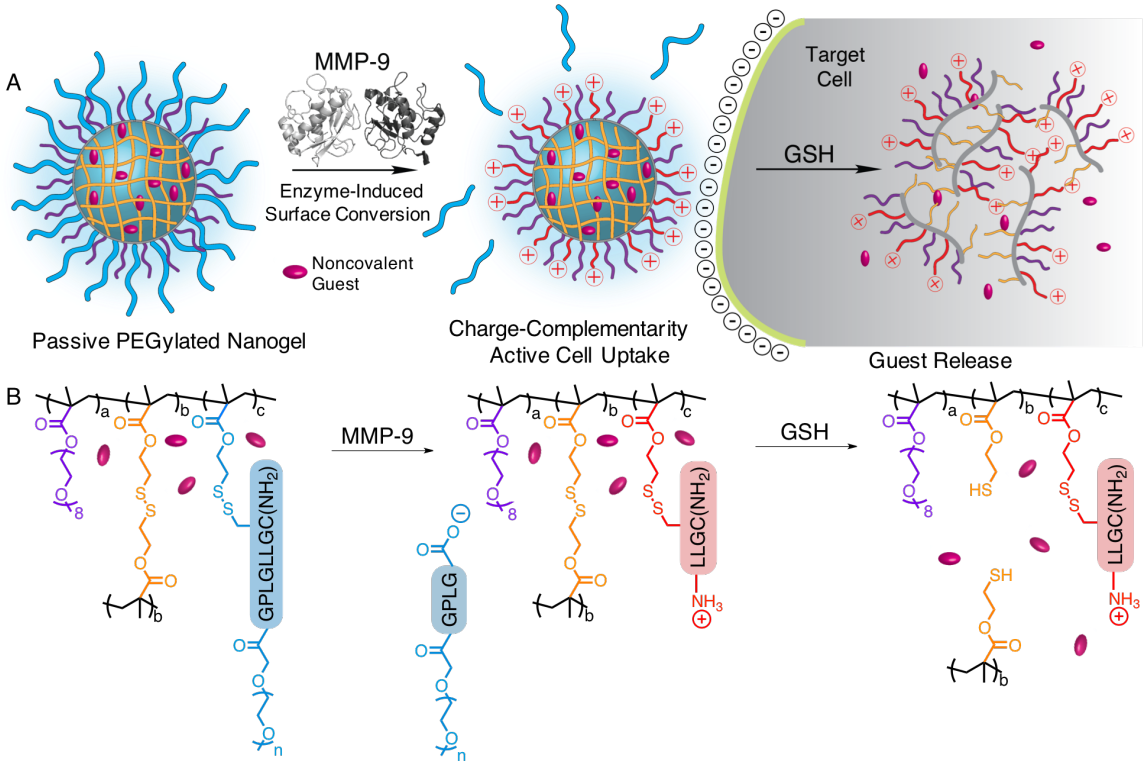

Scheme 7. A) Schematic representation of MMP-9 responsive nanogel and resulting activated cell uptake and GSH release, and B) structural representation of polymer nanogels and stimuli-responsiveness.

4.2 Results and Discussion

4.2.1 Enzyme-Responsive Substrate Synthesis and Proteolysis Validation

Key elements of the suggested nanocarrier are the polymeric nanogel responsible for guest incorporation and intracellular guest release, along with the post-modifiable enzyme responsive substrate that will facilitate cellular internalization. The matrix metalloproteinase-9 responsive peptide-poly(ethylene glycol) monomethyl ether (Mw 350 and 750 g/mol) substrates, mPEG(350)- GPLG↓LLGC(NH_2) and mPEG(750)-GPLG↓LLGC(NH_2), were inspired from collagenous peptide sequences that were shown to be hydrolyzed by type IV collagenases, or MMP-9 between the Gly-Leu bond.[65, 66] Of those investigated, the sequence AcPLG↓LLG-OC_2H_5 was found to be the best substrate for MMP-9, with a similar turnover number (k_{cat}) to denatured collagen and a specific activity of 80 μmol/mg/h.[65] A minimum of six amino acid residues and peptide charge neutrality was found to exhibit more rapid gelatinolytic activity than peptides comprised of less amino acid residues or charged residues. From N- to C-terminus, the substrate for this study was thus designed to contain PEG, an additional glycine residue, the validated PLG↓LLG sequence, and an amide-neutralized cysteine. Two PEG lengths were explored with the expectation that a shorter length may have greater enzyme accessibility, however if proteolysis is sufficient, longer lengths may engender greater difference in cellular interaction from its "passive" to "active" state. The MMP-9 cleavable PEG-peptide conjugates mPEG(350)-GPLG↓LLGC(NH_2) and mPEG(750)-GPLG↓LLGC(NH_2) were made using solid phase peptide synthesis, purified by high performance liquid chromatography, and characterized using electrospray ionization (ESI) and matrix-assisted laser desorption/ionization (MALDI) mass spectrometry (**Figure 66, 67**).

Prior to nanogel conjugation, proteolytic susceptibility of substrates by MMP-9 was evaluated. Synthesized substrates mPEG(350)-GPLG↓LLGC(NH_2) and mPEG(750)-GPLG↓LLGC(NH_2) were incubated with MMP-9 and characterized by liquid chromatography mass spectrometry (LCMS). For both substrates, chromatographic separation of unreacted substrate from digested products was achieved and products were identified (**Figure 71**). For mPEG(350)-GPLG↓LLGC(NH_2) the unreacted substrate eluted at 36-39 min and has a distribution of peaks separated by 44 Da, the mass of one ethylene glycol unit, that is centered at m/z 1020 ($[M+H]^+$, M=1019 g/mol) (**Figure 50**). The expected product LLGC(NH_2) eluted at 15-16 minutes with m/z 404 ($[M+H]^+$, M=403 g/mol), and mPEG(350)-GPLG eluted at 25-31 minutes with a distribution of peaks separated by 44 Da centered at m/z 635 ($[M+H]^+$, M=634 g/mol). The 44 Da mass difference between each peak indicates the repeating ethylene glycol units, which further validate the structure of the cleaved product. Some disulfide LLGC dimer was also observed, which likely occurred during peptide incubation. Likewise, for mPEG(750)-GPLG↓LLGC(NH_2), the unreacted substrate eluted at 39-40 min with m/z 1328 ($[M+H]^+$, M=1327 g/mol). The expected product LLGC(NH_2) eluted at 15-17 minutes with m/z 404, and product mPEG(750)-GPLG eluted at 25-35 minutes with m/z 987 ($[M+H]^+$, M=986 g/mol). The absence of other products supports the specificity of MMP-9 cleavage between the Gly-Leu bond.

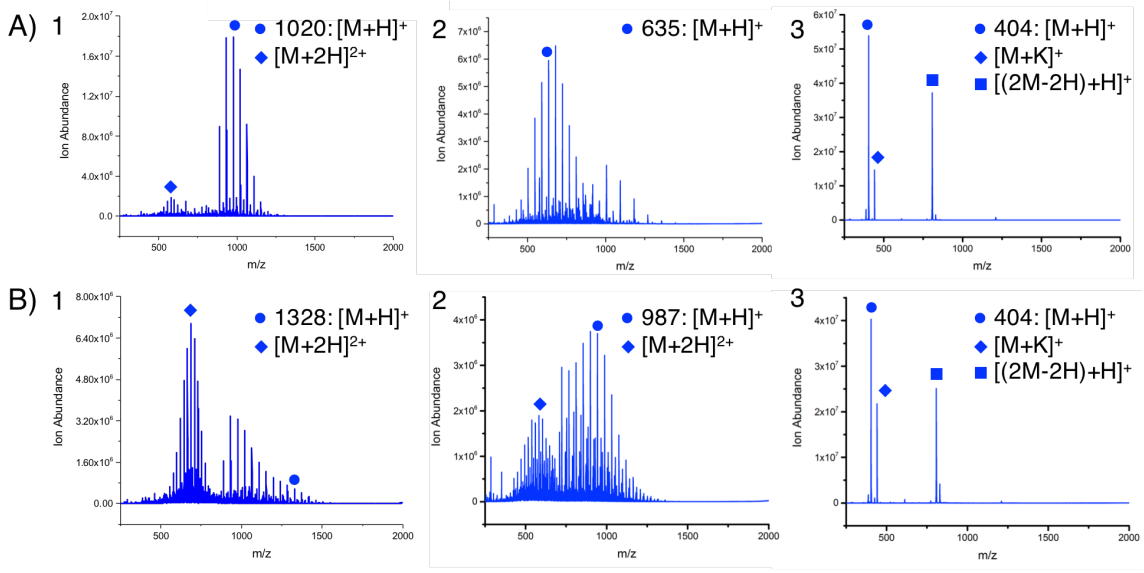

Figure 50. LC-MS ESI characterization of A) mPEG(350)-GPLGLLGC(NH_2) 1) starting material and MMP-9 cleavage products 2) mPEG(350)-GPLG and 3) LLGC(NH_2). ESI characterization of B) mPEG(750)-GPLGLLGC(NH_2) 1) starting material and MMP-9 cleavage products 2) mPEG(750)-GPLG and 3) LLGC(NH_2).

4.2.2 Matrix Metalloproteinase-Responsive Nanogel Synthesis and Characterization

To afford nanoparticles with MMP-9 responsive characteristics, we utilized the previously reported self-crosslinking disulfide-based nanogel scaffold.[67] The polymeric nanogels are achieved using amphiphilic random copolymers that self-assemble into nanoscale aggregates with disulfide functionality that allows for both controlled guest entrapment and stimuli-responsive release. Redox-responsive guest release from nanoassemblies are of significant interest due to their sensitivity to concentrations of glutathione (GSH) in blood plasma (10 μM) compared to the cytosol (10 mM).[67-69] While stable encapsulation is observed at extracellular GSH concentrations, these nanogels release their therapeutic cargo following cellular internalization and exposure to cytosolic concentrations of GSH. In this work, we expanded this platform to include a second stimuli-responsive feature at the particle surface, which can modify its cell interaction and facilitate cellular uptake.

The p(OEGMA-*co*-PDSMA) random copolymer used for nanogel formation was synthesized by a reversible addition–fragmentation chain transfer (RAFT) polymerization of monomers poly(ethylene glycol) methyl ether methacrylate (OEGMA) and pyridyldisulfide ethyl methacrylate (PDSMA). After polymerization, the polymer was purified by dialysis against dichloromethane to remove unreacted monomers, then characterized by NMR and GPC (**Figure 61, 62**). We used the characteristic resonances of the 2-pyridylthio moieties of PDSMA (δH_a = 8.45, δH_b = 7.66, and δH_c = 7.10 ppm) and methoxy moieties of OEGMA (δH_d = 3.37 ppm) to calculate the relative ratios of the monomer incorporated in the polymer as 7:3 PDS to OEG. The GPC obtained number-average molecular weight (M_n) and dispersity ($Đ = M_W/M_n$) of the copolymer was 31.9 kDa and 1.4, respectively.

The nanogel was then formulated by dispersing the p(OEGMA-*co*-PDSMA) random copolymer in an aqueous phase in the presence of Na_2SO_4 (25 mM) to form ~20 nm self-assembled aggregates. The aggregates were then locked in conformation through intra-aggregate disulfide crosslink formation (**Scheme 8**). The covalent crosslinking is achieved via the addition of a sub-stoichiometric amount of reducing agent, DL-dithiothreitol (DTT), which generates the corresponding quantity of free thiols on PDS moieties within the aggregate interior, which then react with remaining activated PDS moieties in the polymer chain. For these nanogels, we used 12.5 mol% DTT, relative to PDS in the aggregates, to result in 25% crosslinked nanogels. The crosslinking for resultant Bare-NG was quantified by the reaction byproduct 2-pyridinethione using its characteristic absorption peak at 343 nm (**Figure 69**).

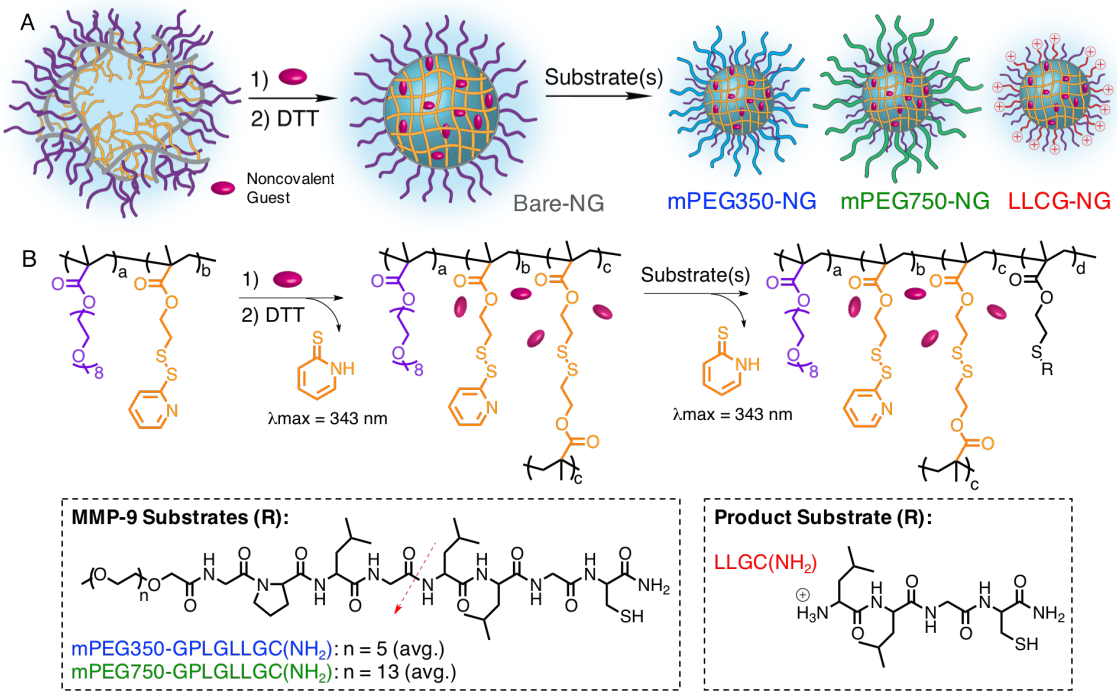

Scheme 8. A) Schematic representation of polymeric nanogel formation, and B) structural representation of polymer nanogels synthesis with structure of substrates.

Next, nanogels were decorated with either mPEG(350)-GPLG↓LLGC(NH_2), mPEG(750)-GPLG↓LLGC(NH_2), or positive control LLGC(NH_2) through a thiol-disulfide exchange reaction between the cysteine thiols of the peptide and PDS groups of the nanogel (**Scheme 8**). Peptides dissolved in methanol were added to the aqueous crosslinked nanogels and post modification was quantified by absorbance using the reaction byproduct 2-pyridinethione (**Figure 69**). The resulting nanogels denoted mPEG350-NG, mPEG750-NG, and LLGC-NG contained ~30% peptide functionalization respective to PDS, for each mPEG(350)-GPLG↓LLGC(NH_2), mPEG(750)-GPLG↓LLGC(NH_2), and LLGC(NH_2), respectively (**Table 23**). Conjugation efficiency for LLGC(NH_2) was 73%, while the conjugation efficiencies for mPEG(350)-GPLG↓LLGC(NH_2) and mPEG(750)-GPLG↓LLGC(NH_2) were 64% and 56%,

respectively. Nanogels were purified by dialysis and MALDI characterization of nanogel confirmed removal of free peptide (**Figure 51**). Post-modification of the peptides to the nanogels did not appreciably change the particle sizes, or cause any observable precipitation or aggregation as characterized by DLS (**Figure 51**). Due to the known lower critical solution temperature (LCST) characteristics of PEG, the temperature responsiveness of these nanogels were characterized by DLS. Size transitions were observed well above 37 °C, suggesting nanoparticle integrity at biologically-relevant conditions (**Figure 70**).

Table 23. Characterization of substrate-functionalized nanogels.

Sample	Crosslink (% PDS)	Substrate Identity	Substrate (% PDS)	Size (nm)
Bare NG	24	--	N/A	16
mPEG350-NG	24	mPEG350-GPLGLLGC(NH_2)	32	18
mPEG750-NG	24	mPEG750-GPLGLLGC(NH_2)	28	18
LLGC-NG	24	LLGC(NH_2)	33	16

4.2.3 Surface-Conversional Validation and Quantification

The proteolytic capability of MMP-9 to cleave peptide from the nanogel surface was confirmed using MALDI-MS. On a substrate decorated particle surface, we expect MMP-9 proteolysis to generate free mPEG-GPLG in solution while LLGC(NH_2) remains conjugated to the particle by the C-terminal cysteine. The nanogels were incubated with active MMP-9 at 37 °C for 24 hours in PBS pH 7.4. Following this incubation, any free cleaved peptide was isolated for analysis using 3 kDa centrifuge filtration. The centrifuged solutions were then mixed with matrix solutions containing CHCA and characterized by MALDI-MS. As a control, nanogels not incubated with MMP-9 were characterized to demonstrate that masses corresponding to free substrates were not observed prior to proteolysis, while their cleavage products were evident following MMP-9 treatment

(**Figure 51**). MALDI analysis of mPEG350-NG incubated with MMP-9 generated a distribution of peaks separated by 44 Da that is centered at m/z 767, which correlates to $[M+H]^+$ of product $mPEG_8$-GPLG. MMP-9 mediated mPEG750-NG proteolysis also exhibited a distribution of peaks separated by 44 Da with a distribution maxima of m/z 1,141, which correlates to $[M+Na]^+$ of product $mPEG_{16}$-GPLG. For both nanogels, these proteolysis products have a slightly higher PEG distribution shift than observed on free substrate. This slight change can be attributed to either preferential conjugation of longer PEG species to the particle due to enhanced aqueous solubility, or higher MALDI ionization efficiency of the longer PEG species.

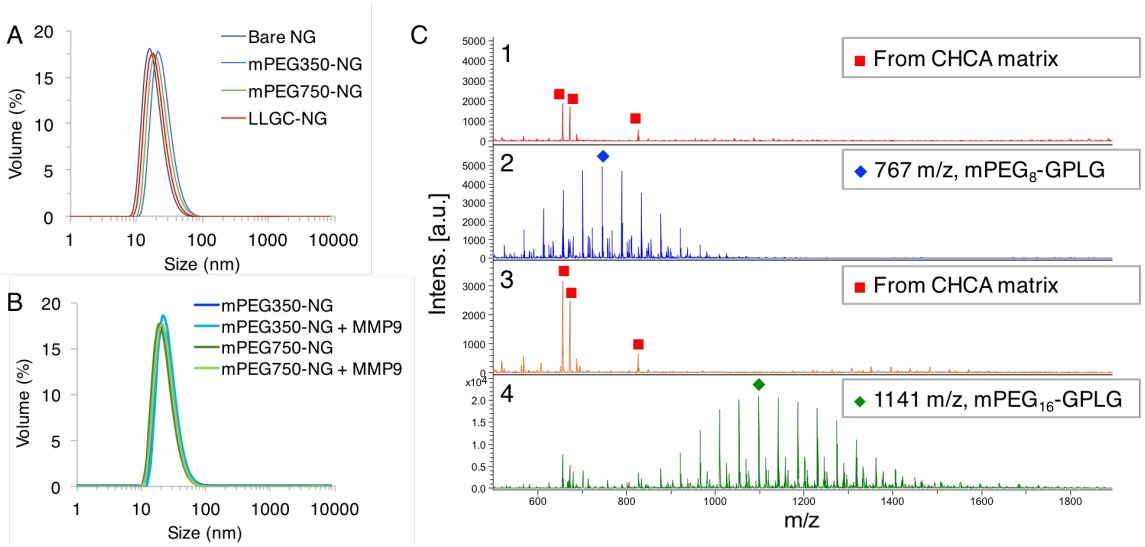

Figure 51. DLS sizes by volume of A) Bare NG and substrate-modified nanogels and B) MMP-9 responsive NGs mPEG350-NG and mPEG750-NG before and after MMP (54 nM) treatment. C) MALDI characterization of substrate containing nanogels 1) mPEG350-NG, 2) mPEG350-NG pretreated with MMP-9 (54 nM), 3) mPEG750-NG, 4) mPE7350-NG pretreated with MMP-9 (54 nM).

We then investigated the generation free amines on the nanogel surfaces by MMP-9 proteolysis and aimed to quantify the reaction using a fluorescamine assay. In this assay, non-fluorescent fluorescamine (4-phenylspiro[furan-2(3H), 1'-phthalan]-3,3'-dione) reacts directly with primary amines to form a fluorescent product (390 nm excitation, 465 nm

emission). Previous reports have observed near complete reaction between lysines and N-terminus of peptides with fluorescamine.[72] Because fluorescence is proportional to the quantity of free amines present, this assay is often used to detect and quantify proteins with high sensitivity.[72-74] The fluorescamine assay has been frequently used to monitor supramolecular processes as well, such as characterization of poly(L-lysine)-DNA complexes that are post-modified a multivalent polymer.[73] Likewise, we expect the N-termini generated by MMP-9 proteolysis on a nanogel surface to be quantifiable using the fluorescamine assay.

Here we used the positive control nanogel, modified with 33% LLGC(NH_2), to demonstrate the reaction between fluorescamine and a modeled MMP-9 created N-terminus. Moreover, the fluorescence generated is proportional to the concentration of N-termini present from the functionalized peptide. Because the fluorescamine reaction is highly efficient, the fluorescence from this sample can be assumed to represent a nanogel with 100% cleavage. A concentration dependent calibration curve was generated using 3 molar excess of fluorescamine in DMSO with various concentrations of LLGC-NG (mg/mL) PBS buffer pH 7.4 and monitoring the fluorescence intensity (**Figure 52**). The fluorescamine assay confirmed that the fluorescence intensity was linearly proportional to the concentration of LLGC-NG, and appropriate for quantification of N-termini in solution.

Nanogels were incubated with low nanomolar concentrations of MMP-9 (0.54-5.4 nM) to evaluate responsivity to levels reported in plasma (50-500 ng/mL) for various cancers.[74-76] There have been significant efforts to determine plasma or serum concentrations of MMP-9 to discern cancer progression and prognosis significance. Local tumor concentrations are expectedly higher, and cell culture of different cancer lines report

MMP-9 excretions in the high nanomolar to low micromolar range.[63, 77] This is heterogeneous across different tumor types[78], so we assigned an MMP-9 concentration of 54 nM (5 μg/mL) as a conservative estimate to evaluate responsivity at tumor-relevant extracellular matrix concentrations. To understand concentration affects, mPEG350-NG and mPEG750-NG nanogels were incubated with 0.54, 5.4, and 54 nM MMP-9, and at determined time points quenched, purified by 100 kDa dialysis, then reacted with fluorescamine for quantification. Obtained fluorescence intensities were calculated against the linear fit of LLGC-NG to determine percentage of N-termini, i.e. cleavage, generated by MMP-9.

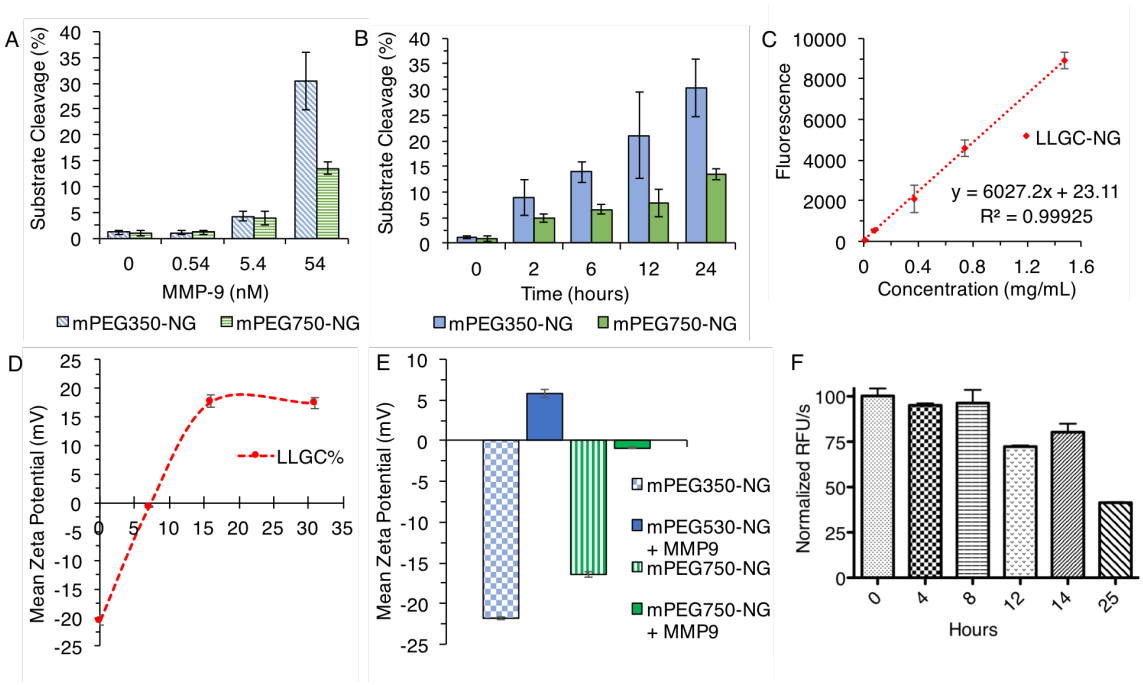

Figure 52. Fluorescamine assay results for MMP-9 substrate cleave percent by A) concentration and B) time for nanogels (avg. ± std, n=3 repeat), and C) fluorescence calibration of LLGC-NG (avg. ± std, n=4 measurements). D) Mean zeta potential of nanogels conjugated with increasing LLGC% (avg. ± std, n=3 measurements). D) Mean zeta potential of mPEG350-NG and mPEG750-NG before and after MMP-9 treatment (avg. ± std, n=3 measurements). F) Confirmation of MMP-9 activity over the 24-hour experiment, expressed as normalized RFU/s with 8 hours ProMMP-9 activation with APMA as time 0 of nanogel incubation (avg. ± std, n=2 repeat).

Nanogels incubated without MMP-9 showed negligible fluorescence, confirming

the expected absence of amines on the starting material (**Figure 52**). At 0.54 nM MMP-9, negligible (~1%) cleavage was observed for both mPEG350-NG and mPEG750-NG after a 24-hour incubation, which were similar in value to those obtained for 0 nM MMP-9. At moderate concentrations (5.4 nM), as expected low cleavage values were still obtained, with ~4% for both nanogels. Under extracellular relevant concentrations of MMP-9 (54 nM), 30±6% of the substrate was cleaved from the mPEG350-NG nanogel surface after 24 hours. For mPEG750-NG, however, approximately half the amount of cleavage was obtained, with 14±1% cleaved at 24 hours. To evaluate this result, time dependent cleavage of 54 nM MMP-9 was obtained. This analysis showed that much higher cleavage occurred with mPEG350-NG compared to mPEG750-NG, however was progressive over the full 24 hours for both systems. We hypothesize that this difference is due to substrate accessibility, as it is expected that the longer PEG lengths can cause more steric hindrance and restrict the extent of protease-mediated substrate cleavage.

We were also interested in evaluating this surface conversional property by examining nanocarrier zeta potential change. Precursor Bare NG and substrate-decorated nanogels mPEG350-NG and mPEG750-NG gave zeta potentials of -21 mV, -22 mV and -17 mV, respectively (**Figure 52**). Although the negative zeta potential of anticipated neutral PEG surface seems unexpected, several reports indicate PEG-decorated nanostructures do have negative zeta potentials.[42, 79, 80] The cause of this, however, is thus far unclear. Nanogels were then decorated with increasing amounts of amine terminus containing peptide LLGC(NH_2) to test the veracity of the amine terminus to inflict a positive zeta potential on these nanogels. Indeed, conjugation of LLGC(NH_2) developed a positive charge, with zeta potential becoming more neutral at -1 mV for 7% conjugation

and +18 mV for 16% conjugation, which did not become more positive with higher peptide conjugation. This guided our rationale that even small amounts of this substrate could impact the surface charge of these nanogels. The zeta potentials of mPEG350-NG did indeed become less negative after incubation with MMP-9, with a mean zeta potential of +6 mV after 24 hours of treatment. This suggests a significant shift in surface character from the initial value of -22 mV. Measurably positive surface charge was not achieved with mPEG750-NG, with maximum value of -1 mV after 24 hour MMP-9 incubation. This is consistent with the lower cleavage extent observed by fluorescamine assay on this particle, further supporting that accessibility of the protease to substrate limited the surface-conversion capability.

4.2.4 Guest Encapsulation and Stimuli-Responsive Release

For this nanocarrier, guest encapsulation under both stimuli GSH and MMP-9 was evaluated. To test the structural stability and guest release in response to stimuli, nanogels encapsulated with a model hydrophobic guest 1,1'-dioctadecyl-3,3,3',3'-tetramethylindocarbocyanine perchlorate (DiI) were prepared for mPEG350-NG, mPEG750-NG, and Bare NG to serve as a MMP-9 non-responsive control (**Figure 53**). Due to the hydrophobicity of DiI, we expect any dye release from the nanogels interior to result in precipitation and resulting fluorescence decrease. Nanogels were prepared in TNC buffer, pH 7.4, and the fluorescence of DiI was monitored over time in response to GSH, ProMMP-9 to serve as non-catalytic protein control, or MMP-9 at various concentrations.

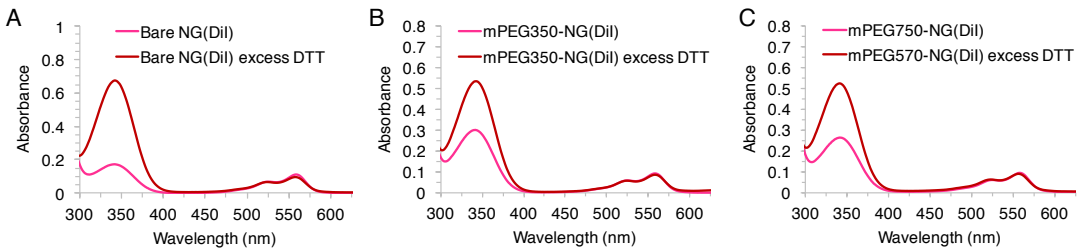

Figure 53. UV-visible spectra of crosslinking of A) Bare NG, and post modification with substrates to give B) mPEG350-NG and B) mPEG750-NG compared to excess DTT for maximum release byproduct 2-pyridinethione (λ_{max} = 343 nm) in nanogels loaded with DiI (λ_{max} = 558 nm).

The trends in guest release were similar for Bare-NG, mPEG350-NG, and mPEG750-NG (**Figure 54**). In all cases, the nanogel control, which is exposed to no stimulus, exhibited some release over 48 hours, with 4±3, 13±7, and 8±4% for Bare-NG, mPEG350-NG, and mPEG750-NG, respectively (**Table 24**). This release is likely due to loss of any adsorbed or poorly encapsulated DiI from buffer dilution. We investigated the release capabilities under cytosolic redox conditions and as expected, the disulfide-based nanogel crosslinks were responsive to reduced glutathione. Over a 48-hour period, we observed 51±3, 42±1, and 48±1% release of encapsulated DiI in the presence of 10 mM GSH at pH 7.4, for Bare-NG, mPEG350-NG, and mPEG750-NG, respectively (**Figure 54**). Release values in response to extracellular reduced GSH concentrations (10 μM) were similar to the controls, supporting low responsivity to extracellular GSH levels.

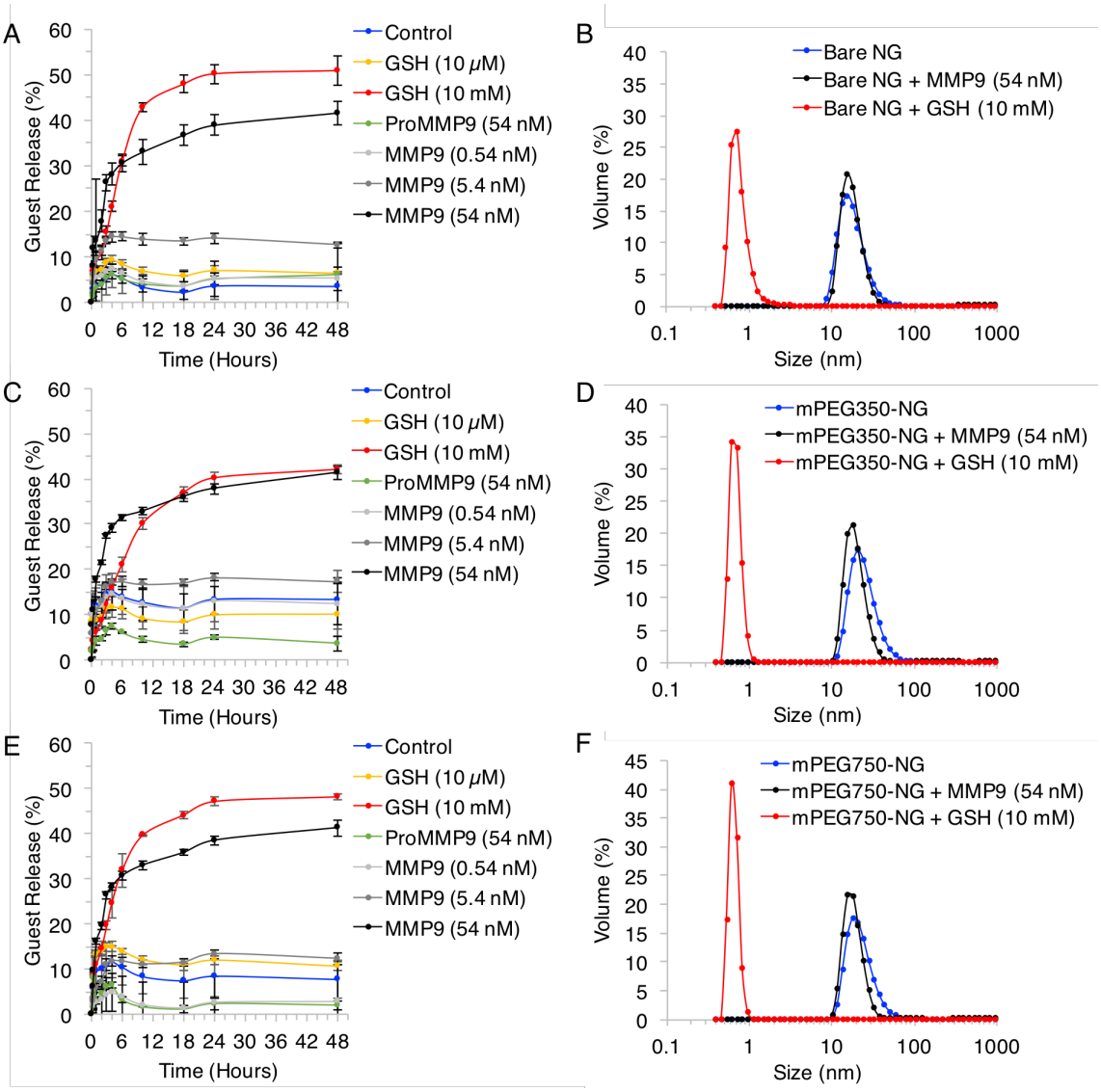

Figure 54. Guest release based on normalized fluorescence for nanogels A) Bare over 48 hours in response to GSH (10 mM and 10 μM), ProMMP-9 (54 nM), and MMP-9 (0.54, 5.4, and 54 nM) compared to no stimulus control, and B) corresponding DLS of nanogel sizes upon exposure to MMP-9 (54 nM) and GSH (10 mM) and serial dilution. C) Guest release and D) DLS plots of mPEG350-NG upon exposure to stimuli, and E) guest release and F) DLS plots of mPEG750-NG upon exposure to stimuli.

Unexpectedly, we also observed some release by MMP-9 with values of 42±3, 41±1, and 41±2% at 48 hours for Bare-NG, mPEG350-NG, and mPEG750-NG, respectively (**Figure 54**). This was heavily dependent on MMP-9 concentration, with far less release observed at serum concentration of MMP (5.4 nM), and values similar to

controls at 0.54 nM. Furthermore, this release was not observed with the inactive proenzyme, ProMMP-9, with 6±7, 4±2, and 2±1% at 48 hours for 54 nM for nanogels Bare-NG, mPEG350-NG, and mPEG750-NG, respectively, which was irrespective of concentration, (**Figure 55**). This suggests that the release mediated by MMP-9 is not due to general non-specific protein interaction with the nanogels, but unique to MMP-9 catalytic activity with the nanogels. However, this is not a result of the MMP-responsive substrates, as the same result was observed with the non-MMP-responsive Bare NG. Further, DLS characterization of the nanogels was executed under severe dilution conditions (1000-fold) and we observed maintained particle integrity of MMP-9 (54 nM) treated nanogels, while those treated with 10 mM GSH lost its aggregation capability (**Figure 54**). One possibility for observed release is that the protease could exhibit some esterase activity, cleaving ester bonds in the polymer structure. This could be easily avoided for these nanogels through use of acrylamide rather than methacrylate-based monomers. Some premature extracellular guest release would still be unique to tumor-relevant high protease concentrations, and therefore in the target region and may not be of concern.

Table 24. Guest release % for A) Bare NG B) mPEG350-NG, and C) mPEG750-NG at 48 h.

	Control	GSH (10 μM)	GSH (10 mM)	ProMMP (.54 nM)	ProMMP (5.4 nM)	ProMMP (54 nM)	MMP (.54 nM)	MMP (5.4 nM)	MMP (54 nM)
A	3.5±3.3	6.4±0.2	50.9 ±3.2	4.6±0.4	5.8±0.3	6.3±6.6	5.3±2.6	12.7±0.6	41.6±2.5
B	13.3±6.6	10.2±4.8	42.0±1.0	6.7±1.4	5.7±0.2	3.8±1.6	12.5±4.8	17.4±0.6	41.3±1.3
C	7.8±4.3	10.6±1.0	48.2±0.7	3.4±1.8	1.6±0.8	2.1±0.9	2.8±8.3	12.3±1.2	41.3±1.7

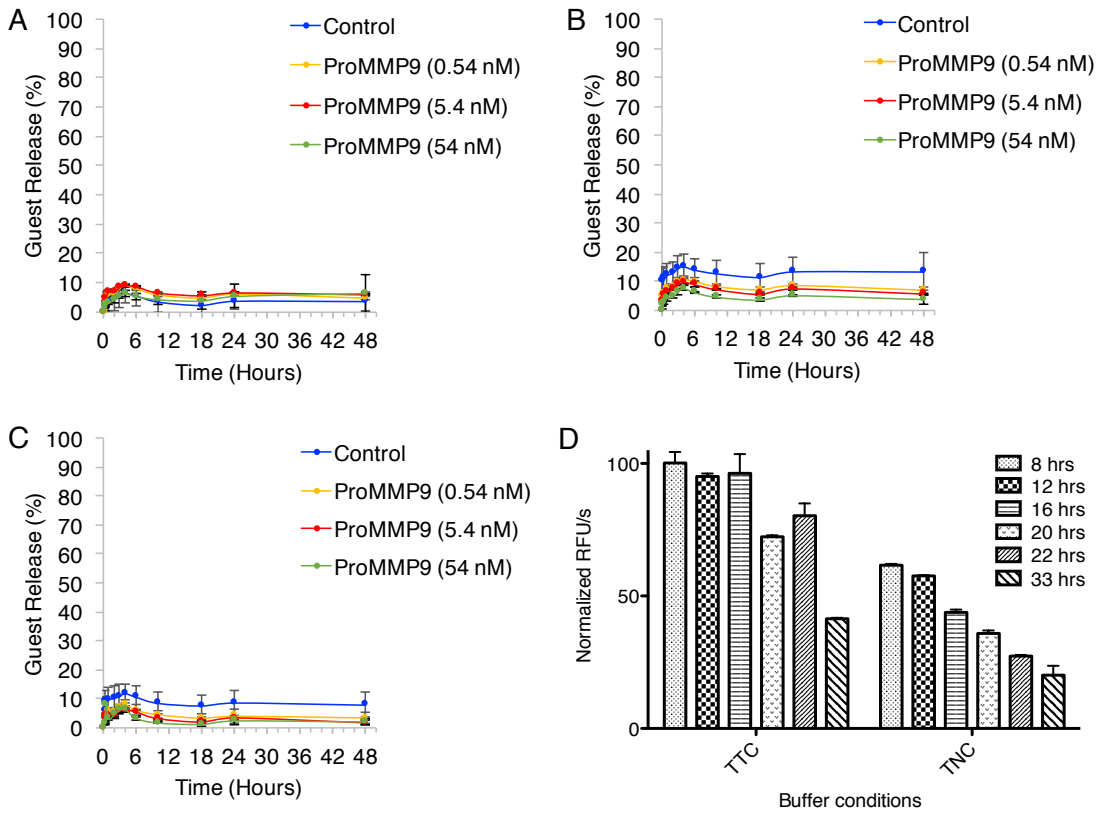

Figure 55. Guest release based on normalized fluorescence for nanogels A) Bare NG B) mPEG350-NG, and C) mPEG750-NG over 48 hours in response to ProMMP-9 (0.54, 5.4, and 54 nM) compared to no stimulus control. D) Activty of MMP-9 monitored in TTC and TNC buffer over 33 hours (8 hour APMA activation is 0 hour of nanogel incubation).

4.2.5 Cellular Uptake Analysis

Confocal microscopy was used to evaluate whether the nanogels were taken up by human HeLa cells at an enhanced rate following MMP-9 treatment. Cytotoxicity of these nanogels was evaluated for the HeLa cell line using the MTT cytotoxicity assay, demonstrating >70% viability even up to 1 mg/mL (**Figure 56**). To monitor the *in vitro* cellular uptake, nanogels were first covalently modified with 5% thiol-modified fluorescein label. Negative "passive" controls mPEG350-NG(F) (fluorescein) and mPEG750-NG(F), amine-decorated positive control LLGC-NG(F), and test samples

MMP-treated mPEG350-NG(F) Active and mPEG750-NG(F) Active were all prepared with fluorescein tag and were the same size by DLS (**Figure 57**).

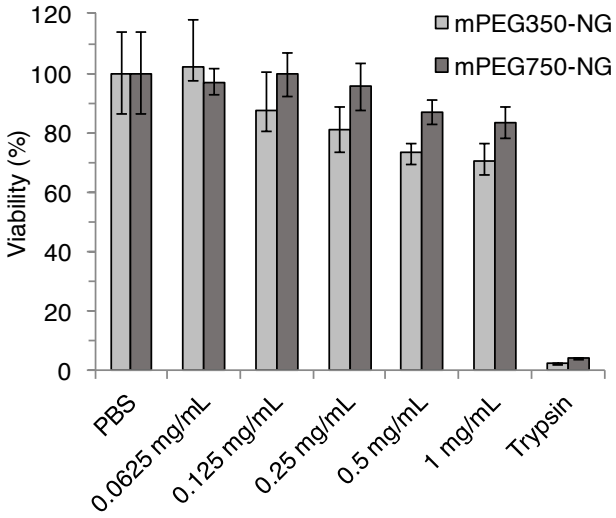

Figure 56. MTT toxicity assay with nanogels mPEG350-NG and mPEG350-NG compared to positive control (PBS) and negative control (trypsin).

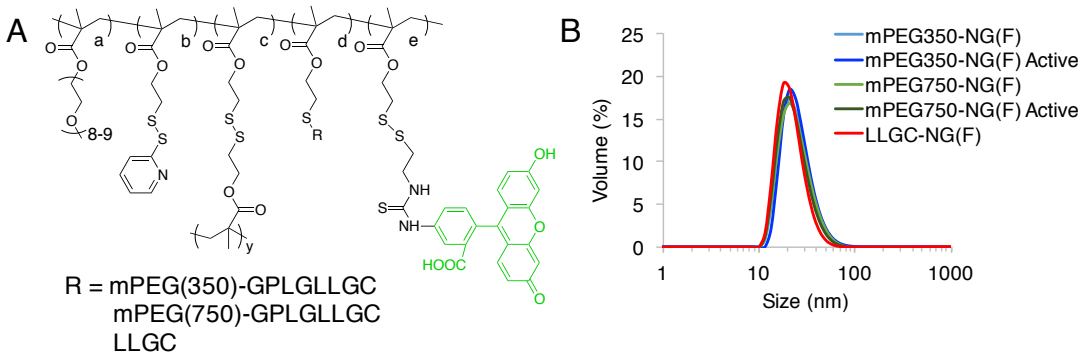

Figure 57. Fluorescein-modified nanogel A) structure and B) sizes by DLS for confocal Microscopy.

Nanogels were incubated with HeLa cells for 2 hours before confocal imaging, and NG uptake was observed using laser excitation at 488 nm. Consistent with expectations, from microscopy images "passive" PEG-decorated mPEG350-NG(F) showed much lower cellular uptake than amine-decorated LLGC-NG(F) (**Figure 58**). This result supported our anticipation that the poly-amine character from N-termini could be sufficient in modifying the adsorption of nanogels on cellular membranes. Indeed, once treated with MMP-9,

mPEG350-NG(F) Active exhibited uptake much more reminiscent of positive control LLGC-NG(F). Therefore, the extent of enzymatic proteolysis achieved on this nanogel was sufficient to achieve a surface-conversion and alter its cellular uptake. The results are likely a combination of PEG reduction of endosomolytic activity and improved charge-charge adsorption of polyvalent amines on the phospholipid bilayer of cells. Microscopy z-stack images at 100× objective supported these results (**Figure 59**). Nanogel mPEG750-NG(F), however, did not exhibit an observable difference in uptake following MMP-9 treatment, which shows that the extent of cleavage that occurs on these particles is crucial in obtaining this improved cell-membrane interaction. These results were supported quantitatively by flow cytometry, which showed highest fluorescence intensities of FITC in HeLa cells with positive control LLGC-NG, and a greater fluorescence intensity for mPEG350-NG Active compared to mPEG350-NG (**Figure 58**). Consistent with microscopy observations, mPEG750-NG did not show uptake enhancement following MMP activation, with similar median FITC fluorescence intensities. It is possible that either higher protease concentrations or longer incubation times could improve the extent of MMP-9 surface charge turnover for longer PEG nanogel, but these results suggest a fine balance is required between substrate PEG shielding and enzyme accessibility to achieve the "passive" to "active" conversion.

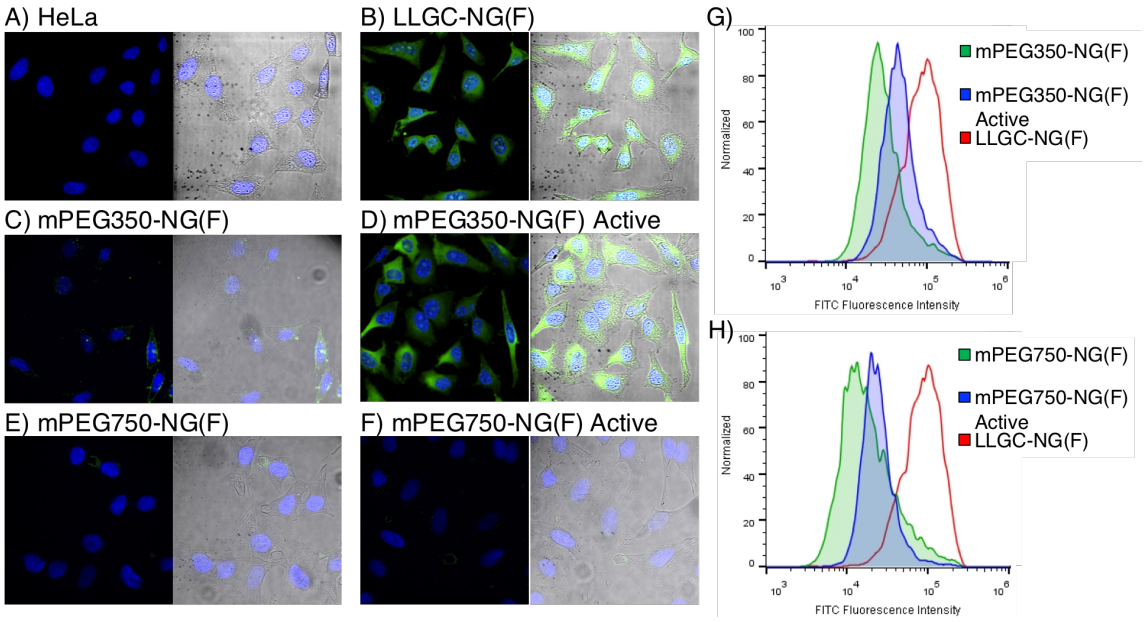

Figure 58. Confocal microscopy images using a 40× objective of composite (left) with nucleus (blue 405 nm) and fluorescein-labeled NG (green, 488 nm), and composite with brightfield (right) image overlays of HeLa cells after 2-hour incubation with A) no sample, and fluorescein-labeled nanogels B) LLGC-NG(F) positive control, C) mPEG350-NG(F), D) mPEG350-NG(F) Active, E) mPEG750-NG(F), F) mPEG750-NG(F) Active. Flow cytometric histogram profiles of FITC fluorescence intensity for HeLa cells incubated with LLGC-NG(F) and G) mPEG350-NG(F) and mPEG350-NG(F) Active, and H) mPEG750-NG(F) and mPEG750-NG(F) Active.

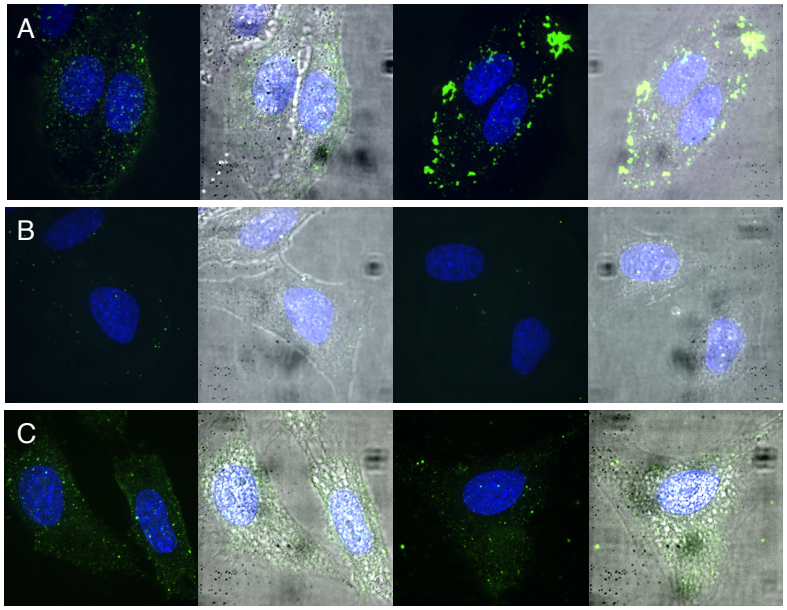

Figure 59. Confocal microscopy 100× composite (left) and brightfield (right) images of HeLa cells after 2-hour incubation with fluorescein-labeled nanogels A) LLGC-NG(F), B) mPEG350-NG(F), C) mPEG350-NG(F) Active. Two images represented for each.

We then investigated the internalization behavior of DiI-encapsulated mPEG350-NG before and after MMP treatment to determine the capability to deliver a hydrophobic guest. This was of interest due to observed DiI release from nanogels under high concentrations of MMP-9. DiI loaded mPEG350-NG was activated with MMP-9, then purified by 100 kDa dialysis and filtration to remove any released free DiI prior to confocal analysis. A loss of ~20% of DiI was observed by absorbance spectra (λ_{max} = 558 nm) following MMP-9 activation compared to untreated control (**Figure 60**). Nanogels were incubated with HeLa cells for 2 hours at the same nanogel concentration (0.1 mg/mL) so that comparative uptake could be evaluated despite the DiI loss. Uptake was observed by confocal microscopy using laser excitation at 540 nm. Even with less fluorophore guest, significantly different cellular uptake was observed for mPEG350-NG(DiI) and mPEG350-NG(DiI) active. These results suggest that the higher internalization is not due to guest quantity or extracellular leakage, but from the greater uptake of MMP-9 activated nanogels, consistent with fluorescein-labeled nanogel results. The enhanced delivery of a hydrophobic guest illustrates the potential for the protease-activation strategy to improve the internalization of therapeutic cargo in MMP-rich environments.

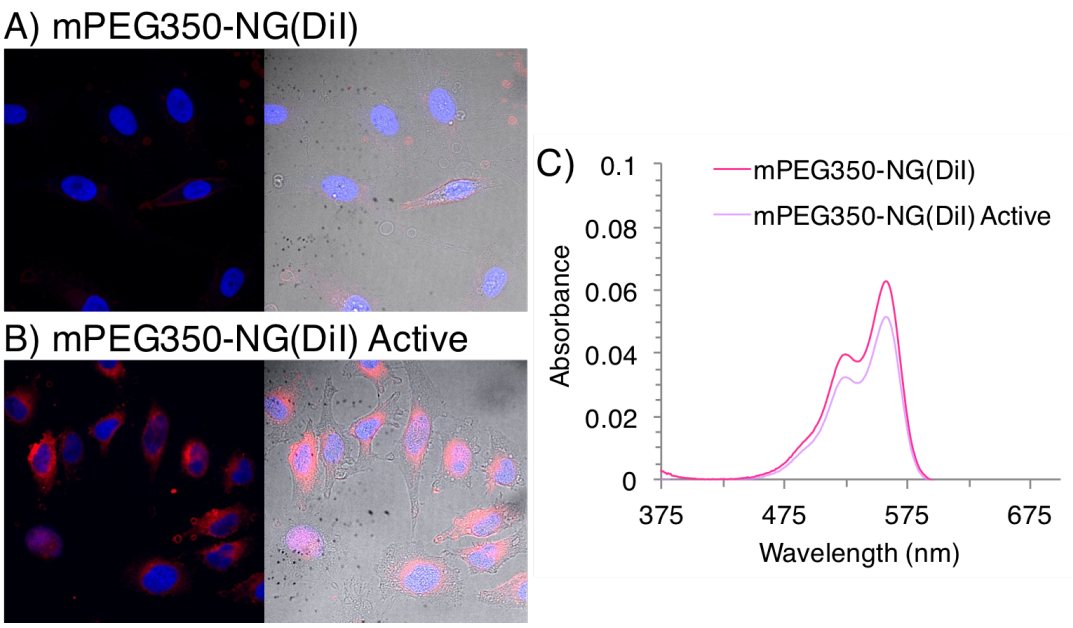

Figure 60. Confocal microscopy images using a 40× objective of composite (left) with nucleus (blue 405 nm) and DiI-loaded NG (red, 540 nm), and composite with brightfield (right) image overlays of HeLa cells after 2-hour incubation with A) mPEG350-NG(DiI) and B) mPEG350-NG(DiI) Active. C) UV-visible absorbance spectra of DiI encapsulation before and after MMP-9 activation. Dye release calculated from decrease in absorbance at λ_{max} 558 nm.

4.3 Conclusion

In summary, we report on a nanogel capable of converting its surface properties from a passive PEGylated particle to an active amine decorated particle in the presence of MMP-9, a protease frequently observed in the tumor extracellular environment. We have shown that: (*i*) the incorporation of MMP-9 substrate on the nanogel surface can lead to a MMP-9 dependent surface conversion from PEG to N-termini, (*ii*) this conversion is dependent on time and the concentration of MMP-9 present, and circulation concentrations of MMP-9 were inadequate while tumor extracellular concentrations of MMP-9 were adequate in achieving surface conversion, (*iii*) the surface conversion process can be used to enhance nanocarrier cellular uptake specifically under desired MMP-9 upregulated environments, and (*iv*) this surface proteolysis on the particle does not lead to nanogel

disassembly, while the intracellular concentrations of reducing glutathione do cause disassembly.

Considering the molecular design, we expect that the sensitivity and specificity of peptidase response can be modified based on the identity of the proteolysis-susceptible peptide incorporated. Because this strategy of N-terminus generation can be achieved by simply installing the substrate to the particle at its C-terminus, it allows for flexible sequence selection and adaptation to the appropriate upregulated MMPs or other proteases in the target tissue. The modular formulation achieved by post-assembly modification with substrate using thiol-disulfide exchange allows for facile incorporation of a variety of responsive sequences, opening a variety of avenues for the design of these protease-responsive surface conversional nanogels.

4.4 Experimental

4.4.1 Materials and Methods

Polyethylene glycol monomethyl ether (average MW 350 and 750 g/mol) , 4-aminophenylmercuric acetate (APMA), methacryloyl chloride, 2-mercaptoethanol, poly(ethyleneglycol) monomethyl ether methacylate (OEGMA; MW 500 g/mol), 4-cyano-4-(phenylcarbonothioylthio)pentanoic acid, chromium trioxide, sulfuric acid, trifluoroacetic acid, triisopropylsilane, 1,2-ethanedithiol, DL-dithiothreitol (DTT), 2-(4-amidinophenyl)-6-indolecarbamidine dihydrochloride (DAPI), fluorescein isothiocyanate isomer 1 (FITC), cystamine dihydrochloride, trimethylamine, tris(2-carboxyethyl)phosphine hydrochloride (TCEP), 1-[bis(dimethylamino)methylene]-1*H*-1,2,3-triazolo[4,5-b]pyridinium 3-oxid hexafluorophosphate (HATU), piperidine solution and fluorescamine were purchased from Sigma Aldrich and used without further

purification. AIBN (2,2'-azobis(2-methylpropionitrile) was purchased from Sigma Aldrich and purified by recrystallization. Amino acids and Rink Amide AM resin (100-200 mesh) for solid phase peptide synthesis were purchased from EMD Millipore. ProMMP-9 was purchased from BioLegend Inc. Fluorogenic peptide substrate Mca-PLGL-Dpa-AR-NH2 was purchased from R&D Systems, Inc. Solvents, Dulbecco's modified Eagle's medium (DMEM), fetal bovine serum (FBS), trypsin-EDTA (0.5%, no phenol red) were purchased from Fisher Scientific. Penicillin-streptomycin-glutamine (100x) solution, PBS 7.4, and 3-(4,5-dimethylthiazol-2-yl)-2,5-diphenyltetrazolium bromide (MTT) were purchased from Thermo Fisher Scientific. Pyridyl disulfide ethyl methacrylate (PDSMA) was prepared as previously reported.[81] Polymers were synthesized using RAFT polymerization and purified by dialysis using a membrane with 3500 MWCO. 1H-NMR spectra were recorded on a 400 MHz Bruker NMR spectrometer using the residual proton resonance of the deuterated solvent as the internal standard. Polymer molecular weights were estimated by gel permeation chromatography (GPC, Waters) using THF as eluent at a flow rate of 1 mL/min by a refractive index detector compared to poly(methyl methacrylate) (PMMA) standard. UV-visible absorption spectra were recorded on a PerkinElmer Lambda 35 UV/Vis Spectrophotometer. High performance liquid chromatography was conducted using a Shimadzu Prominence Modular HPLC.

4.4.2 Experimental Procedures

Synthesis of random copolymer p(OEGMA-*co*-PDSMA): To a Schlenk-flask, monomers PDSMA (5 g, 19.58 mmol) and OEGMA (3.625 g, 7.25 mmol), RAFT reagent 4-cyano-4-(phenylcarbonothioylthio)pentanoic acid (60 mg, 0.362 mmol), and initiator AIBN (12 mg, 0.0731 mmol) were dissolved in DMF (10 mL). The mixture was degassed

by performing three freeze-pump-thaw cycles and filled with argon. The reaction mixture was then sealed and transferred into a pre-heated oil bath at 70 °C and stirred for 18 h. The reaction flask was submerged in an ice bath to quench the polymerization, then dialyzed against dichloromethane in a MWCO 3500 regenerated cellulose membrane for 48 hours to remove unreacted monomers. The solution was dried to yield the random copolymer as an oil. GPC (THF) *Mn*: 31.9 KDa; Đ: 1.4. ^{1}H NMR (400 MHz, $CDCl_3$) δ (ppm): 8.45, 7.66, 7.10, 4.37-3.94, 3.76-3.47, 3.37, 3.01, 2.15-1.56, 1.14-0.65. The molar ratio of the two monomers in the polymer was determined by the relative integrations of the aromatic protons of PDS and methoxy protons of oligoethylene glycol to give 3:7 (OEG:PDS).

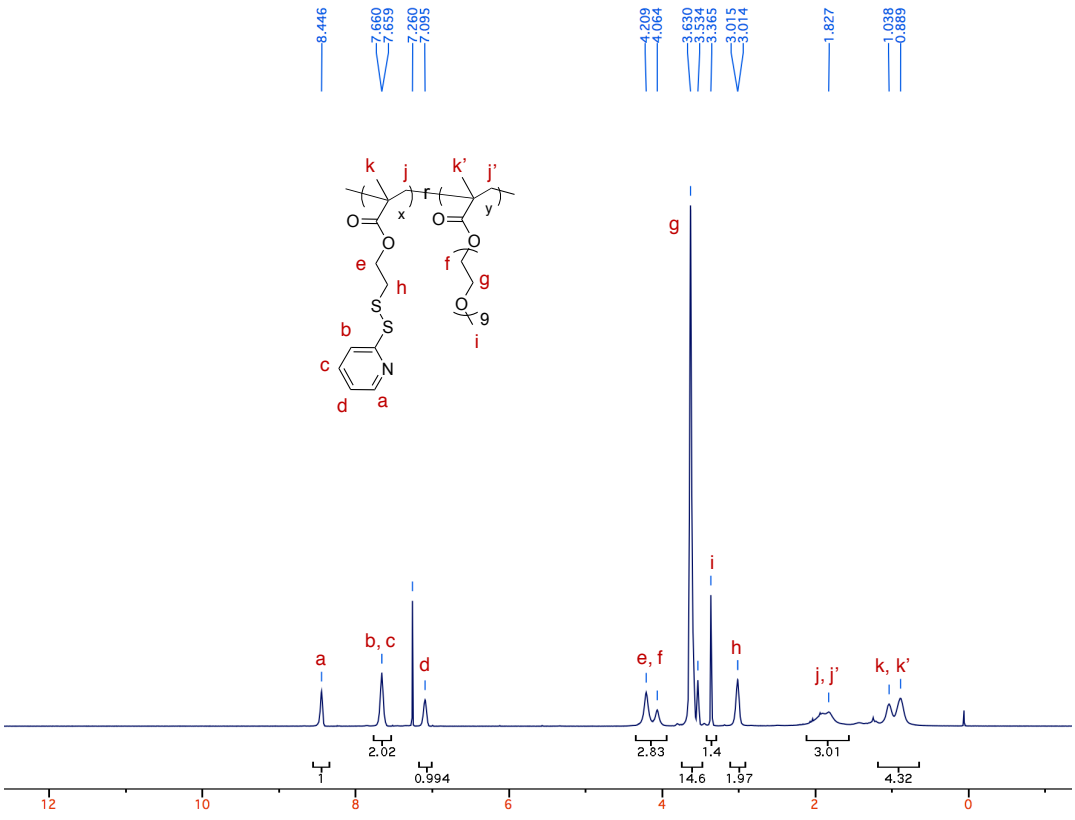

Figure 61. ^{1}H-NMR spectrum of random copolymer p(OEGMA-*co*-PDSMA).

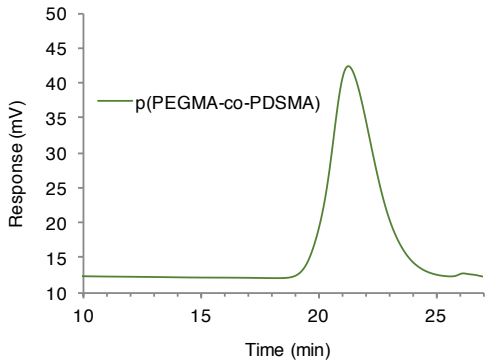

Figure 62. GPC (THF) for polymer p(OEGMA-co-PDSMA) Mn: 31.9 KDa; Đ 1.4.

Synthesis of mPEG(350) carboxylic acid: Poly(ethylene glycol) monomethyl ether carboxylates were prepared from Jones' Oxidation of poly(ethylene glycol) monomethyl ether following previously published procedures.[82-84] Jones' Reagent (1.25 M) was prepared by dissolving chromium trioxide (5 g, 50 mmol) in 35.7 mL of water at 10 °C with stirring, to which 4.36 mL of concentrated sulfuric acid was added in small portions. The solution was stirred for ten minutes then allowed to reach room temperature. Poly(ethylene glycol) monomethyl ether MW 350 (4 g, 11.43 mmol) was dissolved in 250 mL acetone and 1.25 M Jones' Reagent (18.3 mL, 22.86 mmol) was added in a single portion and stirred at room temperature for 12 hours. The solution was filtered to remove excess chromium salts, then evaporated under reduced pressure to remove acetone. The green-blue oil was then dissolved in dichloromethane, dried with anhydrous Na_2SO_4, and filtered to remove remaining chromium salts. The solution was dried to yield the poly(ethylene glycol) monomethyl ether carboxylic acid (MW 350) as an oil with 99% yield. ^{1}H NMR (400 MHz, $CDCl_3$) δ (ppm): 4.16 (s, 2H, CH_2), 3.88-3.49 (m, 27H, 13×CH_2), 3.38 (s, 3H, CH_3). MALDI characterization confirmed product conversion, with distribution of 44 Da centered around m/z 419.55 ($[M+Na]^+$, M=396.5 g/mol) (**Figure 63, 65**).

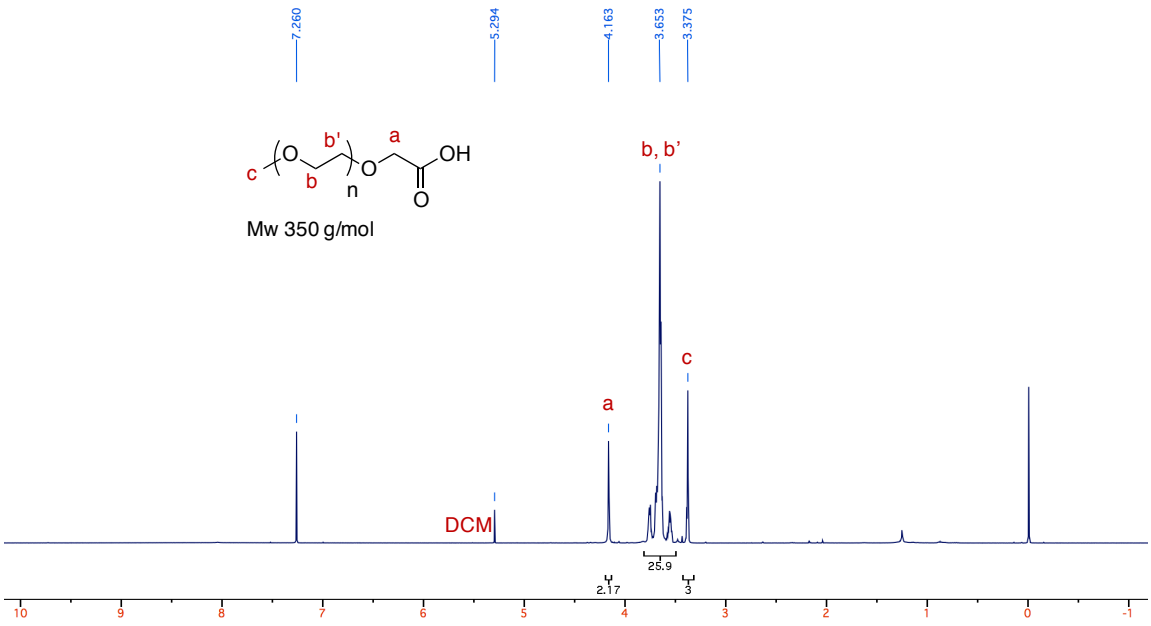

Figure 63. ^{1}H-NMR spectrum of random copolymer mPEG(350) carboxylic acid.

Synthesis of mPEG(750) carboxylic acid: Polyethylene glycol monomethyl ether MW 750 (5 g, 6.667 mmol) was dissolved in 250 mL acetone and 1.25 M Jones' Reagent (10.7 mL, 13.33 mmol) was added in a single portion and stirred at room temperature for 12 hours. The solution was filtered to remove excess chromium salts, then evaporated under reduced pressure to remove acetone. The green-blue oil was then dissolved in dichloromethane (100 mL), dried with anhydrous Na_2SO_4, and filtered to remove remaining chromium salts. The solution was dried to yield the Poly(ethylene glycol) monomethyl ether carboxylic acid (MW 350) as an oil with quantitative yield. ^{1}H NMR (400 MHz, $CDCl_3$) δ (ppm): 4.12 (s, 2H, CH_2), 3.85-3.42 (m, 60H, 30×CH_2), 3.34 (s, 3H, CH_3). MALDI characterization confirmed product conversion, with distribution of 44 Da centered around m/z 729.33 ($[M+Na]^+$, M=706.3 g/mol) (**Figure 64, 65**).

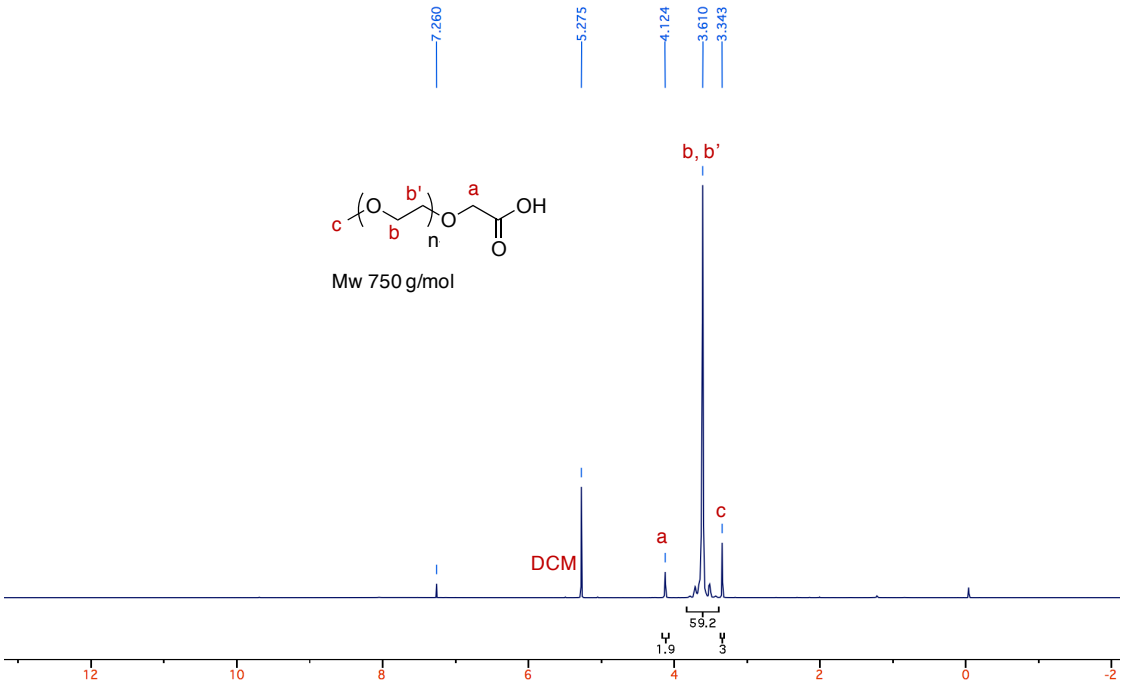

Figure 64. ^{1}H-NMR spectrum of random copolymer mPEG(750) carboxylic acid.

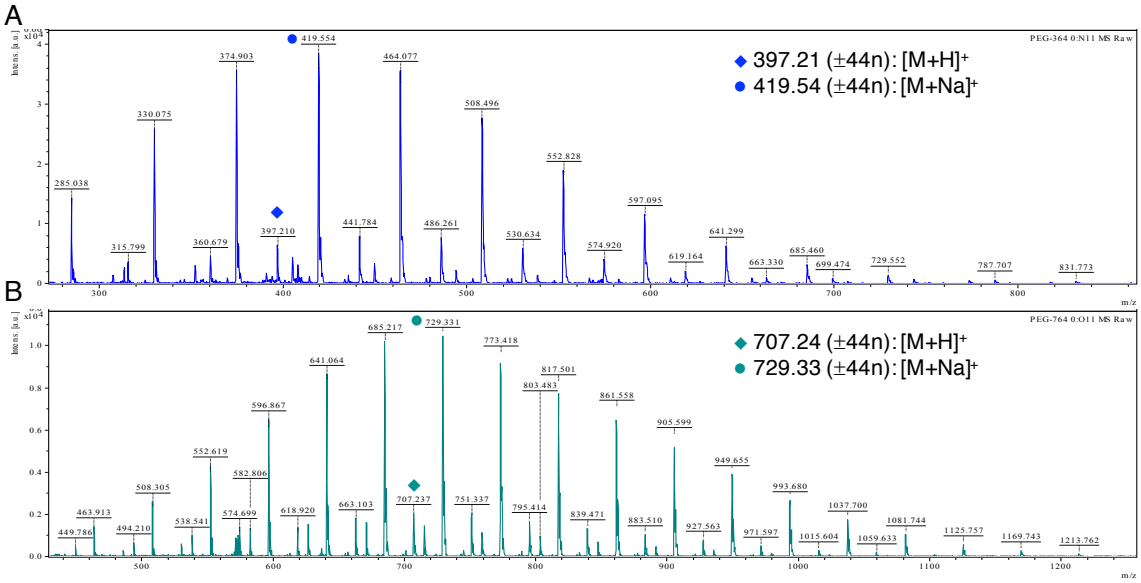

Figure 65. MALDI characterization of A) mPEG(350) carboxylic acid and B) mPEG(750) carboxylic acid.

Synthesis of mPEG(350 and 750)-GPLG↓LLGC(NH_2): The MMP-9 cleavable peptide (GPLG↓LLGC(NH_2); arrow indicates expected MMP-9 cleavage site) was synthesized through standard Fmoc-based solid phase techniques on a rink amide AM resin (500 mg,

0.71 mmol/g loading, 100-200 mesh). Fmoc deprotection was achieved using 20% piperidine in DMF (10 mL) for 20 minutes. Amino acid couplings were achieved by adding Fmoc-protected amino acid (1.06 mmol), HATU (405 mg, 1.06 mmol), and N,N-diisopropylethylamine (190 μL, 1.06 mmol) in DMF (3.55 mL, 0.3 M amino acid) to the resin for 45 minutes. Following each Fmoc deprotection or amino acid coupling, the resin was washed three times with DMF then DCM and then monitored by the Kaiser test. Following the final Fmoc deprotection, either poly(ethylene glycol) monomethyl ether carboxylic acid MW 350 (901 mg, 2.475 mmol) or poly(ethylene glycol) monomethyl ether carboxylic acid MW 750 (1.891 g, 2.475 mmol), with HATU (972 mg, 2.475 mmol), and N,N-diisopropylethylamine (547 μL, 2.475 mmol) to each was dissolved in DMF (8.52 mL 0.3 M carboxylic acid) and added for coupling. The poly(ethylene glycol) monomethyl ether carboxylic acids were left to react for 12 hours, then unreacted reagents were washed from the resin several times with DMF then DCM then monitored by the Kaiser test. The resin was rinsed with DCM and methanol, then dried under vacuum. The PEG-peptide was cleaved from the resin in by incubation in a solution containing trifluoroacetic acid (6.312 mL), 1,2-ethanedithiol (226 μL), triisopropylsilane (129 μL), and water (250 μL), for 6 hours, then filtered and washed two times with small portions of trifluoroacetic acid. The combined filtrates were evaporated under reduced pressure then precipitated with 10-fold volume of cold diethyl ether. The crude precipitate was dissolved in a minimum amount of DCM then precipitated again in diethyl ether several times. The substrates were purified using HPLC on a semi-preparatory C18 column (10 mm x 25 cm, 10 μm particle size) using a gradient mobile phase of acetonitrile 0% to 70% acetonitrile in water, both

containing 0.05% (v/v) trifluoroacetic acid, monitoring absorbance of 214 nm at a flow rate of 5 mL/min.

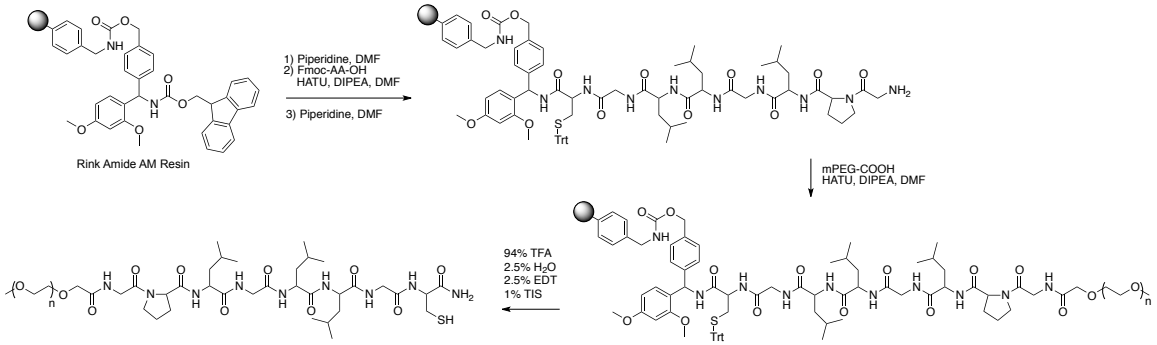

Scheme 9. Synthetic scheme of solid phase peptide synthesis of mPEG(350)-GPLGLLGC(NH_2) and mPEG(750)-GPLGLLGC(NH_2).

Characterization of mPEG(350)-GPLGLLGC(NH_2) and mPEG(750)-GPLGLLGC(NH_2): The peptide mPEG(350)-GPLGLLGC(NH_2) purity was confirmed to be 96%, and the peptide mPEG(750)-GPLGLLGC(NH_2) purity was confirmed to be 91% by analytical HPLC using a C18 column (4.6 mm × 10 cm, 2.7 μm particle size) using a gradient mobile phase of acetonitrile 0% to 50% acetonitrile in water, both containing 0.05% (v/v) trifluoroacetic acid, monitoring absorbance of 214 nm at a flow rate of 1 mL/min (**Figure 66**). The peptide identities were characterized using ESI Mass spectrometry. Mass analysis was carried out on a Bruker AmaZon (Billerica, MA) quadrupole ion trap mass spectrometer equipped with an electrospray ionization source. Typically, the electrospray needle voltage was kept at ~4 kV, and the capillary temperature was set at 220 °C. In mass spectrometry characterization of both mPEG(350)- and mPEG(750)-GPLGLLGC(NH_2), distributions were observed with shifts of m/z 44, consistent with differences in 44 g/mol for one ethylene glycol unit due to the polydispersity of the poly(ethylene glycol) in the substrates. For mPEG(350)-GPLGLLGC(NH_2), the distribution centered around about m/z 1020, which coorelates to

$[M+H]^+$ for expected M of 1019 g/mol and indicates a substrate with an average of 5 ethylene glycol units. The other peaks shifted by m/z of 44 span about ±5 ethylene glycol units. The second distribution observed in the spectrum at m/z 1042 correspond to $[M+Na]^+$ of the same product. Also observed is an $[M+H]^{2+}$ distribution of the same product. From this spectrum, we can conclude the absence of any significant PEG-peptide impurities. Similarly, for mPEG(750)-GPLGLLGC(NH_2), the distribution centered around about m/z of 1350.6 correlates to $[M+Na]^+$ for expected mass 1327.6 g/mol, and indicates a substrate with an average of 12 ethylene glycol units. The other peaks shifted by 44 Da suggests about ±7 ethylene glycol units. Also observed is an $[M+2Na]^{2+}$ distribution of the same product. Likewise, from this spectrum, we can conclude the absence of any significant PEG-peptide impurities.

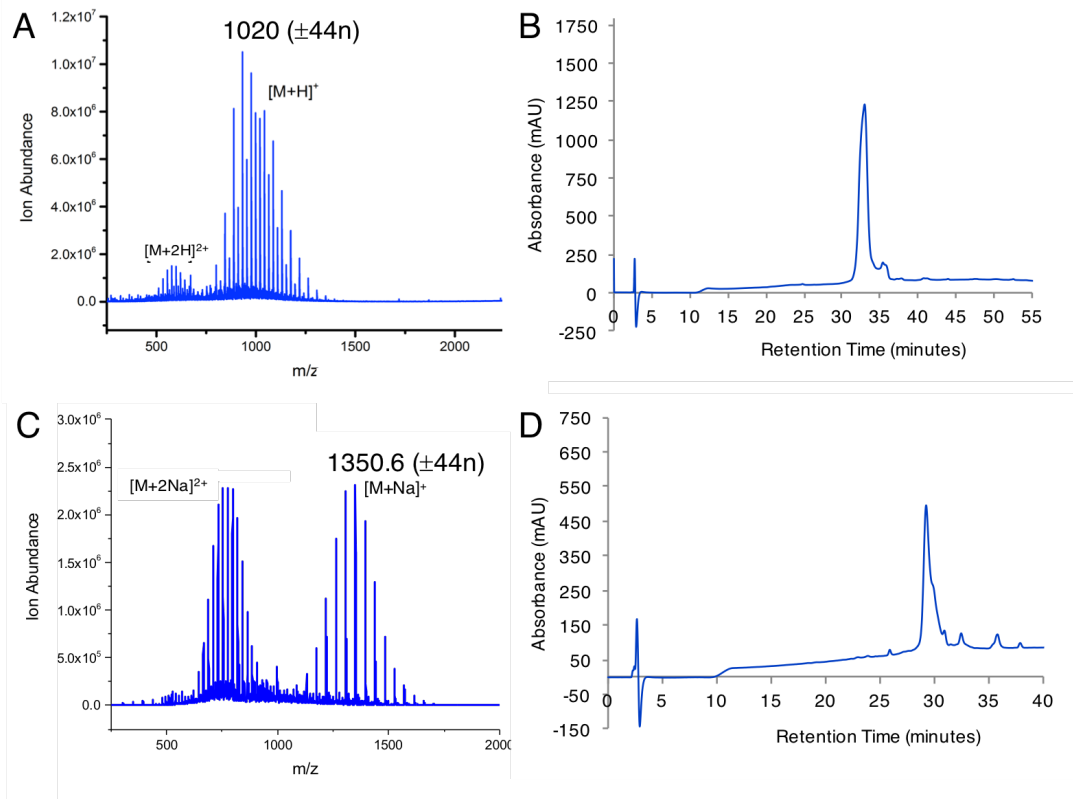

Figure 66. Substrate mPEG(350)-GPLGLLGC(NH_2) A) ESI MS chromatogram and B) reverse phase HPLC chromatogram, and substrate mPEG(750)-GPLGLLGC(NH_2) C) ESI

MS chromatogram and D) reverse phase HPLC chromatogram.

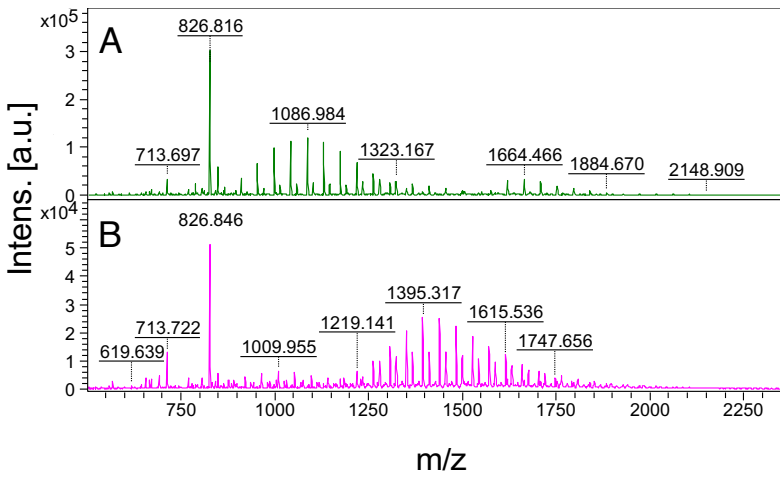

Figure 67. Substrate A) mPEG(350)-GPLGLLGC(NH_2) MALDI MS chromatogram and B) mPEG(750)-GPLGLLGC(NH_2) MALDI MS chromatogram.

Synthesis of LLGC(NH_2): The MMP-9 cleavage product peptide LLGC(NH_2) was synthesized through standard Fmoc-based solid phase techniques on a rink amide AM resin resin (0.2 g, 0.71 mmol/g loading, 100-200 mesh). As described above, Fmoc deprotection was attained using 20% piperidine (5 mL), and amino acid coupling were achieved using Fmoc-protected amino acid (0.4125 mmol), HATU (162 mg, 0.4125 mmol), and N,N-diisopropylethylamine (76.2 µL, 0.4125 mmol) in DMF (1.42 mL, 0.3 M amino acid). Following the final Fmoc deprotection, the resin was rinsed with DCM and methanol, then dried under vacuum. The peptide was cleaved from the resin by incubation in a solution containing TFA (1.052 mL), water (41.7 µL), 1,2-ethanedithiol 37.7 µL) and triisopropylsilane (21.5 µL) for 3 hours, then isolated by diethyl ether precipitation as described above. The peptide was purified using HPLC on a semi-preparatory C18 column (10 mm x 25 cm, 10 µm particle size) using a gradient mobile phase of acetonitrile 0% to 70% acetonitrile in water, both containing 0.05% (v/v) trifluoroacetic acid, monitoring

absorbance of 214 nm and flow rate 5 ml/min.

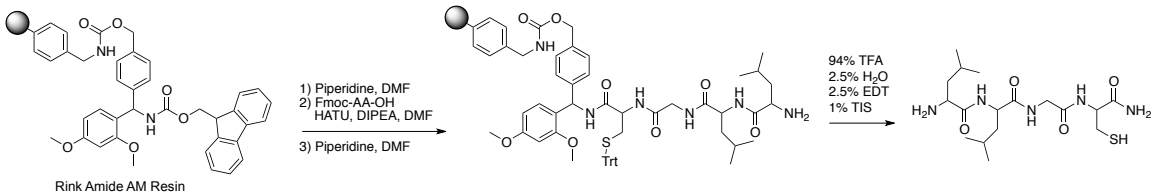

Scheme 10. Synthetic scheme of peptide of LLGC(NH_2).

LLGC(NH_2) Characterization: The peptide purity was confirmed to be 97% by analytical HPLC using a C18 column (4.6 mm × 10 cm, 2.7 μm particle size) (**Figure 68**). The peptide identity was characterized using ESI Mass spectrometry, and the observed peaks at m/z of 404.2 matches $[M+H]^+$ for expected mass of 403 g/mol. A second smaller peak at m/z 805.4 matches $[(2M-2H)+H]^+$ for disulfide formation of the product as a dimer.

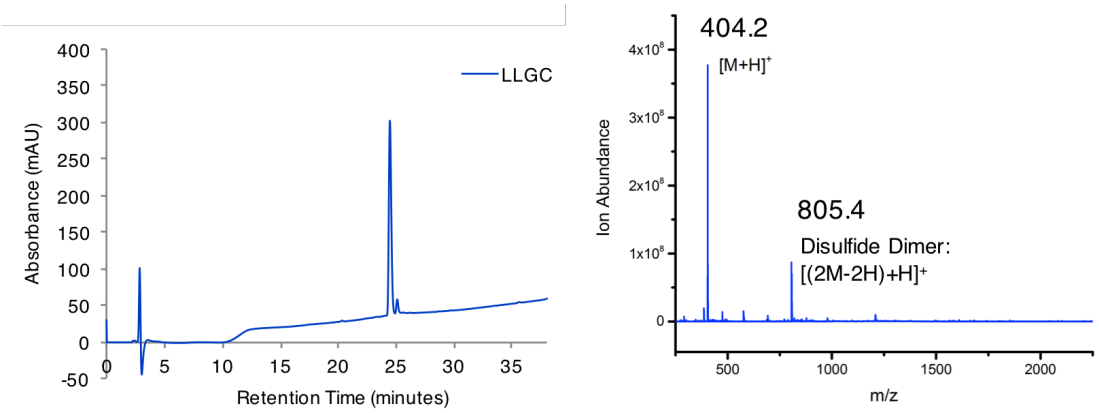

Figure 68. A) Reverse phase HPLC chromatogram of peptide LLCG in 0-70% acetonitrile at 214 nm in water, B) ESI MS of peptide LLGC.

Synthesis of thiol-modified FITC: Fluorescein isothiocyanate (FITC) (61 mg, 0.158 mmol), cystamine dihydrochloride (19 mg, 0.079 mmol) and triethylamine (110 μL, 0.788 mmol) were dissolved in DMSO (1.2 mL) and stirred for 4 hours. Then tris(2-carboxyethyl)phosphine hydrochloride (54 mg, 0.188 mmol) was added and stirred for 1 hour. The mixture was precipitated in diethyl ether and then washed with water. The

resultant crude fluorescein-cysteamine was used for nanogel labeling without further purification.

Formulation of Nanogels: Deionized water was added to the polymer (10 mg/mL) and made into a particle suspension using repeated chill and sonicate cycles until the solution appeared dissolved. Particles of about 20 nm were achieved by chemically crosslinking this equilibrium assembly of the polymer at 25 °C in 25 mM Na_2SO_4 using a calculated amount of DTT for 1 hour as reducing agent as previously reported.[67, 85] Crosslinking was determined to be 25 mole percent PDS by calculating the amount of byproduct, 2-pyridinethione, using its molar extinction coefficient (8.08 x 10^3 M^{-1} cm^{-1} at 343 nm)[86] using UV-Vis spectroscopy. Dynamic light scattering (DLS) experiments to obtain particle size were performed by using a digital correlator and goniometer with a light source operating at 514 nm using a Malvern Nanozetasizer-ZS. Final nanogel size measurements were obtained at 25 °C at a correlation time of 30 seconds. Dust was removed by filtering the solution through 0.45 μm polycarbonate filter. For each sample, 3 readings were recorded averaging 10 runs for the same sample.

PEG-Peptide conjugation to nanogels: The substrates mPEG(350)-GPLG↓LLGC(NH_2) (53.3 mg, 54.6 μmol), or mPEG(750)-GPLG↓LLGC(NH_2) (72.7 mg, 54.6 μmol) were each dissolved in methanol (100 μL) and added separately to 5 mL of aqueous crosslinked nanogel (Bare NG) solutions (10 mg/mL, 109.3 μmol PDS) and stirred open to the atmosphere for 12 hours to allow the methanol to evaporate. The peptide LLGC(NH_2) (3.97 mg, 9.84 μmol) was added to 1 mL of aqueous crosslinked nanogel solution (10 mg/mL, 21.9 μmol PDS) and stirred for 12 hours. The conjugation extent for each mPEG350-NG,

mPEG350-NG, and LLGC-NG, was quantified by UV-Vis spectroscopy by calculating the amount of generated byproduct 2-pyridinethione (**Figure 69**). Unconjugated peptide and 2-pyridinethione byproduct was removed by dialysis against DI water in a 100 KDa MWCO cellulose dialysis membrane for 48 hours. DLS of peptide-conjugated nanogels were obtained in phosphate buffer pH 7.4 at a concentration of 2.5 mg/mL.

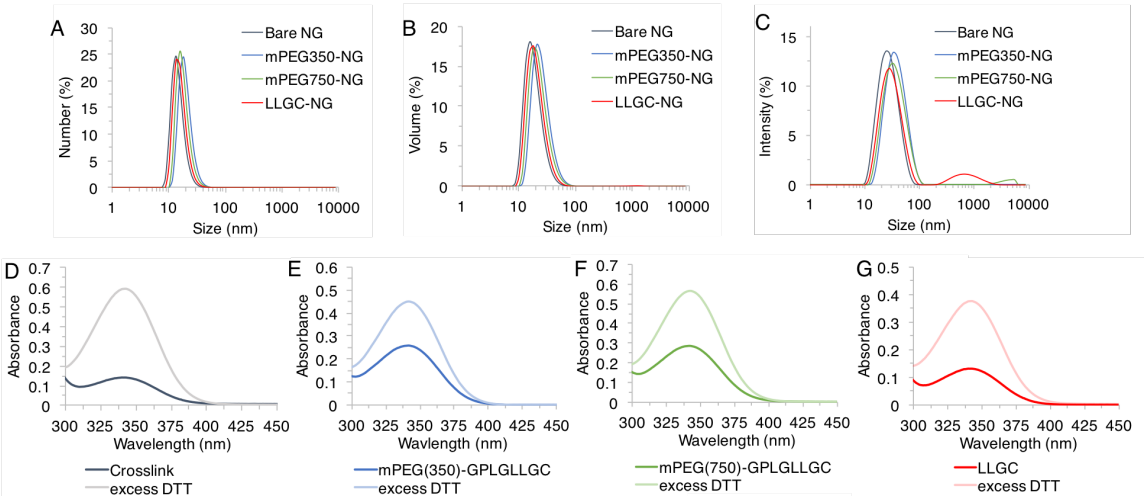

Figure 69. DLS sizes of Bare NG and substrate-modified nanogels by A) number, B) volume, and C) intensity. Absorption spectra of D) nanogel crosslinking, E) mPEG(350)-GPLGLLGC conjugation, F) mPEG(750)-GPLGLLGC conjugation, and G) LLGC conjugation, represented with excess DTT for 100% 2-pyridinethione byproduct release for comparison. Note: for LLGC conjugation, free 2-pyridinethione from crosslinking was removed prior to conjugation, so lower absorption is observed respective to excess DTT.

LCST Determination of Nanogels: Dynamic light scattering (DLS) experiments to obtain temperature dependent nanogel size. The stability of these crosslinked and PEG-peptide decorated nanogels were evaluated at biologically-relevant conditions due to the lower critical solution temperature (LCST) characteristic of PEG. Final nanogel size measurements in PBS buffer pH 7.4 were obtained at 25-65 °C at a correlation time of 30 seconds. Dust was removed by filtering the solution through 0.45 µm polycarbonate filter. For each sample, 3 readings were recorded averaging 10 runs for the same sample. For

mPEG(350)-NG the LCST transition was observed at 45 °C, and for mPEG(750)-NG the LCST transition was observed at 59 °C, both well above biological temperatures (**Figure 70**).

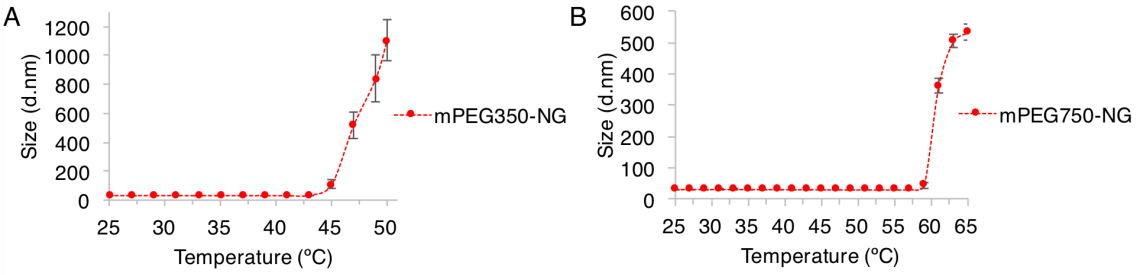

Figure 70. LCST characterization of A) mPEG(350)-NG and B) mPEG(750)-NG.

ProMMP-9 AMPA Activation: APMA (3.5 mg mmol) was dissolved in 1 mL of 0.1 M NaOH solution, then diluted four times with reaction buffer (TCC buffer: 50 mM TRIS HCl, pH 7.5, 1 mM $CaCl_2$, 0.05% triton X-100) to give a 2.5 mM stock of APMA. The pH was adjusted to pH 7.4 using 0.1 M HCl, then the APMA solution (250 µmol, 100 µL) was added to MMP-9 solution (10 µg; 109 pmol, 100 µL) and incubated with shaking for 24 hours at 37 °C in 5% CO_2.

Activity Assay of MMP-9: MMP-9 activity of APMA incubated ProMMP-9 was assayed using the fluorogenic peptide substrate Mca-PLGL-Dpa-AR-NH_2. Protease cleavage between the Gly-Leu bond releases the fluorescent 7-methoxycoumarin group from the quenching 2, 4-dinitrophenyl group, which can be monitored overtime with excitation at 320 nm and emission at 405 nm. After 8 hours of APMA activation, MMP-9 enzymatic activity at 5 nM was assayed using 10 µM substrate (supplied in 6.07 mM stock in DMSO) in a 100 µL reaction mixture in buffer (TTC or TNC) with 10% v/v DMSO. These 100 µL

assays were performed in triplicate in a 96-well microplate at 37 °C using a Molecular Devices Spectramax M5 spectrophotometer. Activity of APMA incubated MMP-9 sample was monitored over 33 hours in both buffers.

Substrate Cleavage by LC-MS: MMP-9 cleavable substrates mPEG(350)-GPLG↓LLGC(NH_2) (1 mg, 0.1 mmol) and mPEG(750)-GPLG↓LLGC(NH_2) (1.3 mg, 0.1 mmol) were incubated with activated MMP-9 (1 μg, 10.9 nM) in TTC buffer 7.4 (1 mL) at 37 °C in 5% CO_2 with shaking for 24 hours. The mixture was analyzed by LCMS. Chromatographic separation was conducted by a Thermo Scientific (Waltham, MA) Ultimate 3000 HPLC with a Thermo Acclaim PepMap RSLC C18 column (300 μm x 15 cm, 2 μm particle size). MMP-9 incubated substrates were eluted using a gradient of acetonitrile containing 0.1% formic acid that increased from 5% to 50% for 45 min at a flow rate of 4 μl/min. Chromatographic separation was successful for mPEG(350)-GPLG↓LLGC(NH_2), with remaining starting material eluted at 37-39 min, product LLGC(NH_2) eluted at 15-16 minutes, and mPEG(350)-GPLG eluted at 25-31 minutes (**Figure 71**). For mPEG(750)-GPLG↓LLGC(NH_2), the remaining starting material eluted at 39-40 min, product LLGC(NH_2) eluted at 15-17 minutes, and product mPEG(750)-GPLG eluted at 25-35 minutes. Substrate products were measured immediately by mass spectrometry. Mass analysis was carried out on a Bruker HCTultra (Billerica, MA) ion trap mass spectrometer equipped with an electrospray ionization source. Typically, the electrospray needle voltage was kept at ~4 kV, and the capillary temperature was set at 220 °C.

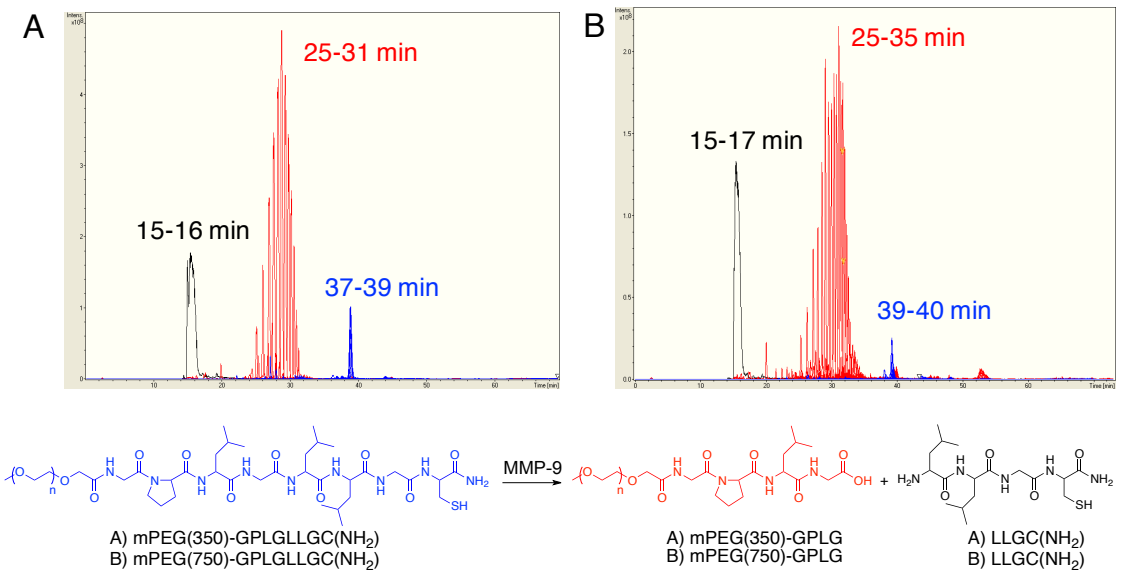

Figure 71. LC-MS extracted ion chromatograms of MMP-9 cleavage of substrates A) mPEG(350)-GPLGLLGC(NH_2) (37-39 min), with products mPEG(350)-GPLG (25-31 min) and LLGC(NH_2) (15-16 min) and B) mPEG(750)-GPLGLLGC(NH_2) (39-40 min), with products mPEG(750)-GPLG (25-35 min) and LLGC(NH_2) (15-17 min), and corresponding chemical structures of substrate and products.

Nanogel Activation with MMP-9: Nanogels (2.5 mg/mL polymer) decorated with MMP-9 cleavable substrates (3 mM) in TTC buffer pH 7.4 was incubated with activated MMP-9 at final enzyme concentrations of 0.54, 5.4, and 54 nM (0.05, 0.5, and 5 μg/mL MMP-9, respectively) at 37 °C in 5% CO_2 with shaking. At determined time points the enzyme activity was quenched with 1% (v/v) acetic acid to pH 3.5, then cleaved peptide was isolated from the mixture for MALDI characterization using a regenerated cellulose Amicon Ultra centrifugal filter with 3KDa MWCO. Activated nanogel was purified by dialysis against DI water in a 100 KDa MWCO cellulose dialysis membrane for 24 hours.

MALDI Characterization: Matrix solutions were prepared dissolving α-cyano-4-hydroxycinnamic acid (CHCA) (10 mg/mL) in a solution containing ACN (50 μL), H_2O (47.5 μL) and TFA (2.5 μL). The matrix solution was then mixed with the centrifuge

filtered nanogel solution that had been incubated with MMP-9. A Bruker Autoflex III time-of-flight mass spectrometer was used for the MALDI-MS analysis of all samples. Acquisition of all mass spectra was done in reflectron mode with an accelerating voltage of 19 kV. Each spectrum is the average of 500 laser shots at 50% laser power.

Fluorescamine Assay: The percentage of cleavage on the particle was determined by quantifying the N-terminal amines using fluorescamine Assay. Formulated product of cleavage nanogel (LLGC-NG) was used to generate a concentration dependent fluorescence calibration curve. Various concentrations of LLGC-NG (7.4 μg/mL- 0.74 mg/mL) were prepared in PBS buffer pH 7.4. MMP-9 incubated and purified nanogels mPEG350-NG and mPEG750-NG were diluted in PBS buffer pH 7.4 (to 0.74 mg/mL) so that their maximum expected amine content would be within the LLGC-NG calibration curve. Non-activated mPEG350-NG and mPEG350-NG (0.74 mg/mL) were prepared as negative controls. In a 96 well (flat-bottomed) plate PBS buffer pH 7.4 (150 μL) and sample solutions (20 uL) were added to each well. Then, fluorescamine solution in DMSO (12 uL, 0.68 mg/mL) was added to each well. The fluorescence was obtained using a Molecular Devices Spectramax M5 plate reader (excitation: 390 nm; emission 465 nm). Average fluorescence values and deviation were obtained from replicate readings (n=3). Concentration of LLGC-NG versus fluorescence was used to generate an amine calibration curve, and the fluorescence of known test samples were used to determine amine content.

Fluorescein Nanogel Labeling: To aqueous nanogel solutions (2.5 mg/mL, 0.5 mL) fluorescein-cysteamine (0.128 mg, 0.273 μmol) in acetone (10 μL) was added and stirred

open for 6 hours until acetone evaporated. The conjugation was characterized by release of 2-pyrinedithione by UV-Vis prior to dialysis against DI water in a 100 KDa MWCO cellulose dialysis membrane for 24 hours to remove any unconjugated fluorescein-cysteine. Feed ratio of 10 mole percent PDS groups gave 8-9 mole percent conjugated fluorescein was achieved on nanogels LLGC-NG, mPEG350-NG, and MMP-9 activated mPEG350-NG.

Cell Culture: Human cervical carcinoma (HeLa) cell line was grown in DMEM supplemented with 10% (FBS), 1% L-glutamine, and 1% antibiotic-antimycotic (comprised of 100 units/mL penicillin and 100 μg/mL streptomycin). All cells were grown at 5% CO_2 and 37 °C. Digestion of cells for culture was done according to HeLa and 293A protocols from ATCC.

Cytotoxicity Assay: Nanogel *in vitro* cytotoxicity was determined using the MTT assay for HeLa cell line. In a 96 well flat-bottomed plate 10,000 cells per well (16,000-32,000 cells/cm^2) in culture medium were seeded and incubated for 24 hours at 5% CO_2 and 37 °C. Nanogel samples in PBS buffer 7.4 were diluted with culture medium for final nanogel concentrations ranging from 0-1 mg/mL with 10 % PBS total. The plate's culture medium was replaced with sample culture medium, or a solution of trypsin (0.5%) as the negative control, and incubated for 24 hours. MTT (10 μL, 5 mg/mL in culture media) was added to each well and incubation was continued for 3 hours. Culture plates were spun down (3,700 rpm, 10 minutes) and supernatant was removed. DMSO (100 μL) was added to each well and absorbance was obtained using a Molecular Devices Spectramax M5 plate reader

(λmax 540 nm and background subtraction 650 nm). Average absorbance values and deviation were obtained from replicate readings (n=4) and were compared to 100% viability of the positive control (10 % PBS, respective to sample dilutions) and 0.5 % trypsin as negative control.

Confocal Microscopy Intracellular Uptake: HeLa cells were seeded at 30-50% confluency (~10,400 cells/cm^2) in 4-chamber 35 mm glass bottom dishes and incubated overnight at 37 °C overnight in 5% CO_2 before performing uptake. Culture media was removed and cells washed with PBS one time before adding new culture media containing fluorescein-labeled nanogels diluted to 0.1 mg/mL in DMEM (10×, diluted to 1× with PBS). Samples were incubated for 2 hours. Nuclear staining (NucBlue, 80 μL per mL media) was added in the final 30-60 min of incubation. Media was removed from cells and washed 2-4 times with PBS, then live cell imaging buffer was added for confocal imaging. Assessment of fluorescein-conjugated nanogel intracellular uptake was recorded using 488 nm laser and nuclear stain was detecting using a 405 nm wavelength laser. Assessment of DiI-loaded nanogel intracellular uptake was recorded using 540 nm laser and nuclear stain was detecting using a 405 nm wavelength laser. Confocal microscopy was performed on a Nikon Yokogawa spinning disk confocal microscope equipped with 40x or 100x oil objectives and an Andor EMCCD camera.

Flow Cytometry: HeLa cells were seeded at 100,000 cells/mL in a glass bottom dish and maintained at 37 °C overnight in 5% CO_2 before performing uptake. Culture media was removed and cells washed with PBS one time before adding new culture media containing

fluorescein-labeled nanogels diluted to 0.05 mg/mL in DMEM (10×, diluted to 1× with PBS). Samples were incubated for 2 hours, then washed with PBS, trypsinized and collected by centrifugation. The cells were re-suspended in 200 μL PBS buffer and stored at 4 °C. A minimum of 100,000 cells were analyzed for each sample using a BD LSRFortessa.

Table 25. HeLa cell Median FITC obtained by flow cytometry with 2 hour nanogel incubation.

Sample	Median FITC
LLGC-NG(F)	85821
mPEG350-NG(F)	26048
mPEG350-NG(F) Active	42983
mPEG750-NG(F)	15972
mPEG750-NG(F) Active	22417

Release Studies: The release of encapsulated model guest DiI was monitored by fluorescence spectroscopy using a Molecular Devices Spectramax M5 plate reader. DiI (0.35 mg) was dissolved in acetone (100 μL) then added to a 350 μL solution of 10 mg/mL aggregate of polymer p(OEGMA-*co*-PDSMA) and stirred was for 8 hours at room temperature, open to the atmosphere to allow for acetone to evaporate. Aggregates were crosslinked then post-functionalized with substrates as previously described. Nanogels were purified by dialysis using 100 KDa MWCO membrane and any non-encapsulated DiI was removed by filtration through a 0.45 μm filter. In a 96 well (flat-bottomed) plate TNC buffer pH 7.4 (90 μL) containing relevant stimuli (GSH, ProMMP-9, or MMP-9) and concentrations were added to each well. Then, nanogel solutions (10 μL, 17 μg/mL) of either Bare NG, mPEG350-NG, and mPEG750-NG were added to each well. The fluorescence was obtained for each well (excitation: 520 nm; emission 565 nm), and the average fluorescence values and deviation were obtained from replicate readings (n=3)

over 48 hours.

DiI-loaded Nanogel Activation with MMP-9: DiI encapsulated mPEG350-NG (2.5 mg/mL polymer) decorated with MMP-9 cleavable substrates (3 mM) in TNC buffer pH 7.4 was incubated with activated MMP-9 (54 nM) at 37 °C in 5% CO_2 with shaking. After 24 hours, the enzyme activity was quenched with 1% (v/v) acetic acid to pH 3.5, then purified by dialysis against DI water in a 100 KDa MWCO cellulose dialysis membrane for 24 hours, and filtered.

4.5 References

1. Liu, D. L.; Chang, X.; Dong, C. M. Reduction- and thermo-sensitive star polypeptide micelles and hydrogels for on-demand drug delivery. *Chem. Commun*. **2013**, *49 (12)*, 1229−1231.

2. Bae, Y. H.; Park, K. Targeted drug delivery to tumors: myths, reality and possibility. *J. Controlled Release* **2011**, *153*, 198-205.

3. Kobayashi, H.; Watanabe, R.; Choyke, P. L. Improving Conventional Enhanced Permeability and Retention (EPR) Effects; What Is the Appropriate Target? *Theranostics* **2014**, *4*, 81-89.

4. Jain, R. K.; Stylianopoulos, T. Delivering nanomedicine to solid tumors. *Nat. Rev. Clin. Oncol.* **2010**, *7*, 653-653.

5. Molineux, G. PEGylation: engineering improved pharmaceuticals for enhanced therapy. *Cancer Treat Rev*. **2002**, *28 (Suppl. A)*, 13−16.

6. Moribe, K.; Maruyama, K. Reviews on PEG coated liposomal drug carriers. *Drug Delivery Syst*. **2001**, *16 (3)*, 165−171.

7. Romberg B.; Hennink W. E.; Storm G. Sheddable coatings for long-circulating nanoparticles. *Pharm. Res*. **2008**, *25*, 55–71.

8. Moghimi S. M.; Hunter A. C.; Murray J. C. Long-circulating and target-specific nanoparticles: Theory to practice. *Pharmacol. Rev*. **2001**, *53*, 283–318.

9. Vittaz M.; Bazile, D.; Spenlehauer, G.; Verrecchia, T.; Veillard, M.; Puisieux, F.; Labarre, D. Effect of PEO surface density on long-circulating PLA-PEO nanoparticles which are very low complement activators. *Biomaterials* **1996**, *17*, 1575–1581

10. Owens, D. E. III; Peppas, N. A. Opsonization, biodistribution, and pharmacokinetics of polymeric nanoparticles. *Int. J. Pharm*. **2006**, *307*, 93–102.

11. Verbaan, F. J.; Oussoren, C.; Snel, C. J.; Crommelin, D. J.; Hennink, W. E.; Storm, G. Steric stabilization of poly(2-(dimethylamino)ethyl methacrylate)-based polyplexes mediates prolonged circulation and tumor targeting in mice. *J. Gene Med.* **2004**, *6*, 64-75.

12. Vader, P.; van der Aa, L. J.; Engbersen, J. F.; Storm, G.; Schiffelers, R. M. Physicochemical and Biological Evaluation of siRNA Polyplexes Based on PEGylated Poly(amido amine)s. *Pharm. Res.* **2012**, *29*, 352.

13. Crownover, E.; Duvall, C. L.; Convertine, A.; Hoffman, A. S.; Stayton, P. S. RAFT-synthesized graft copolymers that enhance pH-dependent membrane destabilization and protein circulation times. *J. Controlled Release* **2011**, *155*, 167-174.

14. Chaudhari, K. R.; Ukawala, M.; Manjappa, A. S.; Kumar, A.; Mundada, P. K.; Mishra, A. K. Mathur, R.; Monkkonen, J.; Murthy, R.S. Opsonization, biodistribution, cellular uptake and apoptosis study of PEGylated PBCA nanoparticle as potential drug delivery carrier. *Pharm. Res*. **2012**, *29*, 53-68.

15. Li, Y.; Kröger, M.; Liu, W. K.; Endocytosis of PEGylated nanoparticles accompanied by structural and free energy changes of the grafted polyethylene glycol. *Biomaterials*, **2014**, *35*, 8467-8478.

16. Matsumura, Y.; Maeda, H. A new concept for macromolecular therapeutics in cancer chemotherapy: mechanism of tumoritropic accumulation of proteins and the antitumor agent smancs. *Cancer Res.* **1986**, *46*, 6387–6392.

17. Guo, M.; Que, C.; Wang, C.; Liu, X.; Yan, H.; Liu, K. Multifunctional superparamagnetic nanocarriers with folate-mediated and pH-responsive targeting properties for anticancer drug delivery. *Biomaterials* **2011**, *32*, 185-194.

18. Narayanan, S.; Binulal, N. S.; Mony, U.; Manzoor, K.; Nair, S.; Menon, D. Folate targeted polymeric 'green' nanotherapy for cancer. *Nanotechnology* **2010**, *21*, 285107.

19. Zhang, Q.; Liu, F.; Nguyen, K. T.; Ma, X.; Wang, X.; Xing, B.; Zhao, Y. Multifunctional Mesoporous Silica Nanoparticles for Cancer-Targeted and Controlled Drug Delivery. *Adv. Funct. Mater.* **2012**, *22*, 5144-5156.

20. Davis, M. E.; Zuckerman, J. E.; Choi, C. H.; Seligson, D.; Tolcher, A.; Alabi, C. A.; Yen, Y.; Heidel, J. D.; Ribas, A. Evidence of RNAi in humans from systemically administered siRNA via targeted nanoparticles. *Nature* **2010**, *464*, 1067-1070.

21. Sarko, D.; Beijer, B.; Boy, R. G.; Nothelfer, E.-M.; Leotta, K.; Eisenhut, M.; Altmann, A.; Haberkorn, U.; Mier, W. The Pharmacokinetics of Cell-Penetrating Peptides. *Mol. Pharmaceutics* **2010**, *7*, 2224−2231.

22. Jin, E.; Zhang, B.; Sun, X.; Zhou, Z.; Ma, X.; Sun, Q.; Tang, J.; Shen, Y. Q.; Kirk, E. V.; Murdoch, W. J.; Radosz, M. Acid-Active Cell- Penetrating Peptides for in Vivo Tumor-Targeted Drug Delivery. *J. Am. Chem. Soc*. **2013**, *135*, 933−940.

23. Ruoslahti, E. RGD and Other Recognition Sequences for Integrins. *Annu. Rev. Cell. Dev. Biol*. **1996**, *12*, 697–715.

24. Friden, P. M.; Walus, L. R.; Musso, G. F.; Taylor, M. A.; Malfroy, B.; Starzyk, R. M. Anti-Transferrin Receptor Antibody and Antibody Drug Conjugates Cross the Blood Brain Barrier. *Proc. Natl. Acad. Sci. U.S.A*. **1991**, *88*, 4771–4775.

25. Iakoubov, L. Z.; Torchilin, V. P. A Novel Class of Antitumor Antibodies: Nucleosome-Restricted Antinuclear Autoantibodies (ANA) from Healthy Aged Nonautoimmune Mice. *Oncol. Res.* **1997**, *9*, 439–446.

26. Lukyanov, A. N.; Elbayoumi, T. A.; Chakilam, A. R.; Torchilin, V. P. Tumor-Targeted Liposomes: Doxorubicin-Loaded Long-Circulating Liposomes Modified with Anti-Cancer Antibody. *J. Controlled Release* **2004**, *100*, 135–144.

27. Gabizon, A.; Horowitz, A. T.; Goren, D.; Tzemach, D.; Mandelbaum-Shavit, F.; Qazen, M. M.; Zalipsky, S. Targeting Folate Receptor with Folate Linked to Extremities of Poly(ethylene glycol)-Grafted Liposomes: In Vitro Studies. *Bioconjugate Chem*. **1999**, *10*, 289–298.

28. Zhu, L.; Ye, Z.; Cheng, K.; Miller, D. D.; Mahato, R. I. Site-Specific Delivery of Oligonucleotides to Hepatocytes after Systemic Administration. *Bioconjugate Chem*. **2008**, *19*, 290–298.

29. Zhu, L.; Mahato, R. I. Targeted Delivery of siRNA to Hepatocytes and Hepatic Stellate Cells by Bioconjugation. *Bioconjugate Chem*. **2010**, *21*, 2119–2127.

30. Phillips, M. A.; Gran, M. L.; Peppas, N. A. Targeted Nanodelivery of Drugs and Diagnostics. *Nano Today*, **2010,** *5(2),*143-159.

31. Lee, H.; Fonge, H.; Hoang, B.; Reilly, R. M.; Allen, C. The effects of particle size and molecular targeting on the intratumoral and subcellular distribution of polymeric nanoparticles. *Mol. Pharm*. **2010**, *7*, 1195–1208.

32. Muro S. New biotechnological and nanomedicine strategies for treatment of lysosomal storage disorders. *Wiley Interdiscip. Rev. Nanomed. Nanobiotechnol.* **2010**, *2*, 189–204.

33. Mutsaers, S. E.; Papadimitriou, J. M. Surface charge of macrophages and their interaction with charged particles. *J. Leukocyte Biol*. **1988**, *44*, 17–26.

34. Richard, J. P.; Melikov, K.; Vives, E.; Ramos, C.; Verbeure, B.; Gait, M. J.; Chernomordik, L. V.; Lebleu, B. Cell-penetrating peptides. A reevaluation of the mechanism of cellular uptake. *J. Biol. Chem*. **2003**, *278*, 585–590.

35. Ulbrich, K.; Subr, V. Polymeric anticancer drugs with pH-controlled activation. *Adv. Drug Delivery Rev*. **2004**, *56*, 1023–1050.

36. Lee, H. J.; Pardridge, W. M. Monoclonal Antibody Radiopharmaceuticals: Cationization, Pegylation, Radiometal Chelation, Pharmacokinetics, and Tumor Imaging. *Bioconjugate Chem*. **2003**, *14*, 546–553.

37. Li, W.; Nakayama, M.; Akimoto, J.; Okano, T. Effect of block compositions of amphiphilic block copolymers on the physicochemical properties of polymeric micelles. *Polymer* **2011**, *52*, 3783-3790.

38. Dobrovolskaia, M. A.; Patri, A. K.; Simak, J.; Hall, J. B.; Semberova, J.; De Paoli Lacerda, S. H.; McNeil, S. E. Nanoparticle size and surface charge determine effects of PAMAM dendrimers on human platelets in vitro. *Mol. Pharm*. **2012**, *9*, 382.

39. Ganta, S.; Devalapally, H.; Shahiwala, A.; Amiji, M. A review of stimuli-responsive nanocarriers for drug and gene delivery. *J. Controlled Release* **2008**, *126 (3)*, 187−204.

40. Fleige, E.; Quadir, M. A.; Haag, R. Stimuli-responsive polymeric nanocarriers for the controlled transport of active compounds: Concepts and applications. *Adv. Drug Delivery Rev*. **2012**, *64 (9)*, 866−884.

41. Kato, Y.; Ozawa, S.; Miyamoto, C.; Maehata, Y.; Suzuki, A.; Maeda, T.; Baba, Y. Acidic extracellular microenvironment and cancer, *Cancer Cell Int*. **2013**, *13*, 89.

42. Li, L.; Raghupathi, K.; Yuan, C.; Thayumanavan, S. Surface charge generation in nanogels for activated cellular uptake at tumor-relevant pH. *Chem. Sci*. **2013**, *4*, 3654-3360.

43. Gu, J.; Cheng, W. P.; Liu, J.; Lo, S. Y.; Smith, D.; Qu X.; Yang, Z. pH-Triggered Reversible “Stealth” Polycationic Micelles, *Biomacromolecules*, **2008**, *9*, 255–262.

44. Gao, Y.; Yang, C.; Liu, X.; Ma, R.; Kong D.; Shi, L. A Multifunctional Nanocarrier Based on Nanogated Mesoporous Silica for Enhanced Tumor-Specific Uptake and Intracellular Delivery. *Macromol. Biosci*. **2011**, *12*, 251–259.

45. Ding, C. X.; Gu, J. X.; Qu, X. Z.; Yang, Z. Z. Preparation of Multifunctional Drug Carrier for Tumor-Specific Uptake and Enhanced Intracellular Delivery through the Conjugation of Weak Acid Labile Linker. *Bioconjugate Chem*. **2009**, *20*, 1163–1170.

46. Ding, D.; Kwok, R. T. K.; Yuan, Y.; Feng, G.; Tang, B. Z.; Liu, B. A Fluorescent Light-up Nanoparticle Probe with Aggregation-induced Emission Characteristics and Tumor-acidity Responsiveness for Targeted Imaging and Selective Suppression of Cancer Cells. *Mater. Horiz.* **2015**, *2*, 100−105.

47. Sun, C.-Y.; Shen, S.; Xu, C.-F.; Li, H.-J.; Liu, Y.; Cao, Z.-T.; Yang, X.-Z.; Xia, J.-X.; Wang, J. Tumor Acidity-Sensitive Polymeric Vector for Active Targeted siRNA Delivery. *J. Am. Chem. Soc*. **2015**, *137*, 15217−15224.

48. Mizuhara, T.; Saha, K.; Moyano, D. F.; Kim, C. S.; Yan, B.; Kim, Y.-K.; Rotello, V. M. Acylsulfonamide-Functionalized Zwitterionic Gold Nanoparticles for Enhanced Cellular Uptake at Tumor pH. *Angew. Chem., Int. Ed*. **2015**, *54*, 6567−6570.

49. Wilson, W. R.; Hay, M. P. Targeting hypoxia in cancer therapy. *Nature Reviews Cancer,* **2011***,* 11, 393-410

50. Brown, J. M. Tumor hypoxia in cancer therapy. *Methods Enzymol*. **2007**, *435*, 297-321.

51. Choi, K. Y.; Swierczewska, M.; Lee, S.; Chen, X. Y. Protease- Activated Drug Development. *Theranostics* **2012**, *2*, 156−178.

52. de la Rica, R.; Aili, D.; Stevens, M. M. Enzyme-responsive nanoparticles for drug release and diagnostics. *Adv. Drug Delivery Rev*. **2012,** *64*, 967−978.

53. Coleman, J. D.; Thompson, J. T.; Smith, R. W., 3rd; Prokopczyk, B.; Vanden, H. J. P. Role of Peroxisome Proliferator-Activated Receptor β/δ and B-Cell Lymphoma-6 in Regulation of Genes Involved in Metastasis and Migration in Pancreatic Cancer Cells. *PPAR Res*. **2013**, *2013*, 121956.

54. Li, H.; Yu, S. S.; Miteva, M.; Nelson, C. E.; Werfel, T.; Giorgio, T. D.; Duvall, C. L. Matrix Metalloproteinase Responsive, Proximity-Activated Polymeric Nanoparticles for siRNA Delivery. *Adv. Funct. Mater*. **2013**, *23*, 3040–3052.

55. Li, J.; Ge, Z.; Liu, S. PEG-sheddable polyplex micelles as smart gene carriers based on MMP-cleavable peptide-linked block copolymers, *Chem. Commun*., **2013**, *49*, 6974−6976.

56. Crisp J. L.; Savariar, E. N.; Glasgow, H. L.; Ellies, L. G.; Whitney, M. A.; Tsien, R.Y. Dual targeting of integrin αvβ3 and matrix metalloproteinase-2 for optical imaging of tumors and chemotherapeutic delivery. *Molecular Cancer Therapeutics* **2014**, *13*, 1514-1525.

57. Harris, T. J.; von Maltzahn, G.; Lord, M. E.; Park, J. H.; Agrawal, A.; Min, D. H.; Sailor, M. J.; Bhatia, S. N. Protease-Triggered Unveiling of Bioactive Nanoparticles. *Small* **2008**, *4*, 1307-1312.

58. Zhu, L.; Kate, P.; Torchilin, V. P. Matrix Metalloprotease 2-Responsive Multifunctional Liposomal Nanocarrier for Enhanced Tumor Targeting. *ACS Nano*, **2012**, *6(4)*, 3491-3498.

59. Fay, F.; Hansen, L.; Hectors, S. J. C. G.; Sanchez-Gaytan, B. L.; Zhao, Y.; Tang, J.; Munitz, J.; Alaarg, A.; Braza, M. S.; Gianella, A.; Aaronson, S. A.; Reiner, T.; Kjems, J.; Langer, F. J. M. Hoeben, H. M. Janssen, C. Calcagno, G. J. Strijkers, Z. A. Fayad, C. Peŕez-Medina, R.; Mulder. W. J. M. Investigating the Cellular Specificity in Tumors of a Surface-Converting Nanoparticle by Multimodal Imaging. *Bioconjugate Chem*. **2017**, *28*, 1413−1421.

60. Zhang, J.; Yuan, Z. F.; Wang, Y.; Chen, W. H.; Luo, G. F.; Cheng, S. X.; Zhuo, R. X.; Zhang, X. Z. Multifunctional Envelope- Type Mesoporous Silica Nanoparticles for Tumor-Triggered Targeting Drug Delivery. *J. Am. Chem. Soc*. **2013**, *135*, 5068−5073.

61. Yu, S. S.; Lau, C. M.; Thomas, S. N.; Jerome, W. G.; Maron, D. J.; Dickerson, J. H.; Hubbell, J. A.; Giorgio, T. D. Size- and charge-dependent non-specific uptake of PEGylated nanoparticles by macrophages. *Int. J. Nanomed*. **2012**, *7*, 799-813.

62. Callmann, C. E.; Barback, C.V.; Thompson, M. P.; Hall, D. J.; Mattrey, R. F.; Gianneschi, N. C. Therapeutic Enzyme-Responsive Nanoparticles for Targeted Delivery and Accumulation in Tumors. *Adv. Mater*. **2015**, *27*, 4611–4615.

63. Kulkarni, P. S.; Haldar, M. K.; Nahire, R. R.; Katti, P.; Ambre, A. H.; Muhonen, W. W.; Shabb, J. B.; Padi, S. K. R.; Singh, R. K.; Borowicz, P. P.; Shrivastava, D. K.; Katti, K. S.; Reindl, K.; Guo, B.; Mallik, S. MMP-9 Responsive PEG Cleavable Nanovesicles for Efficient Delivery of Chemotherapeutics to Pancreatic Cancer. *Mol. Pharmaceutics*. **2014**, *11*, 2390−2399.

64. Liu, Y.; Ding, X.; Li, J.; Luo, Z.; Hu, Y.; Liu, J.; Dai, L.; Zhou, J.; Hou, C.; Cai, K. Enzyme responsive drug delivery system based on mesoporous silica nanoparticles for tumor therapy in vivo. *Nanotechnology* **2015**, *26*, 145102-145116.

65. Seltzer, J. L.; Weingarten; H.; Akers, K. T.; Eschbach, M. L.; Grant, G. A.; Eisen, A. Z. Cleavage Specificity of Type IV Collagenase (Gelatinase) from Human Skin. Use of synthetic peptides as model substrates. *The Journal of Biological Chemistry* **1989**, *264(33)*, 19583-19586.

66. Collier, I. E.; Wilhelm, S. M.; Eisen, A. Z.; Marmer, B. L.; Grant, G. A.; Seltzer, J. L.; Kronberger, A.; He, C.; Bauer, E. A.; Goldberg, G. I. The Structure OF THE Human Skin Fibroblast Collagenase Gene. *J. Biol. Chem*. **1988**, *263*, 6579-6587.

67. Ryu, J. -H.; Chacko, R. T.; Jiwpanich, S.; Bickerton, S.; Babu R. P.; Thayumanavan, S. Self-cross-linked polymer nanogels: a versatile nanoscopic drug delivery platform. *J. Am. Chem. Soc*. **2010**, *132*, 17227–17235.

68. Saito, G.; Swanson, J. A.; Lee, K. D. Drug delivery strategy utilizing conjugation via reversible disulfide linkages: role and site of cellular reducing activities. *Adv. Drug Delivery Rev*. **2003**, *55*, 199-215.

69. Meister, A.; Anderson, M. E. Glutathione. *Ann. Rev. Biochem*. **1983**, *52*, 711-760.

70. Udenfriend, S.; Stein, S.; Böhlen, P.; Dairman, W.; Leimgruber, W.; Weigele, M. Fluorescamine: A Reagent for Assay of Amino Acids, Peptides, Proteins, and Primary Amines in the Picomole range. *Science*, **1972**, *178(4063)*, 871-872

71. Gore, M. Spectrophotometry and Spectrofluorimetry: A Practical Approach. Ed. Oxford University Press, Incorporated (New York, NY 2000) p. 63.

72. Böhlen, P.; Stein, S.; Dairman, W.; Udenfriend, S. Fluorometric assay of proteins in the nanogram range. *Arch. Biochem. Biophys.* **1973**, *155*, 213-220.

73. Read, M. L.; Etrych, T.; Ulbrich, K.; Seymoura, L. W. Characterisation of the binding interaction between poly(L-lysine) and DNA using the fluorescamine assay in the preparation of nonviral gene delivery vectors. *FEBS Lett*. **1999**, *461*, 96-100.

74. Tutton, M. G.; George, M. L.; Eccles, S. A.; Burton, S.; Swift, R. I.; Abulafi, A. M. Use of Plasma MMP-2 and MMP-9 Levels as a Surrogate for Tumor Expression in Colorectal Cancer Patients. *Int. J. Cancer*, **2003**,*107*, 541–550.

75. İnce, A. T.; Yıldız, K.; Gangarapu, V.; Kayar, Y.; Baysal, B.; Karatepe, O.; Kemik, A. S.; Şentürk, H. Serum and biliary MMP-9 and TIMP-1 concentrations in the diagnosis of cholangiocarcinoma. *Int. J. Clin. Exp. Med*. **2015**, *8(2)*, 2734-2740.

76. Jumper, C.; Cobos, E.; Lox, C. Determination of the serum matrix metalloproteinase-9 (MMP-9) and tissue inhibitor of matrix metalloproteinase-1 (TIMP-1) in patients with either advanced small-cell lung cancer or non-small-cell lung cancer prior to treatment. *Respiratory Medicine* **2004**, *98*, 173-177.

77. Hyuga, S.; Nishikawa, Y.; Sakata, K.; Tanaka, H.; Yamagata, S.; Sugita, K.; Saga, S.; Matsuyama, M.; Shimizu, S. Autocrine Factor Enhancing the Secretion of M_r 95,000 Gelatinase (Matrix Metalloproteinase 9) in Serum-free Medium Conditioned with Murine Metastatic Colon Carcinoma Cells. *Cancer Research*, **1994**, *54*, 3611-3616.

78. Sun, Q.; Ojha, T.; Kiessling, F.; Lammers, T.; Shi, Y. Enhancing Tumor Penetration of Nanomedicines. *Biomacromolecules* **2017**, *18*, 1449-1459.

79. Radovic-Moreno, A. F.; Lu, T. K.; Puscasu, V. A.; Yoon, C. J.; Langer, R.; Farokhzad, O. C. Surface Charge-Switching Polymeric Nanoparticles for Bacterial Cell Wall-Targeted Delivery of Antibiotics. *ACS Nano* **2012**, *6*, 4279–4287.

80. Bahadur, K. C. R.; Xu, P. Multicompartment Intracellular Self-Expanding Nanogel for Targeted Delivery of Drug Cocktail. *Adv. Mater*. **2012**, *24*, 6479–6483.

81. Ghosh, S.; Basu, S.; Thayumanavan, S. Simultaneous and Reversible Functionalization of Copolymers for Biological Applications. *Macromolecules* **2006**, *39*, 5595-5597.

82. Li, J.; Kao, W. J. Synthesis of Polyethylene Glycol (PEG) Derivatives and PEGylated−Peptide Biopolymer Conjugates. *Biomacromolecules*, **2003**, *4*, 1055-1067.

83. Xu, J. Z.; Moon, S. H.; Jeong, B.; Sohn, Y. S. Thermosensitive micelles from PEGylated oligopeptides. *Polymer*, **2007**, *48*, 3673-3678.

84. Adidou, O.; Goux-Henry, C.; Safi, M.; Soufiaoui, M.; Framery, E. PEG_{350}-based di-(2-pyridyl)methylamine as a ligand in the Pd-catalyzed water Suzuki–Miyaura reaction of aryl chlorides. *Tetrahedron Letters*, **2008**, *49*, 7217–7219.

85. Ryu, J. -H.; Jiwpanich, S.; Chacko, R.; Bickerton S.; Thayumanavan, S. Surface functionalizable polymer nanogels with facile hydrophobic guest encapsulation capabilities. J. *Am. Chem. Soc*. **2010**, *132*, 8246–8247.

86. Kavimandan, N. J.; Losi, E.; Wilson, J. J.; Brodbelt, J. S.; Peppas, N. A.; Synthesis and Characterization of Insulin-Transferrin Conjugates. *Bioconjugate Chem*. **2006**, *17*, 1376-1384.

CHAPTER 5

BIOCOMPATIBLE POLY(L-GLUTAMIC ACID)-BASED POLYMERS FOR DRUG DELIVERY APPLICATIONS

5.1 Introduction

Use of biodegradable polymers as nanocarriers is of great importance as they can delivery therapeutics to the target site with minimal toxicity and side effects as a result of the vehicle.[1] Biodegradable polymers, those that enzymatically or hydrolytically degrade within the body[2], have become of increasing interest for a variety of medical applications including implants, prostheses, tissue engineering or regeneration, and delivery of therapeutics.[3-4] For therapeutics, many systems are controlled by the rate of biochemical erosion or degradation and/or drug diffusion within the nanocarrier matrix leading to content release. Little investigation has been done on systems where the drug release mechanism is independent of the polymer degradation. Nanocarriers comprised of polymer precursors that have been synthesized by radical polymerization methods such as ATRP or RAFT are generally not biodegradable.[3] Regardless of the apparent toxicity of such nanocarriers, a variety of diseases may benefit from therapeutic delivery using nanocarrier formulation for continual and long-term treatment that has known biocompatible degradation through catabolism and excretion. For therapeutic purposes such as chemotherapeutic delivery to tumors, for example, these materials should still maintain desirable cargo protection and structural stability until exposed to designed stimulus for release.[5] Nanocarriers with stimuli and site-specific drug release and predictable biochemical degradation thus allow for greater control of targeted delivery.

The biocompatibility and biodegradability of polymeric assemblies can be affected by a variety of polymer characteristics including the solubility, hydrophilicity or

lipophilicity, molecular weight, and chemical composition of the material. Naturally occurring polymers are typically degradable by enzyme digestion, and thus have variable degradation rates.[3] Variability is based on the polymer type, location of administration, enzyme type, and enzyme concentration. Such biologically derived materials, however, are commonly bioactive and thus have the disadvantage of invoking a strong immune response. Synthetic polymers produced through ring opening polymerization (ROP) and condensation polymerization have potential to be biologically inactive and can be designed to include hydrolytically or enzymatically cleavable bonds.[3] Various functional groups that could be incorporated into polymers for biodegradation include esters, orthoesters, anhydrides, carbonates, amides, imines, and ureas, among others.[6]

Poly(L-glutamic acid), PG, is an artificial water soluble polypeptide polymer comprised of L-glutamic acid. Both the polymer and its degraded product, L-glutamic acid, are generally recognized as safe (GRAS) by the American Food and Drug Administration (FDA) evaluation and regulation.[7] Cysteine proteases, namely cathepsin B, have been found largely responsible for lysosomal degradation of PG.[7-8] Results from addition of lysosomal enzymes to PG, poly(L-aspartic acid) and poly(D-glutamic acid) have shown that PG is the most susceptible to degradation in the lysosome.[9] Biodistribution analysis has shown that PG was mostly located in the kidney and urine, with very little accumulation in other tissues.[10] The modification of PG with hydrophilic functionalities showed that the polymer was mainly excreted through the renal system, with little clearance by the RES.[11] It has been found to be non-immunogenic in humans with tolerated doses relevant to drug carrier quantities.[12] However, the biodistribution results also found that within an hour of injection a large portion of the PG will have already left circulation.[10]

While the lack of toxicity for some of these materials are promising, their fast degradation and clearance reduce their applicability in drug delivery. However, because of the possibility for modification of these materials, this pitfall may be circumvented. The surface chemistry of nanoparticles has been shown to largely determine the immune systems response to the vehicle.[13] PG has pendent carboxyl groups that are available for conjugation, which is promising for use in drug delivery applications. The degradation of PG has been shown to occur at lower charge density and at random coil regions of the polymer, as it has pH-dependent rod-like alpha-helix secondary structure.[14] Functionalization can affect the alpha-helix secondary structure of PG, and likewise lysosomal degradation has also been shown to increase with side chain modification.[7] Therefore, it would be interesting to develop a PG-based polymer that has compatible lysosomal degradation in the disassembled polymer state, but is resistant to this degradation in the assembled nanocarrier form.

We therefore envisaged an amphiphilic PG-derivative comprised of hydrophilic PEG corona, and hydrophobic and cross-linkable disulfide-based core. We expect that these amphiphilic polymers will self-assemble into micellar aggregates in aqueous conditions and be capable of sequestering lipophilic guests. PEG has been shown to improve the circulation time *in vivo* for a variety of nanocarrier platforms including polymeric nanoassemblies through steric hindrance and reduction of non-specific interactions.[15, 16] It is reasonable to expect that surface decoration of biodegradable polymers with PEG should decrease the rate of clearance and possibly also the rate of enzymatic degradation in circulation. The incorporation of redox-sensitive components in a molecular design has been extensively investigated[34], including our own group work on

disulfide-crosslinked nanogels[17, 18], which are promising for intracellular release of nanocarrier contents. With this project we aim to *i)* design and synthesize PG-based amphiphilic derivatives while having appropriate control over the polymer molecular weight, side chain composition, and solubility, ii) form self-assembled nanoscale aggregates capable of encapsulating hydrophobic guests, and chemical core-crosslinking into stable nanogels, similar to its poly(methyl methacrylate)-based counterparts, and iii) evaluate the polymer and nanogel cytotoxicity and potential use as a delivery vehicle by cellular internalization.

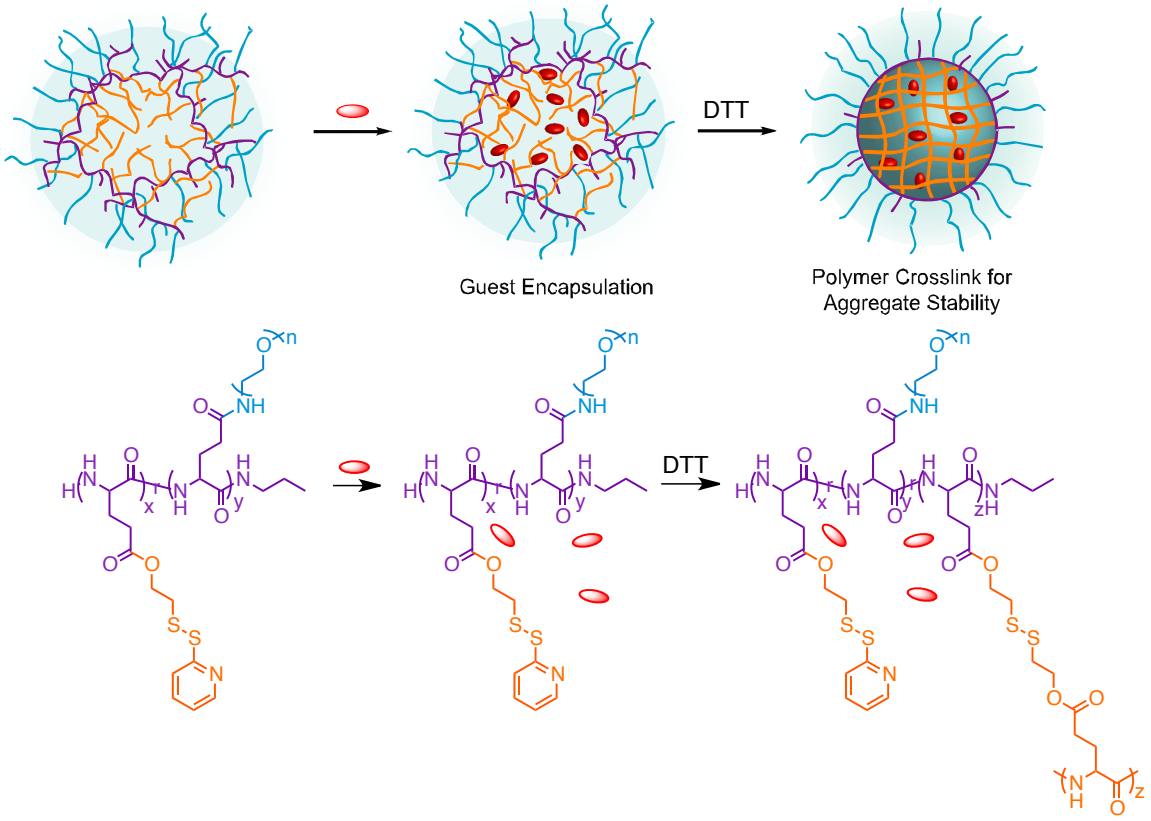

Scheme 11. Pictorial representation and corresponding chemical structures of PG-modified derivative, its amphiphilic self-assembly in aqueous media with hydrophobic guest, and crosslinking in response to reducing agent DTT.

5.2 Results and Discussion

5.2.1 Synthesis and Characterization of Poly(L-glutamic acid) Derivatives

Consistent with previous reports, synthesis was achieved by first the reaction of γ-benzyl-L-glutamate with triphosgene to form α-benzyl-L-glutamate-N-carboxyanhydride (NCA) monomer, which was polymerized through ring opening polymerization (ROP) to form poly(γ-benzyl-L-glutamate) (PBLG) (**Scheme 12**).[19] The polymerization was achieved using primary amine *N*-propylamine initiator. The use of non-nucleophilic bases and primary amines have been shown to form PBLG, with lesser polydispersity using nucleophilic amines.[19-21] Various polymer molecular weights ranging from 9.5 to 43.2 KDa were prepared by varying the monomer and initiator feed ratio, so that any change in aggregation characteristics with molecular weight could be assessed (**Table 26, Figure 72**). Further, these polymerizations were performed at room temperature so that 71lymerizations would be terminated by amine terminus cyclization to form a substituted pyrrolidone ring.[22] This can prohibit the use of PBLG to further polymerize other NCAs, however the amine group can be maintained by polymerization at low temperatures.[23, 24] In this synthetic scheme, amine terminus is not desirable due to subsequent coupling chemistries. Matrix Assisted Laser Desorption/Ionization (MALDI) mass spectrometry characterization of PBLG supported that the amine terminus is a cyclized pyrrolidone ring (**Figure 72**).

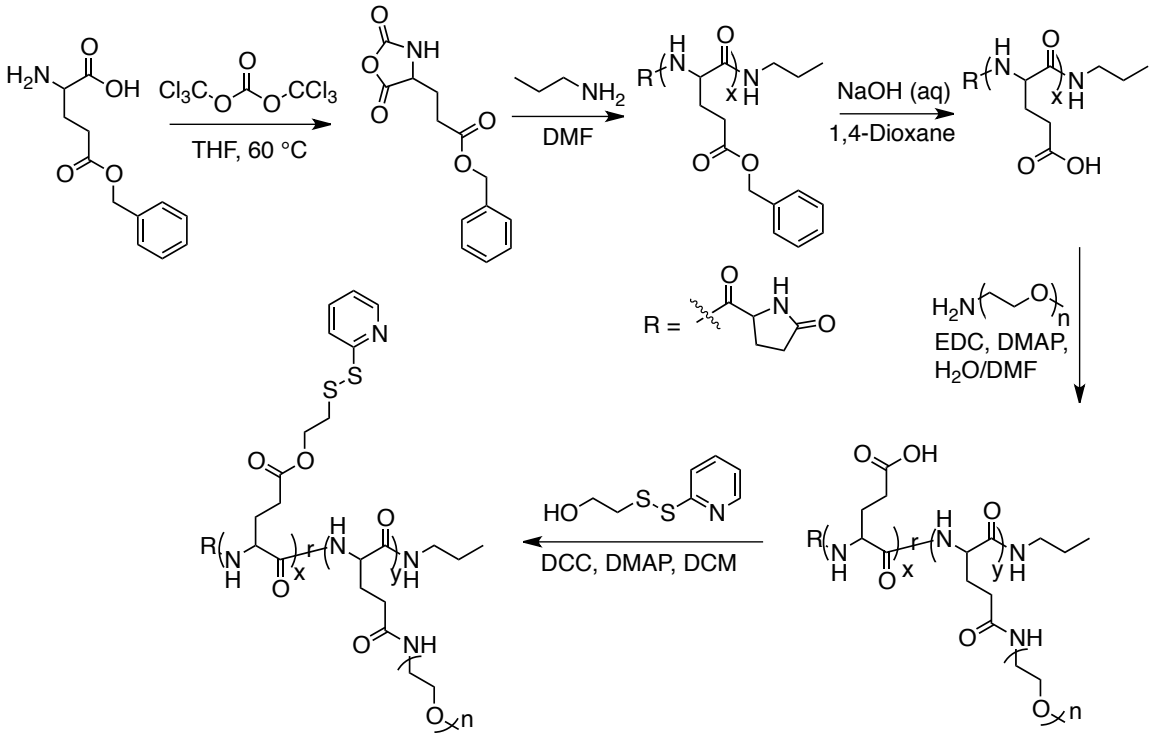

Scheme 12. Synthesis of amphiphilic poly(L-glutamic acid) derivatives PG-*g*-PEG-*g*-PDS.

The benzyl protecting groups on PBLG polymers were then be removed by NaOH to yield poly(L-glutamic acid) polymers. Benzyl deprotection was confirmed by ^{1}H NMR spectroscopy by the disappearance of benzyl peaks (7.28 and 5.07 ppm). A portion of the PG carboxylic acid side chains were then functionalized with PEG using EDC coupling, resulting in grafting ratios of 28-30% PEG on PG-*g*-PEG polymers, determined by the relative integrations of methylene protons of PEG (3.36 ppm) compared to ethylene groups of total glutamic acid side chains (2.98-1.18 ppm). The remaining side chains were then functionalized with (2-pyridyldithio)ethanol (PDS) using DCC coupling, resulting in grafting rations of 68-70% PDS on PG-*g*-PEG- *g*-PDS polymers, determined by the relative integrations of the aromatic protons of PDS (8.46 ppm) compared to methylene protons of PEG (3.36 ppm).

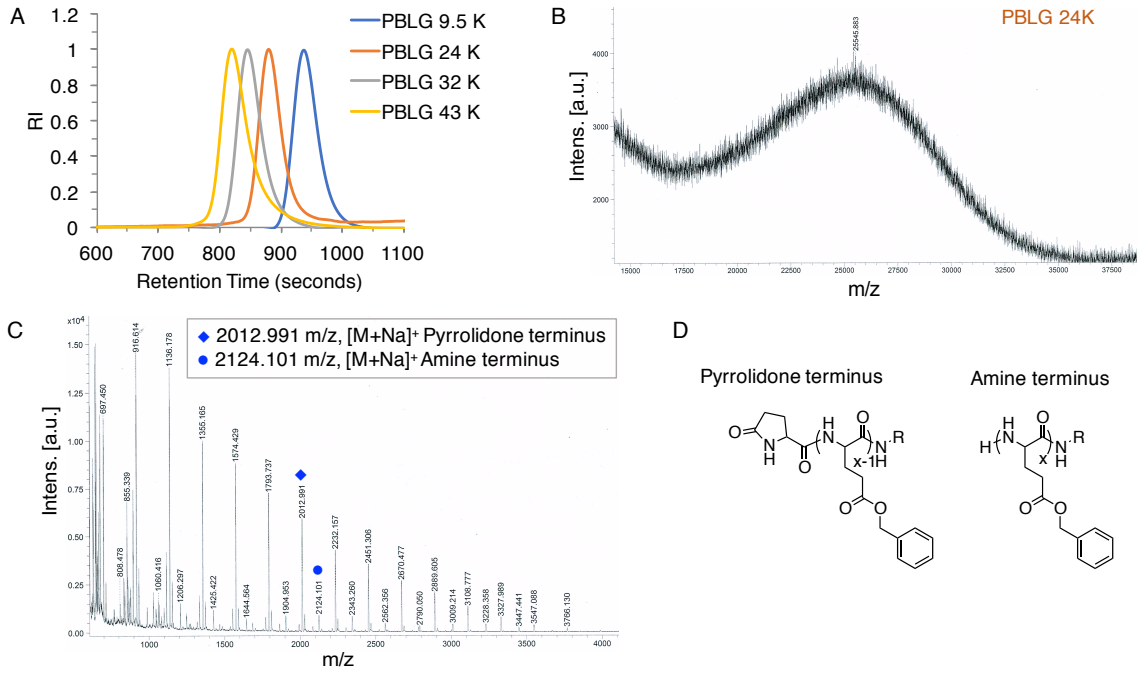

Figure 72. PBLG characterization by A) DMF GPC chromatograms of various molecular weights, B) low resolution MALDI chromatogram of 24K PBLG, C) high resolution MALDI chromatogram for amine-terminus characterization, and D) chemical structures of pyrrolidone and amine terminus for PBLG.

Table 26. Characteristics of PBLG and resultant PG-*g*-PEG-*g*-PDS derivatives.

	PBLG			PG-g-PEG-PDS			
	Mn (expected KDa)	Mn (KDa)[a]	Đ	Mn (KDa)[a]	Đ	PEG (%)[b]	PDS (%)[b]
1	7	9.53	1.11	10.6	1.32	30	70
2	15	23.6	1.06	12.5	1.44	30	68
3	25	32.2	1.15	12.3	1.53	28	65
4	35	43.2	1.23	12.8	1.46	30	70

Note: Based on a) DMF GPC against a PMMA standard, b) ^{1}H-NMR spectroscopy.

Gel permeation chromatography (GPC) analysis of PG-*g*-PEG-*g*-PDS polymers gave similar Mn for polymers 1-4, ranging from 10.6-12.8 KDa, which were smaller than expected based on starting PBLG polymers. Because GPC analysis is calibrated against a poly(methyl methacrylate) (PMMA) standard, which is structurally very different to these polypeptide with secondary structure confirmations, we also examined molecular weight by ^{1}H-NMR. ^{1}H-NMR end group analysis of *N*-propyl amine composition for PG polymers 1-4 gave molecular weights of 5.2, 13, 21, and 29 KDa, respectively, which are consistent

with expected masses following benzyl deprotection of PBLG precursors. End group analysis in PG-*g*-PEG-*g*-PDS polymers, however, gave 7.7, 9.0, 11, and 15 KDa for polymers 1-4, respectively. These values suggest some main chain hydrolysis occurred during aqueous grafting and purification steps. Some hydrolysis during post-modifications isn't surprising, due to the hydrolytic susceptibility of PG. [8, 9, 14]

Fourier transform infrared (FTIR) analysis was evaluated to for functional group composition and determination of poly(peptide) secondary structure (**Figure 73**). The FTIR spectrum of PBLG demonstrates peaks appearing at 1735 cm^{-1} (consistent with C=O stretching band of the benzyl ester group), 3293 cm^{-1} (consistent with amide N-H stretching in main chain), 1651 cm^{-1} (confirming the α-helix amide I band), and 1551 cm^{-1} (confirming the α-helix amide II band), consistent with expectations that segments in PBLG are a α-helix conformational structure.[25, 26] The absence of characteristic anhydride (C=O stretch) peaks at 1774 and 1832 cm^{-1} supports the conversion of NCA monomer to PLBG.[26] The FTIR spectrum of PG detects the same peaks consistent with α-helix amide I and α-helix amide II band at 1643 and 1545 cm^{-1}, respectively, and the absence of ester (C=O stretch) supporting successful benzyl deprotection. For PG-*g*-PEG-*g*-PDS, the presence of these peaks at 1653 cm^{-1}, and 1546 cm^{-1}, like those of PBLG and PG, demonstrate the grafted polymer also contains α-helix conformational structure, consistent with observations of PBLG-grafted polymers.[27] It is possible the polymer contain random coil regions, as broadness of peak at 1653 and 1545 cm^{-1} may also contain signatures from amide I and amide II random coil, which can appear at 1657 and 1535 cm^{-1}, respectively.[26] Further, the peaks at 1096 cm^{-1} (C-O-C stretch) and 2857 cm^{-1} (C-H stretch) are consistent with the PEG segments in PG-*g*-PEG-*g*-PDS. This peak at 2857 cm^{-1} could also be due to

PDS segments (C-H stretch) while aromatic signatures (C=C stretch) are within the same region of peaks observed for the amide I and amide II bands.

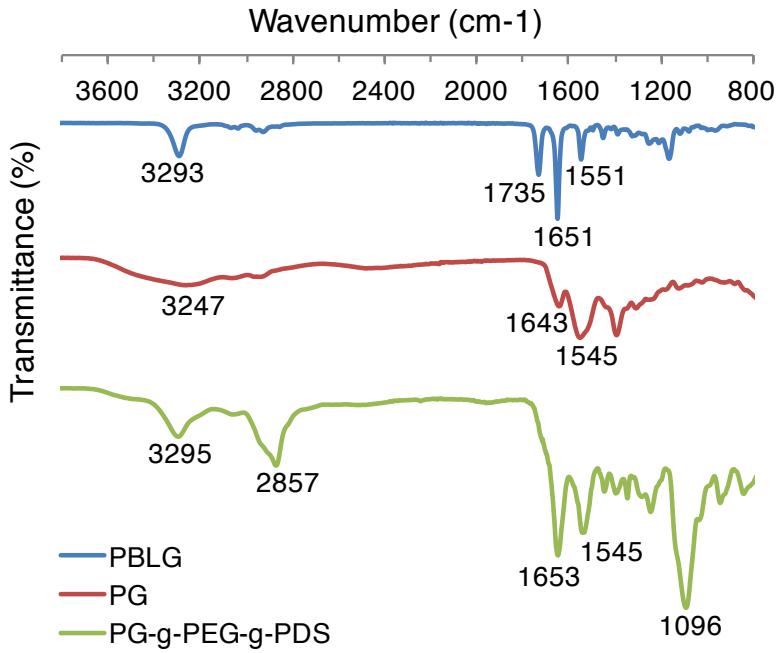

Figure 73. FTIR spectrum of PBLG, PG, and PG-*g*-PEG-*g*-PDS polymers.

5.2.2 Supramolecular Assembly Characterization of Polymers

We then investigated the aggregation characteristics of these polymers to establish their capability to perform as nanocarrier materials. Due to their amphiphilicity, we expect that the polymers will assemble into micelle-type aggregates in aqueous media (**Scheme 11**). Random copolymers PG-*g*-PEG-*g*-PDS (P1-4) were dispersed in an aqueous phase using repeated sonicate and chill cycles until they appeared dissolved. The formation of an amphiphilic aggregates of P1-4 with average hydrodynamic diameters of 10-18 nm were confirmed using dynamic light scattering (DLS) at concentrations of 5 and 10 mg/mL (**Figure 74**). While the polymers were slightly different in molecular weight, their aggregation sizes did not vary when prepared at the same concentration. Due to the known lower critical solution temperature (LCST) characteristics of PEG, the temperature

responsiveness of these polymer aggregates was characterized by DLS to determine if particle sizes could be manipulated. Size transitions were observed above 50 °C, with 130 nm aggregates achieved at 60 °C.

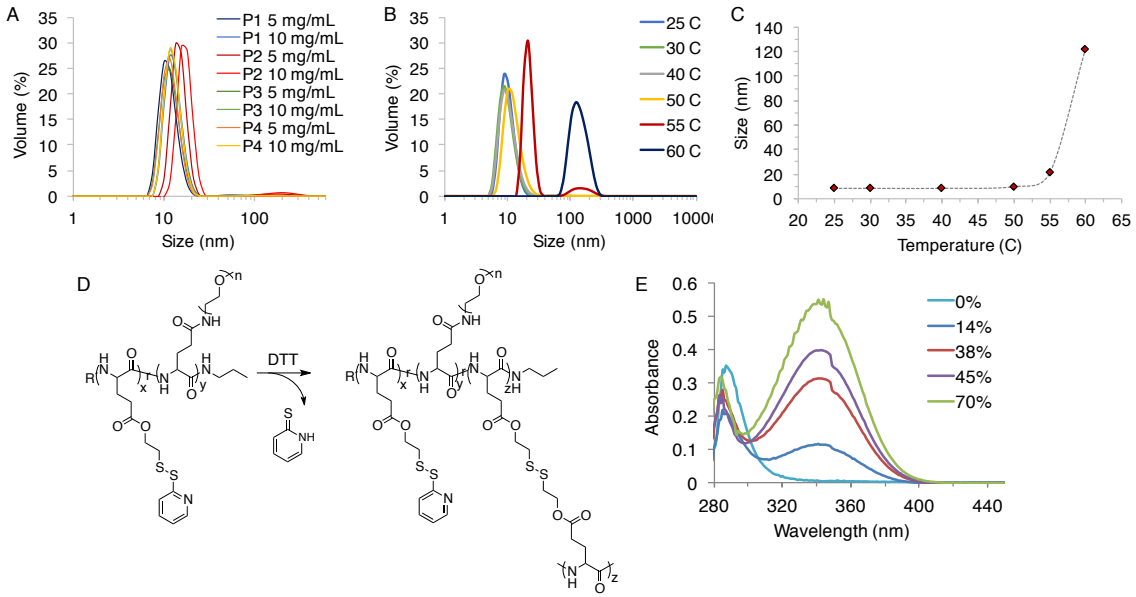

Figure 74. DLS characterization of PG-g-PEG-g-PDS aggregates A) P1-P4 at 5 and 10 mg/mL, B) P1 size at various temperatures, C) corresponding plot of mean particle size vs. temperature, D) chemical structure of crosslink reaction, and D) absorption spectrum of nanogel crosslinking to various extents.

The aggregates were then locked in confirmation through intra-aggregate disulfide crosslink formation using reducing agent DL-dithiothreitol (DTT) as previously reported for poly(methyl methacrylate)-based polymeric nanogels containing PDS moieities.[28, 29] The covalent crosslinking was achieved via the addition of a stoichiometric amount of DTT, which generates the corresponding quantity of free thiols on PDS moieties in the aggregate, which then reacts with remaining PDS moieties in the polymer chain. Controlled crosslinking to various extents was achieved by addition 5, 12.5, 25 and 50% DTT respective to mol PDS, calculated to be 14, 38, 45, and 100% crosslinked, respectively, by the amount of byproduct, 2-pyridinethione, observed by UV-Vis spectroscopy (**Figure 74**). After confirming this stoichiometric control in core crosslinking for this polymer, we then

evaluated the sizes of nanogels after crosslinking. Aggregates P2-P4 were crosslinked ~50 and ~100% and then compared to their non-crosslinked precursor by DLS (**Figure 75**). Interestingly, we observed a slight increase in size for nanogels P2-P4 after crosslinking to 20-30 nm, which was a greater increase for ~100% crosslinked than ~50% crosslinked. It is possible this size increase is a result of nanogel swelling from reduction in particle hydrophobicity that occurs from the loss of 2-(2-pyridyldithio groups during this crosslinking process. Transmission electron microscopy (TEM) analysis of crosslinked nanogels and showed the presence of spherical assemblies in the range of 10-30 nm (**Figure 76**). Crosslinked nanogels gave more distinct particles with size correlation with DLS than the polymer aggregate solution, which may be result of aggregation, or loss of particle integrity, during the drying process.

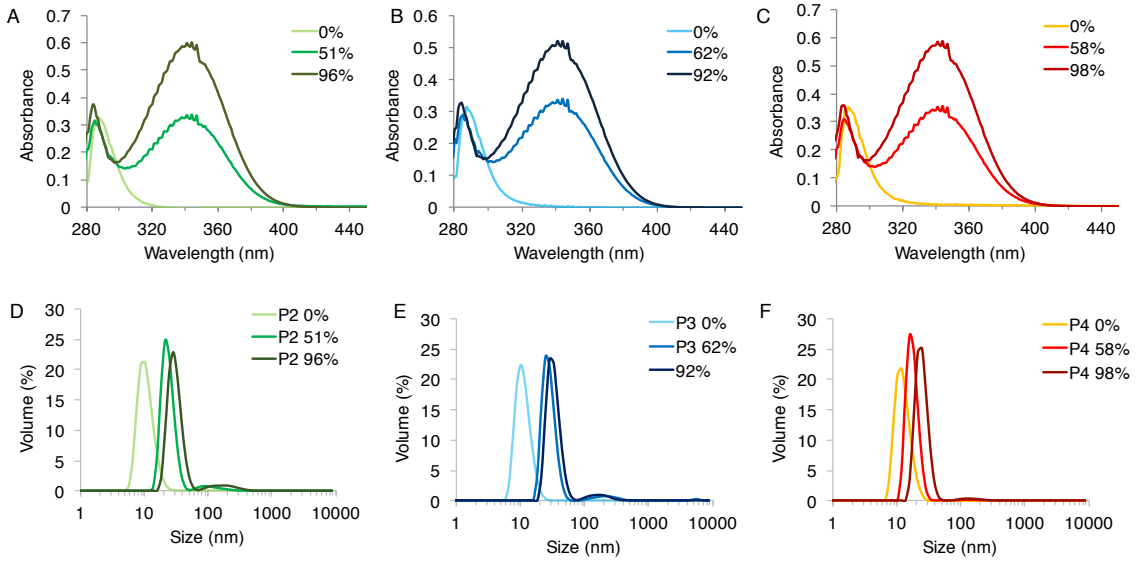

Figure 75. UV-vis absorbance spectra of crosslinking for A) P2, B) P3, and C) P4, and the DLS of aggregates after crosslinking for D) P2, E) P3, and F) P4.

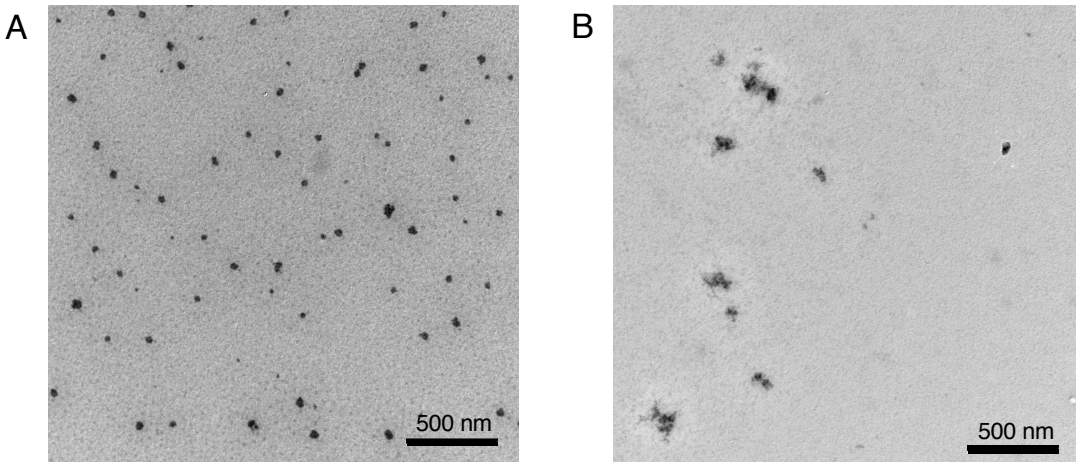

Figure 76. TEM of A) crosslinked nanogel and B) polymer solutions (2.5 mg/mL) drop casted then dried on carbon coated Cu grid.

Next, we investigated the ability of this PG-*g*-PEG-*g*-PDS polymer to act as host for a hydrophobic model guest 1,1'-dioctadecyl-3,3,3',3'-tetramethyl indocarbocyanine perchlorate (DiI) in aqueous medium. DiI is not soluble in water unless a hydrophobic pocket of a suspension is provided. Polymer P2 was used to evaluate this amphiphilic random copolymer to encapsulate this host property, and following DiI addition, aggregates were crosslinked 0, 30, and 70%. Following dialysis purification and filtration to remove any non-encapsulated DiI, their absorbance spectrum and sizes were evaluated (**Figure 77**). This guest loading slightly increased the size of the aggregates, generating particles of 20-30 nm for 0, 30, and 70% crosslinked. As apparent by UV-vis spectroscopy, this polymer can perform as a nanocarrier host for water insoluble guest DiI, with absorption maximum at 562 nm.

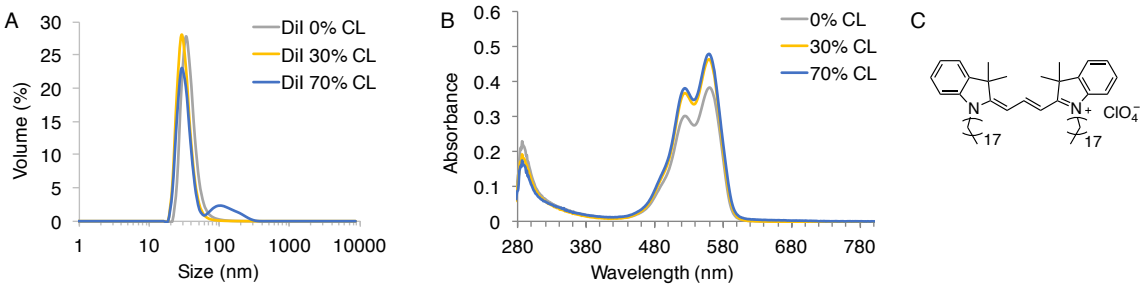

Figure 77. DiI loaded nanogels of different crosslink density A) size by DLS and B) absorbance spectra, and C) chemical structure of DiI.

5.2.2 Cytotoxicity and Cellular Internalization of Polymers

Confocal microscopy was used to evaluate whether these nanogels are capable of internalizing in HeLa cells and 293T cells to evaluate their potential use as delivery vehicles. First cytotoxicity of both the 100% crosslinked nanogel and the polymer (both from polymer P4) was evaluated for both HeLa and 293T cell lines using the Alamar blue cytotoxicity assay. For the nanogel in both cell lines, viability >80% was observed up to 1 mg/mL (**Figure 78**). However, the non-crosslinked polymer exhibited significant toxicity over 0.5 mg/mL for both HeLa and 293T cell lines. This could be attributed to the toxicity from PDS groups, due to known toxicity of 2-(2-pyridyldithio)ethanol, which are removed in the crosslink process. We therefore determined the nanogel to be compatible with cells tested, pending that the PDS groups are removed by crosslinking. To then evaluate the cellular internalization, nanogels were covalently modified with a thiol-modified fluorescein label. Nanogels were incubated with HeLa cells or 293T for 4 hours before confocal imaging, and uptake was observed using laser excitation at 488 nm for fluorescein (**Figure 79**). The cell nuclei were stained with the addition of DRAQ5 and was detecting using a 543 nm wavelength laser. From microscopy images the polymeric nanogel was shown to internalize in both 293T and HeLa cells. These results signify that these particles

are capable of cellular uptake, and therefore should be considered a candidate as a drug delivery vehicle.

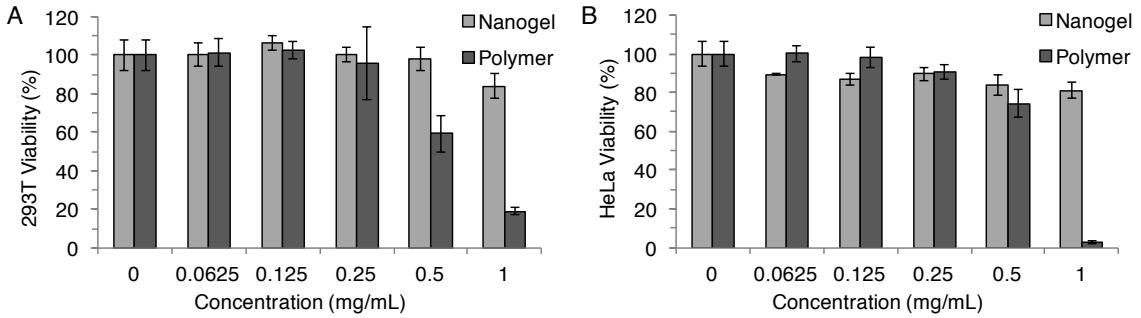

Figure 78. Alamar blue toxicity assay with 100% crosslinked nanogels and polymer PG-g-PEG-g-PDS with A) 293T cell line and B) HeLa cell line.

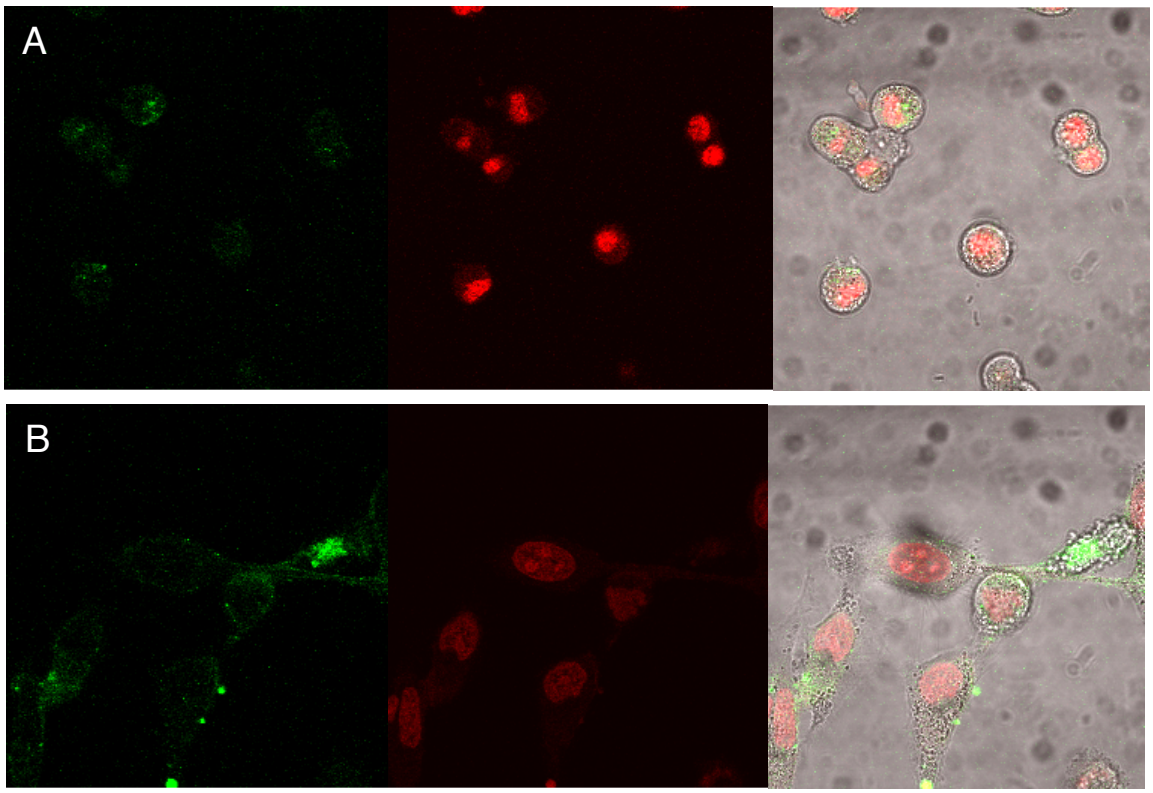

Figure 79. Confocal microscopy images using a 63× × oil-immersion objective of right: fluorescein-labeled NG (green, 488 nm), middle: DRAQ5 nucleus stain (red 543 nm), and left: composite with brightfield image overlays of A) 293T cells and B) HeLa cells after 4-hour incubation.

5.3 Conclusions

In summary, we have designed and synthesized an amphiphilic poly(L-glutamic acid)-based derivative capable of supramolecular self-assembly into nanoscale aggregates,

which can be chemically crosslinked with stoichiometric control. Furthermore, this nanocarrier can perform as a host, by encapsulation of hydrophobic guest in aqueous media. The potential for the use of such materials as delivery vehicles was evaluated by cell cytotoxicity analysis, finding high viability with both HeLa and 293T cell lines. The cellular internalization of these nanogels were also confirmed using confocal microscopy, by monitoring uptake of covalently-conjugated fluorescein tag.

5.4 Experimental

5.4.1 Materials and Methods

All reagents were purchased from commercial source and used without further purification unless otherwise mentioned. The compound 2-(2-pyridyldithio)ethanol (PDS) was prepared as previously reported.[28] Polymers were synthesized using ROP polymerization and purified by dialysis using a membrane with 3500 MWCO. ^{1}H-NMR spectra were recorded on a 400 MHz Bruker NMR spectrometer using the residual proton resonance of the deuterated solvent as the internal standard. Polymer molecular weights were estimated by gel permeation chromatography (GPC, Waters) using DMF as eluent at a flow rate of 1 mL/min by a refractive index detector compared to poly(methyl methacrylate) (PMMA) standard. UV-visible absorption spectra were recorded on a Carry 100 Scan spectrometer. Dynamic Light Scattering (DLS) measurements were carried out on a Malvern NanoZetasizer. TEM images were recorded using a JEOL-2000FX instrument operating at an accelerating voltage of 100 KV. Fourier transform infrared (FTIR) spectra were recorded on Spectrum 100 FTIR spectrometer. Cytotoxicity assays were performed using Molecular Devices Spectramax M5 plate reader. Confocal experiments were obtained using Zeiss510 META confocal laser scanning microscope.

5.4.2 Experimental Procedures

Synthesis of α-benzyl-L-glutamate-N-carboxyanhydride (NCA): Monomer α-benzyl-L-glutamate-N-carboxyanhydride was prepared following a previously published procedure.[30] L-glutamic acid γ-benzyl ester (2 g, 8.47 mmol) was dissolved in dry THF (50 mL) in a 100 mL round bottomed flask and placed in a preheated oil bath at 60 °C under argon atmosphere. Triphosgene (1.25 g, 4.23 mmol) was dissolved in dry THF (2 mL) in a glass vial and added to the L-glutamic acid γ-benzyl ester solution. The reaction mixture was stirred for 6 hours, then stopped and allowed to cool to room temperature. Following evaporation under reduced pressure to 50 mL THF, the solution was precipitated in cold hexane to get a white color solid product in 94% yield. ^{1}H NMR (400 MHz, $CDCl_3$) δ (ppm): 7.35 (m, 5H, C_6H_5), 6.49 (s, 1H, NH), 5.14 (s, 2H, CH_2), 4.37 (t, 1H, *J*=6.12, CH), 2.60 (t, 2H, *J*=6.76, CH_2), 2.27 (sex, 1H, *J*=7.32, CH_2), 2.13 (sex, 1H, *J*=7.32, CH_2).

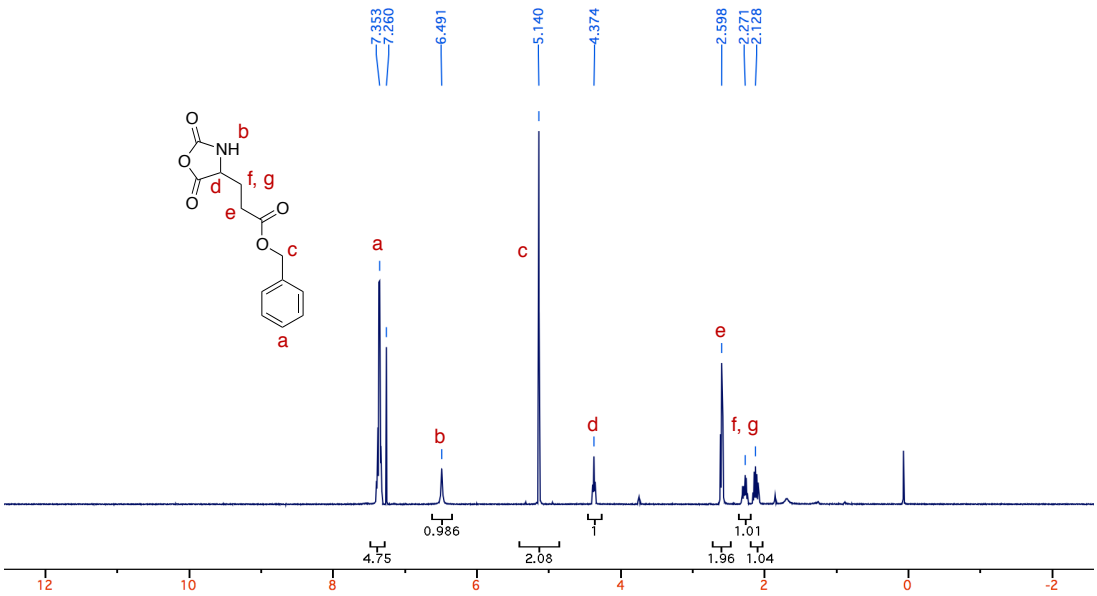

Figure 80. ^{1}H NMR spectrum of α-benzyl-L-glutamate-N-carboxyanhydride.

Synthesis of poly(γ-benzyl-L-glutamate) (PBLG) 1: Poly(γ-benzyl-L-glutamate) polymers were prepared according to a previously published procedure.[31] NCA monomer

(800 mg, 3.04 mmol) was added to a Schlenk flask and dissolved in anhydrous DMF (3 mL) under argon atmosphere. Then propyl amine (7.81 µL, 0.095 mmol) initiator was dissolved in anhydrous DMF (0.39 mL) and added to the Schlenk flask. The reaction mixture was stirred at room temperature for 48 hours. The reaction was stopped and the product was precipitated from diethyl ether to get the polymer as an off-white sticky product. GPC (DMF) *Mn*: 9.5 KDa; Đ: 1.11. ^{1}H NMR (400 MHz, $CDCl_3$) δ (ppm): 7.28 (broad peak, 5H, C_6H_5), 5.07 (broad peak, 2H, CH_2), 3.96 (s, 1H, CH), 2.85-1.95 (broad peaks, 4H, 2xCH_2), 1.70 (s, 2H, CH_2), 0.96 (S, 2H, CH_3).

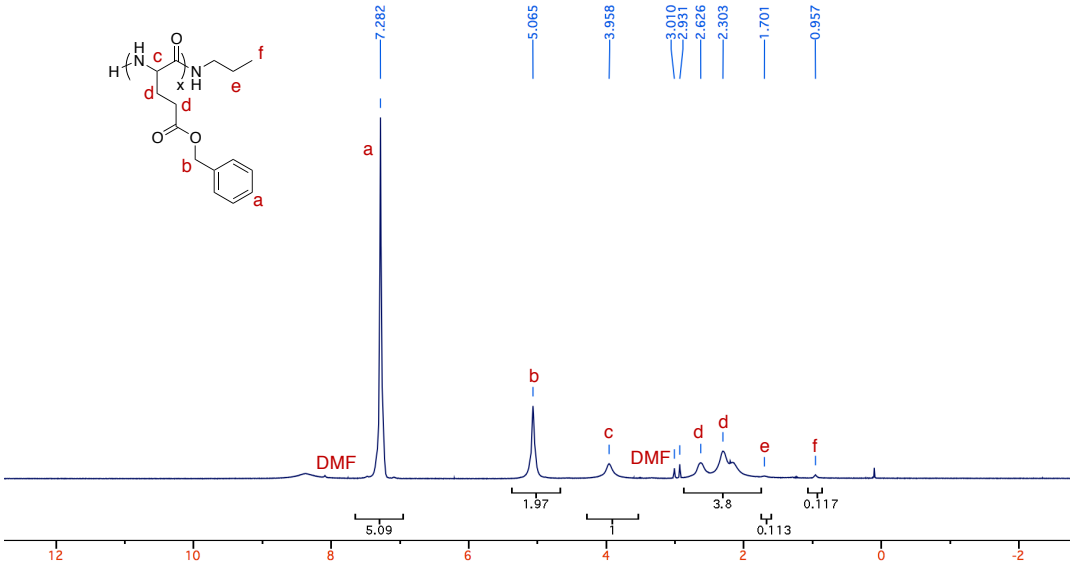

Figure 81. ^{1}H NMR spectrum of poly(γ-benzyl-L-glutamate) (PBLG) 1.

Synthesis of poly(γ-benzyl-L-glutamate) (PBLG) 2: NCA monomer (800 mg, 3.04 mmol) was added to a Schlenk flask and dissolved in anhydrous DMF (3 mL) under argon atmosphere. Then propyl amine (3.68 µL, 0.044 mmol) initiator was dissolved in anhydrous DMF (0.18 mL) and added to the Schlenk flask. The reaction mixture was stirred at room temperature for 48 hours. The reaction was stopped and the product was precipitated from diethyl ether to get the polymer as an off-white sticky product. GPC

(DMF) *Mn*: 23.6 KDa; Đ: 1.06. ^{1}H NMR (400 MHz, $CDCl_3$) δ (ppm): 7.28 (broad peak, 5H, C_6H_5), 5.07 (broad peak, 2H, CH_2), 3.95 (s, 1H, CH), 3.05 (s, 1H, CH), 2.96 (s, 1H, CH), 2.83-1.77 (broad peaks, 4H, 2xCH_2), 1.29 (s, 2H, CH_2), 0.87 (s, 2H, CH_3).

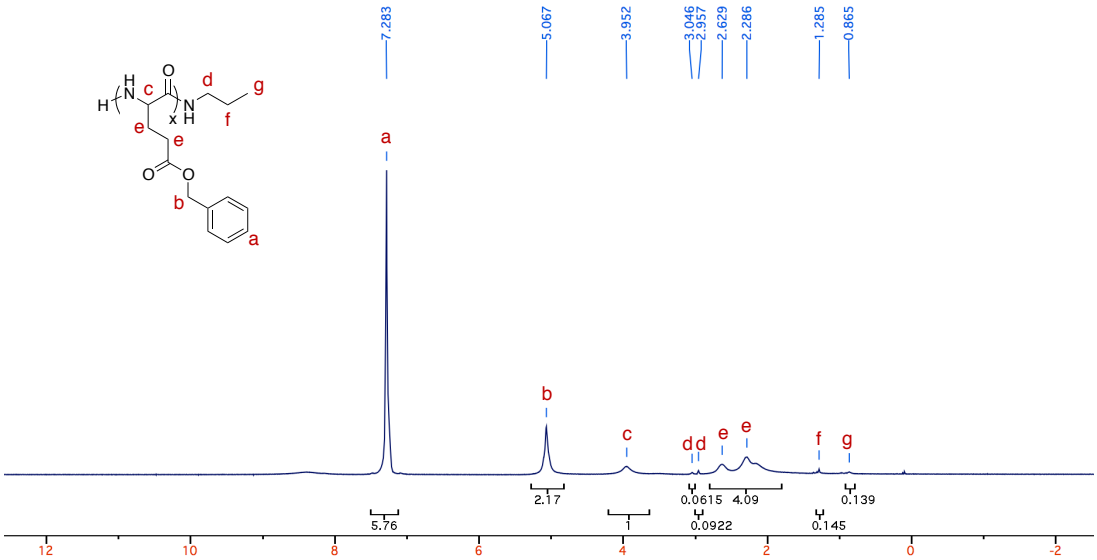

Figure 82. ^{1}H NMR spectrum of poly(γ-benzyl-L-glutamate) (PBLG) 2.

Synthesis of poly(γ-benzyl-L-glutamate) (PBLG) 3: NCA monomer (800 mg, 3.04 mmol) was added to a Schlenk flask and dissolved in anhydrous DMF (3 mL) under argon atmosphere. Then propyl amine (2.19 µL, 0.027 mmol) initiator was dissolved in anhydrous DMF (0.11 mL) and added to the Schlenk flask. The reaction mixture was stirred at room temperature for 48 hours. The reaction was stopped and the product was precipitated from diethyl ether to get the polymer as an off-white sticky product. GPC (DMF) *Mn*: 32.2 KDa; Đ: 1.15. ^{1}H NMR (400 MHz, $CDCl_3$) δ (ppm): 7.28 (broad peak, 5H, C_6H_5), 5.07 (broad peak, 2H, CH_2), 3.95 (s, 1H, CH), 2.86-1.21 (broad peaks, 4H, 2xCH_2), 1.24 (s, 2H, CH_2).

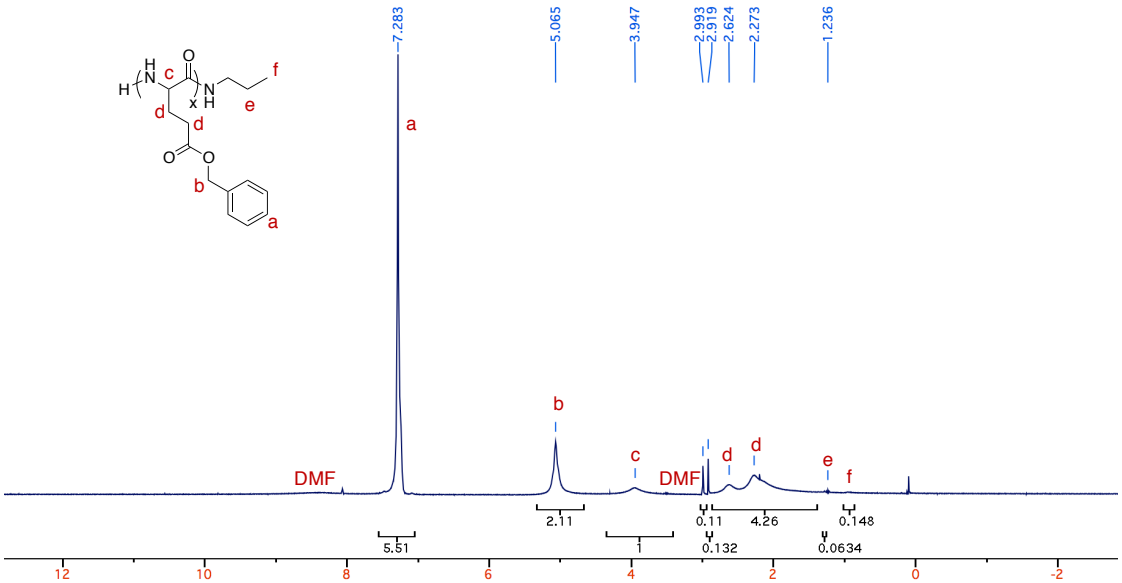

Figure 83. ^{1}H NMR spectrum of poly(γ-benzyl-L-glutamate) (PBLG) 3.

Synthesis of poly(γ-benzyl-L-glutamate) (PBLG) 4: NCA monomer (800 mg, 3.04 mmol) was added to a Schlenk flask and dissolved in anhydrous DMF (3 mL) under argon atmosphere. Then propyl amine (1.56 µL, 0.019 mmol) initiator was dissolved in anhydrous DMF (78 µL) and added to the Schlenk flask. The reaction mixture was stirred at room temperature for 48 hours. The reaction was stopped and the product was precipitated from diethyl ether to get the polymer as an off-white sticky product. GPC (DMF) *Mn*: 43.2 KDa; Đ: 1.23. ^{1}H NMR (400 MHz, $CDCl_3$) δ (ppm): 7.28 (broad peak, 5H, C_6H_5), 5.07 (broad peak, 2H, CH_2), 3.96 (s, 1H, CH), 2.99 (s, 1H, CH), 2.92 (s, 1H, CH), 2.81-1.50 (broad peaks, 4H, 2xCH_2), 1.28 (s, 2H, CH_2), 0.91 (S, 2H, CH_3).

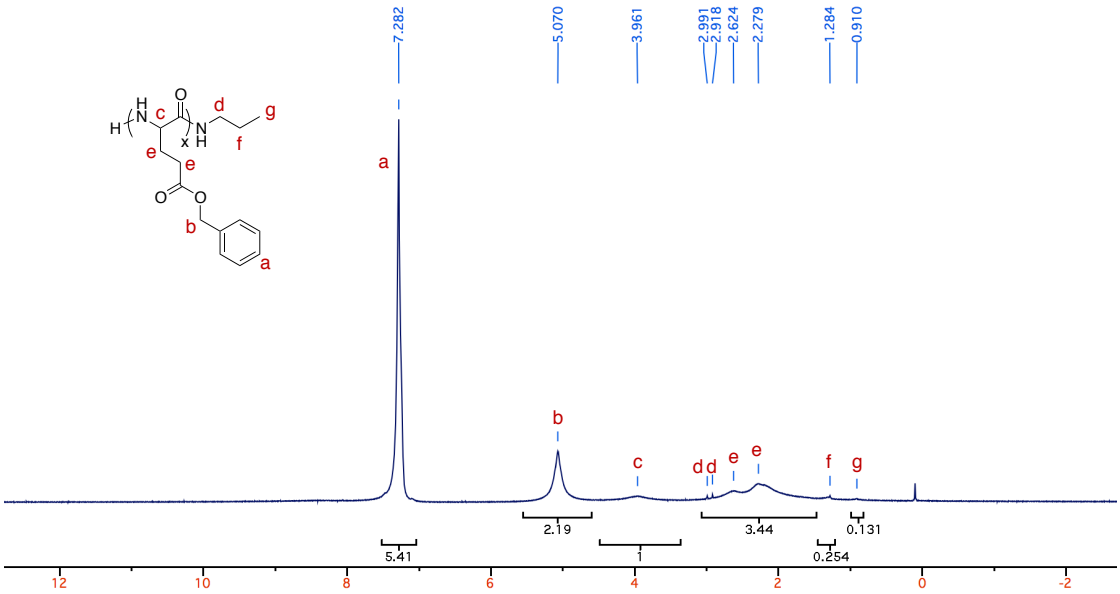

Figure 84. ^{1}H NMR spectrum of poly(γ-benzyl-L-glutamate) (PBLG) 4.

Synthesis of poly(L-glutamic acid) (PG) 1: Poly(L-glutamic acid) polymers were prepared following a previously published procedure.[32] PBLG 1 (551 mg, 2.51 mmol) was dissolved in 1,4-dioxane (5 mL) in 25 mL round bottom, then 1 M NaOH (151 mg, 3.78 mmol) in deionized water was added dropwise, with stirring. The reaction mixture was stirred at room temperature for 12 hours, then purified by dialysis against deionized water for 48 hours. The product was lyophilized to get the polymer as an off-white powder. ^{1}H NMR (400 MHz, D_2O) δ (ppm): 4.34 (broad peak, 1H, CH), 3.16 (s, 2H, CH_2), 2.45-1.81 (broad peaks, 4H, 2xCH_2), 1.51 (s, 2H, CH_2), 0.88 (S, 2H, CH_3). Benzyl deprotection was confirmed by the disappearance of benzyl peaks (7.28 and 5.07 ppm).

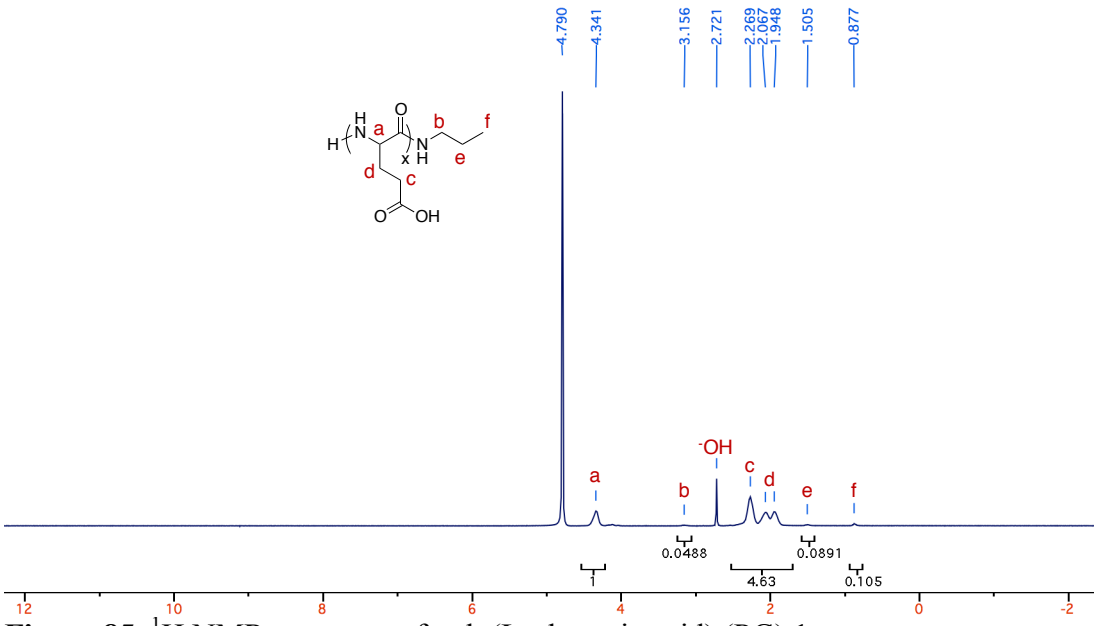

Figure 85. ^{1}H NMR spectrum of poly(L-glutamic acid) (PG) 1.

Synthesis of poly(L-glutamic acid) (PG) 2: PBLG 2 (510 mg, 2.32 mmol) was dissolved in 1,4-dioxane (5 mL) in 25 mL round bottom, then 1 M NaOH (140 mg, 3.45 mmol) in deionized water was added dropwise, with stirring. The reaction mixture was stirred at room temperature for 12 hours, then purified by dialysis against deionized water for 48 hours. The product was lyophilized to get the polymer as an off-white powder. ^{1}H NMR (400 MHz, D_2O) δ (ppm): 4.34 (broad peak, 1H, CH), 3.16 (s, 2H, CH_2), 2.27-2.16 (broad peaks, 2H, CH_2), 2.16-1.83 (broad peaks, 2H, CH_2), 1.50 (s, 2H, CH_2), 0.88 (S, 2H, CH_3). Benzyl deprotection was confirmed by the disappearance of benzyl peaks (7.28 and 5.07 ppm).

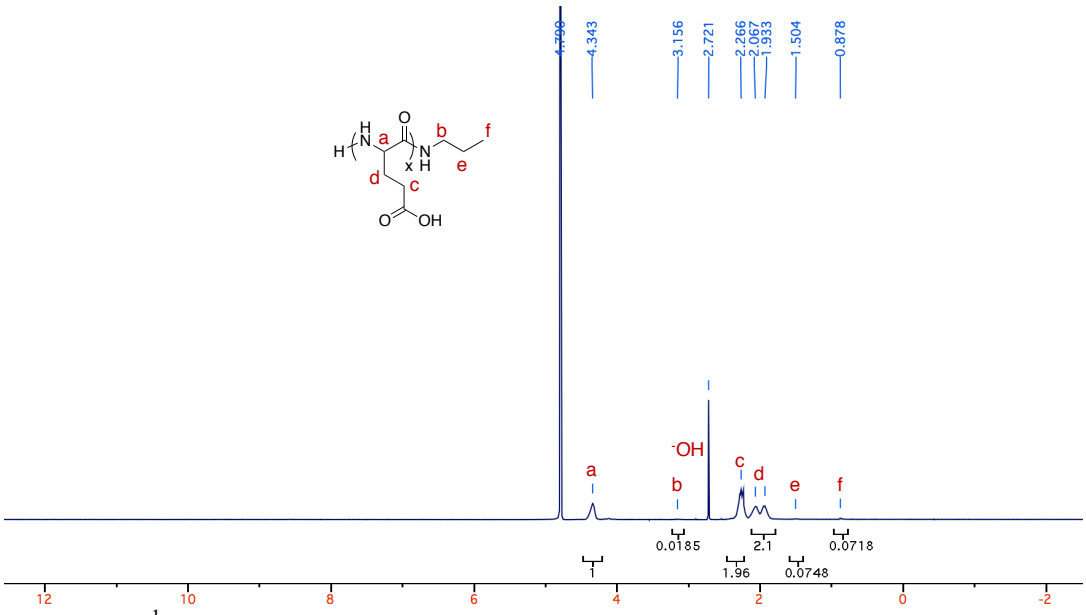

Figure 86. ^{1}H NMR spectrum of poly(L-glutamic acid) (PG) 2.

Synthesis of poly(L-glutamic acid) (PG) 3: PBLG 3 (510 mg, 2.32 mmol) was dissolved in 1,4-dioxane (5 mL) in 25 mL round bottom, then 1 M NaOH (140 mg, 3.45 mmol) in deionized water was added dropwise, with stirring. The reaction mixture was stirred at room temperature for 12 hours, then purified by dialysis against deionized water for 48 hours. The product was lyophilized to get the polymer as an off-white powder. ^{1}H NMR (400 MHz, D_2O) δ (ppm): 4.34 (broad peak, 1H, CH), 3.16 (s, 2H, CH_2), 2.40-2.17 (broad peaks, 2H, CH_2), 2.17-1.83 (broad peaks, 2H, CH_2), 1.49 (s, 2H, CH_2), 0.88 (S, 2H, CH_3). Benzyl deprotection was confirmed by the disappearance of benzyl peaks (7.28 and 5.07 ppm).

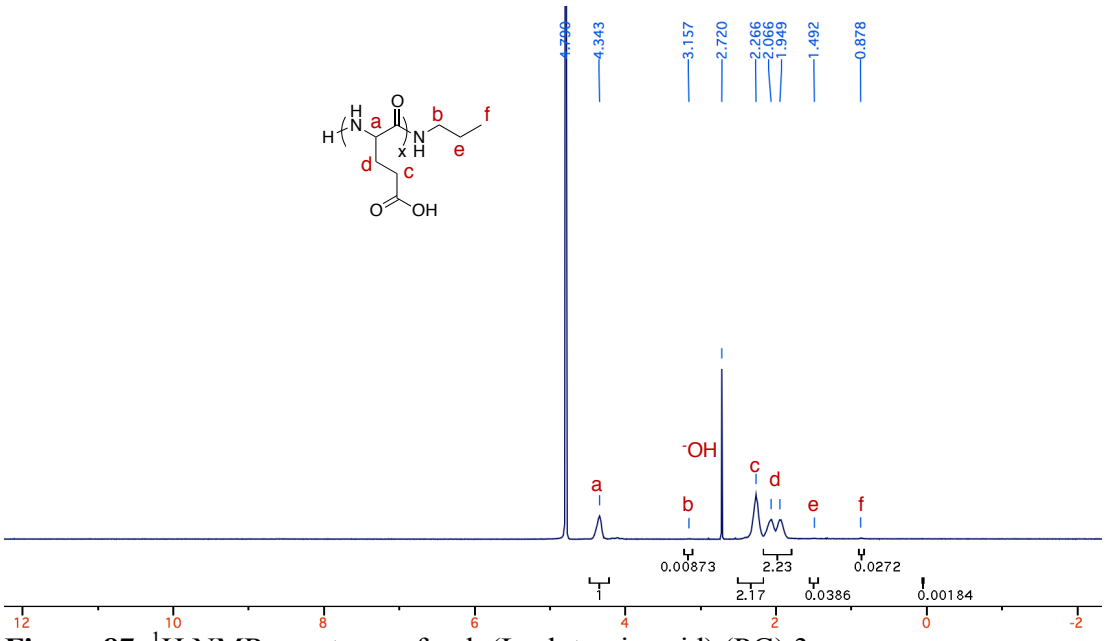

Figure 87. ^{1}H NMR spectrum of poly(L-glutamic acid) (PG) 3.

Synthesis of poly(L-glutamic acid) (PG) 4: PBLG 4 (446 mg, 2.04 mmol) was dissolved in 1,4-dioxane (5 mL) in 25 mL round bottom, then 1 M NaOH (122 mg, 3.05 mmol) in deionized water was added dropwise, with stirring. The reaction mixture was stirred at room temperature for 12 hours, then purified by dialysis against deionized water for 48 hours. The product was lyophilized to get the polymer as an off-white powder. ^{1}H NMR (400 MHz, D_2O) δ (ppm): 4.34 (broad peak, 1H, CH), 2.44-2.17 (broad peaks, 2H, CH_2), 2.17-1.81 (broad peaks, 2H, CH_2). Benzyl deprotection was confirmed by the disappearance of benzyl peaks (7.28 and 5.07 ppm).

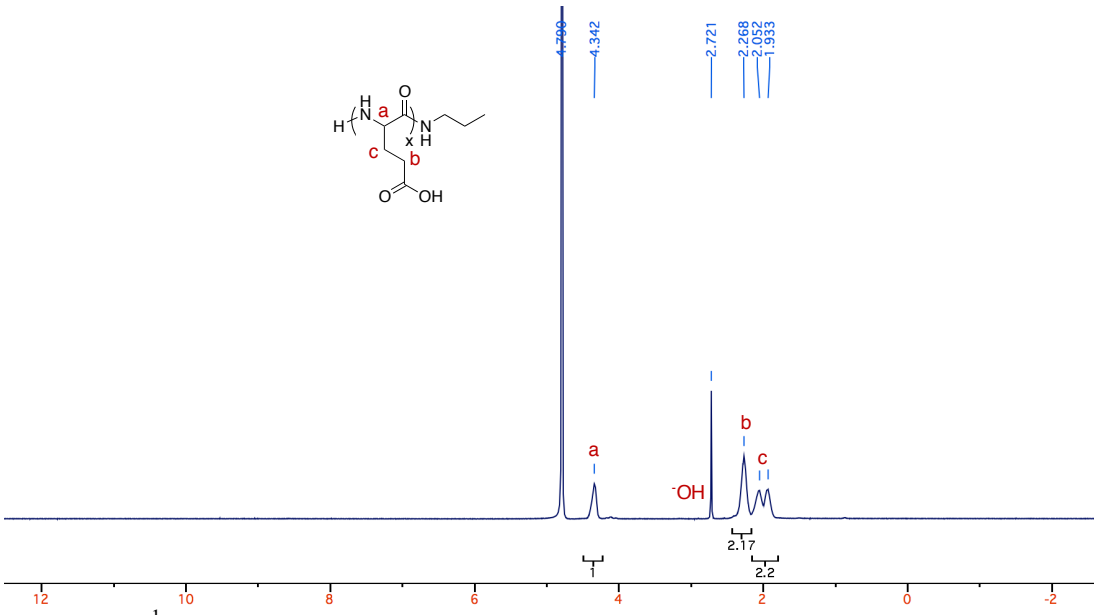

Figure 88. ^{1}H NMR spectrum of poly(L-glutamic acid) (PG) 4.

Synthesis of poly(L-glutamic acid)-*g*-(polyethylene glycol) (PG-*g*-PEG) 1: PG 1 (97.1 mg, 0.759 mmol) was dissolved in a 1:1 mixture of distilled water and DMF (3 mL), then EDC (43.6 mg, 0.227 mmol) and DMAP (27.8 mg, 0.227 mmol) were added and stirred for 20 minutes. Then poly(ethylene glycol) methyl ether amine, Mw 550, (125.2 mg, 0.227 mmol) was added and stirred for 12 hours. The mixture was then purified by dialysis against acetone then DCM for 48 hours, then dried by evaporation under reduced pressure to yield of poly(L-glutamic acid)-*g*-(polyethylene glycol) (PG-*g*-PEG) as a sticky solid. ^{1}H NMR (400 MHz, $CDCl_3$) δ (ppm): 3.64 (broad peak, 28H, 14×CH_2), 3.37 (s, 3H, CH_3), 3.22 (s, 2H, CH_2), 2.96-1.13 (broad peaks, 4H, 2×CH_2), 1.07 (s, 2H, CH_2), 0.87 (s, 3H, CH_3). The amount of PEG grafted was determined as 30% side chains by the relative integrations of methylene protons of PEG (3.36 ppm) compared to ethylene groups of total glutamic acid side chains (2.98-1.18 ppm).

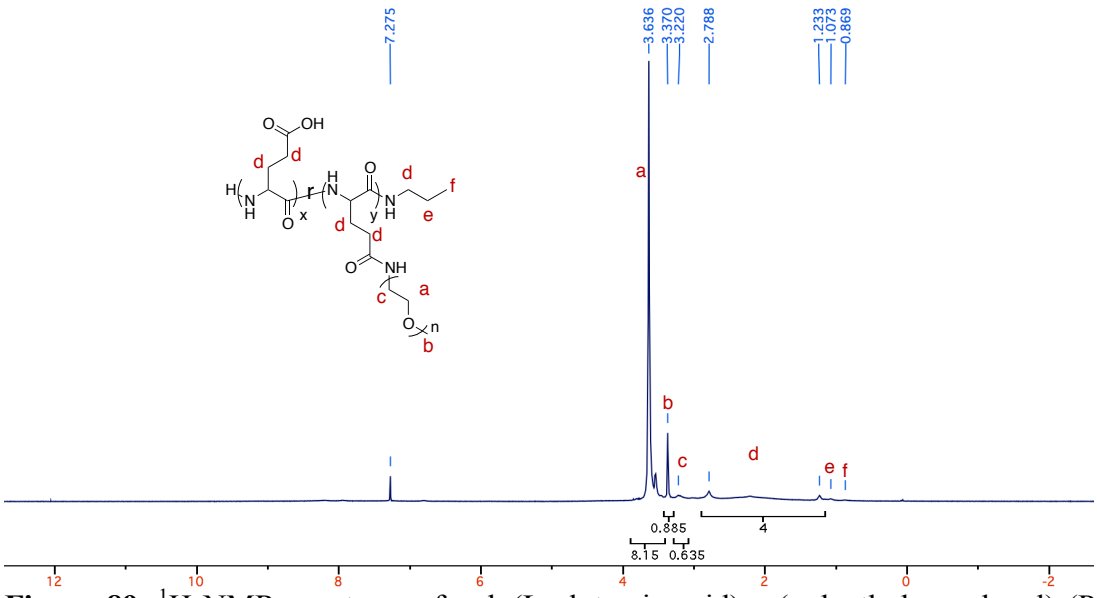

Figure 89. ^{1}H NMR spectrum of poly(L-glutamic acid)-*g*-(polyethylene glycol) (PG-*g*-PEG) 1.

Synthesis of poly(L-glutamic acid)-*g*-(polyethylene glycol) (PG-*g*-PEG) 2: PG 2 (149.1 mg, 1.164 mmol) was dissolved in a 1:1 mixture of distilled water and DMF (3 mL), then EDC (67.0 mg, 0.349 mmol) and DMAP (42.6 mg, 0.349 mmol) were added and stirred for 20 minutes. Then poly(ethylene glycol) methyl ether amine, Mw 550, (192.2 mg, 0.349 mmol) was added and stirred for 12 hours. The mixture was then purified by dialysis against acetone then DCM for 48 hours, then dried by evaporation under reduced pressure to yield of poly(L-glutamic acid)-*g*-(polyethylene glycol) (PG-*g*-PEG) as a sticky solid. ^{1}H NMR (400 MHz, $CDCl_3$) δ (ppm): 3.62 (broad peak, 26H, 13×CH_2), 3.36 (s, 3H, CH_3), 3.22 (s, 2H, CH_2), 2.98-1.18 (broad peaks, 4H, 2×CH_2), 1.07 (s, 2H, CH_2). The amount of PEG grafted was determined as 30% side chains by the relative integrations of methylene protons of PEG (3.36 ppm) compared to ethylene groups of total glutamic acid side chains (2.98-1.18 ppm).

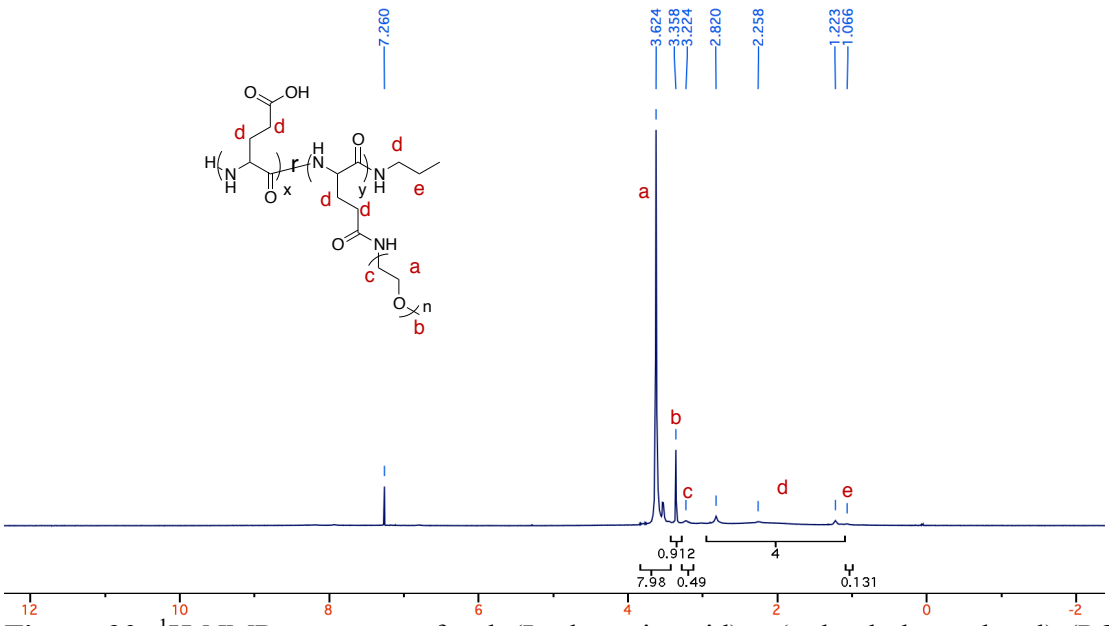

Figure 90. ^{1}H NMR spectrum of poly(L-glutamic acid)-*g*-(polyethylene glycol) (PG-*g*-PEG) 2.

Synthesis of poly(L-glutamic acid)-*g*-(polyethylene glycol) (PG-*g*-PEG) 3: PG 3 (124 mg, 0.969 mmol) was dissolved in a 1:1 mixture of distilled water and DMF (3 mL), then EDC (55.8 mg, 0.291 mmol) and DMAP (35.6 mg, 0.291 mmol) were added and stirred for 20 minutes. Then poly(ethylene glycol) methyl ether amine, Mw 550, (159.8 mg, 0.291 mmol) was added and stirred for 12 hours. The mixture was then purified by dialysis against acetone then DCM for 48 hours, then dried by evaporation under reduced pressure to yield of poly(L-glutamic acid)-*g*-(polyethylene glycol) (PG-*g*-PEG) as a sticky solid. ^{1}H NMR (400 MHz, $CDCl_3$) δ (ppm): 3.62 (broad peak, 28H, 14×CH_2), 3.36 (s, 3H, CH_3), 3.21 (s, 2H, CH_2), 2.90-1.13 (broad peaks, 4H, 2×CH_2), 1.06 (s, 2H, CH_2). The amount of PEG grafted was determined as 28% side chains by the relative integrations of methylene protons of PEG (3.36 ppm) compared to ethylene groups of total glutamic acid side chains (2.90-1.13 ppm).

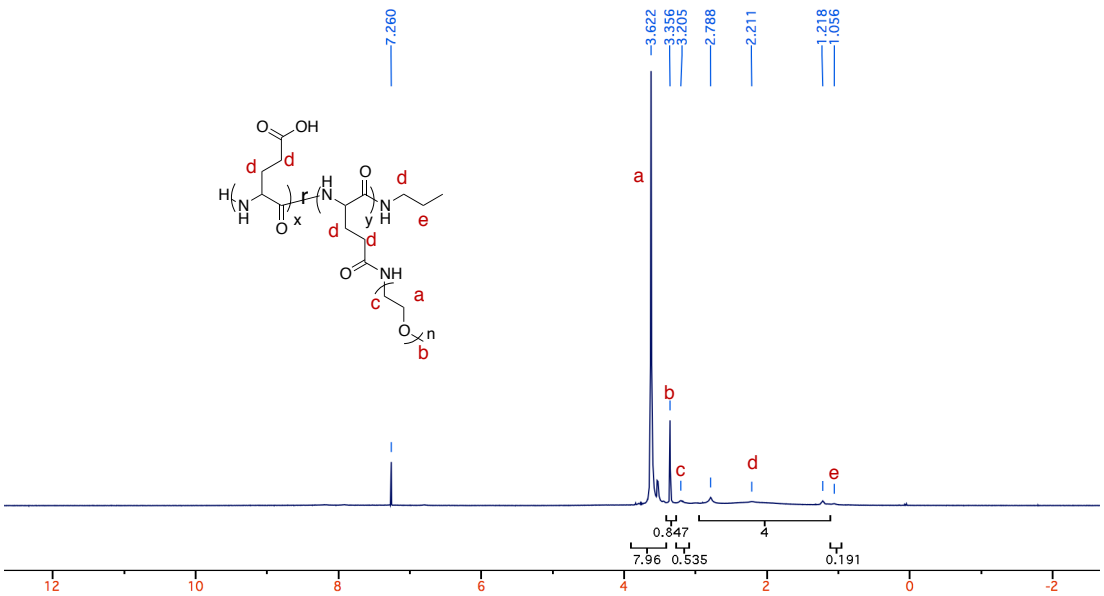

Figure 91. ^{1}H NMR spectrum of poly(L-glutamic acid)-*g*-(polyethylene glycol) (PG-*g*-PEG) 3.

Synthesis of poly(L-glutamic acid)-*g*-(polyethylene glycol) (PG-*g*-PEG) 4: PG 3 (195 mg, 1.522 mmol) was dissolved in a 1:1 mixture of distilled water and DMF (3 mL), then EDC (87.6 mg, 0.456 mmol) and DMAP (55.8 mg, 0.456 mmol) were added and stirred for 20 minutes. Then poly(ethylene glycol) methyl ether amine, Mw 550, (251.1 mg, 0.456 mmol) was added and stirred for 12 hours. The mixture was then purified by dialysis against acetone then DCM for 48 hours, then dried by evaporation under reduced pressure to yield of poly(L-glutamic acid)-*g*-(polyethylene glycol) (PG-*g*-PEG) as a sticky solid. ^{1}H NMR (400 MHz, $CDCl_3$) δ (ppm): 3.63 (broad peak, 28H, 14×CH_2), 3.37 (s, 3H, CH_3), 3.19 (s, 2H, CH_2), 2.99-1.08 (broad peaks, 4H, 2×CH_2), 1.04 (s, 2H, CH_2). The amount of PEG grafted was determined as 30% side chains by the relative integrations of methylene protons of PEG (3.36 ppm) compared to ethylene groups of total glutamic acid side chains (2.99-1.08 ppm).

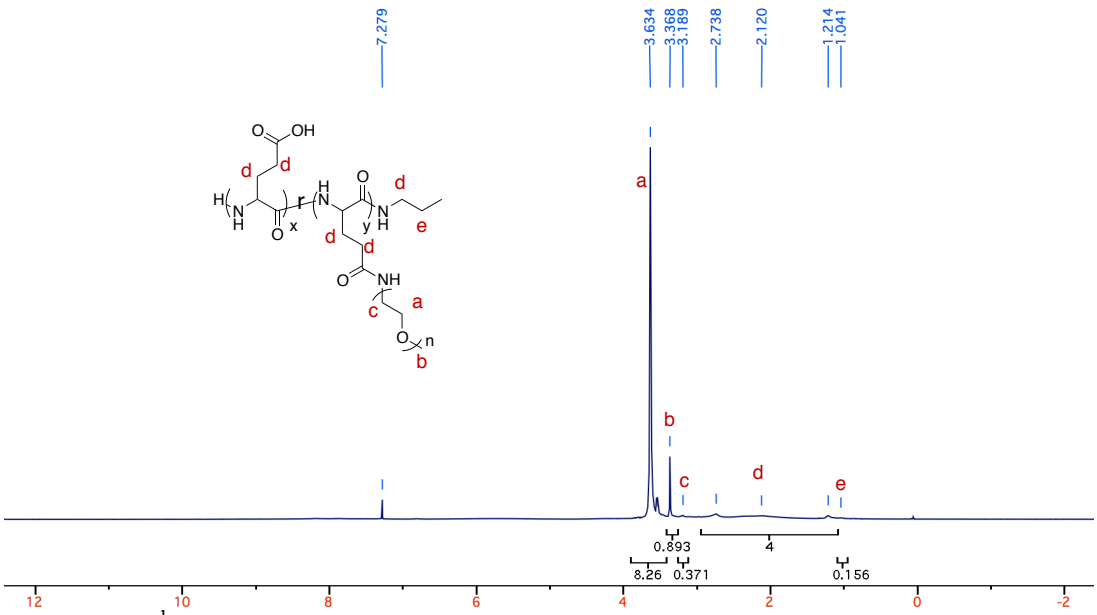

Figure 92. ^{1}H NMR spectrum of poly(L-glutamic acid)-*g*-(polyethylene glycol) (PG-*g*-PEG) 4.

Synthesis of poly(L-glutamic acid)-*g*-(polyethylene glycol)-*g*-2-(2-pyridyldithio)ethanol (PG-*g*-PEG-*g*-PDS) P1: PG-*g*-PEG 1 (43.3 mg, 0.388 mmol) was dissolved in a DCM (3 mL), then DCC (69.7 mg, 0.388 mmol) and DMAP (4.1 mg, 0.039 mmol) were added and stirred for 20 minutes. Then 2-(2-pyridyldithio)ethanol (PDS) (126.5 mg, 0.677 mmol) was added and stirred for 24 hours. The mixture was then purified by dialysis against DCM for 48 hours, then dried by evaporation under reduced pressure to yield of poly(L-glutamic acid)-*g*-(polyethylene glycol)-*g*-pyridyldisulfide (PG-*g*-PEG-*g*-PDS) as a sticky solid. GPC (DMF) *Mn*: 10.6 KDa; Đ: 1.32. ^{1}H NMR (400 MHz, $CDCl_3$) δ (ppm): 8.46, 7.71, 7.13, 4.28, 3.62, 3.36, 3.01, 2.76-1.18, 1.12, 0.86. The amount of PDS grafted was determined as 70% of side chains by the relative integrations of the aromatic protons of PDS (8.46 ppm) compared to methylene protons of PEG (3.36 ppm).

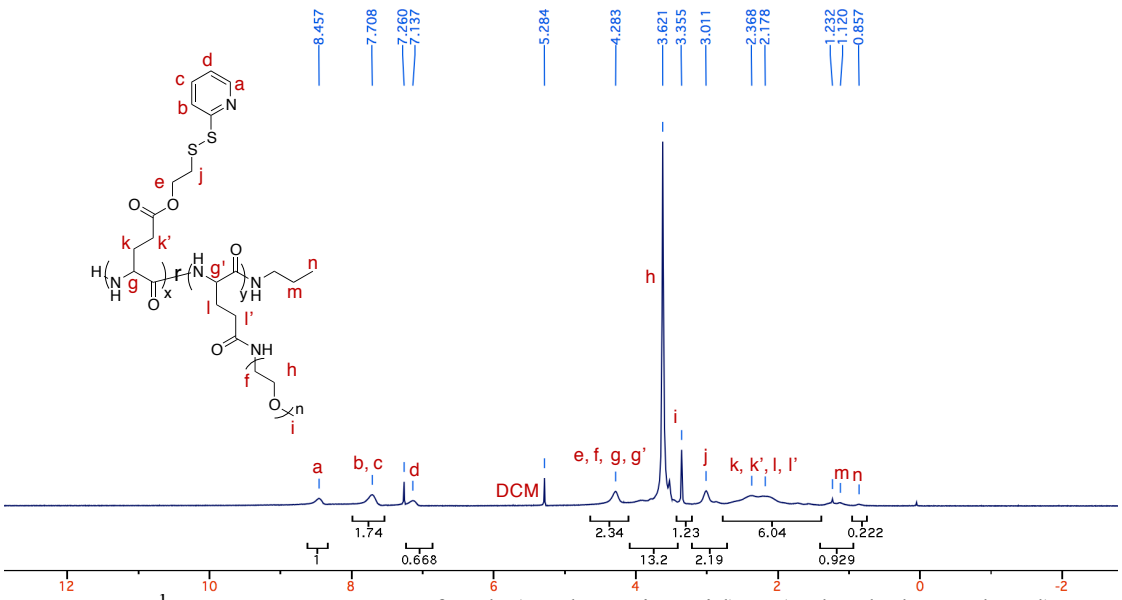

Figure 93. ^{1}H NMR spectrum of poly(L-glutamic acid)-*g*-(polyethylene glycol)-*g*-2-(2-pyridyldithio)ethanol (PG-*g*-PEG-*g*-PDS) 1.

Synthesis of poly(L-glutamic acid)-*g*-(polyethylene glycol)-*g*-2-(2-pyridyldithio)ethanol (PG-*g*-PEG-*g*-PDS) P2: PG-*g*-PEG 2 (42.3 mg, 0.33 mmol) was dissolved in a DCM (3 mL), then DCC (68.1 mg, 0.33 mmol) and DMAP (4.0 mg, 0.033 mmol) were added and stirred for 20 minutes. Then 2-(2-pyridyldithio)ethanol (PDS) (123.6 mg, 0.661 mmol) was added and stirred for 24 hours. The mixture was then purified by dialysis against DCM for 48 hours, then dried by evaporation under reduced pressure to yield of poly(L-glutamic acid)-*g*-(polyethylene glycol)-*g*-pyridyldisulfide (PG-*g*-PEG-*g*-PDS) as a sticky solid. GPC (DMF) *Mn*: 12.5 KDa; Đ: 1.44**.** ^{1}H NMR (400 MHz, $CDCl_3$) δ (ppm): 8.45, 7.69, 7.21, 4.28, 3.62, 3.36, 3.01, 2.75-1.22, 1.12, 0.86. The amount of PDS grafted was determined as 68% of side chains by the relative integrations of the aromatic protons of PDS (8.46 ppm) compared to methylene protons of PEG (3.36 ppm).

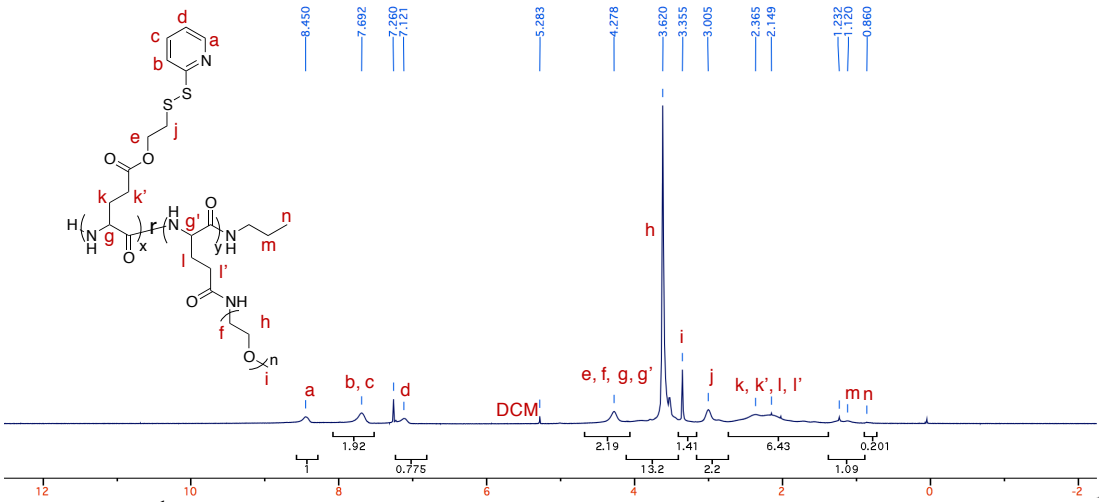

Figure 94. ^{1}H NMR spectrum of poly(L-glutamic acid)-*g*-(polyethylene glycol)-*g*-2-(2-pyridyldithio)ethanol (PG-*g*-PEG-*g*-PDS) 2.

Synthesis of poly(L-glutamic acid)-*g*-(polyethylene glycol)-*g*-2-(2-pyridyldithio)ethanol (PG-*g*-PEG-*g*-PDS) P3: PG-*g*-PEG 3 (46.1 mg, 0.36 mmol) was dissolved in a DCM (3 mL), then DCC (74.2 mg, 0.36 mmol) and DMAP (4.4 mg, 0.036 mmol) were added and stirred for 20 minutes. Then 2-(2-pyridyldithio)ethanol (PDS) (134.7 mg, 0.72 mmol) was added and stirred for 24 hours. The mixture was then purified by dialysis against DCM for 48 hours, then dried by evaporation under reduced pressure to yield of poly(L-glutamic acid)-*g*-(polyethylene glycol)-*g*-pyridyldisulfide (PG-*g*-PEG-*g*-PDS) as a sticky solid. GPC (DMF) *Mn*: 12.3 KDa; Đ: 1.53**.** ^{1}H NMR (400 MHz, $CDCl_3$) δ (ppm): 8.44, 7.69, 7.11, 4.28, 3.62, 3.35, 3.00, 2.75-1.19, 1.12, 0.86. The amount of PDS grafted was determined as 65% of side chains by the relative integrations of the aromatic protons of PDS (8.46 ppm) compared to methylene protons of PEG (3.36 ppm).

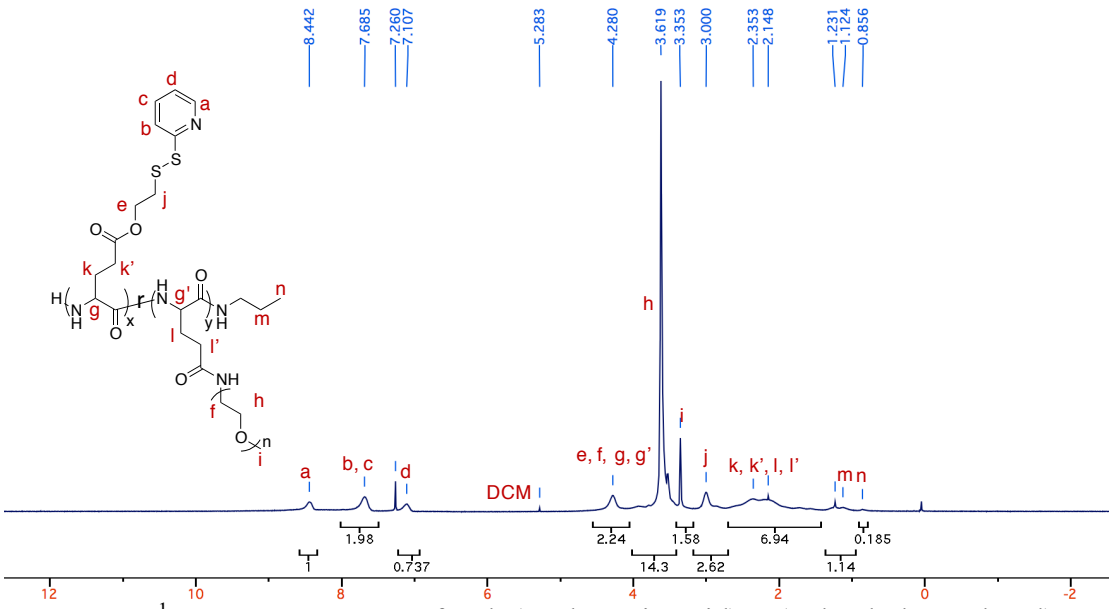

Figure 95. [1]H NMR spectrum of poly(L-glutamic acid)-*g*-(polyethylene glycol)-*g*-2-(2-pyridyldithio)ethanol (PG-*g*-PEG-*g*-PDS) P3.

Synthesis of poly(L-glutamic acid)-*g*-(polyethylene glycol)-*g*-2-(2-pyridyldithio)ethanol (PG-*g*-PEG-*g*-PDS) P4: PG-*g*-PEG 3 (62.5 mg, 0.49 mmol) was dissolved in a DCM (3 mL), then DCC (100.6 mg, 0.49 mmol) and DMAP (6.0 mg, 0.049 mmol) were added and stirred for 20 minutes. Then 2-(2-pyridyldithio)ethanol (PDS) (182.6 mg, 0.98 mmol) was added and stirred for 24 hours. The mixture was then purified by dialysis against DCM for 48 hours, then dried by evaporation under reduced pressure to yield of poly(L-glutamic acid)-*g*-(polyethylene glycol)-*g*-pyridyldisulfide (PG-*g*-PEG-*g*-PDS) as a sticky solid. GPC (DMF) *Mn*: 12.8KDa; Đ: 1.46. [1]H NMR (400 MHz, $CDCl_3$) δ (ppm): [1]H NMR (400 MHz, $CDCl_3$) δ (ppm): 8.46, 7.70, 7.12, 4.29, 3.62, 3.36, 3.01, 2.79-1.20, 1.14, 0.86. The amount of PDS grafted was determined as 70% of side chains by the relative integrations of the aromatic protons of PDS (8.46 ppm) compared to methylene protons of PEG (3.36 ppm).

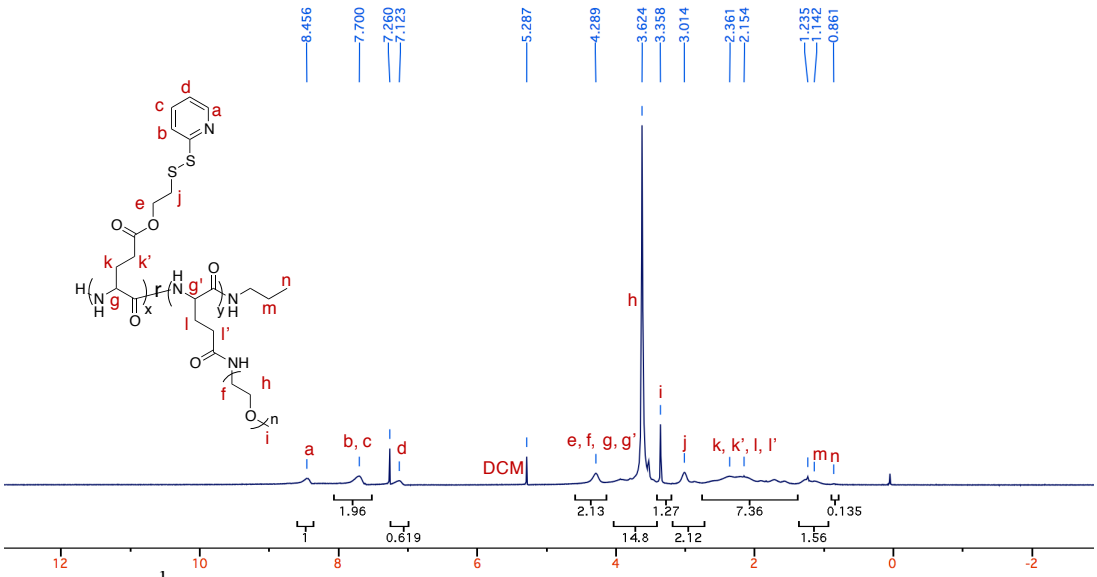

Figure 96. ^{1}H NMR spectrum of poly(L-glutamic acid)-*g*-(polyethylene glycol)-*g*-2-(2-pyridyldithio)ethanol (PG-*g*-PEG-*g*-PDS) P4.

MALDI Characterization: Matrix solutions were prepared dissolving α-cyano-4-hydroxycinnamic acid (CHCA) (10 mg/mL) in a solution of THF. The matrix solution was then mixed with PBLG polymer for analysis. Acquisition of all mass spectra was obtained on a Bruker Omniflex time-of-flight mass spectrometer.

Nanogel Formulation and Characterization: Deionized water was added to the polymer (2.5 mg/mL) and made into a particle suspension using cycles of sonication and chilling until the polymer appeared dissolved. Particles at 25 °C were crosslinked using a calculated amount of DTT for 1 hour as reducing agent as previously reported.[28, 29] Controlled crosslinking was achieved by addition 5, 12.5, 25 and 50% DTT respective to mol PDS, calculated to be 14, 38, 45, and 100% crosslinked, respectively, by the amount of byproduct, 2-pyridinethione, using its molar extinction coefficient (8.08 x 10^3 M^{-1} cm^{-1} at 343 nm)[33] using UV-Vis spectroscopy. Dynamic light scattering (DLS) experiments to obtain aggregate and particle size were performed by using a digital correlator and

goniometer with a light source operating at 514 nm using a Malvern Nano Zetasizer-ZS. Dust was removed by filtering the solution through 0.45 μm polycarbonate filter. Aggregate temperature responsivity was evaluated from 25-60 °C at a correlation time of 30 seconds. For each sample, 3 readings were recorded averaging 10 runs for the same sample. Final nanogel size measurements were obtained at 25 °C at a correlation time of 30 seconds.

DiI Encapsulation: Model guest 1,1'-dioctadecyl-3,3,3',3'-tetramethyl indocarbocyanine perchlorate (DiI) was dissolved in acetone (10 μL) then added to a solution of 1 mg/mL aggregate of polymers PG-g-PEG-g-PDS (P2) and stirred was for 8 hours at room temperature, open to the atmosphere to allow for acetone to evaporate. Aggregate solution was separated into three solutions and two were crosslinked using DTT and quantified by byproduct, 2-pyridinethione at 343 nm to be 30 and 70% crosslinked. Nanogels were purified by dialysis using 100 KDa MWCO membrane and any non-encapsulated DiI was removed by filtration through a 0.45 μm filter.

Transmission Electron Microscope (TEM) Study: The polymer and nanogel solutions (2.5 mg/mL) characterized by DLS were analyzed by TEM measurements. The sample was drop casted (1 drop) on carbon coated Cu grid, then air dried for 12 hours.

Synthesis of thiol-modified FITC: Fluorescein isothiocyanate (FITC) (61 mg, 0.158 mmol), cystamine dihydrochloride (19 mg, 0.079 mmol) and triethylamine (110 μL, 0.788 mmol) were dissolved in DMSO (1.2 mL) and stirred for 4 hours. Then tris(2-

carboxyethyl)phosphine hydrochloride (54 mg, 0.188 mmol) was added and stirred for 1 hour. The mixture was precipitated in diethyl ether and then washed with water. The resultant crude fluorescein-cysteamine was used for nanogel labeling without further purification, as previously reported.[29]

Fluorescein Nanogel Labeling: To nanogel solutions (2.5 mg/mL, 0.5 mL) fluorescein-cysteamine (0.625 mg, 1.34 μmol) in DMF (62.5 μL) was added and stirred for 8 hours until. The nanogel was purified by dialysis against DI water in a 100 KDa MWCO cellulose dialysis membrane for 24 hours to remove any unconjugated fluorescein-cysteamine.

Cell Culture: Human cervical carcinoma (HeLa) and human embryonic kidney (293T) cell lines were grown in DMEM supplemented with 10% (FBS), 1% L-glutamine, and 1% antibiotic-antimycotic (comprised of 100 units/mL penicillin and 100 μg/mL streptomycin). All cells were grown at 5% CO_2 and 37 °C. Digestion of cells for culture was done according to HeLa and 293T protocols from ATCC.

Cytotoxicity Assay: Nanogel *in vitro* cytotoxicity was determined using the Alamar blue assay for HeLa and 293T cell lines. In a 96 well flat-bottomed plate 10,000 cells per well (16,000-32,000 cells/cm^2) in culture medium were seeded and incubated for 12 hours at 5% CO_2 and 37 °C. Nanogel samples in PBS buffer 7.4 were diluted with culture medium for final nanogel concentrations ranging from 0-1 mg/mL with 50% PBS total, in triplicate. The plate's culture medium was replaced with sample culture medium and incubated for 24 hours. The cells were then incubated with a 10% Alamar blue in media for 4 hours.

Fluorescence was obtained using a Molecular Devices Spectramax M5 plate reader (excitation 560 nm, emission 590 nm) in a black 96-well flat bottom plate. Average fluorescence values and deviation were obtained from replicates (n=3) and were compared to 100% viability of the positive control (0 mg/mL nanogel).

Confocal Microscopy Intracellular Uptake: HeLa (500K) and 293T cells (100k) were seeded in a single chamber 35 mm glass bottom dishes and incubated overnight at 37 °C overnight in 5% CO_2 before performing uptake. Culture media was removed and new culture media containing fluorescein-labeled nanogels diluted to 0.25 mg/mL in DMEM. Samples were incubated for 4 hours. The cell nuclei were stained with the addition of DRAQ5 (5 μM) Media was removed from cells and washed 2-4 times with PBS, then live cell imaging buffer was added for confocal imaging. Assessment of fluorescein-conjugated nanogel intracellular uptake was recorded using 488 nm laser and nuclear stain was detecting using a 543 nm wavelength laser. Confocal microscopy was performed on a Zeiss510 META confocal laser scanning microscope and images were obtained using a 63× oil-immersion objective.

5.5 References

1. Kreuter, J. Nanoparticles. J. Kreuter (Ed.), Colloidal Drug Delivery Systems, Marcel Dekker, New York, **1994**.

2. Katti, D. S.; Lakshmi, S.; Langer, R.; Laurencin, C. T. Toxicity, biodegradation and elimination of polyanhydrides. *Adv. Drug Deliv. Rev*. **2002**, *54*, 933–961.

3. Nair, L. S.; Laurencin, C. T. Biodegradable polymers as biomaterials. *Prog. Polym. Sci.* **2007**, *32*, 762-789.

4. Vert, M. Aliphatic polyesters: great degradable polymers that cannot do everything. *Biomacromolecules* **2005**, *6*, 538–546.

5. Lloyd, A. W. Interfacial bioengineering to enhance surface biocompatibility. *Med. Device Technol*. **2002**, *13*, 18–21.

6. Li, S. Hydrolytic degradation characteristics of aliphatic polyesters derived from lactic and glycolic acids. *J. Biomed. Mater. Res*. **1999**, *48*, 342–353.

7. Chiu, H.-C.; Kopeckova, P.; Deshmane, S.S.; Kopecek, J. Lysosomal degradability of poly(alpha-amino acids). *J. Biomed. Mater. Res*., **1997**, *34*, 381–392.

8. McCormick-Thomson, L.A.; Duncan, R. Poly(amino acid) copolymers as a potential soluble drug delivery system. 1. Pinocytotic uptake and lysosomal degradation measured in vitro. *J. Bioact. Compat. Polym*., **1989**, *4*, 242–251.

9. Kishore, B.K.; Lambricht, P.; Laurent, G.; Maldague, P.; Wagner, R.; Tulkens, P.M. Mechanism of protection afforded by polyaspartic acid against gentamicin-induced phos- pholipidosis. II. Comparative in vitro and in vivo studies with poly-L-aspartic, poly-L-glutamic and poly-D-glutamic acids. *J. Pharmacol. Exp. Ther*., **1990**, *255*, 875–885.

10. Akamatsu, K.; Yamasaki, Y.; Nishikawa, M.; Takakura, Y.; Hashida, M. Development of a hepatocyte-specific prostaglandin E1 polymeric prodrug and its potential for preventing carbon tetrachloride-induced fulminant hepatitis in mice. *J. Phar- macol. Exp. Ther*., **1999**, *290*, 1242–1249.

11. Bayley, D.; Sancho, M.-R.; Brown, J.; Brookman, L.; Petrak, K.; Goodard, P.; Steward, A. Soluble polymeric carriers for drug delivery. Part 6. Preparation and biodistribution of N^5 -hy- droxyethyl-L-glutamine-co-L-glutamic acid copolymers in rats. J. *Bioact. Compat. Polym*., **1993**, *8*, 51–68.

12. Kenny, A. D. Evaluation of sodium poly(a-L-glutamic acid) as a plasma expander. *Proc. Soc. Exp. Biol. Med.,* **1959**, *100*, 778 – 780.

13. Dobrovolskaia, M. A.; McNeil, S. E. Immunological properties of engineered nanomaterials. *Nature Nanotechnology*, **2007**, *2*, 469-478.

14. Pytela, J.; Kotva, R.; Metalova, M.; Rypacek, F. Degradation of N^5 -(2-hydroxylethyl)-L-glutamine and L-glutamic acid homopolymers and copolymers by papain. *Int. J. Biol. Macromol*., **1990**, *12*, 241–246.

15. Molineux, G. PEGylation: engineering improved pharmaceuticals for enhanced therapy. *Cancer Treat Rev*. **2002**, *28 (Suppl. A)*, 13−16.

16. Moribe, K.; Maruyama, K. Reviews on PEG coated liposomal drug carriers. *Drug Delivery Syst*. **2001**, *16 (3)*, 165−171.

17. Ryu, J.-H.; Jiwpanich, S.; Chacko, R. T.; Bickerton, S.; Thayumanavan, S. Surface-Functionalizable Polymer Nanogels with Facile Hydrophobic Guest Encapsulation Capabilities. *J. Am. Chem. Soc.* **2010**, *132*, 24, 8246-8247.

18. Ryu, J.-H.; Chacko, R. T.; Jiwpanich, S.; Bickerton, S.; Babu, R. P.; Thayumanavan, S. Self-Cross-Linked Polymer Nanogels: A Versatile Nanoscopic Drug Delivery Platform. *J. Am. Chem. Soc*. **2010**, *132*, 17227-17235.

19. Idelson, M.; Blout, E. R. High molecular weight poly(a-L- glutamic acid): preparation and physical rotation changes. *J. Am. Chem. Soc*., **1958**, *80*, 4631–4634.

20. Block, H. Poly(g-benzyl-L-glutamate) and Other Glutamic Acid Containing Polymers, Gordon and Breach, New York, **1983**.

21. Deming, T. Facile synthesis of block copolypeptides of defined architecture. *Nature*, **1997**, *390*, 386–389.

22. Blout, E. R.; Karlson, R. H. Polypeptides. III. The Synthesis of High Molecular Weight Poly-γ-benzyl-L-glutamates. *J. Am. Chem. Soc*. **1956**, *78*, 941– 946.

23. Papadopoulos, P.; Floudas, G.; Klok, H. A.; Schnell, I.; Pakula, T. Self-Assembly and Dynamics of Poly(γ-benzyl-l-glutamate) Peptides. *Biomacromolecules* **2004**, *5*, 81–91.

24. Mitchell, J. C.; Woodward, A. E.; Doty, P. Polypeptides. XVI. The Polydispersity and Configuration of Low Molecular Weight Poly-γ-benzyl-L-glutamates. *J. Am. Chem. Soc.* **1957**, *79*, 3955–3960.

25. Higashi, N.; Kawahara, J.; Niwa, M. Preparation of helical peptide monolayer-coated gold nanoparticles. *J. Colloid Interface Sci.* 2005, *288*, 83.

26. Higashi,N.; Koga, T.; Niwa, M. Helical Superstructures from a Poly(*γ*-benzyl-L-glutamate)-Poly(L-glutamic acid) Amphiphilic Diblock Copolymer: Monolayer Formation on Water and Its Specific Binding of Amino Acids. *Langmuir* 2000, *16,* 3482-3486.

27. Zhu, G.-G.; Wang, F.-G.; Liu, Y.-Y. Effects of Reaction Conditions on the Grafting Percentage of Poly(ethylene glycol)-block-poly(γ-benzyl L-glutamate)-graft-poly(ethylene glycol) Copolymer. *J. Braz. Chem. Soc*. **2010**, *21*, 715-720.

28. Ryu, J. -H.; Chacko, R. T.; Jiwpanich, S.; Bickerton, S.; Babu R. P.; Thayumanavan, S. Self-cross-linked polymer nanogels: a versatile nanoscopic drug delivery platform. *J. Am. Chem. Soc*. **2010**, *132*, 17227–17235.

29. Ryu, J. -H.; Jiwpanich, S.; Chacko, R.; Bickerton S.; Thayumanavan, S. Surface functionalizable polymer nanogels with facile hydrophobic guest encapsulation capabilities. J. *Am. Chem. Soc*. **2010**, *132*, 8246–8247.

30. Yang, Z.; Zhang, Y.; Markland, P.; Yang, V. C. Poly(glutamic acid) poly(ethylene glycol) hydrogels prepared by photoinduced polymerization: Synthesis, characterization, and preliminary release studies of protein drugs. *J Biomed Mater Res*. **2002**, *62*, 14-21.

31. Molla, R. M.; Prasad, P.; Thayumanavan, S. Protein-Induced Supramolecular Disassembly of Amphiphilic Polypeptide Nanoassemblies. *J. Am. Chem. Soc*. **2015**, *137*, 7286−7289.

32. Lee, S. J.; Min, K. H.; Lee, H. J.; Koo, A. N.; Rim, H. P.; Jeon, B.J.; Jeong, S. Y.; Heo, J. S.; Lee, S. C.; Ketal cross-linked poly(ethylene glycol)-poly(amino acid)s copolymer micelles for efficient intracellular delivery of 43 doxorubicin. *Biomacromolecules*, **2011**, *12*, 1224-1233.

33. Kavimandan, N. J.; Losi, E.; Wilson, J. J.; Brodbelt, J. S.; Peppas, N. A.; Synthesis and Characterization of Insulin-Transferrin Conjugates. *Bioconjugate Chem*. **2006**, *17*, 1376-1384.

CHAPTER 6

SUMMARY AND FUTURE DIRECTIONS

6.1 Summary of the Dissertation

Nano-scaled materials have gained immense interest in therapeutic delivery, diagnostics, and sensing applications, among many others. In drug delivery, nanoparticles of various compositions have been pursued, broadly including metals, inorganic materials, polymers, lipids, dendrimers and biologics. Advances in polymerization synthetic techniques has led to the development of diverse block and random copolymers with sophisticated chemical and structural properties. The synthetic feasibility and modification chemistries of amphiphilic random copolymers, as well as their spontaneous self-assembly in aqueous systems, have progressed their candidacy for biological applications. In this dissertation, we investigated structural and stimuli-responsive features of such self-assembling amphiphilic random copolymers towards the development of these nanomaterials for water insoluble therapeutics.

In chapter 1, we examined the requirements of nanoparticles as carriers for water-insoluble guests, and discussed the merits of amphiphilic random copolymers as hosts. In chapter 2, we studied the *in vivo* performance of core-disulfide crosslinked nanogels in tumor bearing mice using triple negative human mammary carcinomas models. Tumor accumulation of the NIR-labeled nanogels were evaluated using *in vivo* FMT imaging over 72 hours following a single nanogel injection. Nanogel sizes and PEG content were optimized to achieve greater retention of total body probe, highest percent injected dose of the nanogel in the tumor, and to evaluate relative accumulations in other tissues. In chapter 3, we further evaluated the safety and efficacy of these nanogels in triple negative human mammary carcinomas using docetaxel as chemotherapeutic guest. Tumor-bearing mice

were treated with regimens of docetaxel-loaded nanogels, and any tumor inhibition or adverse effects were monitored and compared to regimens of free docetaxel. Some minor anti-tumor activity was observed in model BR1282, and anti-tumor activity was achieved for model BR1458, however did not exceed the efficacy of free docetaxel. However, while adverse effects on body weight were observed with free docetaxel, no adverse effects on body weight were observed in docetaxel-loaded nanogel samples.

In chapter 4, we developed a methodology for enhancing the cell uptake of PEGylated nanogels in the presence of tumor-relevant enzyme MMP-9. We reported a nanogel capable of converting its surface properties from a passive PEGylated particle to an active amine decorated particle in the presence of MMP-9. Surface conversion was confirmed using MALDI mass spectrometry characterization of products, zeta potential measurements of surface charge, and fluorescamine assay to establish amine content. The enhanced uptake of protease-treated nanogel was supported by confocal microscopy by both a covalently conjugated fluorophore nanogel tag and non-covalently encapsulated hydrophobic model guest.

We then introduced an alternative amphiphilic random copolymer design based on poly(L-glutamic acid) in chapter 5. The poly(L-glutamic acid) derivatives with grafted PEG and PDS moieties on carboxylate side chains were synthesized, and the resultant amphiphilic polymer were capable of supramolecular self-assembly into nanoscale aggregates. These polypeptide aggregates could be chemical crosslinked under reducing conditions, similar to its poly(methyl methacrylate) counterpart. The nanocarrier host properties were established by encapsulation of model hydrophobic guest, and low

cytotoxicity and cellular internalization were demonstrated on both HeLa and 293T cell lines.

6.2 Future Directions

Further understanding of the *in vivo* biodistribution of these nanogels could benefit from studying any dose-dependent effects of empty of nanogels and overall pharmacokinetic performance. In chapter 2, the smallest nanogels tested (~30-40 nm) achieved the highest tumor accumulation, so it may be worth examining nanogels from 10-30 nm. Smaller particles may be able to achieve deeper tumor penetration, however may suffer from poor tumor retention. Further, smaller particles can have greater susceptibility to renal filtration through the kidneys. Conjugation of targeting ligands may also achieve enhancement in tumor retention and uptake.

For these random copolymer systems, determining spatial density of PEG chains on their surface by particle counting and theoretical methods would improve the understanding of these nanogels. With these random copolymer-based nanogels we have shown fine control in the aggregation sizes with various solution manipulation techniques, including polymer molecular weight, concentration, temperature, and salt. However, thus far we do not have a firm grasp on the number of particles generated in solution under these various conditions. From a fundamental perspective, we may better understand this nanogel system using particle counting methods, and understand how solution manipulations impact the number of polymer chains per particle, and thus the polymer chain density or these particles in relation to size. With this understanding, we can further ascertain the surface coverage from post-modifications such as PEGylation. Likewise, this information

would lend well in active targeting strategies, such that we could quantifiably and reliably predict the number, and spatial arrangement, of targeting ligands on the particle surfaces.

Further *in vitro* investigations of these materials could improve the understanding of *in vivo* performance and overall biological fate. First, evaluating the generation of protein coronas on these particles in serum, with relation to size, PEG weight percent decoration, and PEG length decoration would identify the parameters that would most greatly avoid opsonization and phagocytosis. Second, it is important to evaluate whether these parameters reduce the ability for immune cells in the reticuloendothelial system to clear these nanoparticles, including Kupffer cells in the liver, dendritic cells in the lymph nodes, and B cells in the spleen. We observed considerable localization for the nanogels in the liver, but we do not know whether that is an artifact of the fenestrated liver endothelium, or due to a high extent of Kupffer cell uptake and clearance.

In chapter 3 the efficacy of docetaxel-loaded nanogels may have suffered from their low encapsulation efficiencies. Because these random copolymer nanogels are also being explored for delivery of proteins, it would be interesting to test the parameters determined in chapter 2 with a hydrophilic protein therapeutic cargo, rather than hydrophobic chemotherapeutic cargo. The hydrophilic-lipophilic-balance of these heavily PEGylated nanogels may be better candidates for protein cargo, which should be well protected within the particle interior and not leak. Alternative structural designs or formulation techniques will have to be realized to maintain core hydrophobicity and high surface PEG composition for hydrophobic delivery goals.

In further investigation of tumor-relevant stimuli responsive systems, like those discussed in chapter 4, pursing alternative substrates with responsivity to other upregulated

MMPs would elucidate the versatility of this enhanced uptake strategy. For practical translation of these site-specific activation strategies, it would be beneficial to determine the time scales of *in vivo* extracellular retention and cellular internalization. We expect based on biodistribution studies that nanogels remain in the tumor region on the time scale of hours to days. However, we do not know what proportion of these nanogels are in the extracellular milieu compared to internalized in tumor cells at any given time. Cell internalization of these PEGylated passive nanogels is slow, so it would be fundamentally interesting to evaluate the equilibrium shift of intracellular vs. extracellular particles following activation. For enhanced tumor cell uptake, the nanogel "activation" process would need to be faster than the particle "internalization" process *in situ*. This process could be evaluated *in vitro* using cancer cells in an extracellular matrix mimic hydrogel. The enhanced internalization over time can be monitored and compared between non-activated and activating conditions. One possible design of such an experiment is the co-encapsulation of a FRET donor and acceptor pair inside the nanogel interior. Due to the proximity of the dyes, we'd expect non-internalized particles to primarily exhibit emission of the acceptor fluorescence from excitation of the donor. However, upon cell internalization and GSH guest release, recover of donor fluorescence should be observed as the distance increases between the dyes. In this way, the relative extracellular acceptor fluorescence and intracellular donor fluorescence could be monitored over time. Additionally, using hydrogels as extracellular matrix mimics would allow the investigation of these systems under flow. This surface-conversional strategy is non-reversible, so a concern for these activation designs in the rate at which particles are internalized following

activation, compared to reentry into circulation as “active” particles as a competing process.

Further, the compatibility of this MMP-9 responsive carrier design with protein cargo would give us more understanding of the guest protection and proteolytic susceptibility in polymeric nanogels for the application of protein delivery. Release studies of showed the unexpected result that MMP-9 caused some release of encapsulated guest, which was unique to active MMP-9 and not caused by inactive Pro-MMP-9. It is possible that MMP-9 is exhibiting some esterase behavior and cleaving some of the ester bonds on the poly(methacrylate) backbone of the polymeric nanogel. If this is the case, it would be easily avoided by using a poly(acrylamide)-based polymer. Nevertheless, evaluating the susceptibility of nanogels to MMP-9 and other upregulated proteases is vital for the development of cancer-relevant protein delivery. As proof of concept, trypsin digestion has been used to establish both the protection and release of proteins in nanoscopic systems. Similar evaluation using proteases the nanogels may be exposed to under various cancer-relevant environments would validate their biological stability.

In chapter 5, we established preliminary proof-of-concept validation that grafted poly(peptide)-based amphiphilic random copolymers, with known secondary structure characteristics, would be capable of supramolecular self-assembly and nanocarrier properties. In future work, determining the degradation profiles in response to cathepsin B and other proteases would be important in determining relative serum stability and lysosomal degradation of the nanogel. This lysosomal degradation could also have implications in delivery strategies for lysosomal-relevant therapeutic cargo. Lastly, it

would be fundamentally interesting to determine the secondary structure characteristics of such self-assembling polypeptide derivatives.

BIBLIOGRAPHY

1. Acharya, S.; Sahoo, S. K. PLGA nanoparticles containing various anticancer agents and tumour delivery by EPR effect. *Adv. Drug Deliv. Rev*. **2011**, *63*, 170–183.

2. Adidou, O.; Goux-Henry, C.; Safi, M.; Soufiaoui, M.; Framery, E. PEG_{350}-based di-(2-pyridyl)methylamine as a ligand in the Pd-catalyzed water Suzuki–Miyaura reaction of aryl chlorides. *Tetrahedron Letters*, **2008**, *49*, 7217–7219.

3. Aida, T.; Meijer, E. W.; Stupp, S. I. Functional supramolecular polymers. *Science*, **2012**, *335*, 813–817.

4. Akamatsu, K.; Yamasaki, Y.; Nishikawa, M.; Takakura, Y.; Hashida, M. Development of a hepatocyte-specific prostaglandin E1 polymeric prodrug and its potential for preventing carbon tetrachloride-induced fulminant hepatitis in mice. *J. Pharmacol. Exp. Ther*. **1999**, *290*, 1242–1249.

5. Alexander, C. M.; Hamner, K. L.; Maye, M. M.; Dabrowiak, J. C. Multifunctional DNA-Gold Nanoparticles for Targeted Doxorubicin Delivery. *Bioconjug. Chem*. **2014**, *25*, 1261–1271.

6. Alexis, F.; Pridgen, E.; Molnar, L. K.; Farokhzad, O. C. Factors affecting the clearance and biodistribution of polymeric nanoparticles. *Mol Pharm*. **2008**, *5*, 505–515.

7. Auzenne, E.; Ghosh, S. C.; Khodadadian, M.; Rivera, B.; Farquhar, D.; Price, R. E.; Ravoori, M.; Kundra, V.; Freedman, R. S.; Klostergaard, J. Hyaluronic acid-paclitaxel: antitumor efficacy against CD44(þ) human ovarian carcinoma xenografts. *Neoplasia* **2007**, *9*, 479-486.

8. Bae, Y. H.; Park, K. Targeted drug delivery to tumors: myths, reality and possibility. *J. Controlled Release* **2011**, *153*, 198.

9. Bahadur, K. C. R.; Xu, P. Multicompartment Intracellular Self-Expanding Nanogel for Targeted Delivery of Drug Cocktail. *Adv. Mater*. **2012**, *24*, 6479–6483.

10. Baldwin, R. L. How Hofmeister ion interactions affect protein stability. *Biophys. J.* **1996**, *71*, 2056-2063.

11. Bao, Y.; Guo, Y.; Zhuang, X.; Li, D.; Cheng, B.; Tan, S.; Zhang, Z. d-α-Tocopherol Polyethylene Glycol Succinate-Based Redox-Sensitive Paclitaxel Prodrug for Overcoming Multidrug Resistance in Cancer Cells. *Mol. Pharm*. **2014**, *11*, 3196–3209.

12. Bartczak, D.; Muskens, O. L.; Sanchez-elsner, T.; Kanaras, A. G.; Millar, T. M. Manipulation of *in Vitro* Angiogenesis Using Peptide-Coated Gold Nanoparticles. *ACS Nano* **2013**, *7*, 5628–5636.

13. Bayley, D.; Sancho, M.-R.; Brown, J.; Brookman, L.; Petrak, K.; Goodard, P.; Steward, A. Soluble polymeric carriers for drug delivery. Part 6. Preparation and biodistribution of N^5 -hydroxyethyl-L-glutamine-co-L-glutamic acid copolymers in rats. J. *Bioact. Compat. Polym*., **1993**, *8*, 51–68.

14. Bergström, K.; Holmberg, K.; Safranj, A.; Hoffman, A. S.; Edgell, M. J.; Kozlowski, A.; Hovanes, B. A.; Harris, J. M. Reduction of fibrinogen adsorption on PEG-coated polystyrene surfaces. *J. Biomed. Mater. Res*. 1992, *26(6),* 779–790.

15. Bergström, K.; Osterberg, E.; Holmberg, K.; Hoffman, A. S.; Schuman, T. P.; Kozlowski, A.; Harris, J. M. Effects of branching and molecular weight of surface-bound poly(ethylene oxide) on protein rejection. *J Biomater Sci Polymer Edn*. **1994**, *6*, 123–132.

16. Blanco, E.; Shen, H.; Ferrari, M. Principles of nanoparticle design for overcoming biological barriers to drug delivery. *Nature Biotechnology*, **2015**, *33*, 941-951.

17. Block, H. Poly(g-benzyl-L-glutamate) and Other Glutamic Acid Containing Polymers, Gordon and Breach, New York, **1983**.

18. Blout, E. R.; Karlson, R. H. Polypeptides. III. The Synthesis of High Molecular Weight Poly-γ-benzyl-L-glutamates. *J. Am. Chem. Soc*. **1956**, *78*, 941– 946.

19. Böhlen, P.; Stein, S.; Dairman, W.; Udenfriend, S. Fluorometric assay of proteins in the nanogram range. *Arch. Biochem. Biophys.* **1973**, *155*, 213-220.

20. Brown, J. M. Tumor hypoxia in cancer therapy. *Methods Enzymol*. **2007**, *435*, 297-321.

21. Brunsveld, L.; Folmer, B. J. B.; Meijer, E. W.; Sijbesma, R. P. Supramolecular Polymers. *Chem. Rev*. **2001**, *101*, 4071–4098.

22. Cabral, H.; Nishiyama, N.; Kataoka, K. Supramolecular Nanodevices: From Design Validation to Theranostic Nanomedicine. *Acc. Chem. Res*. **2011**, *44*, 999−1008.

23. Callmann, C. E.; Barback, C.V.; Thompson, M. P.; Hall, D. J.; Mattrey, R. F.; Gianneschi, N. C. Therapeutic Enzyme-Responsive Nanoparticles for Targeted Delivery and Accumulation in Tumors. *Adv. Mater*. **2015**, *27*, 4611–4615.

24. Chaudhari, K. R.; Ukawala, M.; Manjappa, A. S.; Kumar, A.; Mundada, P. K.; Mishra, A. K. Mathur, R.; Monkkonen, J.; Murthy, R.S. Opsonization, biodistribution, cellular uptake and apoptosis study of PEGylated PBCA nanoparticle as potential drug delivery carrier. *Pharm. Res*. **2012**, *29*, 53-68.

25. Chiu, H.-C.; Kopeckova, P.; Deshmane, S.S.; Kopecek, J. Lysosomal degradability of poly(alpha-amino acids). *J. Biomed. Mater. Res*., **1997**, *34*, 381–392.

26. Choi, C. H.; Alabi, C. A.; Webster, P.; Davis, M. E. Mechanism of active targeting in solid tumors with transferrin-containing gold nanoparticles. *Proc. Natl. Acad. Sci. U. S. A*. **2010**, *107*, 1235−1240.

27. Choi, K. Y.; Swierczewska, M.; Lee, S.; Chen, X. Y. Protease- Activated Drug Development. *Theranostics* **2012**, *2*, 156−178.

28. Chung, H. J.; Park, T. G. Self-Assembled and Nanostructured Hydrogels for Drug Delivery and Tissue Engineering. *Nano Today* **2009**, *4*, 429–437.

29. Coleman, J. D.; Thompson, J. T.; Smith, R. W., 3rd; Prokopczyk, B.; Vanden, H. J. P. Role of Peroxisome Proliferator-Activated Receptor β/δ and B-Cell Lymphoma-6 in Regulation of Genes Involved in Metastasis and Migration in Pancreatic Cancer Cells. *PPAR Res*. **2013**, *2013*, 121956.

30. Collier, I. E.; Wilhelm, S. M.; Eisen, A. Z.; Marmer, B. L.; Grant, G. A.; Seltzer, J. L.; Kronberger, A.; He, C.; Bauer, E. A.; Goldberg, G. I. The Structure OF THE Human Skin Fibroblast Collagenase Gene. *J. Biol. Chem*. **1988**, *263*, 6579-6587.

31. Colombo, P.; Sonvico, F.; Colombo, G.; Bettini, R. Novel platforms for oral drug delivery. *Pharm. Res*. **2009**, *26*, 601– 611.

32. Corbett, T.; Griswold, D.; Roberts, B.; Peckham, J.; Schabel, F.; Evaluation of single agents and combinations of chemotherapeutic agents in mouse colon carcinomas. *Cancer*, **1977**, *40(5)*, 2660-2690.

33. Corbett, T.; Polin, L.; Roberts, B. J.; Lawson, A. J.; Wilbur, R.; Leopold, W. R.; White, K.; Kushner, J.; Paluch, J.; Hazeldine, S.; Moore, R.; Rake, J.; Horwitz, J. P. Transplantable Syngeneic Rodent Tumors: Solid Tumors of Mice. Tumor Models in Cancer Research, **2002**, Humana Press, 41-71.

34. Corbett, T.; Valeriote, F.; LoRusso, P.; Polin, L.; Panchapor, C.; Pugh, S.; White, K.; Knight, J.; Demchik, L.; Jones, J.; Jones, L.; Lowichik, N.; Biernat, L.; Foster. B.; Wozniak, A.; Lisow, L.; Valdivieso, M.; Baker, L.; Leopold, W.; Sebolt, J.; Bissery, M.; Mattes, K.; Dzubow, J.; Rake, J.; Perni, R.; Wentland, M.; Coughlin, S.; Shaw, J. M.; Liversidge, G.; Liversidge, E.; Bruno, J.; Sarpotdar, P.; Moore, R.; Patterson, G. Tumor models and the discovery and secondary evaluation of solid tumor active agents. *Int. J. Pharmacognosy*, **1995**, *33*, 102-122.

35. Criscione, J. M.; Le, B. L.; Stern, E.; Brennan, M.; Rahner, C.; Papademetris, X.; Fahmy, T. M. Self-assembly of pH-responsive fluorinated dendrimer-based particulates for drug delivery and noninvasive imaging. *Biomaterials* **2009**, *30*, 3946–3955.

36. Crisp J. L.; Savariar, E. N.; Glasgow, H. L.; Ellies, L. G.; Whitney, M. A.; Tsien, R.Y. Dual targeting of integrin αvβ3 and matrix metalloproteinase-2 for optical imaging of tumors and chemotherapeutic delivery. *Molecular Cancer Therapeutics* **2014**, *13*, 1514-1525.

37. Crownover, E.; Duvall, C. L.; Convertine, A.; Hoffman, A. S.; Stayton, P. S. RAFT-synthesized Graft Copolymers that Enhance pH-dependent Membrane Destabilization and Protein Circulation Times. *J. Controlled Release* **2011**, *155*, 167-174.

38. Cui, J.; Björnmalm, M.; Liang, K.; Xu, C.; Best, J. P.; Zhang, X.; Caruso F. Super-soft hydrogel particles with tunable elasticity in a microfluidic blood capillary model. *Adv. Mater*. **2014**, *26*, 7295–7299.

39. Danhier, F.; Feron, O.; Preat, V. To exploit the tumor microenvironment: passive and active tumor targeting of nanocarriers for anti-cancer drug delivery. *J. Control Release* **2010**, *148*, 135-146.

40. Das, M.; Singh, R. P.; Datir, S. R.; Jain, S. Intranuclear Drug Delivery and Effective in Vivo Cancer Therapy via Estradiol–PEG-Appended Multiwalled Carbon Nanotubes. *Mol. Pharm.* **2013**, *10*, 3404–3416.

41. Davis, M. E.; Zuckerman, J. E.; Choi, C. H.; Seligson, D.; Tolcher, A.; Alabi, C. A.; Yen, Y.; Heidel, J. D.; Ribas, A. Evidence of RNAi in humans from systemically administered siRNA via targeted nanoparticles. *Nature* **2010**, *464*, 1067-1070.

42. de la Rica, R.; Aili, D.; Stevens, M. M. Enzyme-responsive nanoparticles for drug release and diagnostics. *Adv. Drug Delivery Rev*. **2012**, *64*, 967−978.

43. de Las Heras Alarcon, C.; Pennadam, S.; Alexander, C. Stimuli Responsive Polymers for Biomedical Applications. *Chem. Soc. Rev*. **2005**, *34*, 276–285.

44. Deming, T. Facile synthesis of block copolypeptides of defined architecture. *Nature*, **1997**, *390*, 386–389.

45. Diaz D. D.; Kuhbeck, D.; Koopmans, R. J. Stimuli-Responsive Gels as Reaction Vessels and Reusable Catalysts. *Chem. Soc. Rev*. **2011**, *40*, 427–448.

46. Ding, C. X.; Gu, J. X.; Qu, X. Z.; Yang, Z. Z. Preparation of Multifunctional Drug Carrier for Tumor-Specific Uptake and Enhanced Intracellular Delivery through the Conjugation of Weak Acid Labile Linker. *Bioconjugate Chem*. **2009**, *20*, 1163–1170.

47. Ding, D.; Kwok, R. T. K.; Yuan, Y.; Feng, G.; Tang, B. Z.; Liu, B. A Fluorescent Light-up Nanoparticle Probe with Aggregation-induced Emission Characteristics and Tumor-acidity Responsiveness for Targeted Imaging and Selective Suppression of Cancer Cells. *Mater. Horiz.* **2015**, *2*, 100−105.

48. Discher, B. M.; Won, Y. Y.; Ege, D. S.; Lee, J. C.-M.; Bates, F. S.; Discher, D. E.; Hammer, D. A. Polymersomes: Tough Vesicles Made from Diblock Copolymers. *Science* **1999**, *284*, 1143–1146.

49. Dobrovolskaia, M. A.; McNeil, S. E. Immunological properties of engineered nanomaterials. *Nature Nanotechnology*, **2007**, *2*, 469-478.

50. Dobrovolskaia, M. A.; Patri, A. K.; Simak, J.; Hall, J. B.; Semberova, J.; De Paoli Lacerda, S. H.; McNeil, S. E. Nanoparticle size and surface charge determine effects of PAMAM dendrimers on human platelets in vitro. *Mol. Pharm*. **2012**, *9*, 382.

51. Dressman, J. B.; Berardi, R. R.; Dermentzoglou, L. C.; Rusell, T. L.; Schmaltz, S. P.; Barnett, J. L.; Jarvenpaa, K. M. Upper gastrointestinal (GI) pH in young, healthy men and women. *Pharm. Res.* **1990**, *7*, 756–761.

52. Duncan R. Polymer conjugates as anticancer nanomedicines. *Nat. Rev. Cancer* **2006**, *6*, 688-701.

53. Ernsting, M. J.; Foltz, W. D.; Undzys, E.; Tagami, T.; Li, S. D. Tumor-targeted drug delivery using MR- contrasted docetaxel - carboxymethylcellulose nanoparticles. *Biomaterials* **2012**, *33*, 3931–3941.

54. Ernsting, M. J.; Tang, W. L.; Maccallum, N. W.; Li, S. D. Preclinical pharmacokinetic, biodistribution, and anti-cancer efficacy studies of a docetaxel-carboxymethylcellulose nanoparticle in mouse models. *Biomaterials* **2012**, *33*, 1445–1454.

55. Evans, D. F.; Ninham, B. W. Molecular Forces in the Self-Organization of Amphiphiles. *J. Phys. Chem*. **1986**, *90*, 226−234.

56. Evans, D. F.; Wennerstrom, H. The Colloidal Domain, 2nd ed.; Wiley-VCH: New York, 1999.

57. Fang, C.; Shi, B.; Pei, Y. Y.; Hong, M. H.; Wu, J.; Chen, H. Z. In vivo tumor targeting of tumor necrosis factor-R-loaded stealth nanoparticles: Effect of MePEG molecular weight and particle size. *Eur. J. Pharm. Sci.* **2006**, *27*, 27–36.

58. Fang, J.; Nakamura, H.; Maeda, H. The EPR effect: unique features of tumor blood vessels for drug delivery, factors involved, and limitations and augmentation of the effect. *Adv. Drug Deliv. Rev*. **2011**, *63*, 136-151.

59. Fassas, A.; Buffels, R.; Kaloyannidis, P.; Anagnostopoulos, A. Safety of high-dose liposomal daunorubicin (daunoxome) for refractory or relapsed acute myeloblastic leukaemia. *Br. Jo. Haematol*. **2003**, *122*, 161–163.

60. Fay, F.; Hansen, L.; Hectors, S. J. C. G.; Sanchez-Gaytan, B. L.; Zhao, Y.; Tang, J.; Munitz, J.; Alaarg, A.; Braza, M. S.; Gianella, A.; Aaronson, S. A.; Reiner, T.; Kjems, J.; Langer, F. J. M. Hoeben, H. M. Janssen, C. Calcagno, G. J. Strijkers, Z. A. Fayad, C. Peŕez-Medina, R.; Mulder. W. J. M. Investigating the Cellular Specificity in Tumors of a Surface-Converting Nanoparticle by Multimodal Imaging. *Bioconjugate Chem*. **2017**, *28*, 1413−1421.

61. Feng, X.; Lv, F.; Liu, L.; Tang, H.; Xing, C.; Yang, Q.; Wang, S. Conjugated Polymer Nanoparticles for Drug Delivery and Imaging. *ACS Appl. Mater. Interfaces* **2010**, *2*, 2429–2435.

62. Fleige, E.; Quadir, M. A.; Haag, R. Stimuli-responsive polymeric nanocarriers for the controlled transport of active compounds: Concepts and applications. *Adv. Drug Delivery Rev*. **2012**, *64 (9)*, 866−884.

63. Foulkes, W. D.; Smith, I. E.; and Reis-Filho, J. S. Triple-negative breast cancer. *N. Engl. J. Med*. **2010**, *363*, 1938-1948.

64. Friden, P. M.; Walus, L. R.; Musso, G. F.; Taylor, M. A.; Malfroy, B.; Starzyk, R. M. Anti-Transferrin Receptor Antibody and Antibody Drug Conjugates Cross the Blood Brain Barrier. *Proc. Natl. Acad. Sci. U.S.A*. **1991**, *88*, 4771–4775.

65. Fuhrhop, J.-H.; Wang, T. Bolaamphiphiles. *Chem. Rev*. **2004,** *104*, 2901–2937.

66. Gabizon, A.; Horowitz, A. T.; Goren, D.; Tzemach, D.; Mandelbaum-Shavit, F.; Qazen, M. M.; Zalipsky, S. Targeting Folate Receptor with Folate Linked to Extremities of Poly(ethylene glycol)-Grafted Liposomes: In Vitro Studies. *Bioconjugate Chem*. **1999**, *10*, 289–298.

67. Ganta, S.; Devalapally, H.; Shahiwala, A.; Amiji, M. A review of stimuli-responsive nanocarriers for drug and gene delivery. *J. Controlled Release* **2008**, *126 (3)*, 187−204.

68. Gao, W.; Chan, J. M.; Farokhzad, O. C. pH-Responsive Nanoparticles for Drug Delivery. *Mol. Pharm*. **2010**, *7*, 1913–1920.

69. Gao, Y.; Yang, C.; Liu, X.; Ma, R.; Kong D.; Shi, L. A Multifunctional Nanocarrier Based on Nanogated Mesoporous Silica for Enhanced Tumor-Specific Uptake and Intracellular Delivery. *Macromol. Biosci*. **2011**, *12*, 251–259.

70. Gaucher, G.; Marchessault, R. H.; Leroux, J. C. Polyester-based micelles and nanoparticles for the parenteral delivery of taxanes. *J. Control Release* **2010**, *143*, 2-12.

71. Ge, G.; Brus, L. E. Fast Surface Diffusion of Large Disk-Shaped Nanocrystal Aggregates. *Nano Lett.* **2001**, *1*, 219–222.

72. Ge, J.; Lei, J.; Zare, R. N. Bovine Serum Albumin–Poly(methyl methacrylate) Nanoparticles: An Example of Frustrated Phase Separation. *Nano Lett*. **2011**, *11*, 2551–2554.

73. Geisow, M. J.; Evans, W. H. pH in the endosome. Measurements during pinocytosis and receptor-mediated endocytosis. *Exp. Cell Res*. **1984**, *150*, 36–46.

74. Gelderblom, H.; Verweij, J.; Nooter, K.; Sparreboom, A. Cremophor EL: the drawbacks and advantages of vehicle selection for drug formulation. *Eur. J. Cancer* **2001**, *37*, 1590-1598.

75. Ghosh, S.; Basu, S.; Thayumanavan, S. Simultaneous and Reversible Functionalization of Copolymers for Biological Applications. *Macromolecules* 2006, *39*, 5595-5597.

76. Ghosh, S.; Irvin, K.; Thayumanavan, S. Tunable Disassembly of Micelles Using a Redox Trigger. *Langmuir* **2007**, *23*, 7916–7919.

77. Gold, A. A.; Ghosh, P. S.; Kim, C.; Han, G.; Forbes, N. S.; Rotello, V. M. Efficient Gene Delivery Vectors by Tuning the Surface Charge Density of Amino Acid-Functionalized Gold Nanoparticles. *ACS Nano* **2008**, *2*, 2213–2218.

78. Gombotz, W. R.; Guanghui, W.; Horbett, T. A.; Hoffman, A. S. Protein adsorption to poly(ethylene oxide) surfaces. *J. Biomed. Mater. Res*. 1991, *25*, 1547–1562.

79. González-Toro, D. C.; Ryu, J.-H.; Chacko, R. T.; Zhuang, J.; Thayumanavan, S. Concurrent Binding and Delivery of Proteins and Lipophilic Small Molecules Using Polymeric Nanogels. *J. Am. Chem. Soc*., **2012**, *134*, 6964-6967.

80. Gore, M. Spectrophotometry and Spectrofluorimetry: A Practical Approach. Ed. Oxford University Press, Incorporated (New York, NY 2000) p. 63.

81. Gradishar, W. J. Albumin-bound paclitaxel: a next-generation taxane. *Expert Opin. Pharmacother*. **2006**, *7*, 1041-1053.

82. Gref, R.; Lück, M.; Quellec, P.; Marchand, M.; Dellacherie, E.; Harnisch, S.; Blunk, T.; Müller, R. H. 'Stealth' corona-core nanoparticles surface modified by polyethylene glycol (PEG): Influences of the corona (PEG chain length and surface density) and of the core composition on phagocytic uptake and plasma protein adsorption. *Colloids Surf.* **2000**, *18*, 301–313.

83. Gu, J.; Cheng, W. P.; Liu, J.; Lo, S. Y.; Smith, D.; Qu X.; Yang, Z. pH-Triggered Reversible "Stealth" Polycationic Micelles, *Biomacromolecules*, **2008**, *9*, 255–262.

84. Guo, M.; Que, C.; Wang, C.; Liu, X.; Yan, H.; Liu, K. Multifunctional superparamagnetic nanocarriers with folate-mediated and pH-responsive targeting properties for anticancer drug delivery. *Biomaterials* **2011**, *32*, 185-194.

85. Guo, X.; Shi, C.; Yang, G.; Wang, J.; Cai, Z.; Zhou, S. Dual-Responsive Polymer Micelles for Target-Cell-Specific Anticancer Drug Delivery. *Chem. Mater*. **2014**, *26*, 4405–4418.

86. Hage, C.; Gremse, F.; Griessinger, C. M.; Maurer, A.; Hoffmann, S. H. L.; Osl, F.; Pichler, B. J.; Kiessling, F.; Scheuer, W.; Pöschinger, T. Comparison of the Accuracy of FMT/CT and PET/MRI for the Assessment of Antibody Biodistribution in Squamous Cell Carcinoma Xenografts. *J. Nucl. Med*. **2017**.

87. Harris, T. J.; von Maltzahn, G.; Lord, M. E.; Park, J. H.; Agrawal, A.; Min, D. H.; Sailor, M. J.; Bhatia, S. N. Protease-Triggered Unveiling of Bioactive Nanoparticles. *Small* **2008**, *4*, 1307-1312.

88. Hartgerink, J. D.; Beniash, E.; Stupp, S. I. Self-Assembly and Mineralization of Peptide-Amphiphile Nanofibers. *Science* **2001**, *294*, 1684−1688.

89. Hawker, C. J.; Bosman, A. W.; Harth, E. New polymer synthesis by nitroxide mediated living radical polymerizations. *Chem. Rev*. **2001**, *101*, 3661–3688.

90. Higashi, N.; Kawahara, J.; Niwa, M. Preparation of helical peptide monolayer-coated gold nanoparticles. *J. Colloid Interface Sci.* 2005, *288*, 83.

91. Higashi,N.; Koga, T.; Niwa, M. Helical Superstructures from a Poly(*γ*-benzyl-L-glutamate)-Poly(L-glutamic acid) Amphiphilic Diblock Copolymer: Monolayer Formation on Water and Its Specific Binding of Amino Acids. *Langmuir* 2000, *16,* 3482-3486.

92. Hilf, S.; Kilbinger, A. F. M. Functional end groups for polymers prepared using ring-opening metathesis polymerization. *Nat. Chem*. **2009**, *1*, 537–546.

93. Hofmeister, F. On the understanding of the effects of salts, second report. On irregularities in the precipitating effect of salts and their relationship to their physical behavior. *Arch. Exp. Pathol. Pharmocol.* **1888**, *24*, 247-260.

94. Hrkach, J.; Von Hoff, D.; Ali, M. M.; Andrianova, E.; Auer, J.; Campbell, T.; De Witt, D.; Figa, M.; Figueiredo, M.; Horhota, A.; Low, S.; McDonnell, K.; Peeke, E.; Retnarajan, B.; Sabnis, A.; Schnipper, E.; Song, J. J.; Song, Y. H.; Summa, J.; Tompsett, D.; Troiano, G.; Van Geen Hoven, T.; Wright, J.; Lorusso, P.; Kantoff, P. W.; Bander, N. H.; Sweeney, C.; Farokhzad, O. C.; Langer, R.; Zale, S. Preclinical Development and Clinical Translation of a PSMA-Targeted Docetaxel Nanoparticle with a Differentiated Pharmacological Profile. *Sci. Transl. Med*. **2012**, *4*, 128-139.

95. Hu, J.; Zhang, G.; Liu, S. Enzyme-responsive polymeric assemblies, nanoparticles and hydrogels. *Chem. Soc. Rev*. **2012**, *41*, 5933-5949.

96. Huang, X.; Zheng, B.; Liu, Z.; Tan, C.; Liu, J.; Chen, B.; Li, H.; Chen, J.; Zhang, X.; Fan, Z.; Zhang, W.; Guo, Z.; Huo, F.; Yang, Y.; Xie, L.; Huang, W.; Zhang, H. Coating Two-Dimensional Nanomaterials with Metal–Organic Frameworks. *ACS Nano* **2014**, *8*, 8695–8701.

97. Hudis, C. A.; Gianni, L. Triple-Negative Breast Cancer: An Unmet Medical Need. *The Oncologist*. **2011**, *16*, 1–11.

98. Hyuga, S.; Nishikawa, Y.; Sakata, K.; Tanaka, H.; Yamagata, S.; Sugita, K.; Saga, S.; Matsuyama, M.; Shimizu, S. Autocrine Factor Enhancing the Secretion of M_r 95,000 Gelatinase (Matrix Metalloproteinase 9) in Serum-free Medium Conditioned with Murine Metastatic Colon Carcinoma Cells. *Cancer Research*, **1994**, *54*, 3611-3616.

99. Iakoubov, L. Z.; Torchilin, V. P. A Novel Class of Antitumor Antibodies: Nucleosome-Restricted Antinuclear Autoantibodies (ANA) from Healthy Aged Nonautoimmune Mice. *Oncol. Res.* **1997**, *9*, 439–446.

100. Idelson, M.; Blout, E. R. High molecular weight poly(a-L- glutamic acid): preparation and physical rotation changes. *J. Am. Chem. Soc*., **1958**, *80*, 4631–4634.

101. Ikkala, O.; ten Brinke, G. Functional materials based on self-assembly of polymeric supramolecules. *Science* **2002**, *295*, 2407–2409.

102. İnce, A. T.; Yıldız, K.; Gangarapu, V.; Kayar, Y.; Baysal, B.; Karatepe, O.; Kemik, A. S.; Şentürk, H. Serum and biliary MMP-9 and TIMP-1 concentrations in the diagnosis of cholangiocarcinoma. *Int. J. Clin. Exp. Med*. **2015**, *8(2)*, 2734-2740.

103. Israelachvili, J. N.; Mitchell, D. J.; Ninham, B. W. Theory of Self-Assembly of Hydrocarbon Amphiphiles into Micelles and Bilayers. *J. Chem. Soc., Faraday Trans II*. **1976**, *72*, 1525−1568.

104. Jacques, S.L.; Pogue, B.W. Tutorial on diffuse light transport. *J. Biomed. Opt*. **2008**, 13, 041302.

105. Jain, R. K.; Stylianopoulos, T. Delivering nanomedicine to solid tumors. *Nat. Rev. Clin. Oncol.* **2010**, *7*, 653-653.

106. Jain, T. K.; Morales, M. A.; Sahoo, S. K.; Leslie-Pelecky, D. L.; Labhasetwar, V. Iron Oxide Nanoparticles for Sustained Delivery of Anticancer Agents. *Mol. Pharm*. **2005**, *2*, 194–205.

107. Jana, S.; Cooper, A.; Ohuchi, F.; Zhang, M. Uniaxially Aligned Nanofibrous Cylinders by Electrospinning. *ACS Appl. Mater. Interfaces* **2012**, *4*, 4817–4824.

108. Janata, J.; Josowicz, M. Conducting polymers in electronic chemical sensors. *Nat. Mater*. **2003**, *2*, 19–24.

109. Jeon, S. I.; Andrade, J. D. Protein-surface interactions in the presence of olyethylene oxide: Effect of protein size. *J. Colloid Interf. Sci*. **1991**, *142*, 159-166.

110. Jeon, S. I.; Lee, J. H.; Andrade, J. D.; De Gennes, P. G. Protein-surface interactions in the presence of olyethylene oxide: Simplified theory. *J. Colloid Interf. Sci*. **1991**, 142, 149-158.

111. Jiang, G.; Wang, Y.; Zhang, R.; Wang, R.; Wang, X.; Zhang, M.; Sun, X.; Bao, S.; Wang, T.; Wang, S. Preparation of Redox-Sensitive Shell Cross-Linked Nanoparticles for Controlled Release of Bioactive Agents. *ACS Macro Lett*. **2012**, *1*, 489–493.

112. Jiang, S.; Eltoukhy, A. A.; Love, K. T.; Langer, R.; Anderson, D. G. Lipidoid-Coated Iron Oxide Nanoparticles for Efficient DNA and siRNA delivery. *Nano Lett*. **2013**, *13*, 1059–1064.

113. Jin, E.; Zhang, B.; Sun, X.; Zhou, Z.; Ma, X.; Sun, Q.; Tang, J.; Shen, Y. Q.; Kirk, E. V.; Murdoch, W. J.; Radosz, M. Acid-Active Cell- Penetrating Peptides for in Vivo Tumor-Targeted Drug Delivery. *J. Am. Chem. Soc*. **2013**, *135*, 933−940.

114. Jiwpanich, S.; Ryu, J. -H.; Bickerton, S.; Thayumanavan, S. Noncovalent encapsulation stabilities in supramolecular nanoassemblies. *J. Am. Chem. Soc*. **2010**, *132*, 10683-10685.

115. Johnson, J. A.; Lu, Y. Y.; Burts, A. O.; Lim, Y. -H.; Finn, M. G.; Koberstein, J. T.; Turro, N. J.; Tirrell, D. A.; Grubbs, R. H. Core-clickable PEG-branch-azide bivalent-bottle-brush polymers by ROMP: grafting-through and clicking-to. *J. Am. Chem. Soc*. **2010**, *133*, 559–566.

116. Jones S. Head-to-head: docetaxel challenges paclitaxel. *EJC Supplements* **2006**, *4*, 4-8.

117. Jumper, C.; Cobos, E.; Lox, C. Determination of the serum matrix metalloproteinase-9 (MMP-9) and tissue inhibitor of matrix metalloproteinase-1 (TIMP-1) in patients with either advanced small-cell lung cancer or non-small-cell lung cancer prior to treatment. *Respiratory Medicine* **2004**, *98*, 173-177.

118. Kararli, T. T. Comparison of the gastrointestinal anatomy, physiology, and biochemistry of humans and commonly used laboratory animals. *Biopharm. Drug Dispos*. **1995**, *16*, 351–380.

119. Kato, Y.; Ozawa, S.; Miyamoto, C.; Maehata, Y.; Suzuki, A.; Maeda, T.; Baba, Y. Acidic extracellular microenvironment and cancer, *Cancer Cell Int*. **2013**, *13*, 89.

120. Katti, D. S.; Lakshmi, S.; Langer, R.; Laurencin, C. T. Toxicity, biodegradation and elimination of polyanhydrides. *Adv. Drug Deliv. Rev*. **2002**, *54*, 933–961.

121. Kavimandan, N. J.; Losi, E.; Wilson, J. J.; Brodbelt, J. S.; Peppas, N. A.; Synthesis and Characterization of Insulin-Transferrin Conjugates. *Bioconjugate Chem*. **2006**, *17*, 1376-1384

122. Kenny, A. D. Evaluation of sodium poly(a-L-glutamic acid) as a plasma expander. *Proc. Soc. Exp. Biol. Med.,* **1959**, *100*, 778 – 780.

123. Kim D. W.; Kim S. Y.; Kim, H. K.; Kim, S. W.; Shin, S. W.; Kim, J. S.; Park, K.; Lee, M. Y. Heo, D. S. Multicenter phase II trial of Genexol-PM, a novel Cremophor-free, polymeric micelle formulation of paclitaxel, with cisplatin in patients with advanced non-small-cell lung cancer. *Ann. Oncol*. **2007**, *18*, 2009–2014

124. Kim, J.-H.; Bryan, W. W.; Chung, H.-W.; Park, C. Y.; Jacobson, A. J.; Lee, T. R. Gold, Palladium, and Gold−Palladium Alloy Nanoshells on Silica Nanoparticle Cores. *ACS Appl. Mater. Interfaces* **2009**, *1*, 1063–1069.

125. Kim, J. K.; Yang, S. Y.; Lee, Y.; Kim, Y. Functional nanomaterials based on block copolymer self-assembly. *Prog. Polym. Sci*. **2010**, *35*, 1325–1349.

126. Kishore, B.K.; Lambricht, P.; Laurent, G.; Maldague, P.; Wagner, R.; Tulkens, P.M. Mechanism of protection afforded by polyaspartic acid against gentamicin-induced phos- pholipidosis. II. Comparative in vitro and in vivo studies with poly-L-aspartic, poly-L-glutamic and poly-D-glutamic acids. *J. Pharmacol. Exp. Ther*., **1990**, *255*, 875–885.

127. Klaikherd, A.; Nagamani, C.; Thayumanavan, S. Multi-Stimuli Sensitive Amphiphilic Block Copolymer Assemblies. *J. Am. Chem. Soc*. **2009**, *131*, 4830–4838.

128. Kobayashi, H.; Watanabe, R.; Choyke, P. L. Improving Conventional Enhanced Permeability and Retention (EPR) Effects; What Is the Appropriate Target? *Theranostics* **2014**, *4*, 81-89.

129. Kovar, J. L.; Simpson, M. A.; Schutz-Geschwender, A.; Olive, D. M. A systematic approach to the development of fluorescent contrast agents for optical imaging of mouse cancer models. *Anal Biochem.* **2007**, *367*, 1–12.

130. Kozielski, K. L.; Tzeng, S. Y.; Hurtado De Mendoza, B. A.; Green, J. J. Bioreducible Cationic Polymer-Based Nanoparticles for Efficient and Environmentally Triggered Cytoplasmic siRNA Delivery to Primary Human Brain Cancer Cells. *ACS Nano* **2014**, *8*, 3232–3241.

131. Kreuter, J. Nanoparticles. J. Kreuter (Ed.), Colloidal Drug Delivery Systems, Marcel Dekker, New York, **1994**.

132. Kulkarni, P. S.; Haldar, M. K.; Nahire, R. R.; Katti, P.; Ambre, A. H.; Muhonen, W. W.; Shabb, J. B.; Padi, S. K. R.; Singh, R. K.; Borowicz, P. P.; Shrivastava, D. K.; Katti, K. S.; Reindl, K.; Guo, B.; Mallik, S. MMP-9 Responsive PEG Cleavable Nanovesicles for Efficient Delivery of Chemotherapeutics to Pancreatic Cancer. *Mol. Pharmaceutics*. **2014**, *11*, 2390−2399.

133. Langer, R. New Methods of Drug delivery. *Science* **1990**, *249*, 1527–1533.

134. Lee, H.; Fonge, H.; Hoang, B.; Reilly, R. M.; Allen, C. The effects of particle size and molecular targeting on the intratumoral and subcellular distribution of polymeric nanoparticles. *Mol. Pharm*. **2010**, *7*, 1195–1208.

135. Lee, H. J.; Pardridge, W. M. Monoclonal Antibody Radiopharmaceuticals: Cationization, Pegylation, Radiometal Chelation, Pharmacokinetics, and Tumor Imaging. *Bioconjugate Chem*. **2003**, *14*, 546–553.

136. Lee K. S.; Chung, H. C.; Im, S. A.; Park, Y. H.; Kim, C. S.; Kim, S. B.; Rha, S. Y.; Lee, M. Y.; Ro, J. Multicenter phase II trial of Genexol-PM, a Cremophor-free, polymeric micelle formulation of paclitaxel, in patients with metastatic breast cancer. *Breast Cancer Res. Treat*. **2008**, *108*, 241–250.

137. Lee, M.; Cho, B.-K.; Zin, W.-C. Supramolecular Structures from Rod−Coil Block Copolymers. *Chem. Rev*. **2001**, *101*, 3869–3892.

138. Lee, S.; Koo, H.; Na, J. H.; Lee, K. E.; Jeong, S. Y.; Choi, K.; Kim, S. H.; Kwon, I. C.; Kim, K. DNA Amplification in Neutral Liposomes for Safe and Efficient Gene Delivery. *ACS Nano* **2014**, *8*, 4257–4267.

139. Lee, S. J.; Min, K. H.; Lee, H. J.; Koo, A. N.; Rim, H. P.; Jeon, B.J.; Jeong, S. Y.; Heo, J. S.; Lee, S. C.; Ketal cross-linked poly(ethylene glycol)-poly(amino acid)s copolymer micelles for efficient intracellular delivery of 43 doxorubicin. *Biomacromolecules*, **2011**, *12*, 1224-1233.

140. Letchford. K.; Liggins, R.; Wasan, K. M.; Burt, H. In vitro human plasma distribution of nanoparticulate paclitaxel is dependent on the physicochemical properties of poly(ethylene glycol)-block-poly(caprolactone) nanoparticles. *Eur. J. Pharm Biopharm*. **2009**, *71*, 196-206.

141. Li, C. Poly(L-glutamic acid)-anticancer drug conjugates. *Adv. Drug Deliv. Rev.* **2002**, *54*, 695-713.

142. Li, C.; Newman, R. A.; Wu, Q. P.; Ke, S.; Chen, W.; Hutto, T.; Kan, Z.; Brannan, M. D.; Charnsangavej, C.; Wallace, S. Biodistribution of paclitaxel and poly(L-glutamic acid)-paclitaxel conjugate in mice with ovarian OCa-1 tumor. *Cancer Chemother. Pharmacol.* **2000**, *46*, 416-422.

143. Li, H.; Yu, S. S.; Miteva, M.; Nelson, C. E.; Werfel, T.; Giorgio, T. D.; Duvall, C. L. Matrix Metalloproteinase Responsive, Proximity-Activated Polymeric Nanoparticles for siRNA Delivery. *Adv. Funct. Mater*. **2013**, *23*, 3040–3052.

144. Li, J.; Ge, Z.; Liu, S. PEG-sheddable polyplex micelles as smart gene carriers based on MMP-cleavable peptide-linked block copolymers. *Chem. Commun*. **2013**, *49*, 6974−6976.

145. Li, J.; Kao, W. J. Synthesis of Polyethylene Glycol (PEG) Derivatives and PEGylated−Peptide Biopolymer Conjugates. *Biomacromolecules*, **2003**, *4*, 1055-1067.

146. Li, L.; Raghupathi, K.; Yuan, C.; Thayumanavan, S. Surface charge generation in nanogels for activated cellular uptake at tumor-relevant pH. *Chem. Sci*. **2013**, *4*, 3654-3360.

147. Li, L.; Ryu, J. -H.; Thayumanavan, S. Effect of Hofmeister ions on the size and encapsulation stability of polymer nanogels. *Langmuir* **2013**, *29*, 50-55.

148. Li, L.; Thayumanavan, S. Environment-dependent guest exchange in supramolecular hosts. *Langmuir* **2014**, *30*, 12384-12390.

149. Li, Q.; Zeng, L.; Wang, J.; Tang, D.; Liu, B.; Chen, G.; Wei, M. Magnetic Mesoporous Organic−Inorganic $NiCo_2O_4$ Hybrid Nanomaterials for Electrochemical Immunosensors. *ACS Appl. Mater. Interfaces* **2011**, *3*, 1366–1373.

150. Li. S. Hydrolytic degradation characteristics of aliphatic polyesters derived from lactic and glycolic acids. *J. Biomed. Mater. Res*. **1999**, *48*, 342–353.

151. Li, S.-D.; Huang, L. Pharmacokinetics and Biodistribution of Nanoparticles. *Mol. Pharmaceutics*, **2008**, *5 (4)*, 496–504.

152. Li, W.; Nakayama, M.; Akimoto, J.; Okano, T. Effect of block compositions of amphiphilic block copolymers on the physicochemical properties of polymeric micelles. *Polymer* **2011**, *52*, 3783-3790.

153. Li, Y.; Kröger, M.; Liu, W. K.; Endocytosis of PEGylated nanoparticles accompanied by structural and free energy changes of the grafted polyethylene glycol. *Biomaterials*, **2014**, *35*, 8467-8478.

154. Lim, W. T.; Tan, E. H.; Toh, C. K.; Hee, S. W.; Leong, S. S.; Ang, P. C.; Wong, N. S., Chowbay, B. Phase I pharmacokinetic study of a weekly liposomal paclitaxel formulation (Genexol-PM) in patients with solid tumors. *Ann. Oncol*. **2010**, *21*, 382-388.

155. Lipinski, C. A. Drug-like properties and the causes of poor solubility and poor permeability. *J. Pharmacol. Toxicol. Methods* **2000**, *44*, 235-249.

156. Liu, D.; Mori, A.; Huang, L. Role of liposome size and RES blockade in controlling biodistribution and tumor uptake of GM1- containing liposomes. *Biochim. Biophys. Acta* **1992**, *1104*, 95– 101.

157. Liu, D. L.; Chang, X.; Dong, C. M. Reduction- and thermo-sensitive star polypeptide micelles and hydrogels for on-demand drug delivery. *Chem. Commun*. **2013**, *49 (12)*, 1229−1231.

158. Liu, Y.; Ding, X.; Li, J.; Luo, Z.; Hu, Y.; Liu, J.; Dai, L.; Zhou, J.; Hou, C.; Cai, K. Enzyme responsive drug delivery system based on mesoporous silica nanoparticles for tumor therapy in vivo. *Nanotechnology* **2015**, *26*, 145102-145116.

159. Lloyd, A. W. Interfacial bioengineering to enhance surface biocompatibility. *Med. Device Technol*. 2002, *13*, 18–21.

160. Lukyanov, A. N.; Elbayoumi, T. A.; Chakilam, A. R.; Torchilin, V. P. Tumor-Targeted Liposomes: Doxorubicin-Loaded Long-Circulating Liposomes Modified with Anti-Cancer Antibody. *J. Controlled Release* **2004**, *100*, 135–144.

161. Luo, M.; Liu, Y.; Hu, J.; Liu, H.; Li, J. One-Pot Synthesis of CdS and Ni-Doped CdS Hollow Spheres with Enhanced Photocatalytic Activity and Durability. *ACS Appl. Mater. Interfaces* **2012**, *4*, 1813– 1821.

162. Ma, X.; Zhou, Z.; Jin, E.; Sun, Q.; Zhang, B.; Tang, J.; Shen, Y. Facile Synthesis of Polyester Dendrimers as Drug Delivery Carriers. *Macromolecules* **2013**, *46*, 37–42.

163. Maeda, H.; Nakamura, H.; Fang, J. The EPR effect for macromolecular drug delivery to solid tumors: Improvement of tumor uptake, lowering of systemic toxicity, and distinct tumor imaging in vivo. *Adv. Drug Deliv. Rev.* **2013**, *65*, 71–79.

164. Magnusson, J. P.; Khan, A.; Pasparakis, G.; Saeed, A. O.; Wang, W. X.; Alexander, C. Ionsensitive isothermal responsive polymers prepared in water. *J. Am. Chem. Soc*. **2008**, *130*, 10852– 10853.

165. Mai, Y.; Eisenberg, A. Self-assembly of block copolymers. *Chem. Soc. Rev*. **2012**, *41*, 5969– 5985.

166. Matsumura, Y.; Maeda, H. A new concept for macromolecular therapeutics in cancer chemotherapy: mechanism of tumoritropic accumulation of proteins and the antitumor agent smancs. *Cancer Res*. **1986**, *46*, 6387–6392.

167. Matyjaszewski, K.; Tsarevsky, N. V. Macromolecular engineering by atom transfer radical polymerization. *J. Am. Chem. Soc*. **2014**, *136*, 6513–6533.

168. McCormick-Thomson, L.A.; Duncan, R. Poly(amino acid) copolymers as a potential soluble drug delivery system. 1. Pinocytotic uptake and lysosomal degradation measured in vitro. *J. Bioact. Compat. Polym*., **1989**, *4*, 242–251.

169. Medina, S. H.; El-sayed, M. E. H. Dendrimers as Carriers for Delivery of Chemotherapeutic Agents. *Chem. Rev*. **2009**, *109*, 3141–3157.

170. Meister, A.; Anderson, M. E. Glutathione. *Ann. Rev. Biochem*. **1983**, *52*, 711-760.

171. Meng, F.; Zhong, Z.; Feijen, J. Stimuli-Responsive Polymersomes for Programmed Drug Delivery. *Biomacromolecules* **2009**, *10*, 197–209.

172. Menger, F. M. The Structure of Micelles. *Acc. Chem. Res*. **1979**, *12*, 111–117.

173. Merkel, T. J.; Chen, K.; Jones, S. W.; Pandya, A. A.; Tian, S.; Napier, M. E.; Zamboni, W. E.; DeSimone, J. M. The effect of particle size on the biodistribution of low-modulus hydrogel PRINT particles. *J. Control. Release*, **2012**, *162*, 37–44.

174. Mitchell, J. C.; Woodward, A. E.; Doty, P. Polypeptides. XVI. The Polydispersity and Configuration of Low Molecular Weight Poly-γ-benzyl-L-glutamates. *J. Am. Chem. Soc*. **1957**, *79*, 3955–3960.

175. Miyake, M.; Yamada, K.; Oyama, N. Self-Assembling of Guanidine-Type Surfactant. *Langmuir* **2008**, *24*, 8527–8532.

176. Mizuhara, T.; Saha, K.; Moyano, D. F.; Kim, C. S.; Yan, B.; Kim, Y.-K.; Rotello, V. M. Acylsulfonamide-Functionalized Zwitterionic Gold Nanoparticles for Enhanced Cellular Uptake at Tumor pH. *Angew. Chem., Int. Ed*. **2015**, *54*, 6567−6570.

177. Moad, G.; Rizzardo, E.; Thang, S. H. Living radical polymerization by the RAFT process–a third update. *Aust. J. Chem*. **2012**, *65*, 985–1076.

178. Moffitt, M.; Khougaz, K.; Eisenberg, A. Micellization of Ionic Block Copolymers. *Acc. Chem. Res*. **1996**, *29*, 95–102.

179. Moghimi, S. M.; Hunter, A. C.; Murray, J. C. Long-circulating and target-specific nanoparticles: Theory to practice. *Pharmacol. ReV*. **2001**, *53*, 283–318.

180. Molineux, G. PEGylation: engineering improved pharmaceuticals for enhanced therapy. *Cancer Treat Rev*. **2002**, *28* (Suppl. A), 13−16.

181. Molla, R. M.; Prasad, P.; Thayumanavan, S. Protein-Induced Supramolecular Disassembly of Amphiphilic Polypeptide Nanoassemblies. *J. Am. Chem. Soc*. **2015**, *137*, 7286−7289.

182. Moribe, K.; Maruyama, K. Reviews on PEG coated liposomal drug carriers. *Drug Delivery Syst*. **2001**, *16 (3)*, 165−171.

183. Mu, J.; Zhang, L.; Zhao, M.; Wang, Y. Catalase Mimic Property of Co_3O_4 Nanomaterials with Different Morphology and Its Application as a Calcium Sensor. *ACS Appl. Mater. Interfaces* **2014**, *6*, 7090–7098.

184. Muro S. New biotechnological and nanomedicine strategies for treatment of lysosomal storage disorders. *Wiley Interdiscip. Rev. Nanomed. Nanobiotechnol.* **2010**, *2*, 189–204.

185. Murthy, N.; Campbell, J.; Fausto, N.; Hoffman, A. S.; Stayton, P. S. Design and synthesis of pH-responsive polymeric carriers that target uptake and enhance the intracellular delivery of oligonucleotides. *J. Control. Release* **2003**, *89*, 365-374.

186. Mutsaers, S. E.; Papadimitriou, J. M. Surface charge of macrophages and their interaction with charged particles. *J. Leukocyte Biol*. **1988**, *44*, 17–26.

187. Nagarajan, R. Molecular Packing Parameter and Surfactant Self-assembly: The Neglected Role of the Surfactant Tail. *Langmuir* **2002**, *18*, 31−38.

188. Nagayama, S.; Ogawara, K.; Fukuoka, Y.; Higaki, K.; Kimura, T. Time-dependent changes in opsonin amount associated on nanoparticles alter their hepatic uptake characteristics. *Int. J. Pharm.* **2007**, *342*, 215–221.

189. Nahire, R.; Hossain, R.; Patel, R.; Paul, S.; Meghnani, V.; Ambre, A. H.; Gange, K. N.; Katti, K. S.; Leclerc, E.; Srivastava, D. K.; Sarkar, K.; Mallik, S. pH-Triggered Echogenicity and Contents Release from Liposomes. *Mol. Pharm*. **2014**, *11*, 4059–4068.

190. Nahrendorf, M.; Keliher, E.; Marinelli, B.; Waterman, P.; Feruglio, P. F.; Fexon, L.; Pivovarov, M.; Swirski, F. K.; Pittet, M. J.; Vinegoni, C.; Weissleder, R. Hybrid PET-optical imaging using targeted probes. *Proc. Natl. Acad. Sci. U. S. A*. **2010**, *107*, 7910–7915.

191. Nair, L. S.; Laurencin, C. T. Biodegradable polymers as biomaterials. *Prog. Polym. Sci*. **2007**, *32*, 762-789.

192. Nakatani, K.; Ogura, Y.; Koda, Y.; Terashima, T.; Sawamoto, M. Sequence-regulated copolymers via tandem catalysis of living radical polymerization and in situ transesterification. *J. Am. Chem. Soc*. **2012**, *134*, 4373–4383.

193. Narayanan, S.; Binulal, N. S.; Mony, U.; Manzoor, K.; Nair, S.; Menon, D. Folate targeted polymeric 'green' nanotherapy for cancer. *Nanotechnology* **2010**, *21*, 285107.

194. Neiser, M. W.; Muth, S.; Kolb, U.; Harris, J. R.; Okuda, J.; Schmidt, M. Micelle Formation from Amphiphilic “Cylindrical Brush”–Coil Block Copolymers Prepared by Metallocene Catalysis. *Angew. Chem., Int. Ed*. **2004**, *43*, 3192–3195.

195. O'Brien, M. E.; Socinski, M. A.; Popovich, A. Y.; Bondarenko, I. N.; Tomova, A.; Bilynsky, B. T.; Hotko, Y. S.; Ganul, V. L.; Kostinsky, I. Y.; Eisenfeld, A. J.; Sandalic, L.; Oldham, F. B.; Bandstra, B.; Sandler, A. B.; Singer, J. W. Randomized phase III trial comparing single-agent paclitaxel Poliglumex (CT-2103, PPX) with single-agent gemcitabine or vinorelbine for the treatment of PS 2 patients with chemotherapy-naive advanced non-small cell lung cancer. *J. Thorac. Oncol*. **2008**, *3*, 728-734.

196. Owens, D. E. III; Peppas, N. A. Opsonization, biodistribution, and pharmacokinetics of polymeric nanoparticles. *Int. J. Pharm*. **2006**, *307*, 93–102.

197. Papadopoulos, P.; Floudas, G.; Klok, H. A.; Schnell, I.; Pakula, T. Self-Assembly and Dynamics of Poly(γ-benzyl-l-glutamate) Peptides. *Biomacromolecules* **2004**, *5*, 81– 91.

198. Peng, F.; Su, Y.; Zhong, Y.; Fan, C.; Lee, S.-T.; He, Y. Silicon Nanomaterials Platform for Bioimaging, Biosensing, and Cancer Therapy. *Acc. Chem. Res.* **2014**, *47*, 612–623.

199. Perrault, S. D.; Walkey, C.; Jennings, T.; Fischer, H. C.; Chan, W. C. Mediating tumor targeting efficiency of nanoparticles through design. *Nano letters*. **2009**, *9*, 1909–1915.

200. Petzetakis, N.; Robin, M. P.; Patterson, J. P.; Kelley, E. G.; Cotanda, P.; Bomans, P. H. H.; Sommerdijk, N. A. J. M.; Dove, A. P.; Epps, T. H.; O'Reilly, R. K. Hollow Block Copolymer Nanoparticles through a Spontaneous One-step Structural Reorganization. *ACS Nano* **2013**, *7*, 1120–1128.

201. Phillips, M. A.; Gran, M. L.; Peppas, N. A. Targeted Nanodelivery of Drugs and Diagnostics. *Nano Today*, **2010,** *5(2),*143-159.

202. Plowman, J, Dykes D, Hollingshead M, Simpson-Herren L, and Alley M. Human tumor xenograft models in NCI drug development. In: Anticancer drug development guide: preclinical screening, clinical trials, and approval. Teicher (ed) Humana Press Inc. 1993.

203. Pytela, J.; Kotva, R.; Metalova, M.; Rypacek, F. Degradation of N^5 -(2-hydroxylethyl)-L-glutamine and L-glutamic acid homopolymers and copolymers by papain. *Int. J. Biol. Macromol*., **1990**, *12*, 241–246.

204. Quan, Q.; Xie, J.; Gao, H.; Yang, M.; Zhang, F.; Liu, G.; Lin, X.; Wang, A.; Eden, H. S.; Lee, S.; Zhang, G.; Chen, X. HSA Coated Iron Oxide Nanoparticles as Drug Delivery Vehicles for Cancer Therapy. *Mol. Pharm*. **2011**, *8*, 1669–1676.

205. Quémener, D.; Davis, T. P.; Barner-Kowollik, C.; Stenzel, M. H. RAFT and click chemistry: A versatile approach to well-defined block copolymers. *Chem. Commun*. **2006**, *42*, 5051–5053.

206. Quesada, M.; Muniesa, C.; Botella, P. Hybrid PLGA-Organosilica Nanoparticles with Redox-Sensitive Molecular Gates. *Chem. Mater*. **2013**, *25*, 2597–2602.

207. Radovic-Moreno, A. F.; Lu, T. K.; Puscasu, V. A.; Yoon, C. J.; Langer, R.; Farokhzad, O. C. Surface Charge-Switching Polymeric Nanoparticles for Bacterial Cell Wall-Targeted Delivery of Antibiotics. *ACS Nano* **2012**, *6*, 4279–4287.

208. Ranucci, E.; Suardi, M. a; Annunziata, R.; Ferruti, P.; Chiellini, F.; Bartoli, C. Poly(amidoamine) Conjugates with Disulfide-Linked Cholesterol Pendants Self-Assembling into Redox-Sensitive Nanoparticles. *Biomacromolecules* **2008**, *9*, 2693–2704.

209. Read, M. L.; Etrych, T.; Ulbrich, K.; Seymoura, L. W. Characterisation of the binding interaction between poly(L-lysine) and DNA using the fluorescamine assay in the preparation of nonviral gene delivery vectors. *FEBS Lett*. **1999**, *461*, 96-100.

210. Richard, J. P.; Melikov, K.; Vives, E.; Ramos, C.; Verbeure, B.; Gait, M. J.; Chernomordik, L. V.; Lebleu, B. Cell-penetrating peptides. A reevaluation of the mechanism of cellular uptake. *J. Biol. Chem*. **2003**, *278*, 585–590.

211. Romberg, B.; Hennink, W. E.; Storm, G. Sheddable coatings for long-circulating nanoparticles. *Pharm. Res*. **2008**, *25*, 55–71.

212. Rosebrugh, L. E.; Marx, V. M.; Keitz, B. K.; Grubbs, R. H. Synthesis of highly cis, syndiotactic polymers via ring-opening metathesis polymerization using ruthenium metathesis catalysts. *J. Am. Chem. Soc*. **2013**, *135*, 10032–10035.

213. Rosenholm, J. M.; Meinander, A.; Peuhu, E.; Niemi, R.; Eriksson, J. E.; Sahlgren, C.; Linde, M. Targeting of Porous Hybrid Silica Nanoparticles to Cancer Cells. *ACS Nano* **2009**, *3*, 197–206.

214. Rösler, A.; Vandermeulen, G. W. M.; Klok, H.-A. Advanced drug delivery devices via selfassembly of amphiphilic block copolymers. *Adv. Drug Delivery Rev*. **2012**, *64*, 270–279.

215. Ruoslahti, E. RGD and Other Recognition Sequences for Integrins. *Annu. Rev. Cell. Dev. Biol*. **1996**, *12*, 697–715.

216. Ryu, J.-H.; Chacko, R. T.; Jiwpanich, S.; Bickerton, S.; Babu, R. P.; Thayumanavan, S. Self-Cross-Linked Polymer Nanogels: A Versatile Nanoscopic Drug Delivery Platform. *J. Am. Chem. Soc*. **2010**, *132*, 17227–17235.

217. Ryu, J. -H.; Jiwpanich, S.; Chacko, R.; Bickerton S.; Thayumanavan, S. Surface functionalizable polymer nanogels with facile hydrophobic guest encapsulation capabilities. J. *Am. Chem. Soc*. **2010**, *132*, 8246–8247.

218. Ryu, J.-H.; Roy, R.; Ventura, J.; Thayumanavan, S. Redox-Sensitive Disassembly of Amphiphilic Copolymer Based Micelles. *Langmuir* **2010**, *26*, 7086–7092.

219. Saeki, S.; Kuwahara, N.; Nakata, M.; Kaneko, M. Upper and lower critical solution temperature in poly (ethylene glycol) solutions. *Polymer* **1976**, *17*, 685–689.

220. Safra, T.; Muggia, F.; Jeffers, S.; Tsao-Wei, D. D.; Groshen, S.; Lyass, O.; Henderson, R.; Berry, G.; Gabizon, A. Pegylated liposomal doxorubicin (doxil): Reduced clinical cardiotoxicity in patients reaching or exceeding cumulative doses of 500 mg/m^2. *Ann. Oncol*. **2000**, *11*, 1029–1033.

221. Saito, G.; Swanson, J. A.; Lee, K. D. Drug delivery strategy utilizing conjugation via reversible disulfide linkages: role and site of cellular reducing activities. *Adv. Drug Delivery Rev*. **2003**, *55*, 199-215.

222. Sarko, D.; Beijer, B.; Boy, R. G.; Nothelfer, E.-M.; Leotta, K.; Eisenhut, M.; Altmann, A.; Haberkorn, U.; Mier, W. The Pharmacokinetics of Cell-Penetrating Peptides. *Mol. Pharmaceutics* **2010**, *7*, 2224−2231.

223. Schabel, F.; Griswold, D.; Corbett, T.; Laster, R.; Mayo, J.; Lloyd, H. Testing therapeutic hypotheses in mice and man: Observations on the therapeutic activity against advanced solid tumors of mice treated with anticancer drugs that have demonstrated or potential clinical utility for treatment of advanced solid tumors of man. *Methods in Cancer Research* **1979**, *17*, 3-51.

224. Schabel, F.; Griswold, D.; Laster, W.; Corbett, T.; Lloyd, H. Quantitative evaluation of anticancer agent activity in experimental animals. *Pharmac. Ther. A*. **1977**, *1*, 411-435.

225. Schild, H. G. Poly(*N*-isopropylacrylamide): experiment, theory and application. *Prog. Polym. Sci.* **1992**, *17*, 163–249.

226. Seltzer, J. L.; Weingarten; H.; Akers, K. T.; Eschbach, M. L.; Grant, G. A.; Eisen, A. Z. Cleavage Specificity of Type IV Collagenase (Gelatinase) from Human Skin. Use of synthetic peptides as model substrates. *The Journal of Biological Chemistry* **1989**, *264(33)*, 19583-19586.

227. Shao, Y.; Shi, C.; Xu, G.; Guo, D.; Luo, J. Photo and Redox Dual Responsive Reversibly Cross-Linked Nanocarrier for Efficient Tumor-Targeted Drug Delivery. *ACS Appl. Mater. Interfaces* **2014**, *6*, 10381–10392.

228. Shchukin, D. G.; Grigoriev, D. O.; Mohwald, H. Application of Smart Organic Nanocontainers in Feedback Active Coatings. *Soft Matter* **2010**, *6*, 720–725.

229. Shelley, W. B.; Talanin, N.; Shelley, E. D. Polysorbate 80 hypersensitivity. *Lancet* **1995**, *345*, 1312-1313.

230. Shi, Y.; Goodisman, J.; Dabrowiak, J. C. Cyclodextrin Capped Gold Nanoparticles as a Delivery Vehicle for a Prodrug of Cisplatin. *Inorg. Chem*. **2013**, *52*, 9418–9426.

231. Shokeen, M.; Pressly, E. D.; Hagooly, A.; Zheleznyak, A.; Ramos, N.; Fiamengo, A. L.; Welch, M. J.; Hawker, C. J.; Anderson, C. J. Evaluation of Multivalent, Functional Polymeric Nanoparticles for Imaging Applications. *ACS Nano* **2011**, *5*, 738–747.

232. Shou, M. Prediction of pharmacokinetics and drug-drug interactions from in vitro metabolism data. *Curr. Opin. Drug Discov. Devel*. **2005**, *8*, 66-77.

233. Soussan, E.; Cassel, S.; Blanzat, M.; Rico-Lattes, I. Drug Delivery by Soft Matter: Matrix and Vesicular Carriers. *Angew. Chem., Int. Ed*. **2009**, *48*, 274−288.

234. Stolnik, S.; Dunn, S. E.; Garnett, M. C.; Davies, M. C.; Coombes, A. G. A.; Taylor, D. C.; Irving, M. P.; Purkiss, S. C.; Tadros, T. F.; Davis, S. S.; Illum, L. Surface Modification of Poly(lactide-co-glycolide) Nanospheres by Biodegradable Poly(lactide)-Poly(ethylene glycol) Copolymers. *Pharm. Res.* **1994**, *11(12),* 1800–1808.

235. Stuart, M. A. C.; Huck, W. T. S.; Genzer, J.; Muller, M.; Ober, C.; Stamm, M.; Sukhorukov, G. B.; Szleifer, I.; Tsukruk, V. V.; Urban, M.; Winnik, F.; Zauscher, S.; Luzinov, I.; Minko, S. Emerging Applications of Stimuli-Responsive Polymer Materials. *Nat. Mater.* **2010**, *9*, 101–113.

236. Stuker, F.; Ripoll, J.; Rudin, M. Fluorescence Molecular Tomography: Principles and Potential for Pharmaceutical Research. *Pharmaceutics*, **2011**, *3*, 229-274.

237. Sun, C.-Y.; Shen, S.; Xu, C.-F.; Li, H.-J.; Liu, Y.; Cao, Z.-T.; Yang, X.-Z.; Xia, J.-X.; Wang, J. Tumor Acidity-Sensitive Polymeric Vector for Active Targeted siRNA Delivery. *J. Am. Chem. Soc*. **2015**, *137*, 15217−15224.

238. Sun, Q.; Ojha, T.; Kiessling, F.; Lammers, T.; Shi, Y. Enhancing Tumor Penetration of Nanomedicines. *Biomacromolecules* **2017**, *18*, 1449-1459.

239. Suwa, K.; Yamamoto, K.; Akashi, M.; Takano, K.; Tanaka, N.; Kunugi, S. Effects of salt on the temperature and pressure responsive properties of poly(N-vinylisobutyramide) aqueous solutions. *Colloid Polym. Sci*. **1998**, *276*, 529-533.

240. Tagami, T.; Ernsting, M. J.; Li, S. D. Efficient tumor regression by a single and low dose treatment with a novel and enhanced formulation of thermosensitive liposomal doxorubicin. *J. Control Release* **2011**, *152*, 303-309.

241. Tagami, T.; Ernsting, M. J.; Li, S. D. Optimization of a novel and improved thermosensitive liposome formulated with DPPC and a brij surfactant using a robust in vitro system. *J. Control Release* **2011**, *154*, 290-297.

242. Tagami, T.; Foltz, W. D.; Ernsting, M. J.; Lee, C. M.; Tannock, I. F.; May, J. P.; Li, S. P. MRI monitoring of intratumoral drug delivery and prediction of the therapeutic effect with a multifunctional thermosensitive liposome. *Biomaterials* **2011**, *32*, 6570-6578.

243. Tan, Y.; Jiang, H. Diffuse optical tomography guided quantitative fluorescence molecular tomography. *Appl Opt*. **2008**, *47*, 2011–2016.

244. Tan, Y.; Jiang, H. DOT guided fluorescence molecular tomography of arbitrarily shaped objects. Med. Phys. **2008**, *35*, 5703–5707.

245. Torchilin, V. P. Structure and Design of Polymeric Surfactant-based Drug Delivery Systems. *J. Control. Release* **2001**, *73*, 137−172.

246. Torchilin, V. P.; Lukyanov, A. N.; Gao, Z.; Papahadjopoulos-Sternberg, B. Immunomicelles: Targeted pharmaceutical carriers for poorly soluble drugs. *Proc. Natl. Acad. Sci. U. S. A*. **2003**, *100*, 6039–6044.

247. Tung, S. H.; Lee, H. Y.; Raghavan, S. R. A Facile Route for Creating "Reverse" Vesicles: Insights into "Reverse" Self-Assembly in Organic Liquids. *J. Am. Chem. Soc*. **2008**, *130*, 8813– 8817.

248. Tutton, M. G.; George, M. L.; Eccles, S. A.; Burton, S.; Swift, R. I.; Abulafi, A. M. Use of Plasma MMP-2 and MMP-9 Levels as a Surrogate for Tumor Expression in Colorectal Cancer Patients. *Int. J. Cancer*, **2003**,*107*, 541–550.

249. Udenfriend, S.; Stein, S.; Böhlen, P.; Dairman, W.; Leimgruber, W.; Weigele, M. Fluorescamine: A Reagent for Assay of Amino Acids, Peptides, Proteins, and Primary Amines in the Picomole range. *Science*, **1972**, *178(4063)*, 871-872.

250. Ulbrich, K.; Subr, V. Polymeric anticancer drugs with pH-controlled activation. *Adv. Drug Delivery Rev*. **2004**, *56*, 1023–1050.

251. Urien, S.; Barre, J.; Morin, C.; Paccaly, A.; Montay, G.; Tillement, J. P. Docetaxel serum protein binding with high affinity to alpha 1-acid glycoprotein. *Invest New Drugs* **1996**, *14*, 147-151.

252. Vader, P.; van der Aa, L. J.; Engbersen, J. F.; Storm, G.; Schiffelers, R. M. Physicochemical and Biological Evaluation of siRNA Polyplexes Based on PEGylated Poly(amido amine)s. *Pharm. Res.* **2012**, *29(2)*, 352–361.

253. Varkouhi, A. K.; Scholte, M.; Storm, G.; Haisma, H. J. Endosomal escape pathways for delivery of biologicals. *J. Control. Release* **2011**, *151*, 220–228.

254. Vasquez, K. O.; Casavant, C.; Peterson, J. D. Quantitative Whole Body Biodistribution of Fluorescent-Labeled Agents by Non-Invasive Tomographic Imaging. *PLoS ONE*, **2011**, *6(6),* e20594.

255. Vauthey, S.; Santoso, S.; Gong, H.; Watson, N.; Zhang, S. Molecular Self-Assembly of Surfactant-like Peptides to Form Nanotubes and Nanovesicles. *Proc. Natl. Acad. Sci. U.S.A.* **2002**, *99*, 5355–5360.

256. Ventura, J. Eron, S. J. González-Toro, D. C.; Raghupathi, K.; Wang, F.; Hardy, J. A.; Thayumanavan, S. Reactive Self-Assembly of Polymers and Proteins to Reversibly Silence a Killer Protein. *Biomacromolecules*, **2015**, *16(10)*, 3161–3171.

257. Venturoli, D.; Rippe, B. Ficoll and dextran vs. globular proteins as probes for testing glomerular permselectivity: effects of molecular size, shape, charge and deformability. *Am. J. Physiol*. **2005**, *288*, F605–F613.

258. Verbaan, F. J.; Oussoren, C.; Snel, C. J.; Crommelin, D. J.; Hennink, W. E.; Storm, G. Steric stabilization of poly(2-(dimethylamino)ethyl methacrylate)-based polyplexes mediates prolonged circulation and tumor targeting in mice. *J. Gene Med*. **2004**, *6*, 64-75.

259. Vert, M. Aliphatic polyesters: great degradable polymers that cannot do everything. *Biomacromolecules* **2005**, *6*, 538–546.

260. Vittaz, M.; Bazile, D.; Spenlehauer, G.; Verrecchia, T.; Veillard, M.; Puisieux, F.; Labarre, D. Effect of PEO surface density on long-circulating PLA-PEO nanoparticles which are very low complement activators. *Biomaterials* **1996**, *17*, 1575–1581.

261. Von Hippel, P. H.; Wong. K. Y. Neutral salts: the generality of their effects on the stability of macromolecular conformations. *Science* **1964**, *145*, 577-580.

262. Wang, Y.-C.; Wang, F.; Sun, T.-M.; Wang, J. Redox-Responsive Nanoparticles from the Single Disulfide Bond-Bridged Block Copolymer as Drug Carriers for Overcoming Multidrug Resistance in Cancer Cells. Bioconjug. Chem. 2011, 22, 1939–1945.

263. Weissleder, R. A clearer vision for in vivo imaging. *Nat Biotechnol*. **2001**, *19*, 316–317.

264. Wilson, W. R.; Hay, M. P. Targeting hypoxia in cancer therapy. *Nature Reviews Cancer,* **2011***,* 11, 393-410.

265. Wong, C. -H.; Zimmerman, S. C. Orthogonality in organic, polymer, and supramolecular chemistry: from Merrifield to click chemistry. *Chem. Commun*. **2013**, *49*, 1679–1695.

266. Wu, X. L.; Kim, J. H.; Koo, H.; Bae, S. M.; Shin, H.; Kim, M. S.; Lee, B.-H.; Park, R.-W.; Kim, I.-S.; Choi, K.; Kwon, I. C.; Kim, K.; Lee, D. S. Tumor-Targeting Peptide Conjugated pH-Responsive Micelles as a Potential Drug Carrier for Cancer Therapy. *Bioconjug. Chem*. **2010**, *21*, 208–213.

267. Wu, Y.; Phillips, J. A.; Liu, H.; Yang, R.; Tan, W. Carbon Nanotubes Protect DNA Strands during Cellular Delivery. *ACS Nano* **2008**, *2*, 2023–2028.

268. Xu, J. Z.; Moon, S. H.; Jeong, B.; Sohn, Y. S. Thermosensitive micelles from PEGylated oligopeptides. *Polymer*, **2007**, *48*, 3673-3678.

269. Yan, Z.; Yang, Y.; Wei, X.; Zhong, J.; Wei, D.; Liu, L.; Xie, C.; Wang, F.; Zhang, L.; Lu, W.; He, D. Tumor-Penetrating Peptide Mediation: An Effective Strategy for Improving the Transport of Liposomes in Tumor Tissue. *Mol. Pharm*. **2014**, *11*, 218–225.

270. Yang, G.; Gai, S.; Qu, F.; Yang, P. SiO_2@YBO_3:Eu^{3+} Hollow Mesoporous Spheres for Drug Delivery Vehicle. *ACS Appl. Mater. Interfaces* **2013**, *5*, 5788– 5796.

271. Yang, Z.; Leon, J.; Martin, M.; Harder, J. W.; Zhang, R.; Liang, D.; Lu, W.; Tian, M., Gelovani, J. G.; Qiao, A.; Li, C. Pharmacokinetics and biodistribution of near-infrared fluorescence polymeric nanoparticles. *Nanotechnology* **2009**, *20*, 165101-16511.

272. Yang, Z.; Zhang, Y.; Markland, P.; Yang, V. C. Poly(glutamic acid) poly(ethylene glycol) hydrogels prepared by photoinduced polymerization: Synthesis, characterization, and preliminary release studies of protein drugs. *J Biomed Mater Res*. **2002**, *62*, 14-21.

273. Yu, S. S.; Lau, C. M.; Thomas, S. N.; Jerome, W. G.; Maron, D. J.; Dickerson, J. H.; Hubbell, J. A.; Giorgio, T. D. Size- and charge-dependent non-specific uptake of PEGylated nanoparticles by macrophages. *Int. J. Nanomed*. **2012**, *7*, 799-813.

274. Zhang, L.; Cao, Z.; Li, Y.; Ella-Menye, J.-R.; Bai, T.; Jiang, S. Softer zwitterionic nanogels for longer circulation and lower splenic accumulation. *ACS Nano*, **2012**, *6*, 6681–6686.

275. Zhu, L.; Kate, P.; Torchilin, V. P. Matrix Metalloprotease 2-Responsive Multifunctional Liposomal Nanocarrier for Enhanced Tumor Targeting. *ACS Nano*, **2012**, *6(4)*, 3491-3498.

276. Zhuang, J.; Chacko, R. T.; Amado Torres, D. F.; Wang, H.; Thayumanavan, S. Dual Stimuli-Dual Response Nanoassemblies Prepared from a Simple Homopolymer. *ACS Macro Lett*. **2014**, *3*, 1−5.

277. Zhuang, J.; Gordon, M. R.; Ventura, J.; Li, L. Thayumanavan, S. Multi-Stimuli Responsive Macromolecules and Their Assemblies. *Chem. Soc. Rev*. **2013**, *42*, 7421–7435.

278. Zhang, J.; Yuan, Z. F.; Wang, Y.; Chen, W. H.; Luo, G. F.; Cheng, S. X.; Zhuo, R. X.; Zhang, X. Z. Multifunctional Envelope- Type Mesoporous Silica Nanoparticles for Tumor-Triggered Targeting Drug Delivery. *J. Am. Chem. Soc*. **2013**, *135*, 5068−5073.

279. Zhang, L.; Yu, K.; Eisenberg, A. Ion-Induced Morphological Changes in "Crew-Cut" Aggregates of Amphiphilic Block Copolymers. *Science* **1996**, *272*, 1777– 1779.

280. Zhang, Q.; Liu, F.; Nguyen, K. T.; Ma, X.; Wang, X.; Xing, B.; Zhao, Y. Multifunctional Mesoporous Silica Nanoparticles for Cancer-Targeted and Controlled Drug Delivery. *Adv. Funct. Mater.* **2012**, *22*, 5144-5156.

281. Zhang, Q.; Ko, N. R.; Oh, J. K. Recent advances in stimuli-responsive degradable block copolymer micelles: synthesis and controlled drug delivery applications. *Chem. Commun*. **2012**, *48*, 7542–7552.

282. Zhang, Y.; Cremer, P. S. Interactions between macromolecules and ions: the Hofmeister series. *Curr. Opin. Chem. Biol*. **2006**, *10*, 658–663.

283. Zhang, Y. J.; Furyk, S.; Bergbreiter, D. E.; Cremer, P. S. Specific ion effects on the water solubility of macromolecules: PNIPAM and the Hofmeister Series. *J. Am. Chem. Soc.* **2005**, *127*, 14505–14510.

284. Zhang, Y. J.; Furyk, S.; Sagle, L. B.; Cho, Y.; Bergbreiter, D. E.; Cremer, P. S. Effects of Hofmeister anions on the LCST of PNIPAM as a function of molecular weight. *J. Phys. Chem. C*. **2007**, *111*, 8916-8924.

285. Zhigaltsev, I. V.; Winters, G.; Srinivasulu, M.; Crawford, J.; Wong, M.; Amankwa, L.; Waterhouse, D.; Masin, D.; Webb, M.; Harasym, N.; Heller, L.; Bally, M. B.; Ciufolini, M. A.; Cullis, P. R.; Maurer, N. Development of a weak-base docetaxel derivative that can be loaded into lipid nanoparticles. *J Control Release* **2010**, *144*, 332-340.

286. Zhu, G.-G.; Wang, F.-G.; Liu, Y.-Y. Effects of Reaction Conditions on the Grafting Percentage of Poly(ethylene glycol)-block-poly(γ-benzyl L-glutamate)-graft-poly(ethylene glycol) Copolymer. *J. Braz. Chem. Soc*. **2010**, *21*, 715-720.

287. Zhu, L.; Kate, P.; Torchilin, V. P. Matrix Metalloprotease 2-Responsive Multifunctional Liposomal Nanocarrier for Enhanced Tumor Targeting. *ACS Nano*, **2012**, *6(4)*, 3491-3498.

288. Zhu, L.; Mahato, R. I. Targeted Delivery of siRNA to Hepatocytes and Hepatic Stellate Cells by Bioconjugation. *Bioconjugate Chem*. **2010**, *21*, 2119–2127.

289. Zhu, L.; Ye, Z.; Cheng, K.; Miller, D. D.; Mahato, R. I. Site-Specific Delivery of Oligonucleotides to Hepatocytes after Systemic Administration. *Bioconjugate Chem*. **2008**, *19*, 290–298.

290. Zotti, G.; Vercelli, B.; Berlin, A. Monolayers and multilayers of conjugated polymers as nanosized electronic components. *Acc. Chem. Res.* **2008**, *41*, 1098–1109.